

# Long Spans with Transportable Precast Prestressed Girders

**Final Report**

**December 2013**

---

*Principal investigator:*

H. R. Hamilton

*Research assistants:*

Natassia R. Brenkus

Department of Civil and Coastal Engineering  
University of Florida  
P.O. Box 116580  
Gainesville, Florida 32611

---

**Sponsor:**

Florida Department of Transportation (FDOT)

Project Managers:

Sam Fallaha, P.E.

Christina Freeman, P.E.

**Contract:**

UF Project No. 00082953

FDOT Contract No. BDK75 977-30



**University of Florida**

Engineering School of Sustainable Infrastructure and Environment  
Department of Civil and Coastal Engineering

## **Disclaimer**

The opinions, findings, and conclusions expressed in this publication are those of the authors and not necessarily those of the State of Florida Department of Transportation.

## Unit of Measurement Conversions

### SI\* (MODERN METRIC) CONVERSION FACTORS APPROXIMATE CONVERSIONS TO SI UNITS

SYMBOL	WHEN YOU KNOW	MULTIPLY BY	TO FIND	SYMBOL
<b>LENGTH</b>				
<b>in</b>	inches	25.4	millimeters	mm
<b>ft</b>	feet	0.305	meters	m
<b>yd</b>	yards	0.914	meters	m
<b>mi</b>	miles	1.61	kilometers	km
<b>AREA</b>				
<b>in<sup>2</sup></b>	square inches	645.2	square millimeters	mm <sup>2</sup>
<b>ft<sup>2</sup></b>	square feet	0.093	square meters	m <sup>2</sup>
<b>yd<sup>2</sup></b>	square yard	0.836	square meters	m <sup>2</sup>
<b>ac</b>	acres	0.405	hectares	ha
<b>mi<sup>2</sup></b>	square miles	2.59	square kilometers	km <sup>2</sup>
<b>VOLUME</b>				
<b>fl oz</b>	fluid ounces	29.57	milliliters	mL
<b>gal</b>	gallons	3.785	liters	L
<b>ft<sup>3</sup></b>	cubic feet	0.028	cubic meters	m <sup>3</sup>
<b>yd<sup>3</sup></b>	cubic yards	0.765	cubic meters	m <sup>3</sup>
NOTE: volumes greater than 1000 L shall be shown in m <sup>3</sup>				
<b>MASS</b>				
<b>oz</b>	ounces	28.35	grams	g
<b>lb</b>	pounds	0.454	kilograms	kg
<b>T</b>	short tons (2000 lb)	0.907	megagrams	Mg (or "t")
<b>TEMPERATURE (exact degrees)</b>				
<b>°F</b>	Fahrenheit	5(F-32)/9 or (F-32)/1.8	Celsius	°C
<b>ILLUMINATION</b>				
<b>fc</b>	foot-candles	10.76	lux	lx
<b>fl</b>	foot-Lamberts	3.426	candela/m <sup>2</sup>	cd/m <sup>2</sup>
<b>FORCE and PRESSURE or STRESS</b>				
<b>kip</b>	1000 pound force	4.45	kilonewtons	kN
<b>lbf</b>	pound force	4.45	newtons	N
<b>lbf/in<sup>2</sup></b>	pound force per square inch	6.89	kilopascals	kPa

\*SI is the symbol for the International System of Units. Appropriate rounding should be made to comply with Section 4 of ASTM E380.

**SI\* (MODERN METRIC) CONVERSION FACTORS**  
*APPROXIMATE CONVERSIONS FROM SI UNITS*

SYMBOL	WHEN YOU KNOW	MULTIPLY BY	TO FIND	SYMBOL
<b>LENGTH</b>				
<b>mm</b>	millimeters	0.039	inches	in
<b>m</b>	meters	3.28	feet	ft
<b>m</b>	meters	1.09	yards	yd
<b>km</b>	kilometers	0.621	miles	mi
<b>AREA</b>				
<b>mm<sup>2</sup></b>	square millimeters	0.0016	square inches	in <sup>2</sup>
<b>m<sup>2</sup></b>	square meters	10.764	square feet	ft <sup>2</sup>
<b>m<sup>2</sup></b>	square meters	1.195	square yards	yd <sup>2</sup>
<b>ha</b>	hectares	2.47	acres	ac
<b>km<sup>2</sup></b>	square kilometers	0.386	square miles	mi <sup>2</sup>
<b>VOLUME</b>				
<b>mL</b>	milliliters	0.034	fluid ounces	fl oz
<b>L</b>	liters	0.264	gallons	gal
<b>m<sup>3</sup></b>	cubic meters	35.314	cubic feet	ft <sup>3</sup>
<b>m<sup>3</sup></b>	cubic meters	1.307	cubic yards	yd <sup>3</sup>
<b>MASS</b>				
<b>g</b>	grams	0.035	ounces	oz
<b>kg</b>	kilograms	2.202	pounds	lb
<b>Mg (or "t")</b>	megagrams (or "metric ton")	1.103	short tons (2000 lb)	T
<b>TEMPERATURE (exact degrees)</b>				
<b>°C</b>	Celsius	1.8C+32	Fahrenheit	°F
<b>ILLUMINATION</b>				
<b>lx</b>	lux	0.0929	foot-candles	fc
<b>cd/m<sup>2</sup></b>	candela/m <sup>2</sup>	0.2919	foot-Lamberts	fl
<b>FORCE and PRESSURE or STRESS</b>				
<b>kN</b>	kilonewtons	0.225	1000 pound force	kip
<b>N</b>	newtons	0.225	pound force	lbf
<b>kPa</b>	kilopascals	0.145	pound force per square inch	lbf/in <sup>2</sup>

\*SI is the symbol for the International System of Units. Appropriate rounding should be made to comply with Section 4 of ASTM E380.

1. Report No.		2. Government Accession No.		3. Recipient's Catalog No.	
4. Title and Subtitle <b>Long Spans with Transportable Precast Prestressed Girders</b>			5. Report Date <b>December 2013</b>		
			6. Performing Organization Code		
7. Author(s) <b>Natassia R. Brenkus and H. R. Hamilton</b>			8. Performing Organization Report No.		
9. Performing Organization Name and Address <b>University of Florida Department of Civil &amp; Coastal Engineering P.O. Box 116580 Gainesville, FL 32611-6580</b>			10. Work Unit No. (TRAIS)		
			11. Contract or Grant No. <b>BDK75 977-30</b>		
12. Sponsoring Agency Name and Address <b>Florida Department of Transportation Research Management Center 605 Suwannee Street, MS 30 Tallahassee, FL 32399-0450</b>			13. Type of Report and Period Covered <b>Final Report 04-05-10 thru 12-31-13</b>		
			14. Sponsoring Agency Code		
15. Supplementary Notes					
16. Abstract <p>A splice design for prestressed precast segments was developed and integrated into a simply-supported 208-ft span of 96-in.-deep I-girders. In the proposed splice design, transportable segments are pretensioned at a precast yard, and the strands are cut prior to transport and then spliced on site. Prestressing force is applied to the system by a hydraulic jack on each side of the girder web. External brackets transfer the force from the hydraulic jacks to the precast segments by thru-bolts that pass through the web of the beam. The internal restraint provided by the coupled prestressing strand resists the jacking force, and the prestressing strand is stressed.</p> <p>Due to limitations in laboratory capabilities and research budget, behavioral aspects of the splice deemed most critical were tested using an AASHTO Type II cross-section; due to its smaller size, it was possible to construct duplicate test specimens to assess its constructability as well as its behavior under load.</p> <p>Nine precast pretensioned beam specimens were constructed and tested to evaluate the splice assembly procedure behavior: three control specimens and six spliced specimens. Decks were poured on all specimens. Though labor-intensive, the prestressed splice concept was constructible.</p> <p>Load testing of the completed specimens was conducted to evaluate flexural, shear, and fatigue behavior. Prestress losses were measured and cracking development was observed to assess service behavior. Additional component testing of the coupler used in the splice design was performed at the State Materials Office.</p> <p>Flexural strength of spliced specimens exceeded the AASHTO-LRFD code-predicted values for bonded strand (15%) and unbonded strand (24%). Shear behavior was evaluated by testing a high moment-to-shear ratio (of 3.7). In the one specimen that did exhibit the characteristics of a shear failure, the exhibited shear strength exceeded that calculated per AASHTO-LRFD modified compression field theory. All other specimens tested in the shear set-up failed in flexure. Fatigue resistance of the spliced specimen was greater than that of the non-spliced control. While fatigue did not impact the strength or deflection at ultimate, it did affect ductility and failure mode.</p>					
17. Key Word <b>splice; prestressed concrete; coupler; long span; bridge; I-girder</b>			18. Distribution Statement <b>No restrictions. This document is available to the public through the National Technical Information Service, Springfield, VA, 22161</b>		
19. Security Classif. (of this report) <b>Unclassified</b>		20. Security Classif. (of this page) <b>Unclassified</b>		21. No. of Pages <b>322</b>	22. Price

## **Acknowledgments**

The authors would like to thank the many contributors and helping hands involved in this project.

The authors would like to thank the Florida Department of Transportation (FDOT) State Materials Office, specifically Richard DeLorenzo and Mark Conley, for their support in materials testing.

Thanks to Durastress for the special attention and consideration during the specimen construction. Thanks to Stan Landry with Enerpac Precision Sure-Lock for the contribution of several Grabb-its for preliminary testing.

Special thanks go to the University of Florida Structural Laboratory personnel, including Dr. Chris Ferraro. Thank you for the instruction and assistance with the coupler testing.

Thanks to Christina Freeman and Will Potter for the technical guidance during and throughout the splice and prototype design phase.

Thank you to Abraham Alende, Kinsman Pierson, Michael Willis and Dr. Brandon Ross for their help during the specimen precasting.

For their significant help and constant patience, the authors would like to thank the entire team of the FDOT Structures Research Center. Particular thanks to David Wagner, Steve Eudy, David Allen, Justin Robertson and Brandon Winter for their nearly daily support and advice during the splice construction and testing. Specific thanks to Mr. Wagner for providing the motivational and attention-to-detail insight that made all the pieces fit together.

The year would not have gone as smoothly without the help of Sam Fallaha, Paul Tighe, Chris Weigly, Adam Brennan, Frank Cobb, or Tony Hobbs.

## Executive Summary

A splice design for prestressed precast segments was developed and integrated into a simply-supported 208-ft span of 96-in.-deep I-girders. In the proposed splice design, transportable segments are pretensioned at a precast yard, and the strands are cut prior to transport and then spliced on site. Prestressing force is applied to the system by a hydraulic jack on each side of the girder web. External brackets transfer the force from the hydraulic jacks to the precast segments by thru-bolts that pass through the web of the beam. The internal restraint provided by the coupled prestressing strand resists the jacking force, and the prestressing strand is stressed.

Due to limitations in laboratory capabilities and research budget, behavioral aspects of the splice deemed most critical were tested using an AASHTO Type II cross-section; due to its smaller size, it was possible to construct duplicate test specimens to assess its constructability as well as its behavior under load.

To evaluate the splice design assembly procedures and structural behavior, nine specimens were constructed using the AASHTO Type II cross-section; three control specimens and six spliced specimens were fabricated. To accomplish this, fifteen precast prestressed segments were constructed at a precast facility. The precast segments were then transported to the FDOT Structures Research Lab where six spliced specimens were assembled, the splices stressed, and closures poured. The assembly and stressing procedure included instrumentation to evaluate the procedure. Decks were poured on all specimens. Though labor-intensive, the prestressed splice concept was constructible, with typical prestress losses. Observed cracking moments for all specimens-control or spliced-occurred at less than the moment calculated assuming  $7.5\sqrt{f'_c}$  (psi) at the tensile stress causing cracking.

Load testing of the completed specimens was conducted to evaluate flexural, shear, and fatigue behavior. Prestress losses were measured, and cracking development was observed to assess service behavior. Additional component testing of the coupler used in the splice design was performed at the State Materials Office.

Flexural strength of spliced specimens exceeded the AASHTO-LRFD code-predicted values for bonded strand by 15% and for unbonded strand by 24%. Shear behavior was evaluated by testing a moment-to-shear ratio (M/V) of 3.7-higher than is present in the prototype

FIB96 design (32.9). In the one specimen that did exhibit the characteristics of a shear failure, the exhibited shear strength exceeded that calculated per AASHTO-LRFD modified compression field theory. All other specimens tested in the shear set-up failed in flexure.

Spliced specimen (F1) exhibited greater fatigue resistance than the control specimen (FC) when cycled at the same strand stress range of 0.08fpu. F1 survived 2 million cycles while FC survived 518,000 cycles. Fatigue of spliced specimens did not impact the strength or deflection at ultimate load; it did, however, affect ductility and failure mode. At ultimate load, the non-fatigued control specimen failed in compression (as the deck crushed); fatigued spliced specimens failed when strands ruptured. Fatigue affected reserve strength after ultimate load: fatigued specimens collapsed immediately upon strand rupture; non-fatigued spliced specimens exhibited reserve strength after peak load.

## Table of Contents

Disclaimer .....	ii
Unit of Measurement Conversions .....	iii
Acknowledgments.....	vi
Executive Summary .....	vii
List of Figures .....	xi
List of Tables .....	xvi
1 Introduction.....	1
2 Literature Review.....	3
2.1 History of Spliced Concrete Girders.....	3
2.2 Current Design Practice: Continuity vs. Simple Span Design.....	4
2.3 Advantages of Long-span Precast Concrete Girders .....	6
2.4 Disadvantages of Long-span Precast Concrete Girders.....	8
2.5 Current Construction Techniques: Splice Types .....	9
2.6 Current Construction Techniques: Assembly .....	14
2.7 Current Construction Techniques: Design.....	16
2.8 Prestressing Strand Couplers .....	19
3 Prototype Design–FIB96 .....	23
3.1 Splice Conceptual Design.....	23
3.2 Prototype Bridge and Beam.....	25
3.3 Bridge Design Details.....	26
3.4 Loads.....	28
3.5 Prestressing Strand Pattern Design.....	30
3.6 Moment-Curvature.....	34
3.7 Splice Considerations.....	36
4 Strand Coupler Selection and Testing.....	38
4.1 Ultimate Strength Tests of 0.6-in. dia. Coupler .....	39
4.2 Calibration of 0.5-in. dia. Coupler .....	43
5 Test Specimen Design.....	46
5.1 Detailing Considerations.....	48
5.2 Flexure Service and Cracking Test Design.....	53
5.3 Moment Strength Test Design .....	55
5.4 Shear Test Design .....	59
5.5 Fatigue Test Design .....	60
6 Specimen Construction and Splice Assembly .....	64
6.1 Segment Production .....	64
6.2 Segment Assembly Frames.....	68
6.3 Segment Alignment Procedure .....	69
6.4 Strand Stressing .....	75
6.5 Formwork and Concrete Placement.....	76
6.6 Splice Modifications .....	80
7 Test Procedure and Instrumentation .....	83
7.1 Construction and Splice Assembly.....	83
7.2 Flexure .....	88

7.3	Shear .....	92
7.4	Fatigue.....	95
8	Prestress Losses .....	98
9	Splice Assembly Results and Discussion .....	108
10	Flexural Results and Discussion .....	119
10.1	Flexure–XC.....	119
10.2	Flexure–X1 .....	123
10.3	Service and Cracking Behavior .....	126
10.4	Comparison of Flexure Strength.....	134
11	Shear Results and Discussion .....	138
11.1	Shear–SC.....	138
11.2	Shear–SB.....	140
11.3	Shear–SU .....	143
11.4	Shear–SU2 .....	146
11.5	Comparison of Service and Cracking Behavior.....	150
11.6	Comparison of Shear Strength.....	161
12	Fatigue Results and Discussion .....	166
12.1	Specimen FC.....	166
12.1.1	Static Conditioning .....	166
12.1.2	Fatigue Loading .....	169
12.1.3	Ultimate Strength Test .....	171
12.2	Specimen F1.....	174
12.2.1	Static Conditioning .....	174
12.2.2	Fatigue Loading .....	177
12.2.3	Ultimate Strength Test .....	178
12.3	Specimen F2.....	183
12.3.1	Static Conditioning .....	183
12.3.2	Fatigue Loading .....	188
12.3.3	Ultimate Strength Test .....	189
12.4	Discussion and Comparison of Behavior.....	193
12.4.1	Fatigue.....	193
12.4.2	Ultimate.....	199
13	Discussion and Observations .....	207
13.1	Closure Pour Observations .....	208
13.2	Coupler Observations.....	210
14	Summary and Conclusions .....	211
15	Recommendations and Future Research.....	214
16	References.....	217
	Appendix A–Prototype Design .....	222
	Appendix B–Splice Concepts .....	226
	Appendix C–Bracket Fabrication Drawings.....	240
	Appendix D–Precast Fabrication Drawings.....	245
	Appendix E–Precast Yard and Material Reports .....	257
	Appendix F–Splice Assembly Plots.....	297

## List of Figures

Figure 1–Precast segmented spans used with simple supports (Jaber et al. 2006) .....	6
Figure 2–Curved roadway constructed with spliced girders (Abdel-Karim and Tadros 1992b) .....	6
Figure 3–Nonprestressed reinforcement CIP splice (Abdel-Karim and Tadros 1992) .....	9
Figure 4–Post-tensioned CIP splice (PCI 2004) .....	10
Figure 5–Post-tensioned duct for CIP splice (FDOT 1999).....	11
Figure 6–Gandy Bridge splice connection detail (FDOT 1999).....	12
Figure 7–Stitched splice (PCI 2004).....	13
Figure 8–Match-cast splice (Abdel-Karim and Tadros 1992) .....	14
Figure 9–Launching assembled girder using trolley (Nicholls and Prussack 1997).....	15
Figure 10–Prestressing against internal restraint (Gerwick 1993).....	16
Figure 11–Shear keys required by AASHTO-LRFD (AASHTO-LRFD2007) .....	17
Figure 12–204th Street Bridge (Jaber et al. 2006) .....	18
Figure 13–Prestressing strand coupler types: (a) turnbuckle-style, (b) Alberta, (c) swaged for single strand, (d) swaged for two strands (Zobel and Jirsa 1998; Shanafelt and Horn 1985) .....	19
Figure 14–Turnbuckle-style coupler (FDOT 2010c) .....	20
Figure 15–Repair of severed strand using a coupler (Ministry of Transportation of Ontario 2011) .....	20
Figure 16–Prototype splice design.....	24
Figure 17–Elevation view of FIB96 with two splices.....	25
Figure 18–Prototype design (a) FIB96 girder and (b) bridge cross-section.....	26
Figure 19–Composite section .....	28
Figure 20–Strand layouts .....	31
Figure 21–Moment-curvature of FIB96: continuous strand vs. coupled strand .....	35
Figure 22–FIB96 strain at flexural capacity: continuous vs. coupled strand.....	36
Figure 23–Turnbuckle-style coupler components (Waheed et al. 2005) .....	38
Figure 24–SMO tensile tests of 0.6-in. dia. coupler .....	40
Figure 25–Rupture of strand in 0.6-in. dia. coupler.....	40
Figure 26–UF tensile test set-up of 0.6 in. dia. coupler .....	41
Figure 27–Comparison of 0.6-in. dia. coupler and strand behavior.....	42
Figure 28–Stress-strain models and test data for coupled and continuous strand.....	43
Figure 29–SMO tensile test set-up of 0.5 in.-dia. coupler .....	44
Figure 30–Coupler strain gage calibration (a) specimen 1 and (b) specimen 2.....	45
Figure 31–AASHTO II cross-section .....	47
Figure 32–Test specimens.....	48
Figure 33–Detailing considerations .....	48
Figure 34–Bracket attachment to beam .....	50
Figure 35–Shear keys in test specimen .....	51
Figure 36–Rebar coupler.....	53
Figure 37–Protruding strand .....	53
Figure 38–Flexure test set-up.....	55
Figure 39–Simplified bottom flange of FIB96 cross-section.....	57
Figure 40–Material properties of 270 ksi lo-lax strand.....	58
Figure 41–FIB96 prototype vs. AASHTO II test specimen: strain state at flexural capacity.....	59
Figure 42–Shear test set-up.....	60
Figure 43–Bed layout.....	65
Figure 44–Coped region of bonded segments (a) stirrup placement and (b) pipe insert .....	66
Figure 45–Segments after concrete is cast with top roughened for deck placement .....	66
Figure 46–Elevation of assembly frames.....	69
Figure 47–Photo and schematic of splice assembly frame and beam segments .....	70

Figure 48–Coupler installation on unbonded strand.....	71
Figure 49–Coupled strand prior to prestressing.....	71
Figure 50–Coupled stirrups.....	72
Figure 51–Extend plunger.....	72
Figure 52–Detensioning chair, chucks, and load cells on the unbonded segment.....	73
Figure 53–Tightening the turnbuckles to seat detensioning chair.....	74
Figure 54–Tightening the turnbuckles.....	75
Figure 55–Splice stressed with lock-nuts engaged.....	76
Figure 56–Closure formwork in place.....	77
Figure 57–Seams sealed.....	77
Figure 58–Pouring the closure.....	78
Figure 59–Top of finished closure pour.....	78
Figure 60–Formwork removed (Specimen X1 shown).....	79
Figure 61–Splice complete.....	80
Figure 62–(a) Bond at vertical interface X1 (b) scoring of SU.....	81
Figure 63–Additional stirrup.....	81
Figure 64–Epoxy in closure pour.....	82
Figure 65–Gaged stirrup locations.....	83
Figure 66–Placement of VWSG.....	84
Figure 67–VWSG installation near centroid of strand pattern.....	85
Figure 68–Splice assembly: Instrumentation in closure joint.....	86
Figure 69–Splice assembly: Coupler strain.....	87
Figure 70–Splice assembly: Vertical displacement gages.....	87
Figure 71–Splice assembly: Longitudinal displacement string-pots.....	88
Figure 72–Four-point flexural test set-up: (a) XC and (b) X1.....	89
Figure 73–Flexure: Vertical displacement gages.....	91
Figure 74–Flexure: Out-of-plane displacement gages.....	91
Figure 75–Spliced beams: load cells.....	92
Figure 76–Spliced shear test set-ups for (a) SB and (b) SU and SU2.....	93
Figure 77–Control shear test set-up.....	94
Figure 78–Shear: Vertical displacement gages.....	95
Figure 79–Fatigue test set-up.....	96
Figure 80–Fatigue: Vertical displacement gages.....	97
Figure 81–Prestress force.....	98
Figure 82–Measured prestress losses vs. PCI.....	103
Figure 83–Decompression strain gages.....	104
Figure 84–Decompression: (a) FC; (b) F1; (c) F2-joint and (d) F2-crack.....	105
Figure 85–Load history of X1.....	108
Figure 86–Stressing procedure.....	109
Figure 87–Strand load for (a) SB and (b) SU.....	110
Figure 88–Strand load history based on calibrated coupler strain for (a) SU2 and (b) F2.....	111
Figure 89–Tie-down deflections: (a) SB and (b) SU.....	112
Figure 90–Support deflections: (a) SB and (b) SU.....	113
Figure 91–STM: assumed dimensions.....	114
Figure 92–Tie strain (a) X1 and (b) SU.....	116
Figure 93–Strain in top flange for (a) SB (b) SU.....	117
Figure 94–Transfer length strain (a) SB (b) SU.....	118
Figure 95–XC: Ultimate.....	119
Figure 96–XC: First crack at midspan.....	120
Figure 97–XC: Permanent set.....	121
Figure 98–XC: Compressive concrete strain at midspan.....	122

Figure 99–XC: Midspan strain profile.....	122
Figure 100–X1: Ultimate .....	123
Figure 101–X1: Vertical crack at interface.....	124
Figure 102–X1: Superficial cracks at overlap.....	124
Figure 103–X1: Flexural cracking .....	125
Figure 104–X1: Deck strain.....	126
Figure 105–XC and X1: Elastic behavior.....	127
Figure 106–XC: VWSG vs. bottom flange strain gage.....	129
Figure 107–XC vs. X1: first crack.....	130
Figure 108–Dry joint interface post-demolition, looking at (a) the closure pour, (b) the precast .....	131
Figure 109–XC vs. X1: final cracking patterns .....	131
Figure 110–X1: String-pots across closure.....	132
Figure 111–X1: Opening at joint during test .....	133
Figure 112–Out-of-plane displacement: (a) XC (b) X1.....	134
Figure 113–Flexural strength: XC and X1.....	135
Figure 114–Damage to X1 following testing with spalled concrete in compression zone and wide, permanent crack .....	136
Figure 115–X1: Strand load.....	137
Figure 116–SC: Ultimate .....	138
Figure 117–SC: Crack pattern.....	139
Figure 118–SC: Strain at load point.....	140
Figure 119–SB: Ultimate .....	141
Figure 120–SB: First crack .....	142
Figure 121–SB: Strand slip.....	142
Figure 122–SB: Deck at failure .....	143
Figure 123–SB specimen: Strain at load point.....	143
Figure 124–SU: Ultimate.....	144
Figure 125–SU: First crack.....	144
Figure 126–SU: Joint at failure.....	145
Figure 127–SU specimen: Strain at load point .....	146
Figure 128–SU2: Ultimate.....	147
Figure 129–SU2: First crack.....	147
Figure 130–SU2: Flexural crack at 149 kip.....	148
Figure 131–SU2: Joint at failure.....	149
Figure 132–SU2: Strain at load point .....	150
Figure 133–Bond patterns of shear tests.....	151
Figure 134–Shear comparison: Elastic behavior.....	152
Figure 135–Shear specimens: First crack locations .....	153
Figure 136–SC vs SB: Crack pattern .....	155
Figure 137–SU vs SU2: Crack pattern.....	155
Figure 138–SU2: Bottom strain at vertical crack location.....	156
Figure 139–SU2: Strand load.....	157
Figure 140–Coupler strain gages: (a) SU and (b) SU2 .....	158
Figure 141–SU: Strand Load .....	159
Figure 142–Post-test: End view of unbonded segment.....	160
Figure 143–Ultimate behavior: (a) SC and SB and (b) SU and SU2.....	162
Figure 144–Shear location of interest .....	163
Figure 145–FC: Static conditioning.....	167
Figure 146–Specimen FC: First cracks.....	167
Figure 147–FC: Decompression load cycles .....	168
Figure 148–FC: Decompression strain readings.....	169

Figure 149–FC: Fatigue .....	170
Figure 150–FC: Ultimate .....	171
Figure 151–FC crack progression at (a) no load; (b) ultimate (c) second loading.....	172
Figure 152–FC: Ultimate .....	173
Figure 153–FC strand showing (a) fatigue (20X) (b) fatigue (200X) (c) yield (20X).....	174
Figure 154–F1: Static conditioning.....	175
Figure 155 –F1: Joint opening .....	175
Figure 156–F1: Coupler strain .....	176
Figure 157–F1: Decompression load cycles .....	177
Figure 158–F1: Decompression strain readings.....	177
Figure 159–F1: Fatigue.....	178
Figure 160–F1: Ultimate.....	179
Figure 161–F1: Crack pattern at (a) 125 kip, prior to strand rupture (b) after load drop.....	180
Figure 162–F1: Ultimate.....	180
Figure 163–F1: Post-failure .....	181
Figure 164–F1: Deck strain .....	182
Figure 165–F1: (a) top strand showing fatigue (40X ) (b) failure at teeth (20X) (c) misaligned wedges	183
Figure 166–F2: Precrack.....	184
Figure 167–F2: First crack.....	184
Figure 168–F2: Precrack coupler strain.....	185
Figure 169–F2: First cracks with strain gages .....	186
Figure 170–F2: Static load cycles (a) 2-4 and (b) 5-7 .....	187
Figure 171–F2: Decompression strain readings.....	187
Figure 172–F2: Fatigue.....	188
Figure 173–F2: Cracking after 2 million cycles .....	189
Figure 174–F2: Ultimate.....	190
Figure 175–F2 crack progression at (a) 70 kip, (b) 137 kip, and (c) ultimate (cracks marked).....	190
Figure 176–F2: Deck strain .....	192
Figure 177–F2: (a) bottom strand showing fatigue (40X) (b) top strand yield (20X) .....	192
Figure 178–F1: Cracks at start of fatigue.....	193
Figure 179–F2: Cracks at start of fatigue.....	196
Figure 180–F2: Section degradation due to fatigue .....	197
Figure 181–Fatigue: Deflection at start and end of tests.....	198
Figure 182 –Post-fatigue Failure: FC, F1 and F2 .....	199
Figure 183–AASHTO: FC, F1 and F2.....	200
Figure 184–Static vs. Post-fatigue Failure: Control specimens .....	201
Figure 185–Static vs. Post-fatigue Failure: Spliced specimens .....	201
Figure 186–F1: Post-failure .....	203
Figure 187–F1: Wedge seating .....	203
Figure 188–F2: Post-failure .....	204
Figure 189–F2: Fatigue wear.....	204
Figure 190–F1: Load cells .....	205
Figure 191–F2: Load cells .....	206
Figure 192–Bond at vertical interface (a) X1 and (b) F2.....	208
Figure 193–F2: Concrete intruding into unbonded length.....	209
Figure 194–SB: Void at reentrant corner .....	209
Figure 195–Shear keys (a) SU and (b) SU2.....	210
Figure 196–SU: (a) Prior (b) 35 minutes (c) 40 minutes .....	210
Figure 197–Unfactored Dead Loads at Release on Non-composite End Segments .....	222
Figure 198–Unfactored Dead Loads at Release on Non-composite Middle Segment.....	222
Figure 199–Unfactored Dead Loads on Non-Composite Section–Assembled Length.....	223

Figure 200–Unfactored Moment and Shear Envelopes due to Legal Truck.....	224
Figure 201–Unfactored Moment and Shear Envelopes due to Permit Truck .....	224
Figure 202–Unfactored Moment and Shear Envelopes due to Lane Loading .....	225
Figure 203–Unfactored Dead Loads on Composite Section.....	225
Figure 204–Splice Design A .....	226
Figure 205–Splice Design B .....	228
Figure 206–Splice Design C .....	229
Figure 207–Hinging (and attendant camber) caused by inflation of flatjack. Rotation angle is exaggerated to illustrate mechanism.....	230
Figure 208–Splice closure pour .....	231
Figure 209–Splice C with canted ends.....	232
Figure 210–Splice Design D .....	233
Figure 211–Splice Design E .....	234
Figure 212–Internal forces in Splice Design E .....	235
Figure 213–Splice Design F.....	236
Figure 214–Forces of Splice Design F.....	237
Figure 215–Alternative with side brackets .....	238

## List of Tables

Table 1–Typical FIB96 section properties.....	28
Table 2–Non-composite dead loads.....	29
Table 3–Composite dead loads.....	29
Table 4–Design limit states.....	30
Table 5–Summary of Service I limit states check for precast segments at release.....	32
Table 6–Summary of Service I limit states check for loads associated with deck placement.....	32
Table 7–Summary of Service I limit state check at the extreme top fiber.....	33
Table 8–Summary of Service III limit state check at the extreme bottom fiber.....	33
Table 9–Fatigue limit state check at the extreme bottom fiber at splice.....	33
Table 10–Strength I flexure and shear checks for spliced length.....	34
Table 11–Strength II flexure and shear checks for spliced length.....	34
Table 12–0.5 in.-dia. coupler calibration load procedure.....	44
Table 13–Stress state of FIB96: Serviceability.....	54
Table 14–Stress state of test specimen: Serviceability.....	54
Table 15–Stress state of FIB96: Fatigue.....	62
Table 16–Stress state of test specimen: Fatigue.....	62
Table 17–Loading procedure: Fatigue.....	63
Table 18–Construction and testing schedule.....	67
Table 19–Specimen IDs.....	67
Table 20–Spliced specimens.....	88
Table 21–Fatigue specimen load procedure.....	97
Table 22–Jacking prestress.....	100
Table 23–Measured initial prestress.....	101
Table 24–Measured effective prestress.....	101
Table 25–Measured prestress losses.....	102
Table 26–PCI prestress losses.....	103
Table 27–Effective prestress force by decompression.....	106
Table 28–Spliced specimens: strand loads per load cell.....	114
Table 29–First crack of shear specimens.....	152
Table 30–Shear specimens’ ultimate behavior at vertical interface.....	163
Table 31–F1: Stress ranges measured during fatigue cycling.....	194
Table 32–F2: Stress ranges measured during fatigue cycling.....	195
Table 33–Ductility ratios.....	202
Table 34–Flexural cracking behavior.....	207
Table 35–Web shear cracking.....	208
Table 36–Splice Assembly IDs.....	297

## 1 Introduction

Due to truck weight limitations restricting their transport, simply-supported prestressed bridge girder spans have been limited to approximately 180 ft. Splice connections allow longer span bridges to be constructed using shorter, lighter segments that are assembled prior to or during final erection. Spliced girders, however, have typically been designed to span continuously over the supports. Providing continuity at the supports while ensuring redundancy of design and increased material efficiency requires consideration of the stresses generated by time-dependent movements over its life span. The designer must carefully check and accommodate stress changes due to thermal effects, creep, shrinkage, and secondary moments. On the other hand, simple-span designs may reduce the amount of up-front design time required. Furthermore, such systems may prove more accommodating for vertical and horizontal curves in the span.

The recent development and implementation of the new Florida I-beams (FIB) have introduced several new sections capable of achieving spans longer than currently transportable as single pieces. The new FIB96, for example, is capable of spanning a maximum of 208 ft with 8.5-ksi concrete; using 10-ksi concrete, the maximum span is estimated at 215 ft (FDOT Temporary Design Bulletins C09-01 and C09-05). Depending on the specified concrete strength, additional FIB sections are capable of achieving spans beyond 190 ft, the currently transportable length. As AASHTO and Florida bulb-tee sections will not be used in future FDOT projects, available sections for use as a prototype for the splice design were limited to the new Florida I-beams.

The objectives of this research were to identify potential splice techniques to lengthen the span of transportable precast prestressed concrete girders and to develop and test a splice design. A literature review was conducted to identify current construction practices, splice types, and design systems used to lengthen the span of transportable precast prestressed concrete girders. A review of research and past designs using splice connections was also performed (Chapter 2). A prototype design using the FIB96 section was then developed (Chapter 3) along with a number of possible splice configurations (Appendix B–Splice Concepts). A coupler component for the splice design was tested; results are presented in Chapter 4. From the FIB96 prototype, a scaled test specimen was designed and tested. The specimen and splice designs are reported in Chapter

5, with the specimen construction and splice assembly details included in Chapter 6. Test procedures and instrumentation are covered in Chapter 7. Prestress loss measurements and splice assembly results are included in Chapters 8 and 9, respectively. Load tests were then conducted on the assembled specimens to determine flexural service and ultimate behavior (Chapter 10), shear behavior (Chapter 11), and fatigue performance (Chapter 12). Additional discussion is provided in Chapter 13. The research is then summarized along with key findings in Chapter 14. Recommendations are provided in Chapter 15.

## 2 Literature Review

A literature review was conducted to identify current construction practices, splice types, and design systems used to lengthen the span of transportable precast prestressed concrete girders. Section 2.1 covers the history of spliced concrete girders. Section 2.2 covers the current design practices of both continuous and simple spans. The advantages and disadvantages of long-span precast concrete girders are covered in Sections 2.3 and 2.4, respectively. Current construction techniques of splice types, assembly, and design are covered in Sections 2.5, 2.6, and 2.7, respectively. A review of prestressing couplers is covered in Section 2.8.

### 2.1 History of Spliced Concrete Girders

Despite being more cost-effective and easier to maintain than steel superstructures, concrete has long been passed up for use in spans longer than 150 ft due to weight and length limitations preventing their transportation to the jobsite (Abdel-Karim and Tadros 1992). State highway and railway restrictions (imposed by the weight limits of currently in-use bridges) prevent the transport of these massive girders (Abdel-Karim and Tadros 1992; Ralls et al. 2000; PCI 2004). In response, engineers have turned to the development of splice connections for precast concrete girders to reduce segments to more manageable sizes.

The use of a splice to lengthen the span of concrete girders first appeared in the 1950s, while spliced precast concrete segments have been in use since the 1960s as segmental box girders (Lacey et al. 1971). In 1968, the Precast/Prestressed Concrete Institute (PCI) published a report encouraging the use of precast segments in spliced construction, presenting many advantages of precast construction, as well as some design guidance for precast splices. The collective standardization of girder section geometry by AASHTO, PCI, and the Bureau of Public Roads in the 1960s further advanced the use of precast segments in highway bridge construction (Ralls et al. 2000). In 1982, a joint PCI-PTI committee published “Recommended Practice for Precast Post-Tensioned Segmental Construction” (Joint PCI-PTI Committee 1982). Over the years, the technique of splicing precast concrete girders has been used more frequently, with other innovations such as high-performance concrete, optimized section geometries and advances in pre- and post-tensioning techniques allowing the use of longer spans. Rabbat and Russell (1982) proposed optimized I-girder sections. Lounis et al. (1997) proposed optimized bulb-tee sections for conventional and segmental post-tensioned construction.

Nevertheless, despite a growing body of research and limited implementation by some state transportation departments, utilization of long-span splicing has not become widespread. Instead, knowledge gained and techniques used have remained mostly job-specific, and have not been made widely available to the engineering community for use on similar projects. In an effort to disseminate a collection of information on prior projects, as well as provide design recommendations and standardized specifications, the Transportation Research Board published NCHRP Report 517 in 2004. Ultimately, research has found that incremental changes in conventional design methods and materials result in relatively small increases in span, but splicing techniques can increase the span lengths of precast prestressed concrete girders greatly. The advantages of spliced concrete girders have encouraged increasing use and further research. (Castrodale and White 2004)

## *2.2 Current Design Practice: Continuity vs. Simple Span Design*

Lounis et al. (1997) noted a change in the design trend from simple-span to continuous-span bridge girders. This change allowed longer spans and the elimination of costly and difficult to maintain deck joints (Lounis et al. 1997). According to the PCI Bridge Manual, simple-spans have some performance issues, citing beam end rotation at the piers. This rotation results in significant cracking of the deck, allowing water to leak through the deck and cause corrosion of the reinforcing steel and deterioration of the beam ends (PCI 2004). Elimination of the deck joint enhances deck durability and minimizes maintenance and life cycle costs (Lounis et al. 1997); continuity designs are more structurally efficient and perform better in the long term in certain types of construction (PCI 2004). The NCHRP Report 517 identified circumstances in which continuity designs were considered viable (Castrodale and White 2004):

- 1) Long span crossings, especially over waterways;
- 2) Sites with restricted overhead clearance;
- 3) Sites with limited substructure locations;
- 4) Designs where the reduction of pier quantity results in the most economical design.

By 2004, in a survey of several hundred spliced girder projects, Castrodale and White (2004) found that continuity designs account for a majority of spliced precast concrete (PCC) bridges in North America. In these continuous span designs, the splice location is chosen at the

inflection point of the moment caused by dead load. Continuity is achieved through several methods: deck reinforcement, post-tensioning, or the use of coupling beams with either prestressing or nonprestressed high-strength rods (Ralls et al. 2000). A common method of achieving continuity is through full-length post-tensioning (Abdel-Karim and Tadros 1992).

Advantages of continuous span designs include redundancy of design, elimination of deck joints, and material efficiency; however, continuity designs have their own drawbacks. Continuity designs are complex and require careful consideration of the long-term effects of camber and deflection caused by creep, shrinkage, thermal effects, and secondary moments. Furthermore, the on-site construction process for continuity designs is more labor-intensive than for simple spans.

In its review of projects in the United States, the NCHRP found spliced concrete girders to be most commonly used in multi-span continuous bridge designs. Nevertheless, the committee suggests several applications where the use of spliced PCC girders in simple-span designs may be advantageous (Castrodale and White 2004):

- 1) Remote locations where midspan piers are impossible;
- 2) Situations where the available or preferred equipment is better suited to handle shorter spans;
- 3) Single-point urban interchanges, where an overpass bridge is used to span over another roadway without a midspan pier.

Jaber et al. (2006) reported on the design and construction of a Nebraska bridge using 207-ft simple span precast girders (Figure 1). The girders were constructed in three segments, thus making them transportable to the site by truck. The segment configuration was such that the wet-joints were located away from the midspan, allowing a reduction in the number of pretensioned strands in the outside segments. Segments were placed on the piers and two falsework towers located under the splices. Post-tensioning tendons with a parabolic profile were placed from end-to-end within the span. The authors indicate that the final bridge cost was competitive with structural steel.

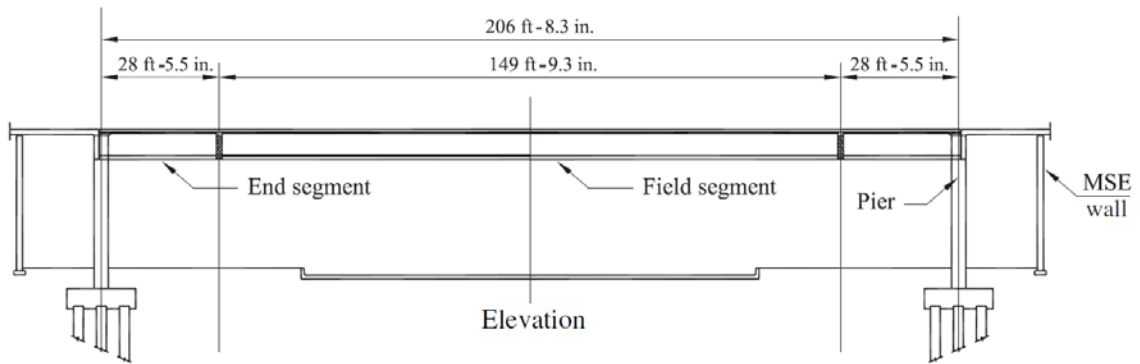


Figure 1–Precast segmented spans used with simple supports (Jaber et al. 2006)

### 2.3 Advantages of Long-span Precast Concrete Girders

One significant benefit of spliced long-span precast concrete girders is their ability to accommodate curved alignments (Figure 2). When a curve in the roadway is required, the splice location can be situated in order to provide a point of curvature between short segment lengths (PCI 2004). Similarly, spliced segments can be arranged such that the placement of the piers avoids obstacles on the ground, such as railroad tracks, utilities or other roadways (Castrodale and White 2004). Because the designer has more flexibility when specifying span lengths and locations of piers, spliced construction allows the placement of piers and spans as necessary for the geometry of the road (Weigel et al. 2003; PCI 2004).



Figure 2–Curved roadway constructed with spliced girders (Abdel-Karim and Tadros 1992b)

The utilization of PCC spliced girders for long spans offers multiple advantages over steel, including increased durability, rapid erection, condensed overall construction time, limited or no environmental impact, reduced cost, and simplified transportation of construction materials (Castrodale and White 2004; Abdel-Karim and Tadros 1992). Furthermore, steel sections require extensive maintenance and present potential environmental risk when being stripped and repainted; again, the use of spliced segmental construction permits concrete bridge girders appears to be an attractive alternative. In environmentally sensitive areas, such as Rock Cut Bridge in Washington, spliced PCC girders provide an ideal solution for eliminating risk to river wildlife (Nicholls and Prussack 1997).

When considering waterway bridges, the increased span length and subsequent elimination of some piers reduces susceptibility to scour, environmental impact, and the risk of barge collision and damage (Abdel-Karim and Tadros 1992). Furthermore, the use of fewer piers results in a reduction of both the quantity of shielding dolphins and accumulated water-borne debris. In locations where minimal disturbance of the waterway is permitted (to reduce the impact on salmon runs, for example), mid-stream piers may not even be an option (Nicholls and Prussack 1997). In extreme marine environments, such as Florida, where scour is a primary concern, the reduction in the quantity of piers is a significant benefit of long-span construction (Ronald 2001).

Comparative costs of steel versus spliced precast concrete (PCC) designs have been investigated by several researchers. Abdel-Karim and Tadros (1992) presented two case studies of bridges in Kentucky, the use of a concrete superstructure instead of steel resulted in a savings of 25-35%. In a separate comparison of six bids—five steel designs and one spliced PCC design—for the construction of a bridge in South Carolina, the concrete design represented a possible savings in all but one bid. Although the most economical design presented was indeed steel, the overall trend of possible savings of up to 50% for the construction phase is noteworthy. Castrodale and White (2004) presented an estimated cost comparison for a number of bridges in North America.

The perceived potential savings of the spliced concrete designs have been large enough for contractors to request a spliced concrete design in favor of a steel superstructure design. (The longest spliced concrete span to date, the Moore Haven Bridge in Florida at 320 ft, was

originally designed with a steel plate superstructure, but was redesigned as a spliced PCC span to reduce overall project cost.) (PCI 2004)

Beyond the construction phase, the use of spliced PCC girders provides further benefits. The use of a concrete superstructure in place of steel eliminates costly repainting, the costs (both economic and environmental) associated with the removal of old paint, as well as the inconvenience of road closures. Abdel-Karim and Tadros noted that maintenance and repair costs were not taken into consideration during selection from the six bids for the South Carolina Bridge; if they had, the concrete design may have proven most cost-effective. Furthermore, with the current trend of rising steel prices, concrete construction is becoming ever more attractive.

In comparison with cast-in-place, precast concrete usually reduces overall construction costs. Because precast segments can be manufactured at the precast plant while the substructure is under construction at the jobsite, the construction work schedule can be significantly condensed. Precast segments also reduce the amount of time dedicated to the construction of formwork and other activities related to cast-in-place construction. The shortened construction schedule limits traffic delays and their associated labor costs.

Several state transportation departments, most notably Washington State Department of Transportation (WSDOT) and the Florida Department of Transportation (FDOT), have implemented the use of long span spliced PCC girders to accommodate longer spans. The WSDOT has been involved in a significant amount of research on spliced segmental construction. To this end, in 1998, WSDOT introduced several standard new deep I-beam sections optimized for use in spliced spans (Seguirant 1998).

#### *2.4 Disadvantages of Long-span Precast Concrete Girders*

Bridge construction making use of long-span precast concrete girders has some disadvantages. Most obviously, without the use of a splice connection, the extreme weight and length of single piece long-span girders restricts their transportation. When a splice connection eliminates this issue, there is increased jobsite labor, falsework, and framing required to assemble the splice. If the splice connection is completed on the ground, there needs to be careful consideration of crane weight limitations. Furthermore, long-span prestressed concrete girders require delicate handling to a degree not needed with long-span steel construction, as they exhibit a tendency to twist and deflect during handling and erection (Ronald 2001).

## 2.5 Current Construction Techniques: Splice Types

There are several types of concrete girder splices currently in use in highway bridge construction, the most common of which being the cast-in-place splice. Whereas the cast-in-place splice is not the most economical, it is the most popular due to its simple construction and flexibility with regards to field tolerances.

Both nonprestressed (conventional) reinforcement and prestressed cast-in-place splices are currently in use. During fabrication of either type of midspan cast-in-place splice, a temporary bent is constructed under the splice location. The two precast girder segments are lifted into place, meeting over the temporary bent. The closure pour is then formed, typically with a high-strength concrete. An example of a nonprestressed reinforcement splice is shown in Figure 3.

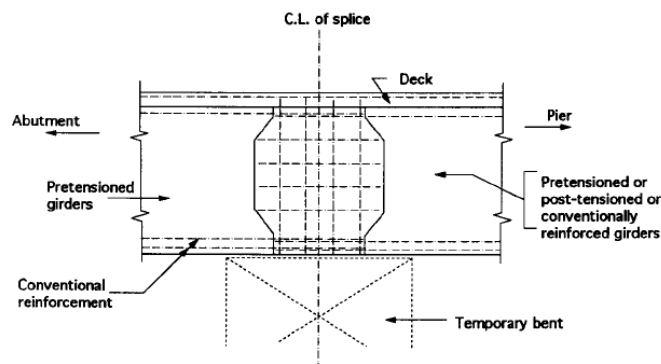


Figure 3–Nonprestressed reinforcement CIP splice (Abdel-Karim and Tadros 1992)

In simple-span construction, nonprestressed splices are located over the piers. The closure pour and deck concrete are poured simultaneously to create continuity over the supports for superimposed dead and live load cases. Under full service load, due to the lack of prestressing in the splice, the surface over the splice is expected to crack. To prevent or limit cracking, and the subsequent corrosion of the splice reinforcement, the designer must specify sufficient deck reinforcement. The splice must be long enough to provide a sufficient lap length of the reinforcing steel. In continuous systems, a nonprestressed splice is located at or near the inflection points of the moment diagram. Once the two girder segments are in place over the temporary bent, the projecting nonprestressed reinforcement is lapped together, and the closure pour is formed. (Abdel-Karim and Tadros 1992).

A typical post-tensioned cast-in-place splice is shown in Figure 4. After the post-tensioning ducts have been adequately aligned, the closure pour is formed at the splice location.

After the splice concrete has cured, the post-tensioning strand is threaded through and stressed to the specified force. In comparison with nonprestressed splices, post-tensioned splices provide significant additional moment capacity.

Several issues must be considered when employing a post-tensioned cast-in-place splice. Frequently, standard I-girder sections must be modified to provide enough space for the PT duct, longitudinal reinforcement, shear stirrups, and code-mandated concrete cover; Florida bulb-tees with modified webs are commonly used in precast, prestressed spliced I-girder spans (Abdel-Karim and Tadros 1992; Ronald 2001). Accurate alignment of the PT duct is important to reduce the prestress losses caused by friction. Rotation of the ends must be controlled by design to limit camber. Care must be taken not to damage the post-tensioning duct during erection; a damaged PT duct cannot be properly grouted. Without fully grouted tendons, the splice may incur additional prestress losses due to friction and may have reduced durability over its lifespan (FDOT 2004). Furthermore, care must be taken to completely seal the coupling zone and PT duct to prevent leakage of the post-tensioning grout and corrosion of the reinforcing steel (PCI 2004; FDOT 2004).

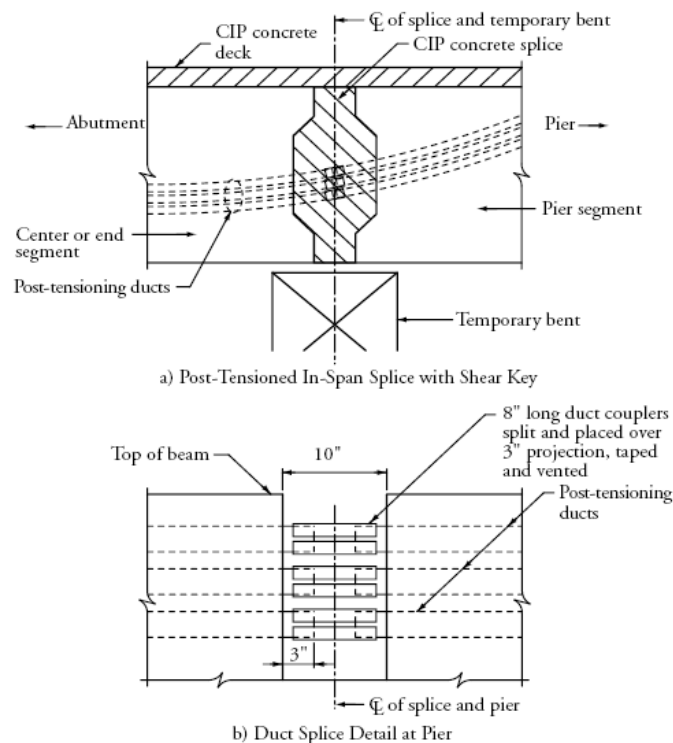


Figure 4—Post-tensioned CIP splice (PCI 2004)

Although cast-in-place splices are not the least expensive option (they require considerable jobsite labor), they are the most commonly used type of splice due to their simplicity and flexibility, accommodating fabrication and construction tolerances with ease; the permitted length of the gap between segments can be from 6 in. to 24 in. (Abdel-Karim and Tadros 1992). The length of the closure pour is controlled by two considerations: the closure length must be sufficient to allow splicing of the conventional reinforcing steel and post-tensioning duct, but is limited to a length by the lack of prestressing steel and the small amount of longitudinal reinforcement (PCI 2004; Ronald 2001). Shear keys are commonly used in cast-in-place splices, such as those shown in Figure 3 and Figure 4, to provide mechanical interlock between two adjacent precast segments and the closure pour. Their presence also provides additional space in which to align the PT ducts and lap the reinforcing steel. (Ronald 2001)

The Westbound Gandy Bridge in Tampa, Florida is an example of a long span bridge with a cast-in-place post-tensioned splice. The center 234-ft channel span was formed by splicing four pairs of precast I-girder segments. Details of the PT duct and CIP splice connections are shown in Figure 5 and Figure 6, respectively.

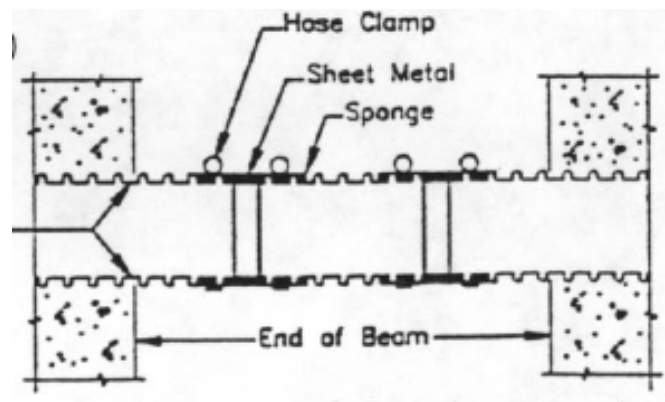


Figure 5–Post-tensioned duct for CIP splice (FDOT 1999)

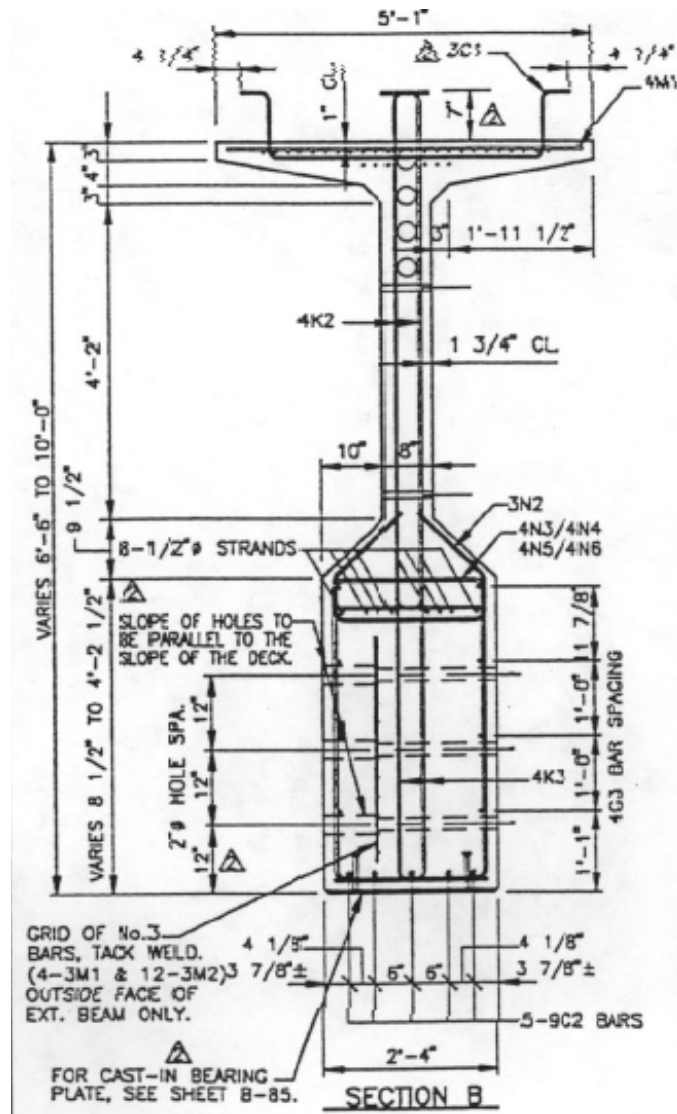


Figure 6–Gandy Bridge splice connection detail (FDOT 1999)

Another type of cast-in-place splice currently in use is the stitched splice, in which short tendons or threaded bars are crisscrossed prior to post-tensioning. In this type of splice, the post-tensioned steel takes up only a short distance of the span, making this an attractive alternative for very long spans where full-length post-tensioning may be ineffective due to the large losses accumulated due to friction (PCI 2004). This method of splicing, however, has a few disadvantages. PT ducts must be quite large to accommodate the quantity of the prestressing steel and to provide additional tolerance for alignment purposes. Furthermore, due to the short length of the prestressing steel, prestress losses during anchorage set may be large. Nevertheless,

this method has been used in a few projects, such as the Shelby Creek Bridge in Kentucky (PCI 2004). An example of a stitched splice detail is shown in Figure 7.

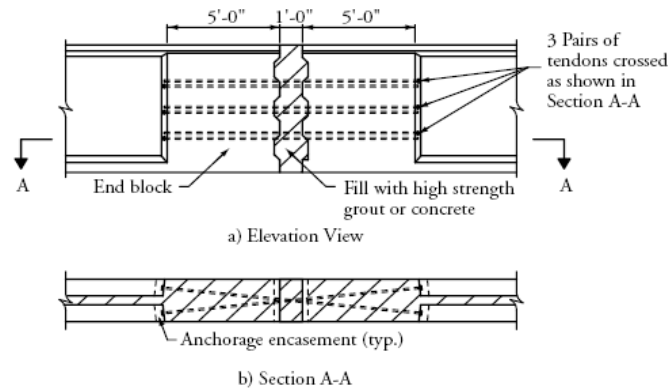


Figure 7–Stitched splice (PCI 2004)

Match-cast splices are an alternative to cast-in-place splices. This method eliminates the need for formwork and a closure pour at the construction site. Instead, the two girder segments are cast adjacent to each other in the precast yard, with a machined steel header precisely aligning the post-tensioning ducts and prestressing strands. After they have each cured, the segments are torch-cut through holes in the header, separated, and hauled to the construction site. On site, one of the segments is placed on its pier and a temporary bent. The second adjoining segment is then slid into place over the temporary pier, matching each segment's post-tensioning duct to form a continuous duct. Once reassembled, the small gap in the concrete is filled with epoxy and the girder surface is sealed. Tendons are then run through the splice and post-tensioned. Finally, the PT duct is grouted to protect the reinforcement against corrosion. An example match-cast splice detail is shown in Figure 8.

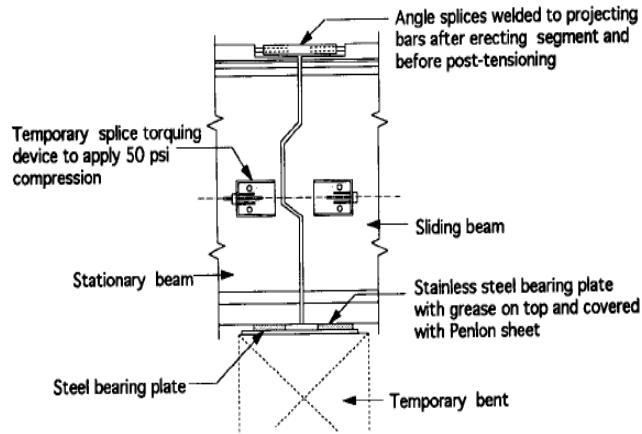


Figure 8–Match-cast splice (Abdel-Karim and Tadros 1992)

## 2.6 Current Construction Techniques: Assembly

Girders segments must be spliced either on the ground or in place (at the final elevation) with the aid of falsework. The preferred assembly location is on the ground if space and crane limits allow, as it eliminates costly temporary falsework. Additionally, construction of the splice on the ground allows easy access to materials and equipment that would otherwise have to be lifted to the mid-air splice location. When space allows, a secondary staging site is selected for assembly and post-tensioning of the girder. The staging site must be level to ensure that the splice is properly formed. Furthermore, sufficient space must be available to allow for maneuvering of the assembled girder during erection. The assembled girder is then transported from the staging site and lifted into place as a single piece. During the erection of the assembled girder, care must be taken to prevent damage to the splice; this method of erection is only recommended when the splice is post-tensioned again after final erection. Using this assembly technique, large-capacity lifting equipment and/or launching truss equipment may be required to handle the final piece weight. (Abdel-Karim and Tadros 1992)

If the weight of an assembled girder is excessive, or if site conditions do not allow the girder to be lifted, the entire girder assembly may be loading onto a rolling trolley and moved laterally into place along a rail on an adjacent temporary structure. After sliding the girder onto the temporary support, two cranes, one on each end of the span, can then place the girder over the supports. An example of this procedure, as done during the construction of Rock Cut Bridge, is shown in Figure 9 (Nicholls and Prussack 1997; Joint PCI-PTI Committee 1982). For more details, see Nicholls and Prussack, 1997.



Figure 9—Launching assembled girder using trolley (Nicholls and Prussack 1997)

Alternatively, when a staging location is not available, the separate pieces are lifted into position and supported with either a strong-back assembly or temporary piers and falsework until the splice connections have been constructed and have reached the specified strength. The construction of a splice in-place requires accurate alignment of the two girder segments. Shimming of the temporary formwork may be necessary to achieve accurate alignment of the post-tensioning ducts. To mitigate the costs, the temporary falsework can be constructed concurrently under all girder lines at the splice location, such that the pairs of girder segments can be spliced simultaneously. The primary advantage to this technique is the reduced handling of the girder segments. Another advantage is that the crane capacity need only be sufficient to handle the heaviest segment (Abdel-Karim and Tadros 1992). Despite these advantages, this method of erection is the least preferred, due to the additional time, cost, and effort expended to complete the difficult mid-air post-tensioning procedure.

A construction technique for splicing together two precast prestressed girders was presented by Gerwick (1993) (Figure 10). In this approach, the tendon for the full span is prestressed and a gap is left in the beam at midspan during casting. The units are folded about the midspan and transported side-by-side to the site. The segments are then placed on falsework in the final configuration and jacked apart in the splice region to stress the prestressing strands.

With the jacks in place, the splice concrete is cast. After curing, the jacks are removed, leaving the splice concrete in a prestressed state.

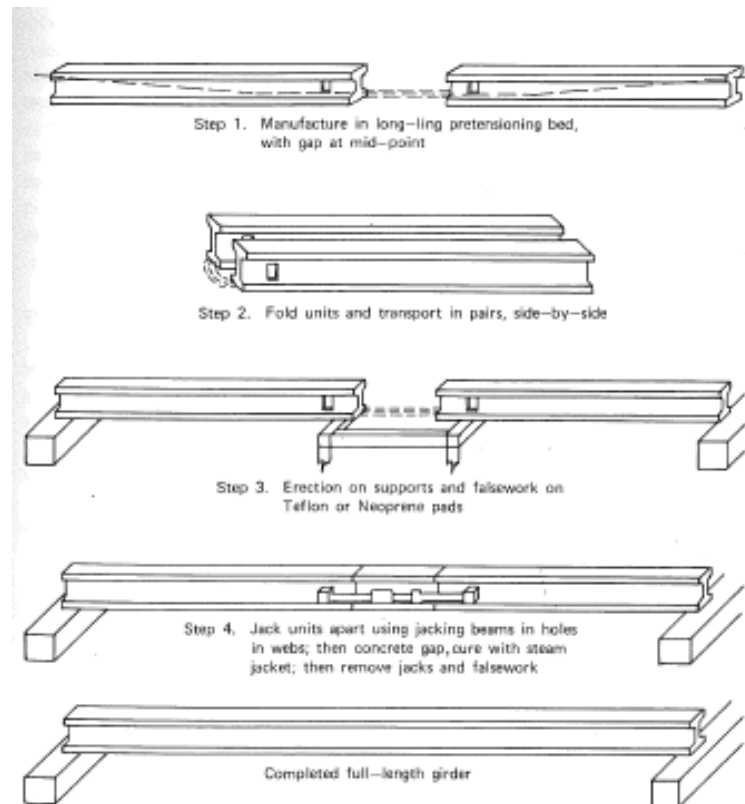


Figure 10–Prestressing against internal restraint (Gerwick 1993)

## 2.7 Current Construction Techniques: Design

The current AASHTO-LRFD code considers precast spliced girder systems as conventional bridge structures with additional requirements for the joint area, distinguishing these systems from segmental construction. Whereas the spliced precast bridge system itself is given separate consideration, the joint area, however, is treated the same as segmental construction joints and is required to meet the same stress limits. (AASHTO-LRFD 2007)

AASHTO-LRFD specifies several construction considerations to be made concerning the joint area. For a cast-in-place joint, when preparing the area for the closure pour, the end of the precast members should either be intentionally roughened to expose the coarse aggregate, or include shear keys (Figure 11). The width of the closure joint between the two precast members is limited to a minimum of 300 mm (12 in.), or 100 mm (4 in.) for joints located within a

diaphragm, in order to allow enough clearance to properly splice the reinforcement, as well as to adequately compact the closure pour concrete. (AASHTO-LRFD 2007)

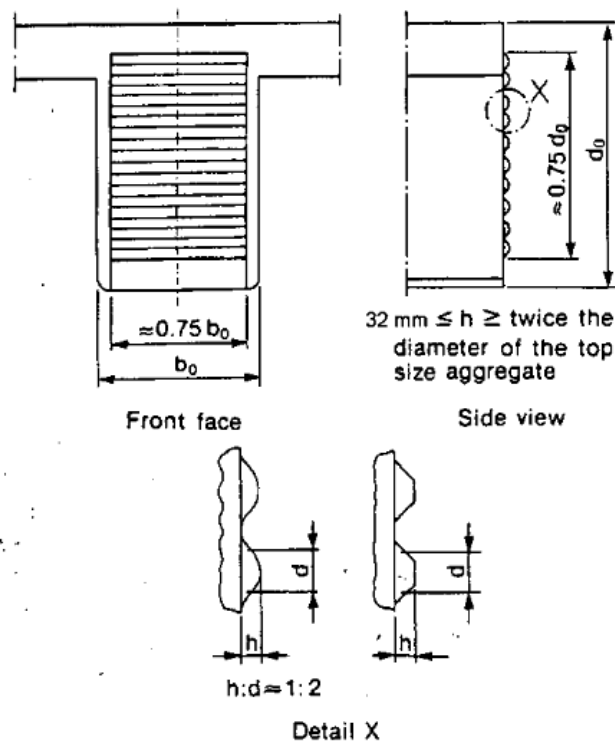


Figure 11–Shear keys required by AASHTO-LRFD (AASHTO-LRFD2007)

Tensile and compressive stress limit states for the joint areas of precast spliced girders are the same as those specified for joints in segmental construction. The joint area may be designed to provide either zero or some tensile capacity, as determined by the joint's location in the span. If the joint area is designed to resist tensile stress, bonded auxiliary reinforcement capable of resisting the calculated tensile force at a maximum tensile stress of  $0.5 f_y$  must be supplied across the joint. The prestressed concrete tensile stress limit for the joint area must be limited to a maximum of  $0.24\sqrt{f'_c}$  (ksi). Both tensile stress limits must be met at all times during the life of the structure (both before and after prestress losses). (AASHTO-LRFD 2007)

After the girder segments have been joined, if the system meets all service limit states prescribed in Section 5.14.1.3, the code provisions indicate that the assembled system may be considered fully continuous for all subsequent load limit states. The joint area, therefore, must provide the same compressive capacity as the rest of the segment for the required service limit states. (AASHTO-LRFD 2007)

The design of the 204<sup>th</sup> Street Bridge (Figure 12) is the closest example of the system type targeted by this research. The simple-span single point interchange, as described by Jaber et al. (2006), consisted of 14 girder lines constructed as two structures (for each lane of traffic). Two short end segments were bridged together with a long center segment to span a total of 207 ft.

Splicing of the segments was completed mid-air, using temporary towers to provide support at the joint. The authors describe as one of the most challenging design aspects the determination of the girder elevations at the splice locations so as to provide a smooth riding surface and to prevent sag in the girder-soffit profile. Screw jacks were used to refine the girder elevation as required. The precast concrete girders were spliced together with a cast-in-place joint, aligning the post-tensioning ducts running through each segment. After the closure pour reached the specified strength, the assembled precast girder system was post-tensioned along its entire length. (Jaber et al. 2006).



Figure 12–204th Street Bridge (Jaber et al. 2006)

The splices were designed to resist zero net tension. No special reinforcement was detailed in the splice area. To prevent tensile stresses in this area during the service life, post-tensioning was specified to provide adequate precompression. The specified compressive

strength at the joint was less than that required in the girders; conventional concrete was adequate for the closure pour. (Jaber et al. 2006)

It is the intent of this research, on the other hand, to investigate methods to splice the girder segments locally, with no or little post-tensioning.

## 2.8 Prestressing Strand Couplers

Prestressing strand couplers provide an economical and time-effective solution for restoring prestress force to severed strands of moderately damaged girders.

Figure 13 shows several examples.

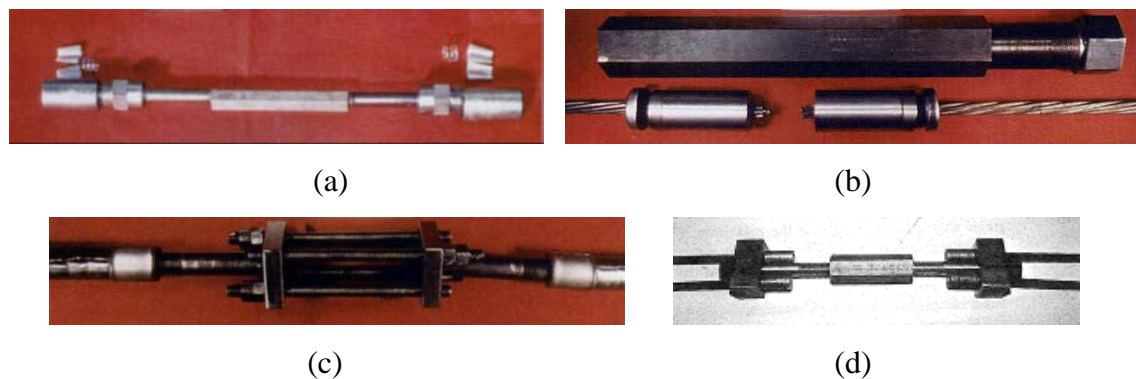


Figure 13–Prestressing strand coupler types: (a) turnbuckle-style, (b) Alberta, (c) swaged for single strand, (d) swaged for two strands (Zobel and Jirsa 1998; Shanafelt and Horn 1985)

Several states, including Florida, California, Texas, and Oregon, have utilized prestressing couplers to repair damaged prestressed concrete bridge girders in place; strand couplers are included as a part of these states' standard practice for girder rehabilitation (Saidii et al. 2000; Johnson 2011). The use of prestressing couplers to restore strength is not a universal practice; in some states, a damaged girder with severed prestressing strands is immediately replaced (Shanafelt and Horn 1980).

Figure 14 shows the strand repair coupler currently permitted by FDOT (FDOT 2010c) for repair of damaged strand in prestressed concrete girders. It is adjustable and 0.5-in. dia. versions of this coupler have been used to repair damaged prestressing strand in concrete girders for approximately the past thirty years (Waheed et al. 2005). The 0.5-in. dia. coupler has been

used to repair bridges in several states. No problems have been reported post-repair (Waheed et al. 2005; Johnson 2011). Figure 15 shows a damaged girder in Ontario that was rehabilitated with couplers (Ministry of Transportation of Ontario 2011).

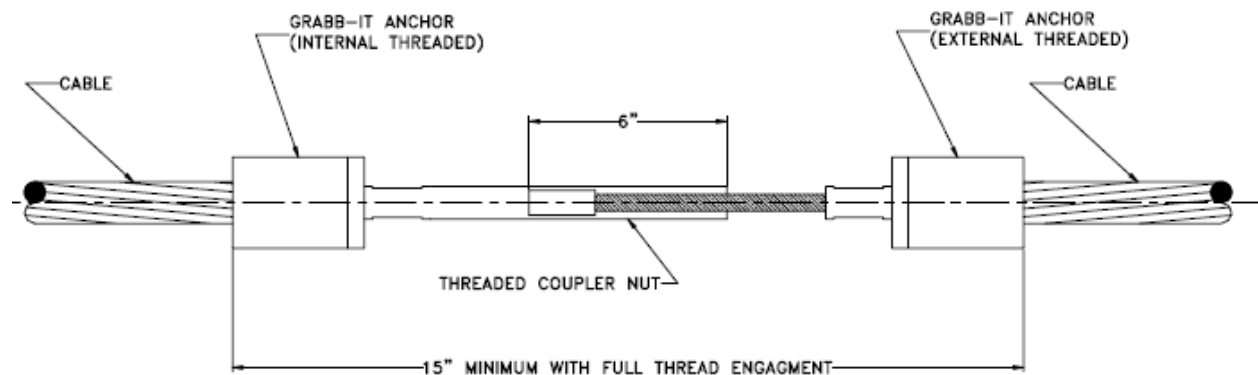


Figure 14–Turnbuckle-style coupler (FDOT 2010c)

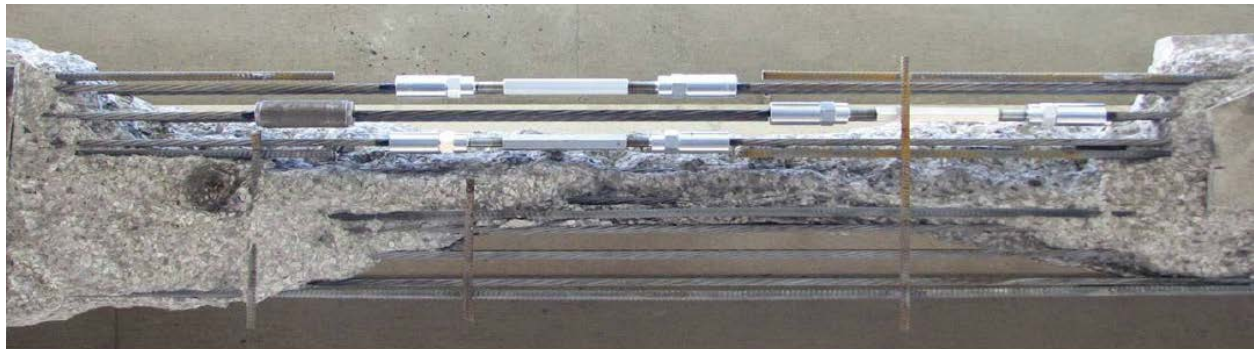


Figure 15–Repair of severed strand using a coupler (Ministry of Transportation of Ontario 2011)

A survey of research on the commercially-available couplers was completed. Shanafelt and Horn (1985) investigated two types of couplers for 0.5-in. dia. prestressing strand: a turnbuckle-style coupler similar to Figure 13(a) and a swaged coupler similar to Figure 13(d). Component tensile testing of both coupler types was performed. In each case, the coupler, with strand attached on either side, was loaded in tension in a Universal Testing Machine (UTM). After several adjustment cycles using a torque wrench to tighten the system and stress the strand, the components were loaded statically to failure. The turnbuckle-style coupler test reached ultimate load when the strand broke at the chuck, at approximately 36.6 kip, or 88% of the

strand's specified strength. The swaged coupler failed at 40.1 kip, or 98% of the strands' specified strength. The coupler appeared to be fabricated from commercially available components, though the manufacturer of the turnbuckle-style coupler was not identified.

In addition to component testing, Shanafelt and Horn (1985) investigated the turnbuckle-style coupler in the repair of severed strand in a full-size AASHTO Type III girder. Using the coupler to reconnect four (of 16 total) strands and preloading the specimen during the repair, they found the coupler capable of restoring the prestress force to that of the non-severed strands—approximately 158 ksi, or  $0.6f_{pu}$ .

Zobel (1997) investigated four mechanical couplers (Figure 13), evaluating their ease of installation and performance as a repair mechanism in a girder previously in service which had been removed brought to the lab for testing. Mock repairs were conducted to investigate the feasibility of repairs using the different coupler types.

Laboratory testing of installed devices provides limited examination of coupler's behavior (Labia et al. 1996). In two tension strength tests by Zobel (1997) of 0.5 in. dia. coupler devices, the prestressing strand ruptured prior to the prestressing strand's specified ultimate strength at notches caused by gripping at wedge anchors. In the first test, the strand ruptured at the test grips at approximately 90% of the strand's specified ultimate strength; it was noted that the strand did begin to yield prior to the strand rupture. In the second test, the strand grips within the wedge anchors of the coupler device notched the strand causing strand rupture at 80% of the strand's specified ultimate strength. Zobel notes that the strand failure appears to result from the quality of the wedges (1997).

In tests commissioned by the manufacturer of 0.5-in. dia. couplers, the prestressing strand ruptures at 95-102% of the prestressing strand's specified strength. Again, the failure occurred as the three-piece wedge anchors bit down on the prestressing strand, causing strand rupture. When tested alone in tension, the 0.5-in.-dia. coupler device itself exceeded the strand's specified ultimate strength by 11%, failing at the base of the externally threaded stem of the turnbuckle. (Law Engineering 1990)

The use of turnbuckle-style prestressing couplers has been covered by several researchers, and is generally prescribed for instances of limited scope. Shanafelt and Horn have described their use as effective for the reconnection of a small quantity of severed strand, recommending that the spliced quantity be limited to no more than approximately 25% of the

total number of strands. In instances where the repair requires splicing of more than 25%, it is recommended that another form of strengthening complement the repair. Based on their test results, Shanafelt and Horn believe that a rupture at the spliced strand will cause local distress. Research on internal strand coupling concluded that such devices are sensitive to cyclic loading, and as such, should only be used to repair a limited number of strands per damaged girder. Potential fatigue issues as one reason for limiting coupler use for ultimate capacity, and list congestion as a second concern. (Shanafelt and Horn 1985).

### 3 Prototype Design–FIB96

The design and development of the splice focused on an intended application: a simply-supported I-girder with a span length of greater than 200 ft. Utilizing the FDOT’s longest spanning I-girder section, the FIB96, a prototype beam design provided the shear and moment demand on the splice. This chapter describes the splice development and prototype beam design for the intended application. Additional details regarding the design are given in Appendix A–Prototype Design.

#### 3.1 Splice Conceptual Design

Several splice concepts were developed and submitted to FDOT for consideration as part of the prototype design process (Appendix A–Prototype Design). Based on this initial submittal and the discussions that followed, the following limitations were imposed on the final design of the splice:

- Concrete in splice region must be prestressed
- Prestressing strands in the splice region must be stressed to a minimum of  $0.6f_{pu}$
- Prestressing strands must be stressed with little or no post-tensioning
- For aesthetic reasons, the cross-section geometry must be maintained through the splice length, which would make the splice visually indiscernible from the rest of the span length.

With these limitations in mind, a variation of the concept presented by Gerwick (1993) was adopted (Figure 10). In this approach, the tendon for the full span is prestressed and a gap is left in the beam at midspan during casting. The units are folded about the midspan and transported side-by-side to the site. The segments are then placed on falsework in the final configuration and jacked apart in the splice region to stress the prestressing strands. With the jacks in place, the splice concrete is cast. After curing, the jacks are removed, leaving the splice concrete in a prestressed state.

As illustrated in Figure 16, Gerwick’s proposed splice method was modified for the prototype design such that the strands are cut prior to transport and then spliced on site. Prestressing force is applied to the system by a hydraulic jack on each side of the girder web. External brackets transfer the force from the hydraulic jacks to the precast segments by thru-bolts that pass through the web of the beam. The internal restraint provided by the coupled

prestressing strand resists the jacking force, and the prestressing strand is stressed. The eccentricity between the applied jacking force and the resisting strand creates in a lifting moment that is resisted by the self-weight of the precast segments and external tie-downs. If the splice is placed low enough on the section, then tie-downs may not be necessary. After the target stress is achieved, the hydraulic jacks are locked and the splice concrete is placed.

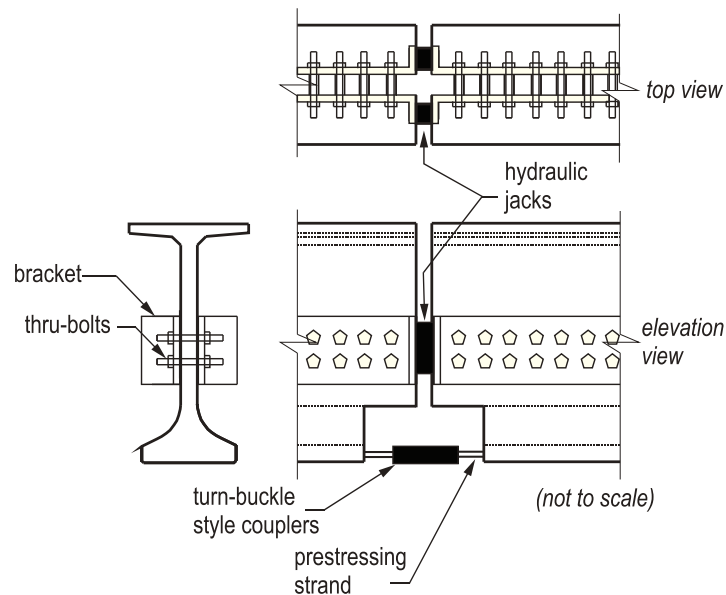


Figure 16–Prototype splice design

The primary aim of incorporating a splice into the prototype design was to reduce the length of the elements so that they can be transported by tractor-trailer. Several options were considered for splice locations with the final configuration illustrated in Figure 17. It was decided to use two symmetrically placed splices rather than a single splice to minimize moment (thus avoiding midspan splice). One added benefit of the symmetrical layout is that the number of prestressing strands required for strength and serviceability need not pass through the splice to the end of the beam. Only the number strands needed for the moment at the splice must be carried through the splice into the end segment. This symmetrical double splice approach was also used in the design of the simply supported 207-ft span 204<sup>th</sup> Street Bridge in Douglas County, NE (Jaber et al. 2006).

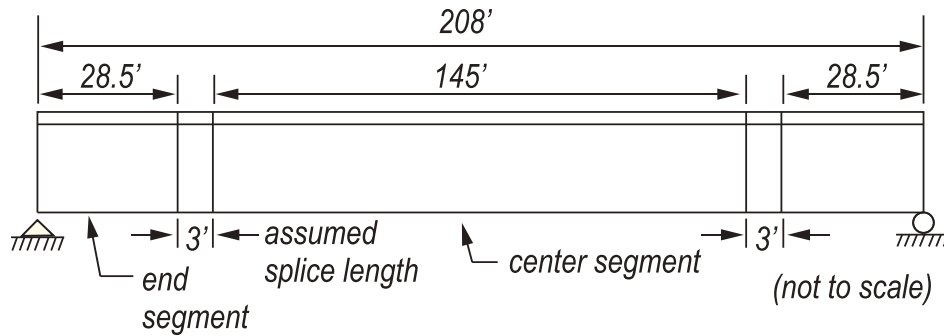


Figure 17–Elevation view of FIB96 with two splices

### 3.2 Prototype Bridge and Beam

To fully utilize its anticipated capacity as a long-span section, the FIB96 (Figure 18(a)) girder was used to develop a prototype splice connection design. The exterior girder of the bridge shown in Figure 18(b) was designed using the FIB96 in accordance with AASHTO-LRFD 2007 (AASHTO 2007) and the FDOT Structural Design Guidelines (SDG) (FDOT 2010).

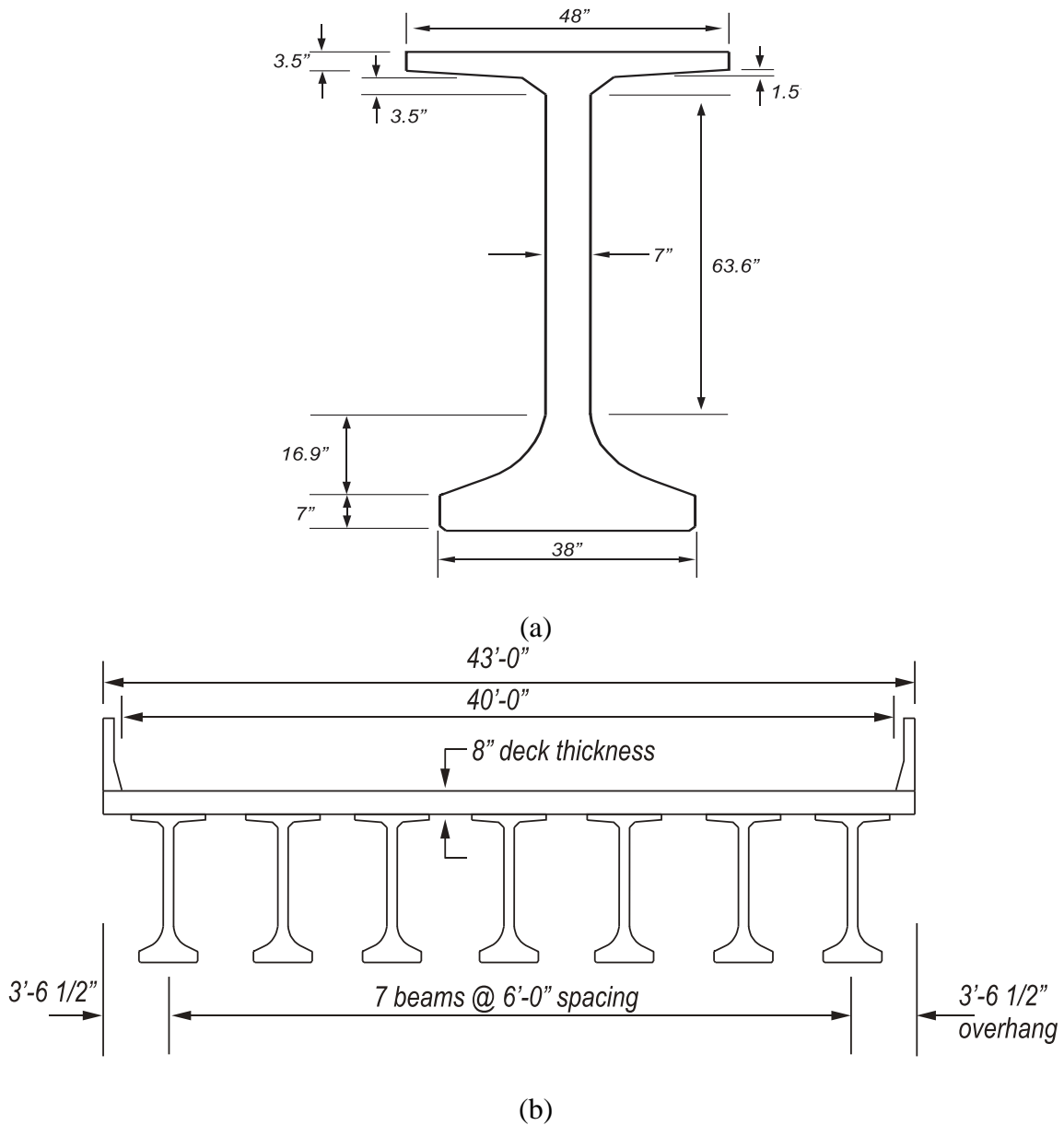


Figure 18–Prototype design (a) FIB96 girder and (b) bridge cross-section

### 3.3 Bridge Design Details

Details of the bridge geometry are:

- Beam length = 208.0 ft
- Design span length = 206.7 ft
- Number of lanes = 4

- Number of beams = 7

Assumed precast beam properties are:

- Concrete strength at transfer,  $f'_{ci} = 6$  ksi
- Concrete strength at 28 days,  $f'_c = 8.5$  ksi
- Initial concrete modulus of elasticity = 4010 ksi (AASHTO-LRFD 5.4.2.4)
- Concrete modulus of elasticity = 4780 ksi (AASHTO-LRFD 5.4.2.4)
- Concrete unit weight = 150 pcf (structural concrete, per SDG)
- Prestressing strands: 0.6-in. dia. ASTM A416, Grade 270, low-relaxation, seven wire strand
- Mild steel reinforcement: ASTM A615, Grade 60.

Assumed cast-in-place deck properties are:

- Slab thickness = 8 in.
- Concrete strength at 28 days = 4.5 ksi
- Slab modulus of elasticity = 3480 ksi

Composite section properties are based on transformed section properties, which incorporate an effective slab width (Figure 19). The effective slab width is calculated for the exterior beam as

$$SlabWidth = \frac{BeamSpacing}{2} + Overhang = 6.54 ft$$

Modular ratio between slab and beam concrete,

$$n = \sqrt{f_{c.beam} / f_{c.slub}} = 1.37$$

Transformed slab width, for use in calculation of composite section properties,

$$b_{eff} = \frac{SlabWidth}{n} = 4.77 ft$$

and result in the non-composite and composite section properties shown in Table 1.

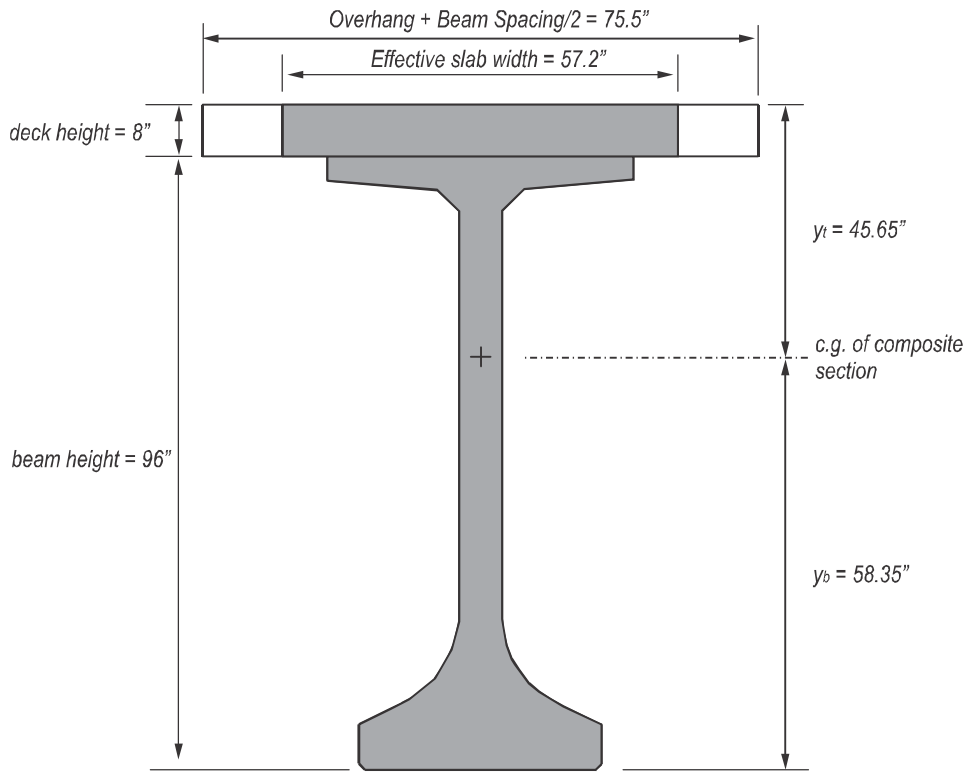


Figure 19–Composite section

Table 1–Typical FIB96 section properties

FIB96	Non-composite	Composite
Area (in. <sup>2</sup> )	1227	1685
I <sub>xx</sub> (in. <sup>4</sup> )	1,516,558	2,608,976
y <sub>t</sub> (in.)	53.22	45.65
y <sub>b</sub> (in.)	42.78	58.35
S <sub>t</sub> (in. <sup>3</sup> )	28496	57152
S <sub>b</sub> (in. <sup>3</sup> )	35450	44713
Depth(in.)	96	104

### 3.4 Loads

Loads were determined per the SDG (FDOT 2010). The dead loads assumed to be acting on the non-composite section are shown in Table 2

Table 2–Non-composite dead loads

Load source	Uniform load (kip/ft)
Girder	1.279
Deck	0.695
Forms	0.02
Total	1.993

The dead loads acting on the composite section are summarized in Table 3.

Table 3–Composite dead loads

Load source	Uniform load (kip/ft)
Future wearing surface	0.075
Barrier	0.21
Total	0.285

The beam was designed for vehicular load requirements prescribed by AASHTO-LRFD, with deviations for load rating as prescribed by SDG 1.7 (FDOT 2010). The design live loads are a combination of:

1. Design truck with dynamic allowance. Three conditions:
  - a. AASHTO-LRFD HL-93 design truck. (32 kip, 32 kip, and 8 kip loads spaced at 14 ft.)
  - b. AASHTO-LRFD HL-93 design tandem. (Two 25 kip loads spaced at 4 ft.)
  - c. Special Florida F-120 truck for permit loading. (53.33 kip, 53.33 kip, and 13.33 kip loads spaced at 14 ft.)
2. Design lane load of 0.64 kip/ft./lane. No dynamic allowance applies.

The dynamic allowance, which applies only to truck loads, is 33% (or 15% for fatigue) as prescribed by AASHTO-LRFD. The AASHTO-LRFD live load distribution factors are not applicable in this beam design. Truck loads were distributed assuming lever rule. All live loads were assumed to act on the composite section.

Because fatigue has been identified as a concern for the coupler device, the amount of prestress force at the splice location was checked to ensure that the section remains uncracked. Stress state checks for fatigue were determined using the fatigue truck with no distributed load, and included the dynamic load allowance of 15%, and by determining the worst case positioning

(transverse and longitudinal) which maximizes the stress range. The beam should remain uncracked for this limit state. The bottom fiber stress at the splice is provided for reference.

The beam design was checked for the limit states described in Table 4, as prescribed in AASHTO-LRFD and modified by the SDG (FDOT 2010).

Table 4–Design limit states

Limit State	Load Combination	Loads
Strength I–Load combination considering normal vehicular use, without wind effects.	$1.5DW + 1.25DC + 1.75LL$	DW: dead load due to the wearing surface DC: dead load due to component and attachments LL: live load due to HL-93 truck (with dynamic amplification) and lane loading
Strength II– Load combination considering permit loads, without wind effects.	$1.5DW + 1.25DC + 1.35LL$	DW: dead load due to the wearing surface DC: dead load due to component and attachments LL: live load due to FL-120 truck (with dynamic amplification) and lane loading
Service I–Load combination relating to normal operational use of the bridge with all loads taken at their nominal value. Wind loads are considered negligible. This limit state is intended to check compression.	$1.0DL + 1.0LL$	DL: total dead load LL: total live load
Service III–This limit state is intended to check tension at midspan for crack control.	$1.0DL + 0.8LL$	DL: total dead load LL: total live load
Fatigue	$0.75LL$	LL: fatigue truck only, with dynamic load allowance

### 3.5 Prestressing Strand Pattern Design

The FDOT LRFD Beam Design MathCAD worksheet (FDOT 2010b) was used to select the number and position of 0.6-in. diameter prestressing strands for each segment. The required number of strands in each segment was dependent on both the construction staging and final configuration and was adjusted to meet both service and strength limit states requirements

(Figure 20). Taking advantage of the segmental nature of the span, 37 of the strands in the center segment were terminated at the splice, leaving 31 strands to continue to the end of the beam.

Continuity of the strands through the splice was necessary to ensure that the strands in the splice were prestressed to  $0.6f_{pu}$  and that there was sufficient flexural strength to resist the factored moment at the splice. This continuity was ensured by using strand couplers. Because the coupler occupies a larger cross-sectional area than the strand, it was necessary to arrange the strand pattern with sufficient space surrounding each strand to prevent interference. This spacing is apparent in the end segment pattern shown in Figure 20. Further, as the strand in the splice region will be prestressed to  $0.6f_{pu}$  and the prestressing strand in the precast segments of the beam will—as is standard—be stressed to  $0.75f_{pu}$ , the discrepancy in stress level required the specification of additional dormant strand, to be prestressed only in the splice region. The final strand pattern for each segment was chosen as closely in accordance with the SDG standard FDOT strand pattern layout as possible (FDOT 2010). A notable exception was a modification of the standard strand pattern in the web to include additional strands to achieve the required moment capacity.

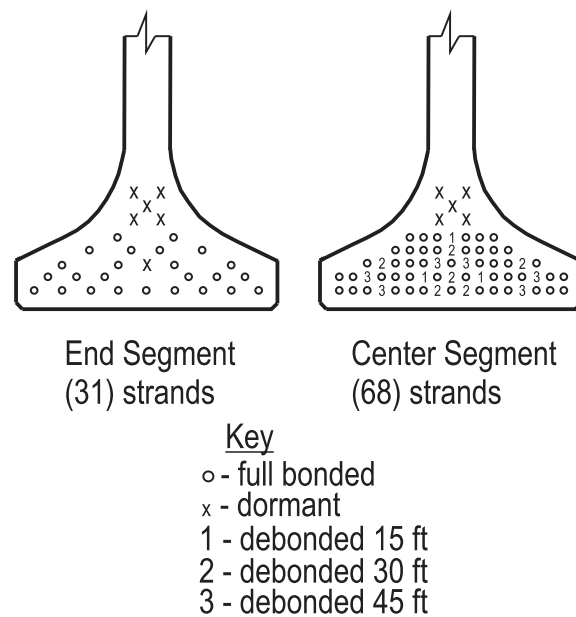


Figure 20—Strand layouts

Initially, the end and center segments were analyzed individually using both the FDOT MathCAD worksheet (FDOT 2010b) and a supplemental worksheet to address the concrete stresses at the time of prestress release for each segment. The transformed section properties

were used for these calculations. Beam segments were assumed to be detailed with tensile reinforcement in the top of the section so that  $0.19\sqrt{f'_c}$ (ksi) limit on concrete tensile stress was used. The following allowable stresses at release were used to check the calculated stresses shown in Table 5.

- Compressive stress limit:  $0.6f'_c = 3600$  psi (AASHTO-LRFD 5.9.4.1.1)
- Tensile stress limit (outer 15% of segment):  $12\sqrt{f'_c}$ (psi) = 930 psi (SDG)
- Tensile stress limit (inner 70% of segment):  $0.19\sqrt{f'_c}$ (ksi) = 533 psi (AASHTO-LRFD 5.9.4.1.2)

Table 5–Summary of Service I limit states check for precast segments at release

Segment	Position (ft)*	Tensile Stress (psi)		Compressive Stress (psi)	
		Applied	Limit	Applied	Limit
End	4.275	485	930	1920	3600
	14.25	452	533	1893	3600
Center	21.75	730	930	3309	3600
	72.5	265	533	3485	3600

\*distance from end of segment

The segments were assumed to be shipped to the site in their separate configurations and spliced and erected for deck placement. Table 6 presents the Service I limit states check using non-composite section properties for loads during deck placement. The following limits were checked:

- Compressive stress limit at 1.0DL:  $0.45f'_c = 3830$  psi
- Tensile stress limit:  $0.19\sqrt{f'_c}$ (ksi) = 533 psi

Table 6–Summary of Service I limit states check for loads associated with deck placement

Position (ft)*	Tensile Stress (psi)		Compressive Stress (psi)	
	Applied	Limit	Applied	Limit
2.8	537	533	2823	3825

\*distance from end of spliced beam

The beam was checked for Service I and Service III limit states load combinations with full dead and live loads (Table 7 and Table 8). Additionally, the bottom fiber stress was checked for the fatigue load combination (Table 9), to ensure that the splice location remained uncracked. The transformed, composite section was used to make these checks. The following limits were used:

- Service I (1.0DL+1.0LL)
  - Compressive stress limit:  $0.6f'_c = 5100$  psi
  - Tensile stress limit:  $0.19\sqrt{f'_c}(\text{ksi}) = 533$  psi
- Service III (1.0DL+0.8LL)
  - Compressive stress limit:  $0.4 f'_c = 3400$  psi
  - Tensile stress limit:  $0.19\sqrt{f'_c}(\text{ksi}) = 533$  psi
- Fatigue (1.0DL+0.75LL):
  - Tensile stress limit:  $7.5\sqrt{f'_c}$  (psi) = 690 psi

Table 7–Summary of Service I limit state check at the extreme top fiber

Position (ft)*	Tensile Stress (psi)		Compressive Stress (psi)	
	Applied	Limit	Applied	Limit
2.8	498	533	n/a	n/a
30	n/a	n/a	1775	5100
104	n/a	n/a	4353	5100

\*distance from end of spliced beam

Table 8–Summary of Service III limit state check at the extreme bottom fiber

Position (ft)*	Tensile Stress (psi)		Compressive Stress (psi)	
	Applied	Limit	Applied	Limit
2.8	n/a	n/a	2727	3400
30	n/a	n/a	1078	3400
104	475	533	n/a	n/a

\*distance from end of spliced beam

Table 9–Fatigue limit state check at the extreme bottom fiber at splice

Position (ft)*	Tensile Stress (psi)	
	Applied	Limit
30	280	690

Table 10 presents the Strength I moment and shear factored combinations at the location of the splice and at the beam midspan, as well as the associated design moment strengths. Table 11 presents the Strength II combinations and limiting values.

Table 10–Strength I flexure and shear checks for spliced length

Position (ft)*	$\phi M_n$ (kip-ft)	$M_u$ (kip-ft)	$\phi M_n/M_u$	$\phi V_n$ (kip)	$V_u$ (kip)	$\phi V_n/V_u$
30	14,700	11,200	1.31	770	340	2.26
104	26,600	23,100	1.15	484	0	n/a

\*distance from end of spliced beam

Table 11–Strength II flexure and shear checks for spliced length

Position (ft)*	$\phi M_n$ (kip-ft)	$M_u$ (kip-ft)	$\phi M_n/M_u$	$\phi V_n$ (kip)	$V_u$ (kip)	$\phi V_n/V_u$
30	14,700	10,100	1.46	770	310	2.48
104	26,600	20,900	1.27	484	0	n/a

\*distance from end of spliced beam

### 3.6 Moment-Curvature

Another important aspect of the splice design that is not explicitly covered in the AASHTO-LRFD is the flexural ductility of the section. Because the strands will be mechanically coupled at the beam splice, the flexural ductility of the section at that location will depend on the stiffness and seating movement of the strand couplers. To evaluate the ductility the beam splice, moment-curvature analysis was conducted considering the effect of the strand couplers on ductility. The coupler stress-strain model (established with testing reported in Chapter 4) was utilized to assess the cross-section with 31 strands coupled using a 0.6-in. dia. coupler (Figure 21). The Ramberg-Osgood model was used to analyze the cross-section as if the strands were continuous across the splice, without any coupling device (Collins and Mitchell 1991).

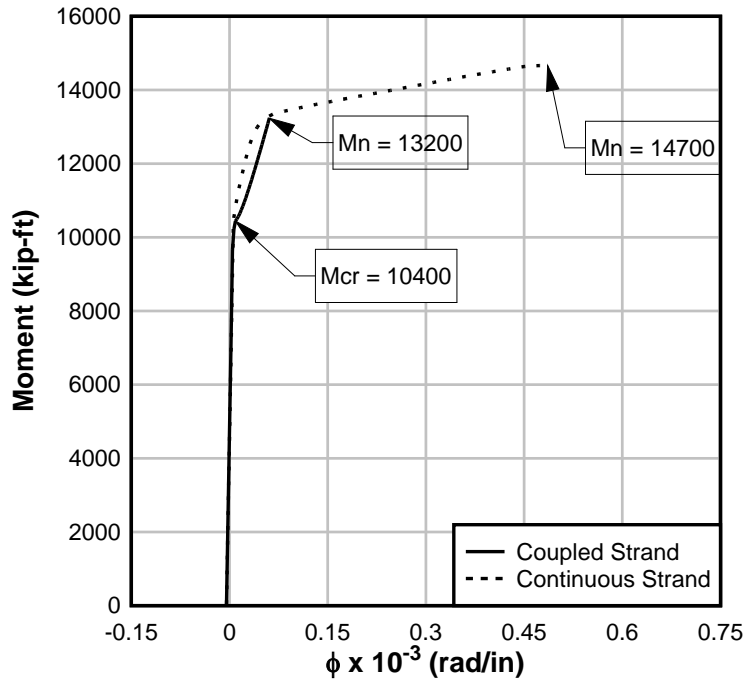


Figure 21–Moment-curvature of FIB96: continuous strand vs. coupled strand

Both models were assumed to have the same effective prestress force. Consequently, both models exhibited the same precracking behavior, with both beams cracking under an applied moment of 10,400 kip-ft.

The predicted ultimate capacity of both sections was also approximately equal. The FIB96 with continuous strand has a moment capacity of 14,700 kip-ft—an additional moment-carrying capacity of 40% beyond the cracking moment. In comparison, the FIB96 with coupled strand has an ultimate capacity of 13,200 kip-ft, approximately 27% beyond the cracking moment. The addition of nonprestressed or partially prestressed strand across the splice region may be required to achieve the design moment capacity.

After cracking, however, the two sections exhibit different behavior: the difference in ductility of the two sections is considerable. Compared with a section reinforced with continuous strand, the lower stiffness of the coupled strand causes greater curvature of the section at lower stress. Because the coupled strand stress-strain model does not include strand yielding, the behavior is similar to that of a section reinforced with mild steel; the moment curvature of the section with coupled strand does not have a smooth rounded shape. At capacity,

the coupled strand ruptures prior to the development of 0.003 compressive strain in the concrete (Figure 22). The failure mode is brittle and sudden.

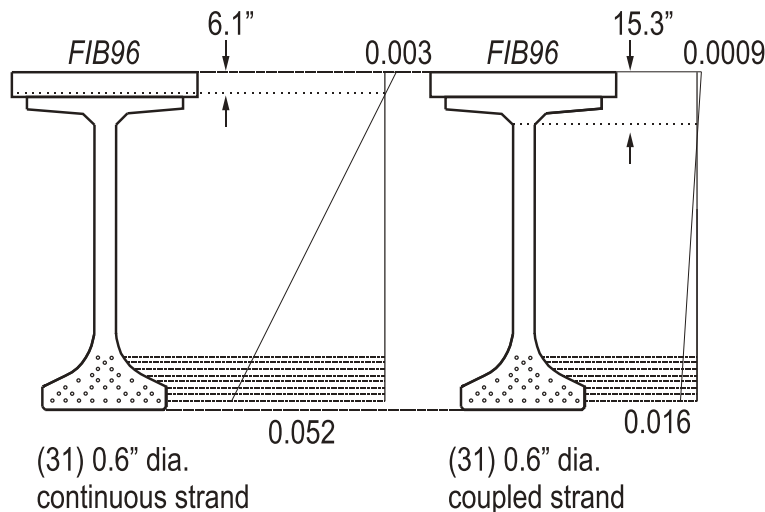


Figure 22–FIB96 strain at flexural capacity: continuous vs. coupled strand

Brittle behavior was similarly observed in ultimate load tests of a box girder repaired with couplers. At ultimate capacity, the repaired box girder (with 2 of 30 strands coupled using 0.5-in. dia. couplers) failed at slightly less load, but considerably less deflection than equivalent intact (non-damaged) box girders; the repaired girder exhibited 35% less deflection. (Labia et al. 1996).

The above moment-curvature analysis was based on test results from a single tensile test of a 0.6-in. dia. coupler (the test is described in Chapter 4) and was completed to develop a prediction of the couplers' influence on the failure behavior. To verify the coupler stress-strain model, it is recommended that additional testing of the couplers be conducted.

### 3.7 Splice Considerations

Figure 16 illustrates the bracket required to push the segments apart after the strands have been coupled. The bracket and connection design itself is relatively simple, but must be capable of transferring shear and moment and requires a slip-resistant connection. Placement of the bracket on the girder web provides an easy-to-access, flat face for the brackets to bear against. Whereas attachment of the brackets to the flat face of the bottom flange would have reduced the eccentricity of the jacking force with that of the prestressing strands, it was considered

impracticable due to the large amount of steel in these regions. The use of thru-bolts allowed for in-line delivery of the jacking force, and reduced the prying action of the brackets on the precast girders. To prevent spalling of the girder web concrete, steel sleeves were detailed for the thru-bolts.

Outside of geometric considerations, the primary objective was to develop moment-carrying capacity at the splice location. To do this, the prestressing strand was designed to be coupled within the splice region, to provide continuous prestressing strand along the span length for ultimate capacity. By relying on couplers to provide continuity of the existing prestressing strand, the cross-section of the FIB section could be maintained. The number of coupled prestressing strands was determined based on the design of the FIB96 prototype and the strand pattern was spaced with the larger volume of the couplers in mind. The coupled prestressing strand was designed to be “prestressed” to achieve the required  $0.6f_{pu}$  for service.

#### 4 Strand Coupler Selection and Testing

Several strand coupler devices were discussed in the literature review. A commercially available turnbuckle coupler (called a Grabb-it) was selected for the test specimen. The use of turnbuckle-style couplers permits adjustment to compensate for different strand lengths; the turnbuckle can be used to equalize the gap length between the precast segments so that prestress force is delivered equally to each strand while also eliminating prestress losses that would otherwise occur due to wedge seating.

Figure 23 shows the components of this turnbuckle-style mechanical connection. A prestressing chuck threaded onto a tensioning bolt is connected by a tensioning nut to another chuck and tensioning bolt pair. One chuck and tensioning bolt pair is threaded opposite to the other pair, so that the device does not “unwind” when the tensioning nut—or turnbuckle—is torqued. Toothed wedges and a tapered spring inside each chuck grab the prestressing strand at each end.

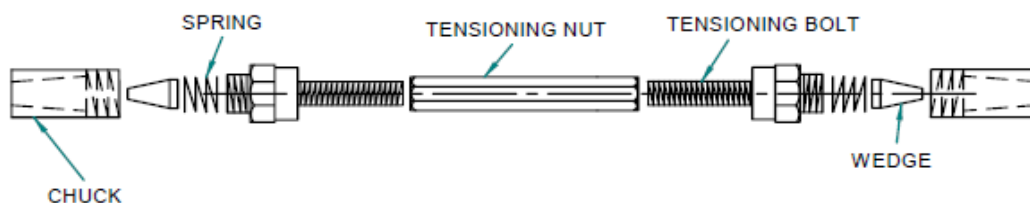


Figure 23–Turnbuckle-style coupler components (Waheed et al. 2005)

Couplers for both 0.5-in. and 0.6-in. diameter strands were tested in tension in a universal test machine. The couplers for 0.6-in. diameter strands were tested to ultimate capacity so that the actual stress-strain relationship of the coupler could be used in the moment-curvature analysis conducted on the prototype girder (Section 3.6). In addition, the results were compared with the ACI and AASHTO-LRFD requirements for post-tensioned anchorages and coupling devices that require the development of at least 95% of the specified ultimate strength of the prestressing strand (ACI 318-08 2008; AASHTO 2007). Although the 0.6-in. dia. coupler was made available for lab testing by the manufacturer, it is not currently in commercial production.

Strain gages were applied to the couplers for 0.5-in. diameter strand and the couplers were tested to develop a calibration of strain versus load. Calibration data were used during the

splice prestressing process to corroborate readings from the load cells placed on the unbonded portion of the prestressing strands in the spliced test specimens.

#### *4.1 Ultimate Strength Tests of 0.6-in. dia. Coupler*

Two tension tests were conducted on the 0.6-in. dia. couplers to be used in the proposed splice design. The first test was performed at the FDOT State Materials Office (Figure 24). In this test, the coupler was used to splice two lengths of 0.6-in. dia. 270 ksi lo-lax prestressing strand. One end of each strand was prepared with white glue and fine sand prior to the test, in accordance with ASTM A1061; the sand-prepared end was gripped by the wedge grips of the test machine (ASTM A1061 2009). Load was applied at a displacement-controlled rate of approximately 0.2 in./min. The test ended when the strand ruptured near the top wedge of the coupler device (Figure 25(a)) at an applied tensile load of 53.6 kip, or 91% of the strand's specified ultimate strength. At rupture, the prestressing strand stress was 247 ksi; though near the proportional limit of lo-lax strand, the stress-strain plot of the coupled device shows that the prestressing strand did not exceed this point, and did not begin to yield prior to rupture. The strand ruptured at notches caused by the wedges (Figure 25(b)).

For comparison purposes, a second test was performed at the UF laboratory in accordance with the static testing requirements of AC303 from the International Code Council Evaluation Service (ICCES) for post-tensioning anchorages (ICCES 2011). In this test, the chuck bodies were disconnected from the turnbuckle and attached to the ends of the prestressing strand - similar to tests of strand chucks (Figure 26).

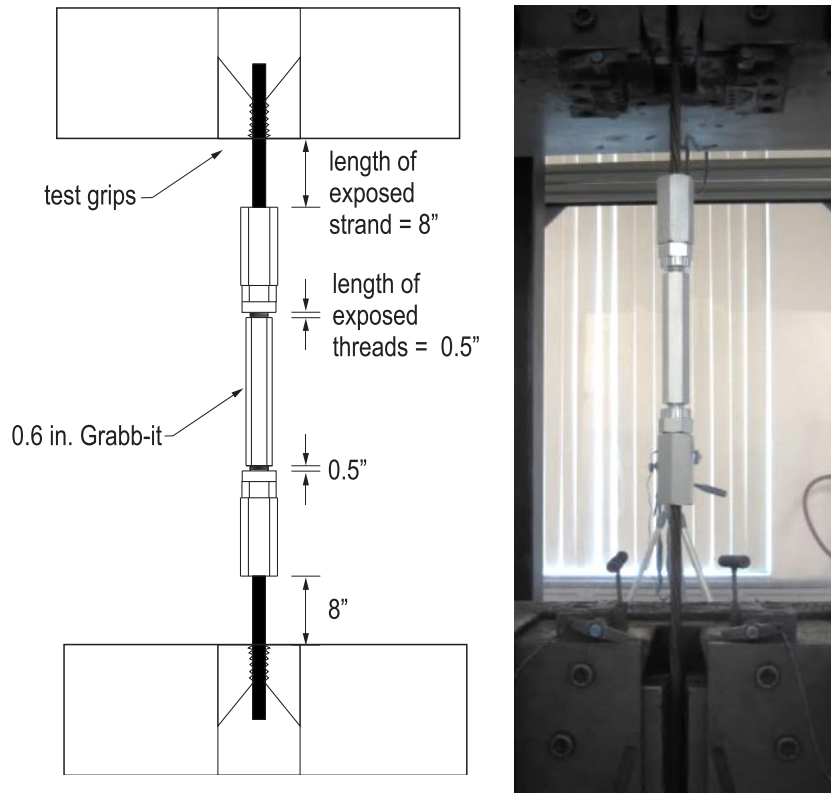


Figure 24–SMO tensile tests of 0.6-in. dia. coupler



(a)



(b)

Figure 25–Rupture of strand in 0.6-in. dia. coupler

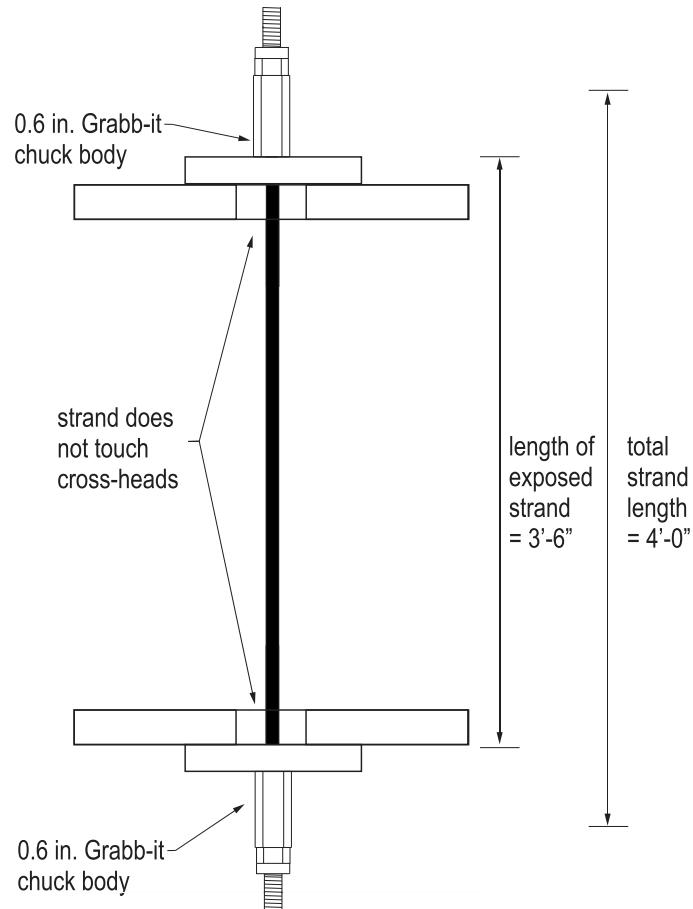


Figure 26–UF tensile test set-up of 0.6 in. dia. coupler

Unlike the first test, no preparation of the strand ends was performed prior to attaching the chucks. The test was performed on the same coupler that was used for the first test with fresh (previously unused) wedges. Load was applied at a displacement-controlled rate of approximately 0.75 in./min., in accordance with ICCES test procedures (ICCES 2011).

The UF test was terminated when the strand ruptured at the chuck, at an applied tensile load of 61.5 kip, or 103% of the strand’s specified ultimate strength. At rupture, the prestressing strand stress was 277 ksi - past the proportional limit of lo-lax strand and into the yield plateau. The stress-strain plot of the coupled device shows that the coupled strand began to yield prior to rupture. It was observed that the strand ruptured at notches caused as the wedge anchors bit into the strand.

Figure 27 shows the stress-strain plot for the two tensile tests of the coupler with strand. Also shown is the stress-strain plot for just the strand (uncoupled), tested per ASTM A1061 (2009).

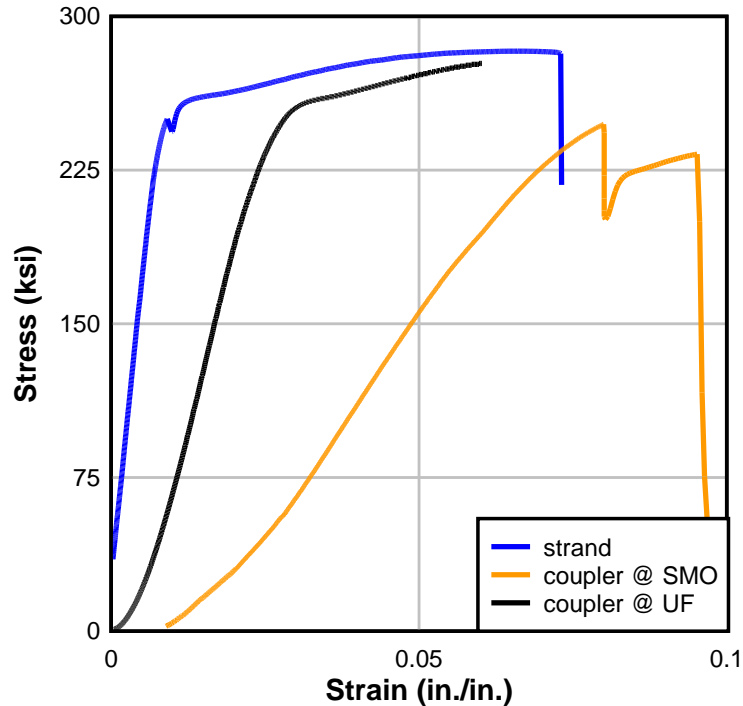


Figure 27—Comparison of 0.6-in. dia. coupler and strand behavior

The increased elongation seen in the coupler in the second (UF) test is unknown. Walsh and Kurama (2010) describe similar observations throughout a series of tests on a single reusable anchor; it is possible that the same phenomenon is occurring in the UF test. Alternately, the apparent strand yield may be due to the increase in the strand length of the UF test set-up. The stress-strain results of the tensile test with the fully assembled coupler (as tested at the SMO) were used in the moment-curvature analysis described in Section 3.6.

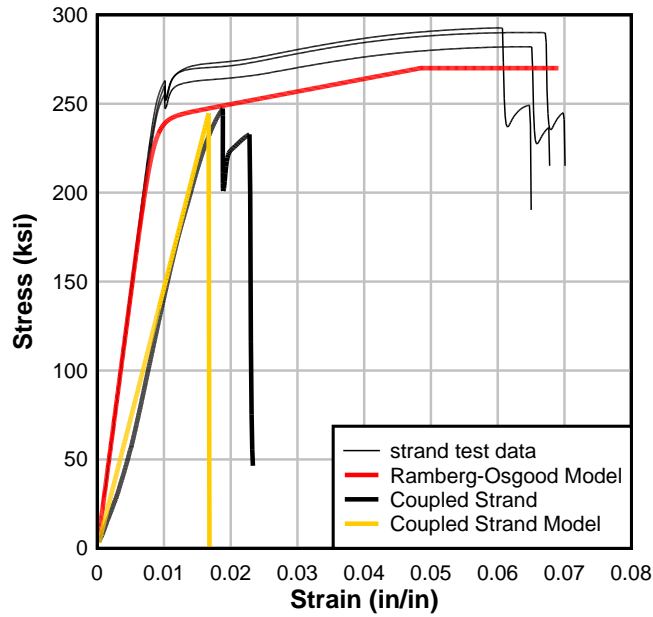


Figure 28–Stress-strain models and test data for coupled and continuous strand

#### 4.2 Calibration of 0.5-in. dia. Coupler

Coupler calibration tests using the test set-up shown in Figure 29 were also performed to develop calibration data for the couplers that were going to be used in the spliced test specimens. Calibration of the strain to applied load allowed for direct measurement of the force in the spliced prestressing strand during the splice assembly procedure.

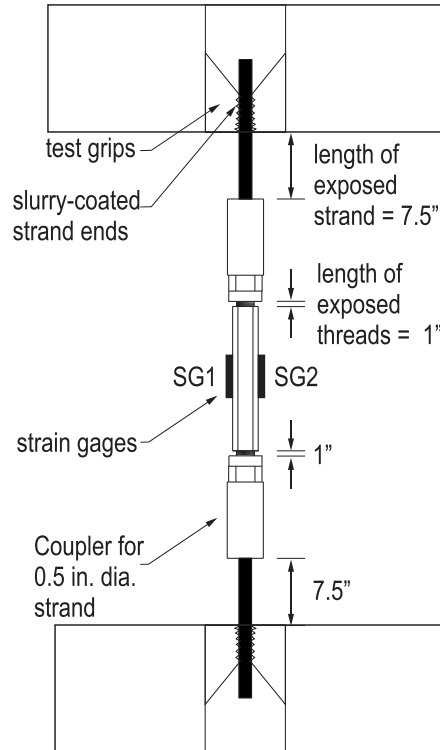


Figure 29–SMO tensile test set-up of 0.5 in.-dia. coupler

Two specimens were tested, each instrumented with two strain gages. Prestressing strand from the same coil as used in the unbonded segment of the spliced specimens was used in the coupler calibration. One end of the prestressing strand was slurry-coated with white glue and fine sand, in accordance with ASTM A1061 (2009). The uncoated end was fit into the chuck body of the coupler; the slurry coated end was fit into the test grips of the crossheads, as shown. Each specimen was loaded to 35 kip three times, as summarized in Table 12.

Table 12–0.5 in.-dia. coupler calibration load procedure

Load Cycle	Procedure
1	0-35 kip, unload to 5 kip
2	5-35 kip, unload to 5 kip
3	5-35 kip, completely unload

Figure 30 shows the plot of the load versus microstrain of the two coupler strain gages. The two strain gages on the couplers produced very consistent readings as load was increased, indicating that there was very little bending of the coupler occurring. The strain readings also

indicate that the coupler was behaving linear-elastically at the tested load range. Also shown in the plot is the approximate linear curve-fit used to relate the coupler strain to an applied tensile load. This relationship was used in later data analysis to relate measured strain in the coupler to strand load.

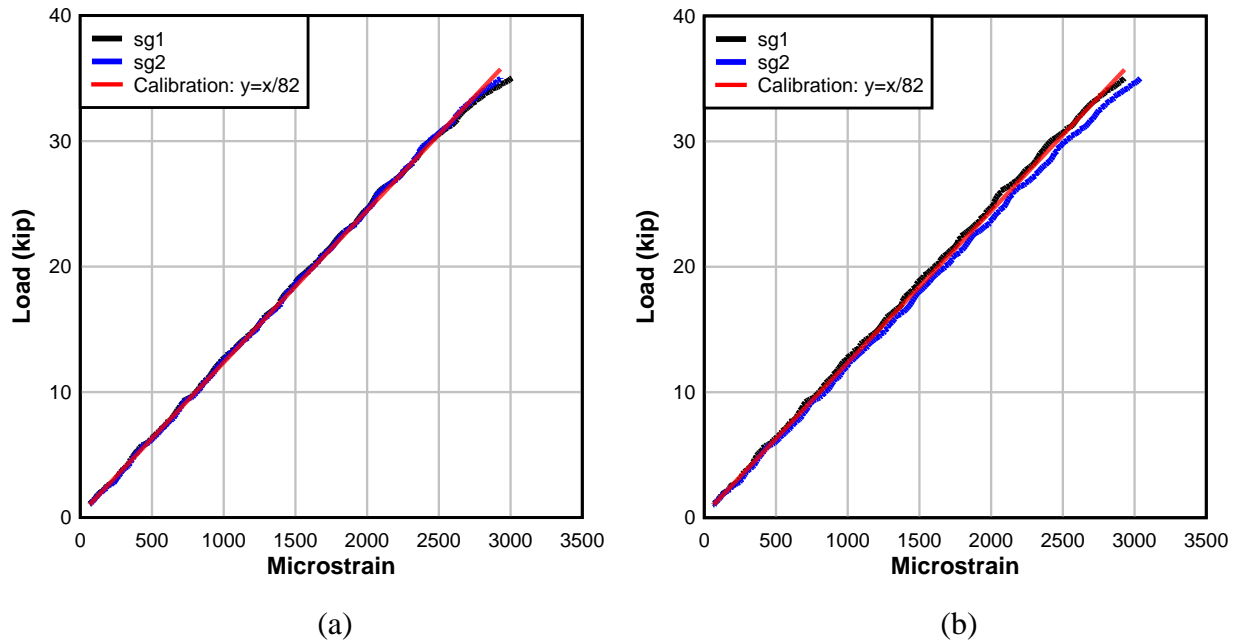


Figure 30–Coupler strain gage calibration (a) specimen 1 and (b) specimen 2

## 5 Test Specimen Design

A comprehensive investigation of the selected splice was necessary to assess its constructability as well as its flexural, shear, and fatigue performance. Comprehensive testing of the FIB96 prototype, however, was not possible due to limitations in laboratory capabilities and research budget. Consequently, the behavioral aspects of the splice deemed most critical were tested using an AASHTO Type II cross-section; due to its smaller size, it was possible to construct duplicate test specimens to investigate the various behaviors.

Matching the strain gradient of the FIB96 prototype to the test specimen was impossible due to the gross height difference of the two geometries. As a result, calibration of the test procedures and loading was based on matching the stress state of the test specimen and the FIB96 prototype at a particular point along the vertical axis of the FIB96 cross-section. The point of interest varied depending on the behavior under investigation.

A 25-ft long AASHTO Type II girder with an 8-in. slab was selected as a test specimen. Based on the capacity of the loading actuators in the laboratory, the strand quantity was limited to five strands. The strand pattern was arranged to create a similar pattern of congestion as would occur in the FIB96 prototype. The intent was to recreate any issues related to clearance that would be encountered in the prototype beam. A sixth strand with an 11-ft bonded length was included to prevent cracking of the unbonded segment during transport to the lab. This additional length of bonded strand was reproduced in the control beams. The AASHTO Type II was fabricated at a precasting yard and the deck was placed by lab personnel following delivery to the laboratory. The specimens are shown in Figure 31 and Figure 32.

The materials chosen for the test specimen beam design were as follows:

Precast beams:    Dimensions and strand pattern (Figure 31): AASHTO Type II

Concrete strength at transfer,  $f'_{ci} = 6$  ksi

Concrete strength at 28 days,  $f'_c = 8.5$  ksi

Initial concrete modulus of elasticity = 4012 ksi (AASHTO-LRFD

5.4.2.4)

Concrete modulus of elasticity = 4,776 ksi (AASHTO-LRFD 5.4.2.4)

Concrete unit weight,  $w_c = 150$  pcf (structural concrete, per SDG)

Beam length = 25.0 ft

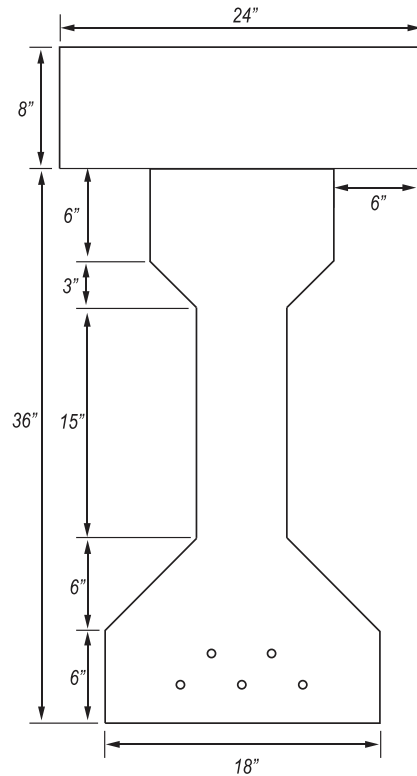


Figure 31–AASHTO II cross-section

- Cast-in-place slab: Slab thickness = 8 in.  
Concrete strength at 28 days = 4.5 ksi
- Prestressing strands: 1/2 in. dia., seven wire lo-lax strand  
Area, per strand = 0.153 in.<sup>2</sup>  
Ultimate strength,  $f_{pu} = 270$  ksi  
Prestressing strand modulus of elasticity = 28,500 ksi  
Prestress level at jacking =  $0.6f_{pu}$

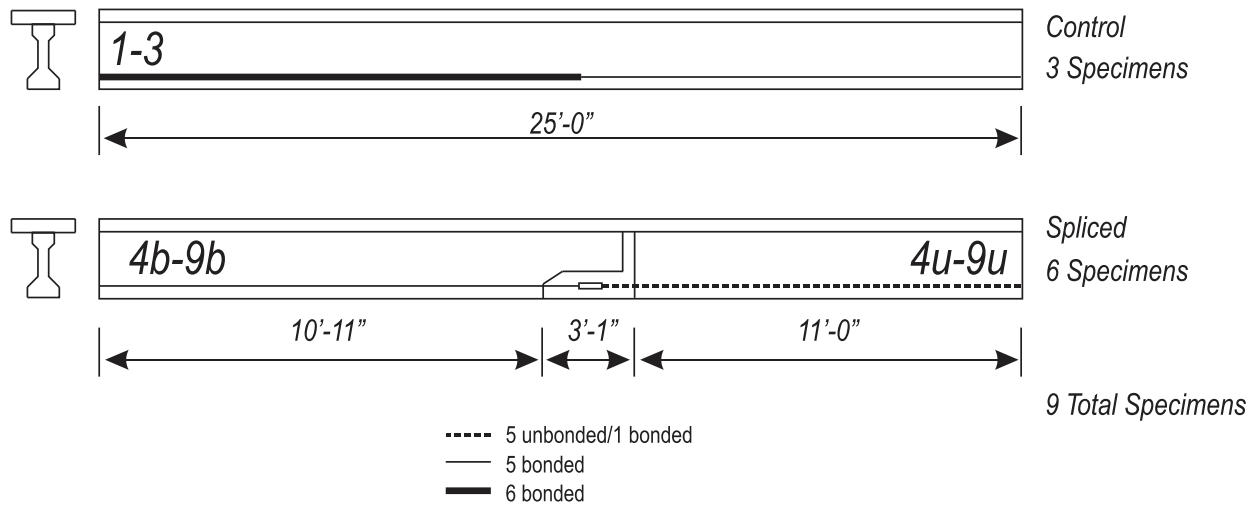


Figure 32–Test specimens

### 5.1 Detailing Considerations

Special detailing was included the segments to be spliced to accommodate personnel during the splice assembly, to prevent cracking, and to provide additional strength capacity. Special detailing for the joint area included shear keys, additional rebar around the notched area of the bonded segment, and special stirrups. Additionally, the geometry of the splice area was also considered. This section covers these detailing considerations. Figure 33 shows the key detailing considerations of the joint area.

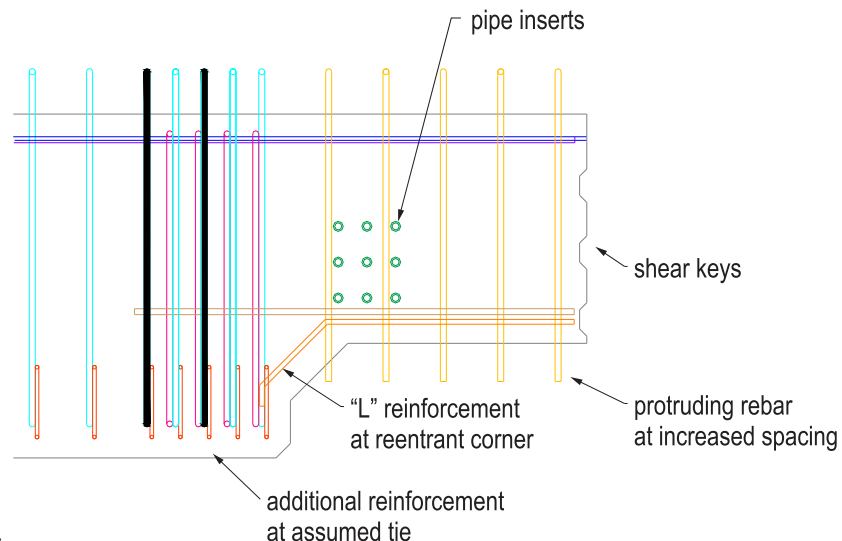


Figure 33–Detailing considerations

The geometry of the splice region was controlled by considerations of working space and the space required for strand coupler installation; common practice and code recommendations for precast joint design were also maintained. As discussed in Section 2.7, the length of the closure pour was controlled by two considerations: the closure length must be sufficient to allow splicing of the prestressing steel, but was limited by design (due to the limited quantity of prestressing steel and the small amount of longitudinal reinforcement). As a minimum, AASHTO-LRFD recommends 12 in. to provide enough clearance to properly splice steel reinforcement (AASHTO 2007). The distance between the top flanges of the closure pour (6 in.) was in accordance with AASHTO-LRFD recommendations for construction joint widths (AASHTO 2007).

The chosen method of introducing prestress force into the coupled strand during splice assembly was to jack the precast segments apart by applying force to removable brackets which are attached to either face of the girder web (Figure 34). Steel brackets were constructed by the FDOT structures lab. The bracket construction drawings are provided in Appendix C–Bracket Fabrication Drawings.

To secure the brackets on the test specimen with thru-bolts, pipes were designed to pass through the girder web. By applying the jacking force via thru-bolts and pipes passing through the girder web, the eccentricity of the applied force was reduced versus attempting to transfer the force through anchored connections on each face of the girder web. This approach is similar to that described by Gerwick (1993) (described further in Section 3.1).

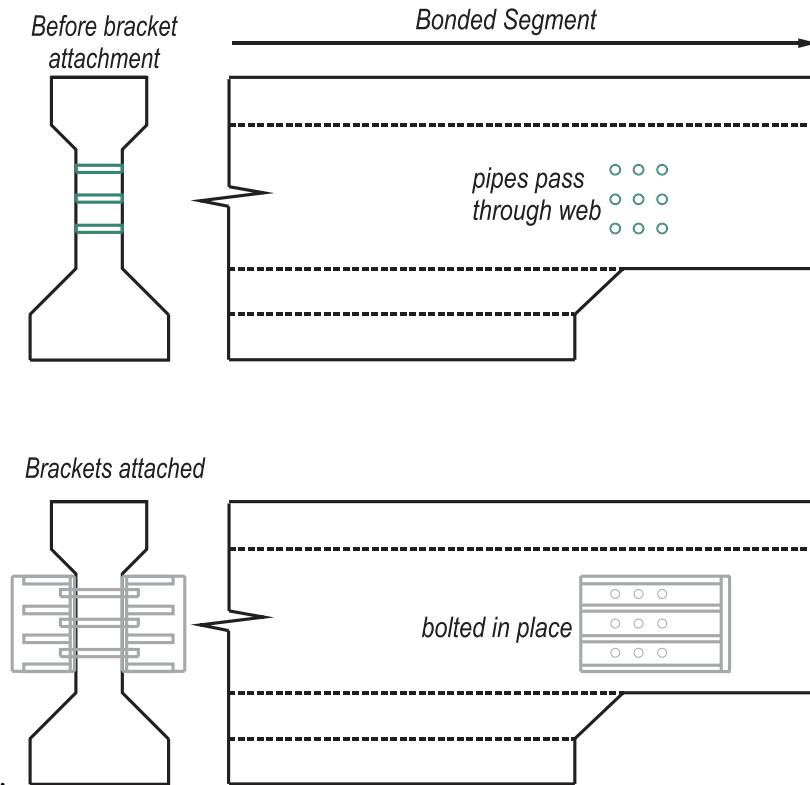


Figure 34—Bracket attachment to beam

Pipe inserts were constructed by the FDOT Structures Lab prior to precast of the beams. To maintain the orientation and alignment of the nine 1-in. dia. schedule 40 steel pipes during beam precast, the pipes were welded to a small rebar cage. Template plates held the pipes in position and relatively in line with one another during welding; accurate alignment of the pipes was crucial to provide non-eccentric load application to the precast concrete during the stressing of the splice region. The alignment and levelness of each pipe insert was checked after the welding was complete.

Small diameter (#3) rebar was used in the pipe insert, in an effort to reduce the steel congestion in this area and allow the concrete to flow around the pipes. The rebar also acted as a convenient tie location when positioning the pipe inserts in the steel reinforcement. Stirrup locations in the region of the pipe inserts were adjusted (spacing in the area was increased) to avoid conflicts with the pipes. Twelve pipe inserts were fabricated by the FDOT Structures Lab and provided to the precaster as assembled units. The pipe inserts were installed at the precast yard during the stirrup placement. Installation of the pipe inserts is covered in Section 6.1. The pipe insert can be seen in Figure 44 and Figure 33.

Detailing of construction joints requires special consideration of the precast ends (PCI 2004). The precast faces were prepared prior to formation of the closure pour to provide adequate shear transfer across the joint. Shear transfer can be accomplished through a number of methods, including roughening the precast concrete after it has cured, providing stirrups which cross the joint or detailing formed shear keys in the precast concrete.

Shear keys were detailed on the to be spliced ends of both the bonded and unbonded segments, to provide mechanical interlock to increase the shear capacity of the interface between the precast concrete and the closure pour concrete. The shear keys are shown in Figure 35. Design recommendations are provided by AASHTO-LRFD (2007) regarding the geometry of shear keys; these recommendations are dependent on the size of the aggregate and the width of the web and were considered for the determination of the shear key dimensions (Figure 11). Dimensions are given in Appendix D–Precast Fabrication Drawings.

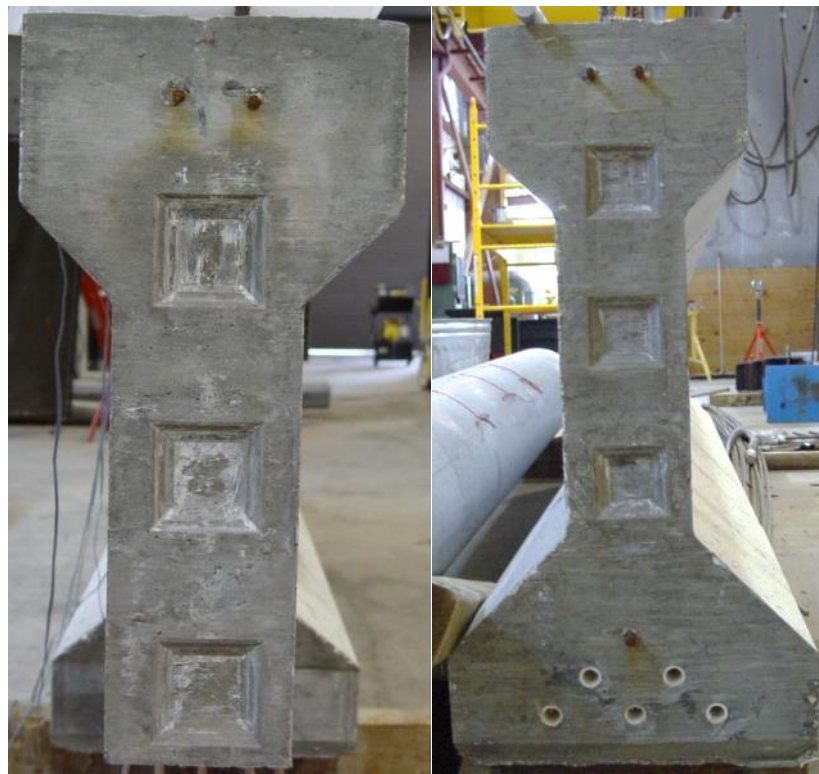


Figure 35–Shear keys in test specimen

In the last four splices, both faces of the precast segments were roughened by gouging the concrete with a cutting disk. This did little to roughen the concrete and likely did not contribute to shear resistance, as will be discussed later. Epoxy application to the faces of the precast

segments of the last four splice assemblies was also done in an effort to increase shear resistance and bond between the precast and the closure pour.

Steel reinforcement of the area near the closure pour was designed with multiple considerations in mind: handling, tie formation during stressing of the closure pour (STM model) the need for additional confinement reinforcement at each end of the precast to control cracking during prestress release, and straight stirrups for shear reinforcement along the closure pour length. These details can be seen in Figure 33. An “L” shaped #5 rebar was placed around the reentrant corner of the bonded segment, to mitigate cracking during handling and transport. Additional rebar were detailed in the region identified by the strut-and-tie model as the area of likely tie-formation. This additional reinforcement also served as confinement reinforcement during prestress transfer. The stirrups in the notched region of the bonded segment were installed without a lower hook. This was done to reduce congestion in the splice region so that the prestressing strand could be more easily reached for coupling during the splice assembly in the laboratory. The bottom hook of the stirrups were later added using a rebar coupler. The stirrup spacing was increased in the region of the coped area of the bonded segment to accommodate the congestion caused by the size of the rebar couplers and pipe inserts.

The selected rebar coupler is a commercially available product which does not require preparation of the rebar. It mechanically connects two pieces of rebar, using a series of screws to engage each rebar piece. Serrated guide rails within the coupler provide additional mechanical grip. A cotter pin serves to set the length of each rebar within the coupler. The rebar coupler is shown in Figure 36.

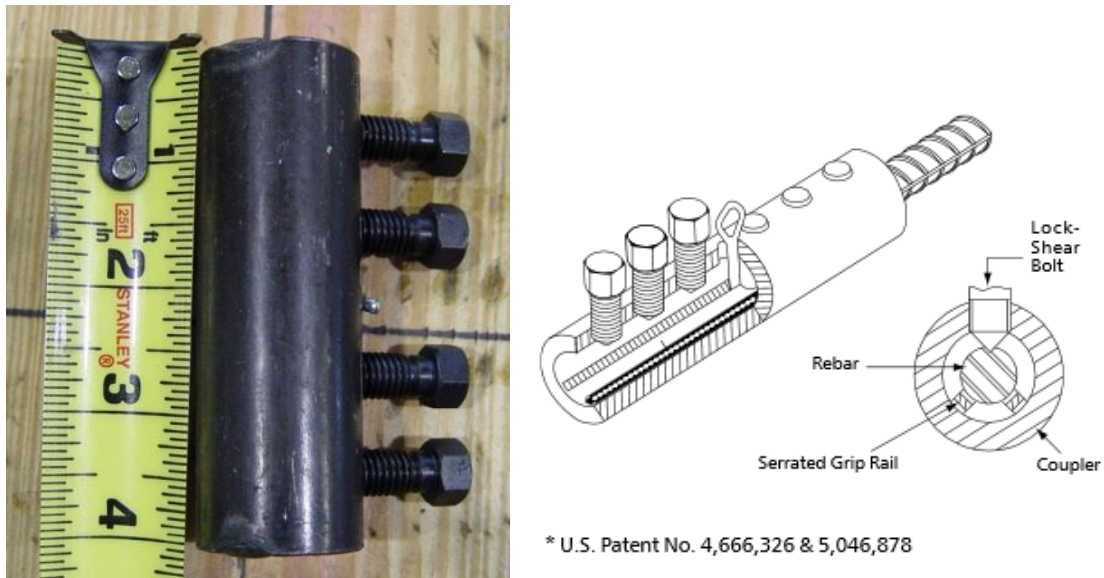


Figure 36–Rebar coupler

Prestressing strand protruding from the bonded segment was detailed to extend into the coped area approximately 26 in., in order to ensure adequate length for later strand splicing. The strand was protected during the precasting and storage by the wooden block-out.



Figure 37–Protruding strand

## 5.2 Flexure Service and Cracking Test Design

The splice location of prototype beam was designed to remain uncracked under service loads; the splice behavior was anticipated to remain linear-elastic under service loads. As a result, the Service I and III load cases were not particularly interesting, unless the prestress losses over time became significant enough to result in cracking. The behavior of the splice under service loads was evaluated for:

- 1) Effective prestress force;
- 2) Splice stiffness vs. precast segment stiffness;
- 3) Strain field.

To match the stress state for Service III, the bottom face was chosen as the reference point, as the prototype beam at the splice location is still compressed. Table 13 presents the Service III bottom fiber stresses for the FIB96 prototype at the splice location.

Table 13–Stress state of FIB96: Serviceability

Load case	$f_{bot}$ (psi)
DL only	-50
Service III	-486

The applied moment required to match the bottom fiber stress of the test specimen to that of the FIB96 prototype under Service III loads was determined and are presented in Table 14. In addition, the applied moment required to reach the cracking stress ( $7.5\sqrt{f'_c}$  (psi)) based on the specified prestress is provided for reference.

Table 14–Stress state of test specimen: Serviceability

Load Level	$f_{bot}$ (psi)	Moment (kip-ft)	Load, 2P (kip)
Service III	-486	409	82
Cracking	-691	445	94

A four-point bending set-up, with the splice region encompassed in the constant moment region, was chosen to investigate the flexural behavior of the test specimen. The 5-ft distance between the load points was selected to encompass the entire splice region. The general flexural test set-up is shown in Figure 38.

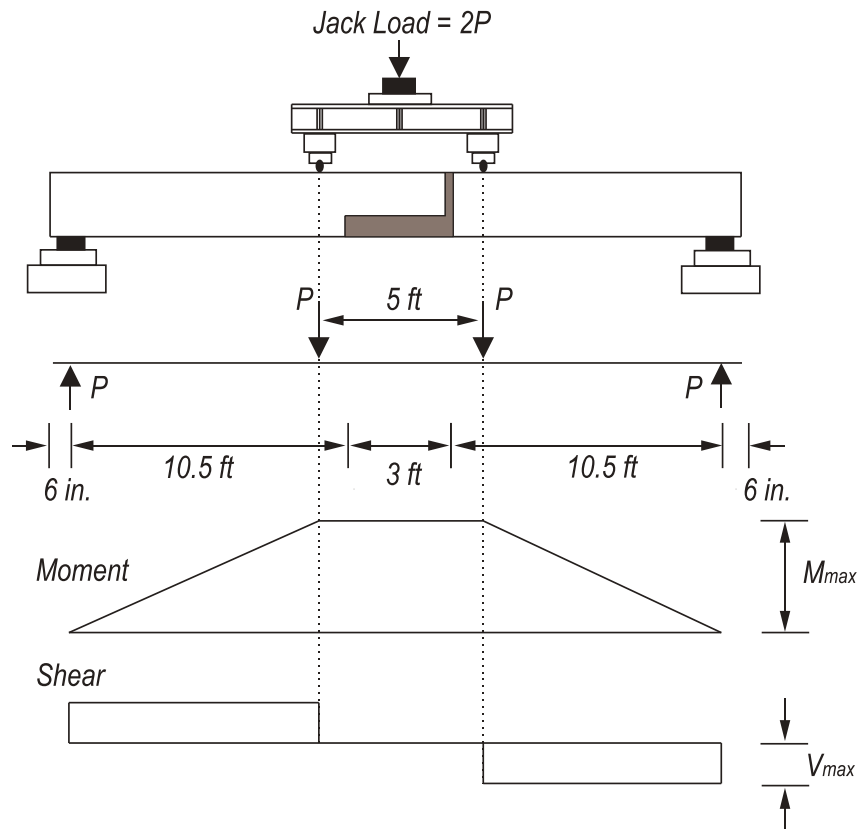


Figure 38–Flexure test set-up

Of primary importance to the long-term performance of the girder is the size and extent of cracking that occurs in the splice when the net tension in the extreme fiber exceeds the cracking strength of the concrete. Such cracking will adversely affect the stiffness and the durability of the girder in the splice region. Although the FIB96 prototype is designed to remain uncracked in service, overloads of a structure do occur. For this reason, cracking behavior of the control versus the spliced test specimens was evaluated.

### 5.3 Moment Strength Test Design

Based on past simple-span highway bridge designs utilizing I-girders (Jaber et al. 2006), a bridge design was developed utilizing FIB96 beams spliced at two locations to achieve a 208-ft simply supported span. Unlike splices for precast I-girder sections in continuous spans, the proposed splice will be located away from any inflection point of the moment diagram and must have significant moment strength. The factored moment in the prototype FIB96 at the splice location (each splice is located 30 ft from a bearing) is approximately 1200 kip-ft.

Because the splice is designed to remain uncracked under service loading, load testing to ultimate strength provides insight into the following performance characteristics for overload conditions, including:

- 1) Splice device (coupler) and strand behavior;
- 2) Crack development;
- 3) Splice stiffness after cracking;
- 4) Changes in the strain field up to capacity;
- 5) Interface issues, including opening of the splice between the precast and cast-in-place concrete;
- 6) Deflections after cracking.

Previous investigation of the FIB54 as a suitable test specimen proved that a shorter section could provide valuable insight into the behavior of the splice region; however, due to concerns regarding the coupler capacity and failure mode, a smaller shape was selected as a test specimen so that more specimens could be constructed, in order to test a variety of loading conditions. Existing equipment in the FDOT structures laboratory can handle an AASHTO Type II cross-section and load it to failure. For these practical reasons, although a deeper FIB section would closer approximate the FIB96 prototype, an AASHTO Type II was chosen as the test specimen. To validate the use of an AASHTO Type II, a moment-curvature analysis was performed to compare the strain states of each cross-section at loads between cracking and ultimate capacity.

Using the high performance compressive concrete strength model as presented in Collins and Mitchell (1991), the tensile concrete strength model by Hsu (1993) and the Ramberg-Osgood empirical steel model presented by Collins and Mitchell (1991) for lo-lax 270 ksi prestressing strand, moment curvature analyses were performed on an AASHTO Type II cross-section and a simplified version (for computation purposes) of the FIB96 cross-section. For this analysis, the prestressing strand was considered to be continuous 270 ksi lo-lax, and the coupler was ignored. This simplification assumes that issues at the coupler can be resolved through additional testing of the coupler, or through selection of an alternate coupler. The entire concrete section was assumed to have a compressive strength of 8.5 ksi. Figure 39 shows the simplified geometry used for calculating section properties of the FIB bottom-flange.

There were 31 strands prestressed to  $0.6f_{pu}$  present in the FIB96 prototype at the splice location (Figure 39).

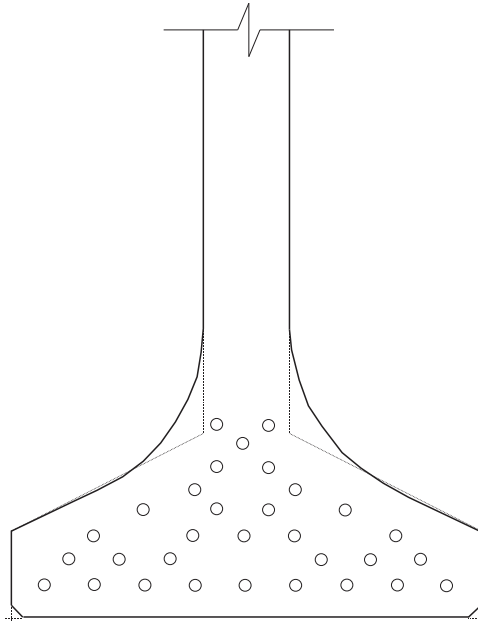


Figure 39–Simplified bottom flange of FIB96 cross-section

To assess its feasibility as a test specimen, a moment-curvature analysis of the AASHTO Type II with a strand pattern of five 270-ksi 0.5-in. diameter lo-lax strands prestressed to  $0.6f_{pu}$  was performed. The AASHTO Type II shape and strand pattern are shown in Figure 31. When the extreme compression fiber was at 0.003, the maximum tensile steel strain in the FIB96 prototype was 0.052 (in./in.) and in the AASHTO Type II test specimen was 0.053 (in./in.).

ASTM A416 tensile testing of 270-ksi lo-lax strand revealed that the steel stress increased approximately 5% from yield to rupture (Figure 40; ASTM A416 2006), though the measured yield and ultimate strengths of the steel samples exceeded those predicted by the Ramberg-Osgood steel model (Collins and Mitchell 1991). Assuming the steel in the splice region follows the Ramberg-Osgood model, both the FIB96 prototype and the AASHTO Type II test specimen began to yield and the prestressing steel stress in each beam reached the stress-strain plateau. The steel strains present at the ultimate capacity of the AASHTO Type II were comparable to those of the full-size FIB96 prototype at its capacity.

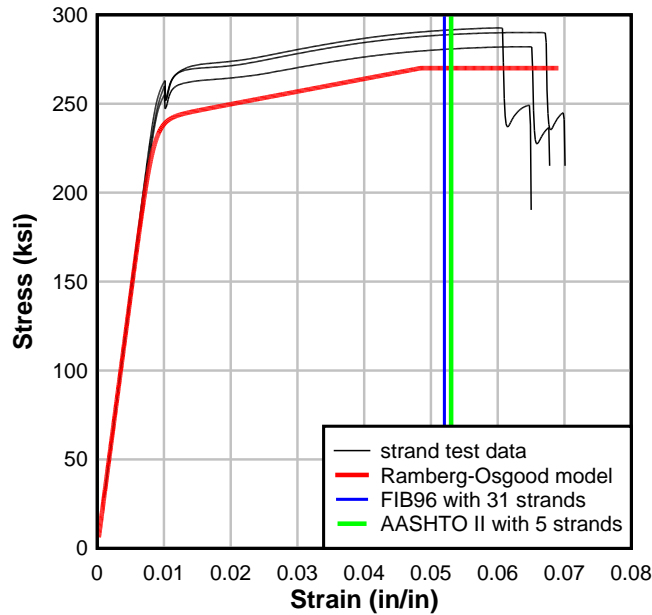


Figure 40–Material properties of 270 ksi lo-lax strand

A scaled representation of the two cross-sections and their respective strain gradients at flexural capacity is shown in Figure 41.

The AASHTO-predicted moment capacity of the test specimen was calculated two ways: assuming the test specimen to be fully bonded and unbonded. Both capacity calculations were performed because the spliced test specimens included unbonded tendons. The bonded flexural capacity of the test specimen is 631 kip-ft; the unbonded capacity is 589 kip-ft. These values do not include the strength reduction factor (phi factor).

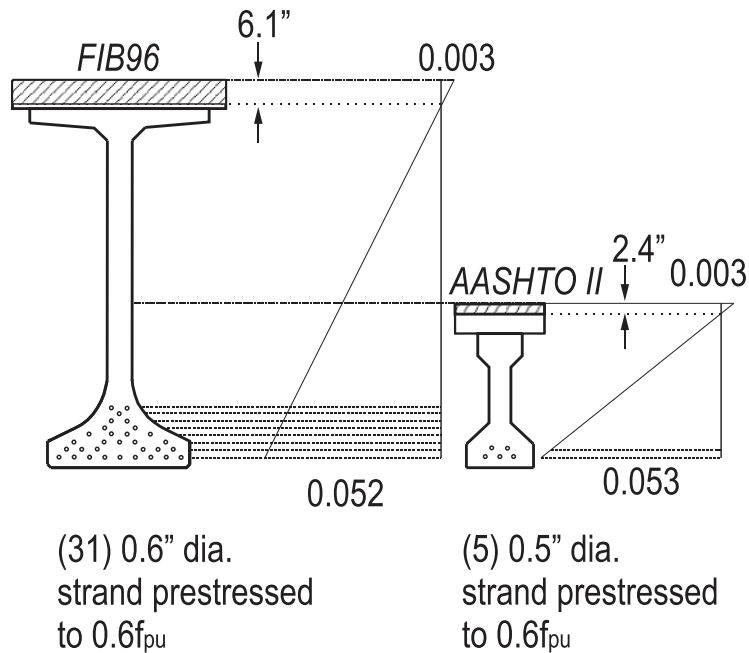


Figure 41–FIB96 prototype vs. AASHTO II test specimen: strain state at flexural capacity

#### 5.4 Shear Test Design

Shear behavior of the splice design was investigated in three spliced specimens. Because the length of the test specimen is much less than the length of the FIB96 prototype, the  $M/V$  ratio could not be matched. Instead, the splice design was tested in a conservative set-up, with a much lower  $M/V$ .

To test the specimen in shear, the shear on the splice region was maximized as much as possible without introducing local effects. To achieve this, one side of the beam was cantilevered to shorten the span, and the main span was loaded in three-point bending. The load point was placed at the midspan of the non-cantilevered span, away from the closure pour. The test set-up is shown in Figure 42.

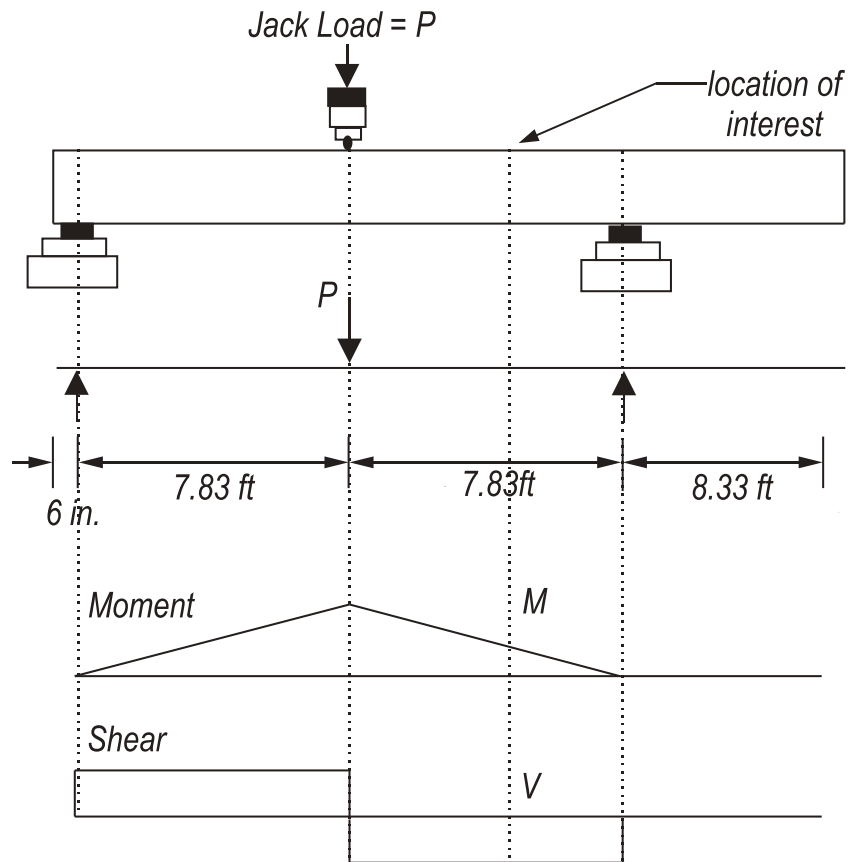


Figure 42–Shear test set-up

The placement of the supports and load points in this orientation ensured that local effects on the splice region were minimized; the applied concentrated load was located as far away from the splice as possible, while still forcing the shear to be greatest across the splice region.

In the prototype design, such direct shear on the splice region would not occur, as the splice region would be located further away from the supports. The selected shear test set-up resulted in a  $M/V$  ratio of 3.7 versus the prototype FIB96 design  $M/V$  ratio of 32.9.

### 5.5 Fatigue Test Design

Fatigue is not a concern if adequate precompression of the splice region can be achieved and maintained such that the service stresses never cause cracking at the splice. However, an overload could cause cracking in the splice region, exposing the splice area to fatigue loading. The mechanical nature of the chosen coupler makes fatigue an important concern; investigation

of the specimen for fatigue was completed to investigate the possibility of brittle failure at the device.

A four-point bending set-up, with the splice region encompassed in the constant moment region, was chosen to investigate the fatigue behavior of the test specimen. The distance of 5ft between the load points was selected to encompass the entire splice region, including all of the closure pour and the couplers. The general test set-up is shown in Figure 38 and is the same set-up used to evaluate static flexural behavior.

All specimens were precracked to expose the critical component—the prestressing strand and the coupler - to the cyclic stress. This approach has been taken in previous research (Rao and Frantz 1996, Russell and Burns 1993, Rabbat et al. 1979). Cracking was determined visually and confirmed by inspection of the load-displacement plot. Cracks were marked prior to load removal.

Decompression tests of each specimen were then performed to evaluate the effective prestress level. Each specimen was statically loaded until the previously formed cracks re-opened. The re-opening of these cracks was determined by the strain readings of gages placed on either side of the crack.

Following the decompressions tests, each specimen was then cycled to evaluate its fatigue life. To assess the test specimen under fatigue loading, the in place state of the FIB96 prototype and the cracking load of the test specimen were used to determine the applied load range. In typical fatigue assessments, the dead load state and the cracking state are used to determine the stress range of the cyclic loading. This approach has been used by other researchers (Russell and Burns 1993, Overman et al. 1984, Roller et al. 1995). Of interest to the current research is the effect of the stress cycling between the in place—dead load only- state of the FIB96 and tensile stress limit—defined in AASHTO-LRFD as limited to  $6\sqrt{f'_c}$  - or the load state associated with cracking. Because the stress range affects the expected life of a beam more than the applied stress magnitude, the dead load of the prototype beam was chosen as the lower load limit, to more closely approximate the stress range expected in the FIB96 prototype. The upper limit of the load was determined based on the cracking load of the test specimen.

The bottom fiber stress in the FIB96 prototype was determined from present dead load and is shown in Table 15. The stress in the FIB96 calculated using the moment induced by the fatigue live load is provided only for reference.

Table 15–Stress state of FIB96: Fatigue

Load case	$f_{bot}$ (psi)
DL only	-50
0.75LL Fatigue	-280

As seen in Table 16, the FIB96 prototype beam at the splice location is designed to remain uncracked in the fatigue load case.

Table 16–Stress state of test specimen: Fatigue

Load Level	$f_{bot}$ (psi)	Moment (kip-ft)	Applied Load (kip)
Specimen DL	468	n/a	n/a
Specimen DL + Preload = Prototype DL	-50	200	42
$6\sqrt{f'_c}$	-553	392	83
$7.5\sqrt{f'_c}$	-691	445	94

The fatigue test parameters were determined by stress matching to equate the stress range in bottom fiber of the test specimen to the calculated stress range in the prototype beam expected between the dead load state and cracking load of the test specimen. Using these two stress states, the load to be applied was calculated and is presented in Table 17.

Because the test specimens have less dead load stress at the bottom fiber than that of the FIB96, a minimum superimposed load must be maintained during fatigue cycling to match the FIB96 dead load stress state. Matching the stress in the bottom fiber, the preload required to match the dead load stress state of the FIB96 prototype is 42 kip–rounded down to 40 kip for simplicity.

Table 17–Loading procedure: Fatigue

Specimen	Lower Limit Load (kip)	Upper Limit Load (kip)	Load Application
FC	40	72	0.2 kip/sec until the mean load of 56 kip was reached. Load amplitude was increased to target load range over 400 cycles.
F1	40	54	0.2 kip/sec until the mean load of 47 kip was reached. Load amplitude was increased to target load range over 200 cycles.
F2	40	72	0.2 kip/sec until the mean load of 56 kip was reached. Load amplitude was increased to target load range over 200 cycles.

The upper limit load was determined on a specimen-by-specimen basis. The load at cracking, as determined from inspection of each specimen’s load-displacement plot, was used as the upper limit load for the control specimen (FC) and the first spliced specimen (F1). Because the stress range of F1 was lower than that of FC, the second spliced specimen (F2) was tested using the load range of the control. In this way, the disparate effective prestress values of the control and spliced specimens were eliminated as a variable.

Following the fatigue testing, each test specimen was statically loaded to failure in the same four-point bending set-up to assess the effects of fatigue degradation.

## **6 Specimen Construction and Splice Assembly**

The intent of this research is to develop and assess a splice design simple enough to be assembled without a subcontractor, for use in future construction projects without needing to post-tension. Throughout the development of the splice for the FIB96 prototype, the ease of the precast segment construction and the splice assembly procedure was considered, guiding development of details, coupler selection, and strand layout. Section 6.1 describes the precast segment production.

Assembly of the splice in the AASHTO II test specimen in the laboratory provided an opportunity to evaluate and adjust the procedure. Dimensions and lay-out of the assembly frame set-up for the splice procedure is described in Section 6.2. The general splice assembly is described in Sections 6.3, 6.4, and 6.5.

### **6.1 Segment Production**

Fifteen precast pretensioned beam segments were constructed at a precast concrete plant. Three beams 25-ft long were constructed as control beams (Specimens 1-3). Six segments with bonded prestressing 13.5 ft long (referred to as segments 4b-9b) and six segments with PVC pipes (in future strand locations; referred to as segments 4u-9u) 11-ft long were also constructed, to be spliced together at the laboratory to form a 25-ft long completed beam (Figure 43). The control beams and bonded segments were constructed in the first pour; due to space limitations and safety concerns regarding completely unbonded strand, the unbonded segments were constructed in a separate pour.

To reduce the likelihood of strand recoil during detensioning, segments for the first pour were arranged in the bed as shown in Figure 43; segments were located close to one another, but away from the abutments.

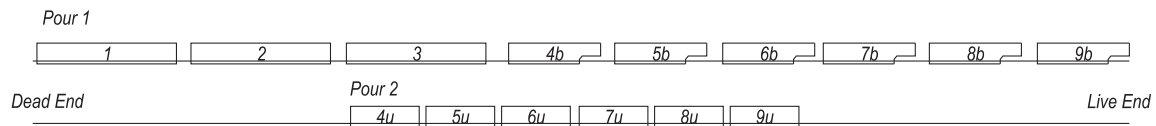


Figure 43–Bed layout

The prestressing strands were stressed to  $0.6f_{pu}$ ; the relatively low level of prestress also acted to reduce the likelihood of strand damage during detensioning. The prestressing report and detensioning sequence are given in Appendix E–Precast Yard and Material Reports. The mild steel reinforcement was tied in, with particular care taken in the coped regions of the bonded segment. The plywood block-out served to form the coped area and protect the protruding strand. Holes were drilled into the block-out to allow for straight-ended stirrups to be placed in this region. Epoxy was used to seal holes to prevent leakage of concrete paste into the wooden block-out.

Following stirrup placement, pipe inserts were aligned and secured with tie wire. Reinforcing bars used to fix the pipe inserts were also used to tie the fixture into place. The pipe assembly was then leveled and supplementary reinforcing bars were tied in to further secure the pipe insert placement. Following the installation of the pipe inserts, the side forms were locked into place. The pipe assembly fit snugly against the side of the forms to prevent intrusion of paste during concrete placement.

A high slump concrete mixture was used to ensure good flow around the congested areas near the pipe inserts. The same concrete mixture design was used for both pours; the mix design and field properties are provided in Appendix E–Precast Yard and Material Reports. The concrete was consolidated with internal and side-form vibrators. Care was taken near

instrumented rebar to ensure gage integrity. The tops of the beams were roughened for future deck placement and the bed was covered with tarps for the curing period. The dates of strand stressing, casting and detensioning are given in Table 18. Identification of which segments correspond to which testing specimens is given in Table 19.

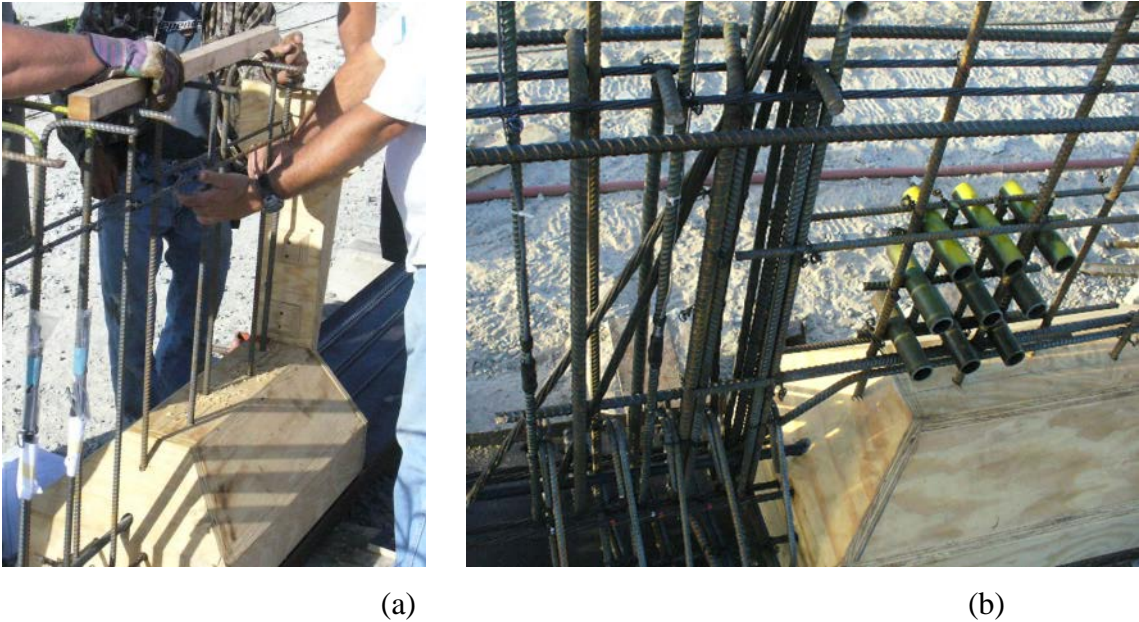


Figure 44–Coped region of bonded segments (a) stirrup placement and (b) pipe insert



Figure 45–Segments after concrete is cast with top roughened for deck placement

Table 18-Construction and testing schedule

Segment	Strand Stressed	Concrete Cast	Strand Detensioned	Splice Assembled	CP Cast	Deck Cast
1	3/20/2012	3/22/2012	3/26/2012	n/a	n/a	08/07/2012
2	3/20/2012	3/22/2012	3/26/2012	n/a	n/a	08/07/2012
3	3/20/2012	3/22/2012	3/26/2012	n/a	n/a	12/13/2013
4b	3/20/2012	3/22/2012	3/26/2012	9/13/2012	9/19/2012	10/02/2013
5b	3/20/2012	3/22/2012	3/26/2012	10/19/2012	10/24/2012	11/06/2012
6b	3/20/2012	3/22/2012	3/26/2012	2/27/2013	3/01/2013	03/21/2013
7b	3/20/2012	3/22/2012	3/26/2012	2/8/2013	2/12/2013	02/22/2013
8b	3/20/2012	3/22/2012	3/26/2012	1/11/2013	1/16/2013	01/31/2013
9b	3/20/2012	3/22/2012	3/26/2012	11/30/2012	12/4/2012	12/13/2012
4u	3/26/2012	3/27/2012	3/30/2012	1/11/2013	1/16/2013	01/31/2013
5u	3/26/2012	3/27/2012	3/30/2012	10/19/2012	10/24/2012	11/06/2012
6u	3/26/2012	3/27/2012	3/30/2012	2/8/2013	2/12/2013	02/22/2013
7u	3/26/2012	3/27/2012	3/30/2012	11/30/2012	12/4/2012	12/13/2012
8u	3/26/2012	3/27/2012	3/30/2012	2/27/2013	3/01/2013	03/21/2013
9u	3/26/2012	3/27/2012	3/30/2012	9/13/2012	9/19/2012	10/2/2013

Table 19–Specimen IDs

Specimen	Segments	Load Test
XC	1	08/24/2012
SC	2	01/04/2013
FC	3	01/30/2013
X1	4b-9u	10/18/2012
SB	5b-5u	11/16/2012
SU	9b-7u	12/20/2012
SU2	8b-4u	02/08/2013
F1	7b-6u	03/06/2013
F2	6b-8u	04/15/2013

The specified concrete strength for transfer,  $f'_{ci}$ , was 6000 psi. The specified compressive strength at 28-days,  $f'_c$ , was 8500 psi. The tested 32-day compressive strengths for the first concrete pour (specimens 1-3 and segments 4b-9b) was 8990 psi; for the unbonded segments completed in the second pour ((segments 4u-9u), the tested 28-day compressive strength was 10700 psi.

Rather than flame-cutting the strands (typical procedure), they were released slowly using a single-strand jack at the live end. After the live end was slack, the strand at the dead end was cut using a plasma torch. No beam movement was visually observed during this process and the

portions of the strands in the cope (that would receive the strand coupler) were not permanently deformed. Completed segments were shipped to the FDOT Structures Laboratory in Tallahassee, FL for splice assembly, deck placement, and load testing.

## **6.2 Segment Assembly Frames**

Pushing the segments apart with hydraulic jacks placed eccentric to the strand centroid created an internal moment. This internal moment caused uplift that was resisted by the structural steel frames and tie-down connections shown in Figure 46. Four steel frames were positioned and bolted to the strong-floor using 1.5-in. diameter threaded rod. Two interior frames were used as tie-downs, resisting the uplift force during the stressing procedure. All four frames were designed to resist beam roll-over and to guide the longitudinal movement of the rolling segment during stressing. Tie-down connections were positioned and welded onto their respective frames. The fixed tie-down connection was constructed of steel plate with a load button receiver welded to a pair of channels bolted to Frame F. The roller tie-down connection was constructed by welding a Hilman roller to a steel plate, which was then welded to a pair of channels bolted to Frame R. To ensure smooth translation of the rolling beam, the Hilman roller was leveled prior to welding it to the frame.

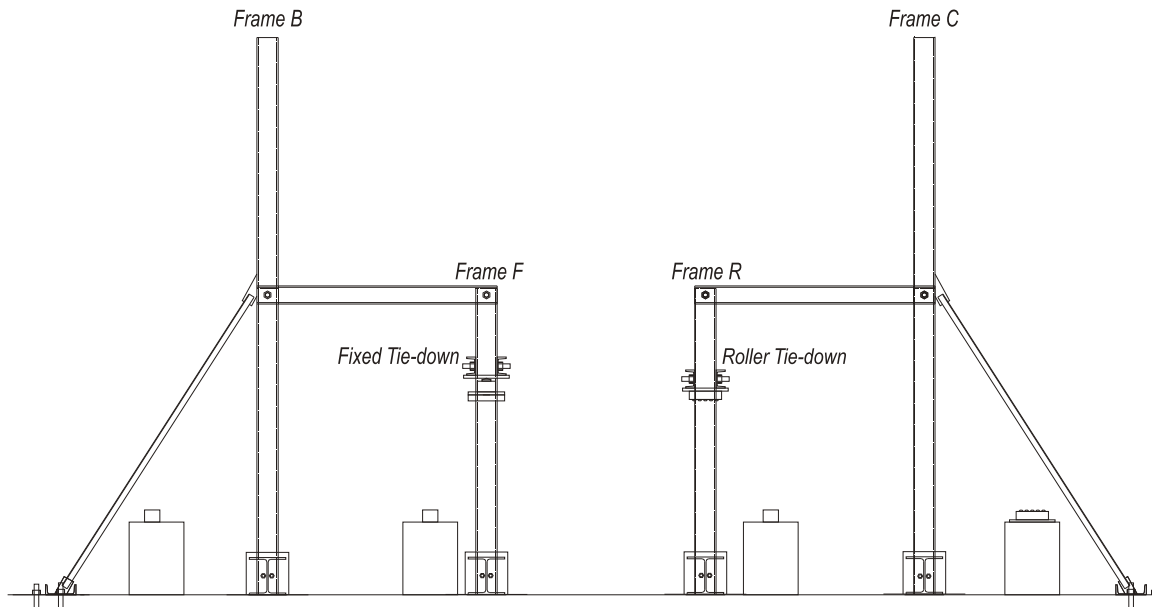


Figure 46–Elevation of assembly frames

### 6.3 Segment Alignment Procedure

Figure 47 shows the placement of the segments along with the strand couplers, beam brackets, and stressing jacks. Segments were maneuvered into position within the assembly frames and set down on their respective supports. The bonded segment was supported at both ends by wooden blocks set on steel blocks. The left end of unbonded segment was supported by a wooden block set on a steel block; the right end of the bonded segment was supported by a Hilman roller welded to a steel block. During the stressing procedure, the beam segments lift off the temporary supports; wood was selected to allow their easy removal.

Segments were then aligned within the frames and relative to one another. To ensure even distribution of uplift force, the segments were first oriented laterally within the frames, centering the beam segments' major axis under the tie-down points of Frames F and R. The beam segments were then aligned longitudinally with one another, ensuring a 5-in. gap between the two segments at the top of the closure gap. Finally, the heights of the segments were adjusted to ensure that the strands to be coupled were in alignment. The height of the prestressing strand was used as the controlling point of reference because each beam segment was of slightly different dimensions; aligning the centroid of the strand provided non-eccentric line of action for the induced prestressing force.

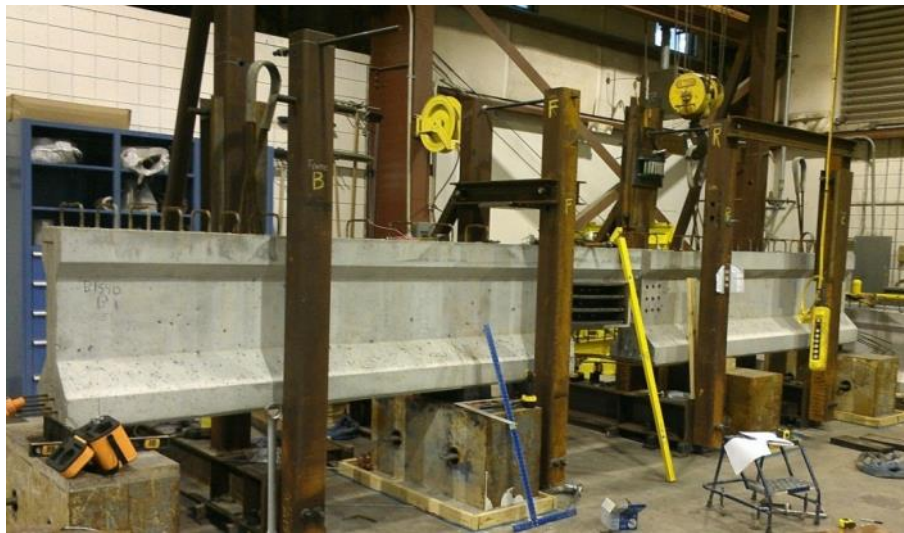
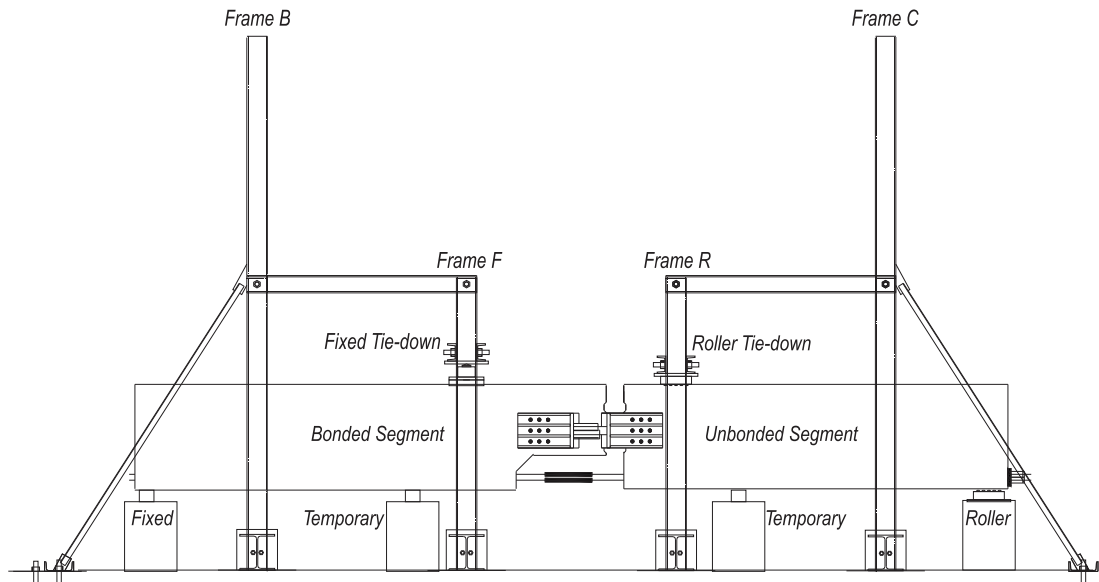


Figure 47—Photo and schematic of splice assembly frame and beam segments

Once the beam segments were aligned, the wooden cribbing was adjusted to allow unrestrained longitudinal movement of the segments along the segment's main longitudinal (same direction as the beam span). The load cell at the fixed tie-down was slid into position and the load button was unthreaded to touch the load button receiver. Proper alignment of this tie-down was critical to prevent rotation of the bonded segment and to ensure accurate readings in the load cell. The prestressing jacks (Enerpac CLL 504s) were placed into the bracket cradles on each side of the segments. Hydraulic hand pumps were attached and set aside.

Strand couplers were adjusted to have approximately 1 in. of thread visible on either side of the turnbuckle, to ensure adequate length for later adjustment. Couplers were first installed on

the strand protruding from the bonded segment. Engagement of the wedges in the coupler was checked by hand. Couplers were then attached to the strand protruding from the unbonded segment (Figure 48). Engagement of the coupler wedges was again checked by hand. At this point, the coupled strands were not taut in the closure pour region and occasionally appeared to bend across the closure pour length (Figure 49). Next, rebar couplers were attached to the rebar protruding into the notch. The couplers were used to attach the bottom hook of the stirrups in the splice region (Figure 50).



Figure 48–Coupler installation on unbonded strand



Figure 49–Coupled strand prior to prestressing



Figure 50–Coupled stirrups

Next, hardware was attached to the end of the unbonded segment. With the string-pots loose, the prestressing jacks were simultaneously pressurized until they engaged the brackets on each side of the unbonded segment. The lock-nuts were engaged and hydraulic pressure was released from the jacks. This was done to prevent translation of the unbonded segment on the Hilman roller during attachment of the hardware and initial adjustment of the coupler turnbuckles.



Figure 51–Extend plunger

The detensioning chair (Figure 52) was then threaded onto the protruding strand from the unbonded segment. The chair was shimmed to the proper height and leveled to provide clear passage of the prestressing strand through each hole. Chucks, load cells, and anchor plates were then installed.



Figure 52–Detensioning chair, chucks, and load cells on the unbonded segment

Prestressing strand couplers were then tightened to hold the detensioning chair against the unbonded segment (Figure 53.). One person was required to adjust each turnbuckle in the closure pour until the coupled strand was taut while the second person monitored and adjusted the alignment of the detensioning chair, the load cells and the prestressing chucks. Proper positioning of the hardware included clear, unrestrained passage of the prestressing strand through the detensioning chair and the load cells; unobstructed placement of each prestressing chuck relative to one another; and flush seating of the detensioning chair on the end of the beam.



Figure 53–Tightening the turnbuckles to seat detensioning chair

With unbonded strands secured with chucks at both ends, an initial load was put into each strand to straighten the prestressing strand across the closure gap, and to provide an “even” starting point for later stressing. This was done by adjusting the turnbuckles on each coupler, alignment of the detensioning chair was monitored to ensure that the protruding strand passed clear through the detensioning chair and the load cells without obstruction. In addition, the load cell and coupler strain gage output were monitored. Alignment of the load cells was monitored to ensure that they were bearing evenly on the detensioning chair and the prestressing chucks. Approximately 1 kip of load was achieved in each strand, or approximately 100 microstrain per coupler. Equalization of the force in each strand was an iterative process, requiring several adjustments to each turnbuckle, as each adjustment affected the force in the nearby strands.



Figure 54–Tightening the turnbuckles

#### 6.4 Strand Stressing

Following initial preloading, the string-pots across the gap between the segments were connected. Preload in each of the load cells was noted, as well as initial strain in the coupler strain gages. The DAQ was zeroed, stressing was initiated, and data acquisition was started. The prestressing jacks were pressurized synchronously with care taken to ensure the splice was stressed evenly. Pressure was held at 100 psi, then every 500 psi until 5600 psi, which corresponded to approximately 25 kip per prestressing strand (approximately 0.6 f.pu).

At 5600 psi, the lock-nuts on both actuators were hand-tightened. In cases where the string-pots at the bottom of the closure indicated 1-in. of displacement prior to achieving 5600 psi in the prestressing jacks, the procedure was halted and the lock-nuts were tightened early. In cases where the gap opening between the segments and the load cell readings were both low, jacking was continued until the jack pressure reached 6100 psi. The hydraulic pressure was then simultaneously and slowly released from the jacks.

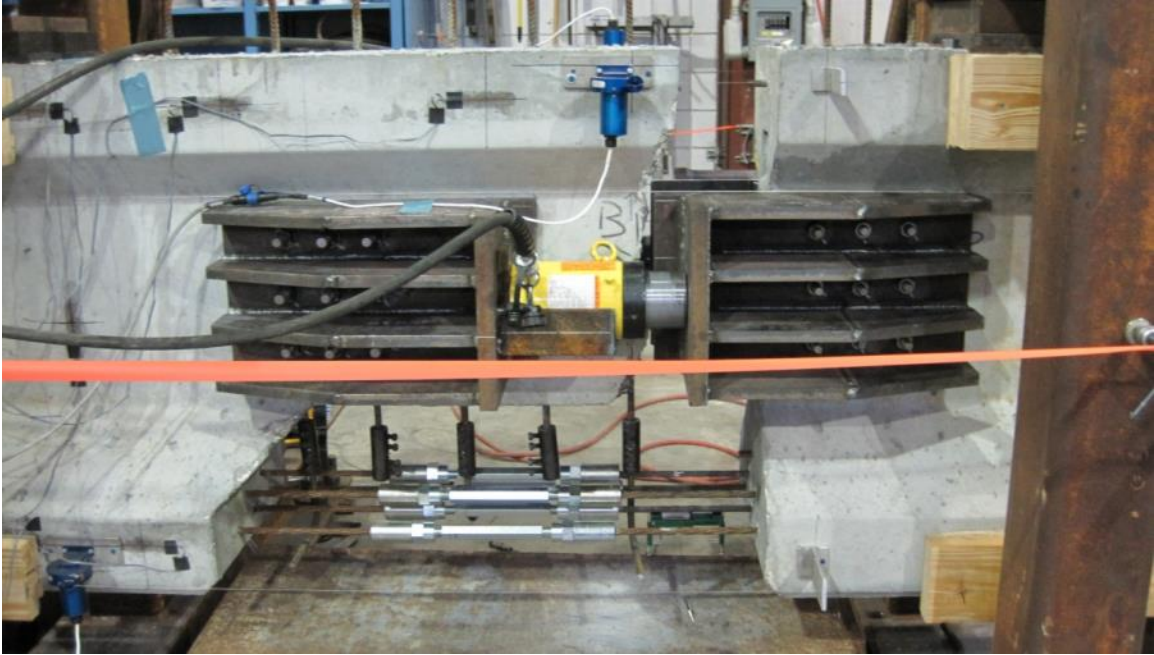


Figure 55–Splice stressed with lock-nuts engaged

### 6.5 *Formwork and Concrete Placement*

Formwork for the closure pour was then attached to the beam segments (Figure 56). The closure pour formwork consisted of two forms for the top flange, two forms for the bottom flange, a long form for the bottom of the beam and small pieces of plywood for the region between the actuators. Side forms were attached to the precast beam using expansion anchors and concrete screws. The bottom form was wedged into place, supported underneath by a steel support block. Seams were caulked and/or duct taped with foam backer rod to prevent leakage during the pour (Figure 57).



Figure 56–Closure formwork in place



Figure 57–Seams sealed

Concrete was lifted using 5-gal. buckets and tremied into the closure with the aid of a plastic traffic cone (Figure 58). The cone was wedged deeply into the form at the start of the pour, and as the concrete level rose, the cone was slowly extracted to mitigate segregation of the mix and void formation.



Figure 58–Pouring the closure

A hand-held vibrator was used to vibrate the accessible parts of the pour; however, limited vibration of the closure concrete was possible due to hardware congestion and the placement of instrumentation.



Figure 59–Top of finished closure pour

The concrete was allowed to cure until the tested compressive strength—as determined by ASTM C39 tests of 6X12 cylinders made from concrete from the same delivery—reached approximately 8500 psi (ASTM C39 2010). This limit was chosen to make sure the concrete developed some tensile strength prior to removal of the prestressing actuators (during which a

small amount of tension is introduced into the joint). The formwork was then removed from the splice region (Figure 60).



Figure 60–Formwork removed (Specimen X1 shown)

To remove the prestressing actuators, the jacks were pressurized until the lock-nuts could be loosened with a spanner wrench. In each case, the pressure required to free the lock-nuts was approximately equal to the pressure in the actuators when the lock-nuts were tightened. Jacks were re-pressurized slowly while monitoring the load in the strand load cells. This was to avoid creating tensile stress in the fresh concrete and potentially cracking the splice concrete.

Tie-down forces were then released. A jack was placed under the beam as near to the support under the bonded segment as possible. The inner support points (wooden supports) were removed to reduce restraint. The jack under the bonded segment was pressurized until the neoprene pad under the beam could be removed. Pressure was then released, which lowered the beam end sufficiently to remove tie-down forces at frames F and R. The stressing brackets were removed, and the assembled beam was removed from the assembly frames, completing the splice procedure.

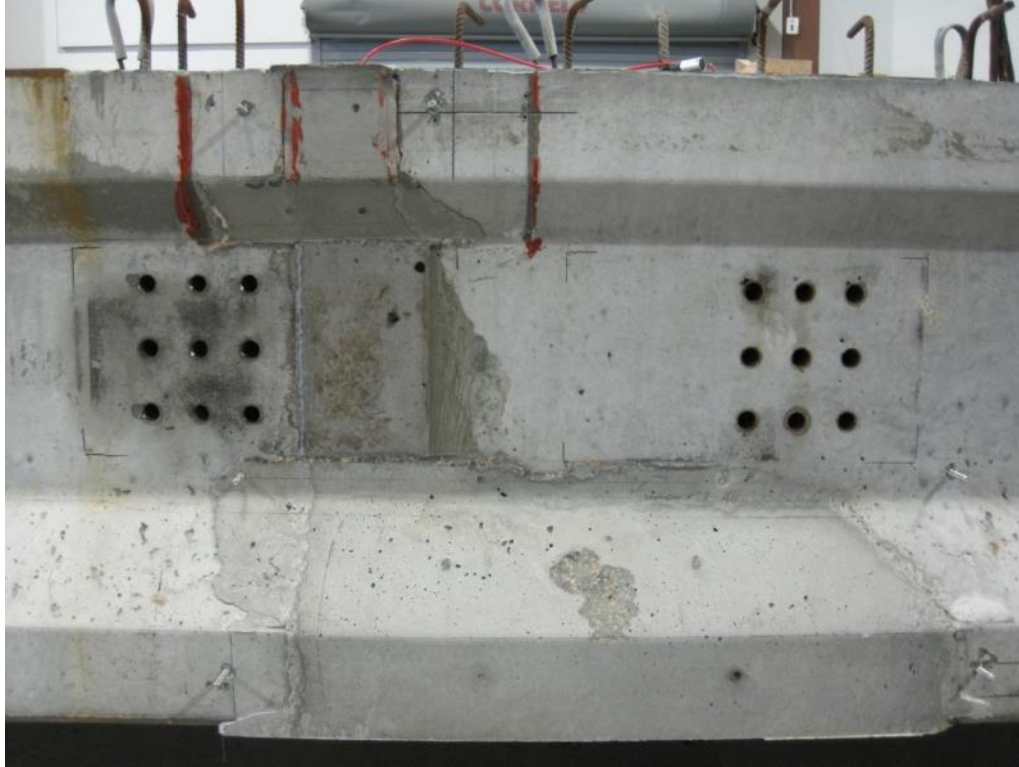


Figure 61–Splice complete

### 6.6 *Splice Modifications*

Several modifications were made to the splice design as specimens were completed and tested. Modifications included: scoring of the closure pour faces with a grinder, the inclusion of an additional rebar in the closure pour, and the use of epoxy on the faces of the closure pour.

After the first two splice assemblies (X1), the precast faces of the closure pour of the remaining spliced beams (SU, SU2, F1 and F2) were scored using a cutting disk. This was done based on the clean break occurring in specimen X1, shown in Figure 62(a) (the first assembled beam).

In specimens SU2, F1 and F2, an additional stirrup was included in the closure to increase the shear capacity of the splice region. The additional stirrup was centered in the vertical portion of the pour and can be seen in Figure 63.

Epoxy was not used in the first three splice assemblies (X1, SB, SU). Figure 62(a) shows the closure after demolition; it can be seen that—for the most part - the closure pour concrete broke away cleanly at the joint. In later specimens (SU2, F1 and F2), an epoxy (Master Builders Concreive Liquid LPL) was used to improve the bond.

Figure 64 shows view of the epoxy application. Approximately 10 minutes prior to the arrival of the closure pour concrete, the epoxy was mixed and applied to the joint. The epoxy was applied from above and below the beam, using a bristle paintbrush. Care was taken to cover the entire surface area with a generous coat. Following the application of the epoxy, the closure was poured; the pour was completed within one hour of epoxy application.

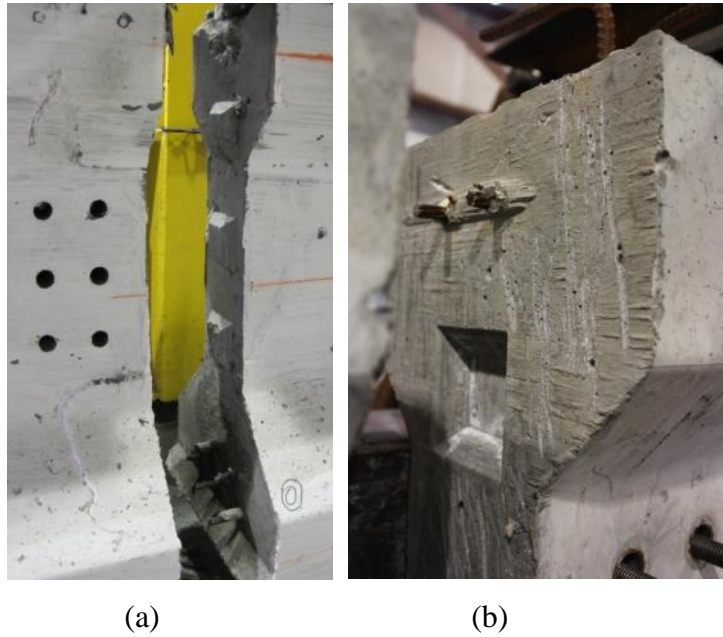


Figure 62–(a) Bond at vertical interface X1 (b) scoring of SU

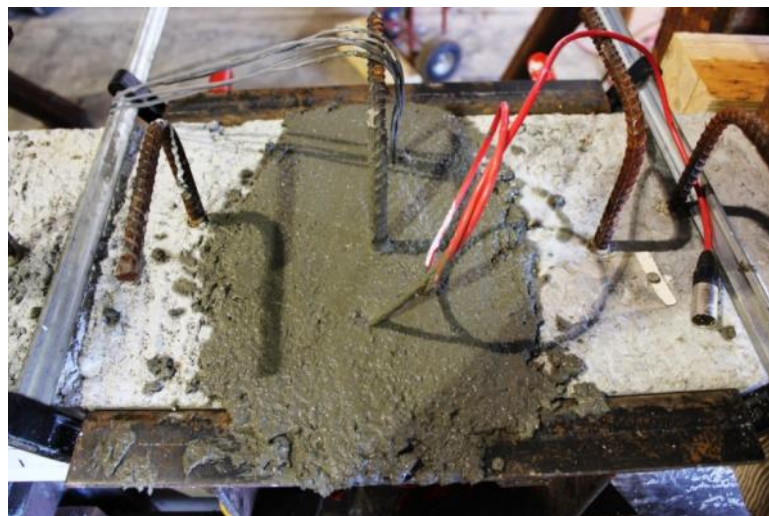


Figure 63–Additional stirrup



Figure 64–Epoxy in closure pour

## 7 Test Procedure and Instrumentation

This section describes the testing procedure and installed instrumentation used in each of the test specimens. In total, six spliced beams were assembled in the laboratory; data was recorded during each splicing procedure. The instrumentation for the splice assembly procedure is covered in Section 7.1; the splicing procedure is described in Chapter 6. One control and two spliced beams were tested in flexure; the instrumentation and testing procedure are covered in Section 7.2. One control and three spliced beams were tested in shear and are presented in Section 7.3. One control and two spliced beams were fatigue tested and are covered in Section 7.4.

### 7.1 Construction and Splice Assembly

Internal gages of two types were included in the specimens during the precasting: foil strain gages and vibrating wire strain gages. The foil strain gages were included to monitor strain in the stirrups during the splice assembly procedure. The vibrating wire strain gages were installed to monitor prestress losses over time, as well as strain changes during the load tests.

A single 3 mm foil strain gage was glued to two prepared rebar stirrups in the laboratory. These are shown in Figure 65. The stirrups were provided to the precaster for inclusion during the construction of the precast segments. The gaged stirrups were located at the assumed tie of the strut-and-tie model used to design the segment for the splice assembly.

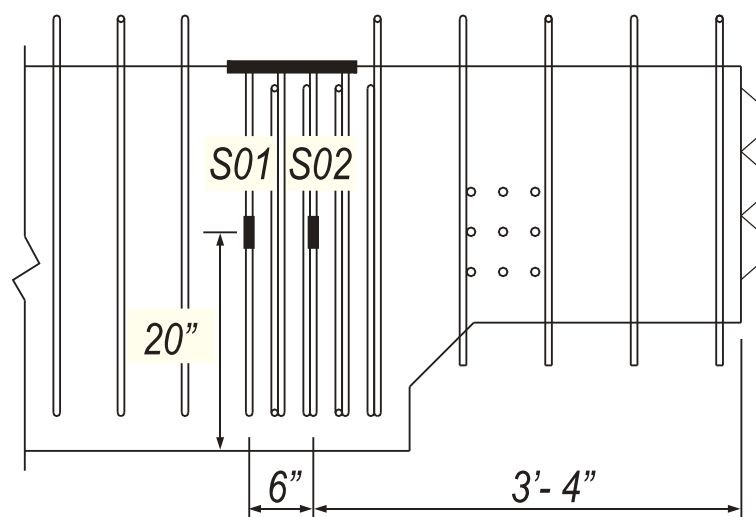


Figure 65–Gaged stirrup locations

Prestress losses were monitored using vibrating wire strain gages (VWSG). During precast construction, gages were installed at the midspan of the control specimens (Segments 1-3) and the bonded segments for the spliced specimens (Segments 4b-9b). VWSG readings were taken prior to and after detensioning to measure the compressive strain in the concrete caused by the prestressing on the section at the time of detensioning; from this an estimate of elastic losses resulting from shortening was calculated. VWSG readings were also taken just prior to load testing to estimate the time-dependent losses that occurred between detensioning and load testing.

During the splice assembly in the laboratory, a gage was installed near the midspan of the full spliced beam length prior to the closure pour. In all cases, the VWSG was installed at the approximate height of the strand pattern centroid. The locations of the VWSGs are shown in Figure 66. To ensure each VWSG remained at the set height, cable ties were used to attach the VWSG to the prestressing strand as shown in Figure 67.

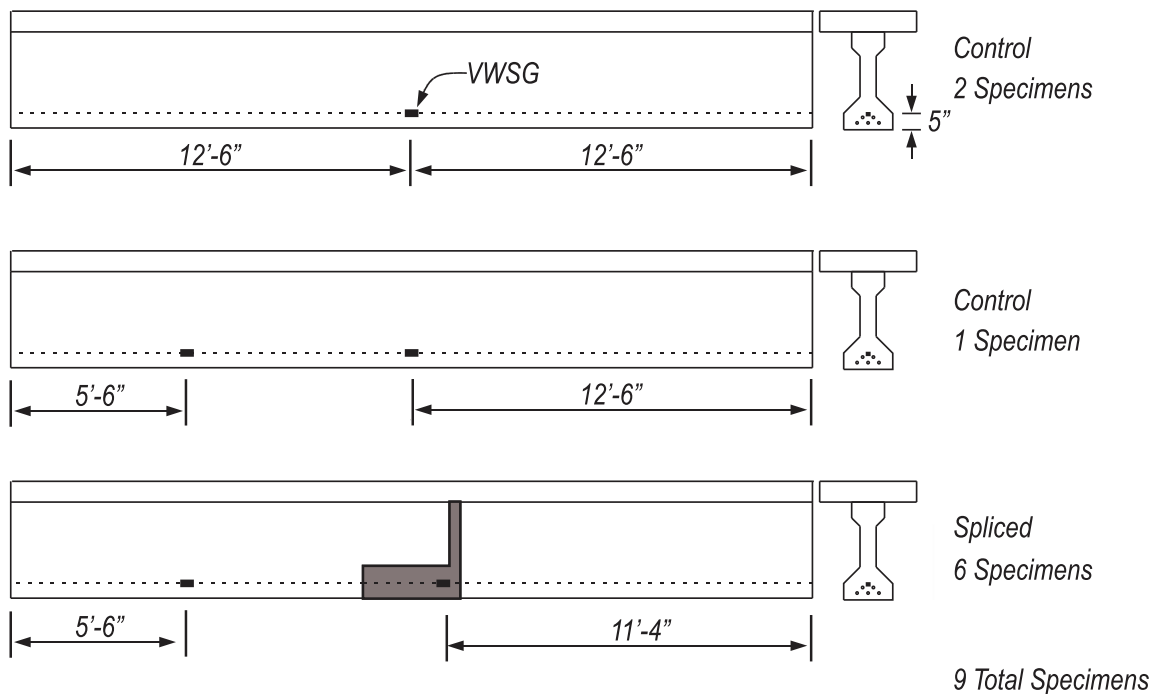


Figure 66–Placement of VWSG



Figure 67–VWSG installation near centroid of strand pattern

Readings were taken with a single-channel Geokon Model GK403 readout box at key points during the construction process and prior to load testing to assess the prestress losses.

Six spliced beams were assembled in the laboratory. Each specimen was arranged in the assembly set-up as shown in Figure 47. Each of the six splice assemblies was instrumented for evaluation of the splice technique and the effect of splicing on the precast segments. Strain, strand slip, load at the fixed tie-down, longitudinal opening at the splice location, and vertical displacement were monitored throughout the stressing of the spliced strand. Four 200 mm displacement transducers were used to monitor vertical displacement. One was placed over each of two exterior bearing to measure the support displacement and one was placed at each of the two tie-down locations. Five strand slip gages were placed on one end of each strand to monitor strand slip. For all but the first splice assembly, strain gages were placed on the flat face of the coupler turnbuckle to indirectly monitor strand load. Load was recorded in conjunction with the strain, strand slip and displacement data. A single vibrating wire gage at midspan of the bonded segment was monitored during loading, with readings taken manually at specified intervals during the strand stressing procedure.

The coupler strain gages (on the face of the turnbuckle with a lead wire coming out) and the VWSG (the blue gage to the right) in the closure pour are shown in Figure 68. Strain gages are shown in Figure 69. Placement of the vertical displacement gages is shown in Figure 70

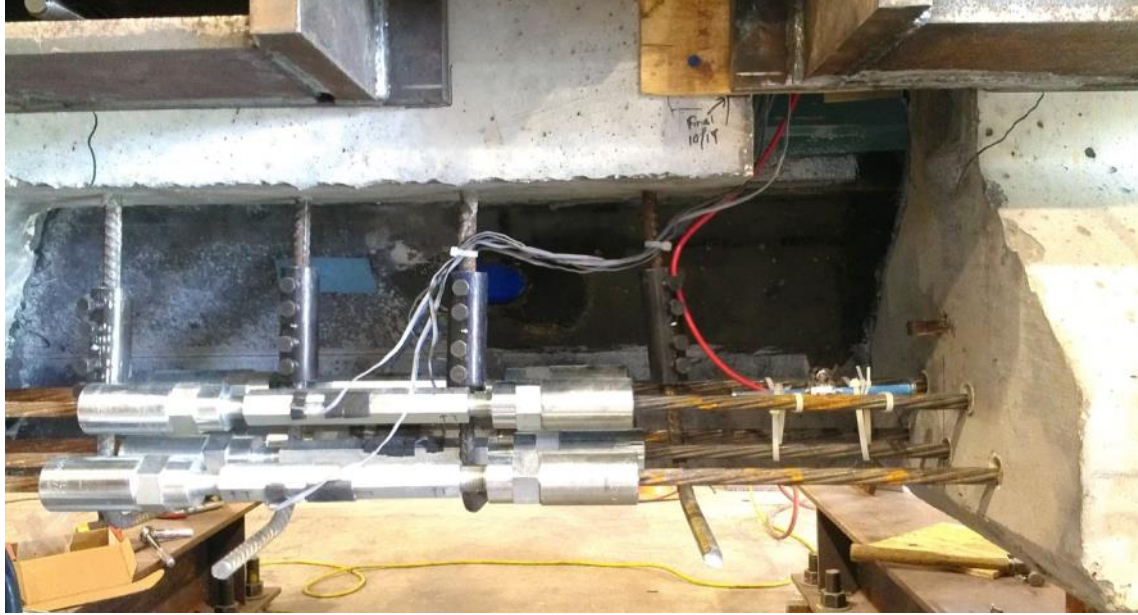


Figure 68–Splice assembly: Instrumentation in closure joint

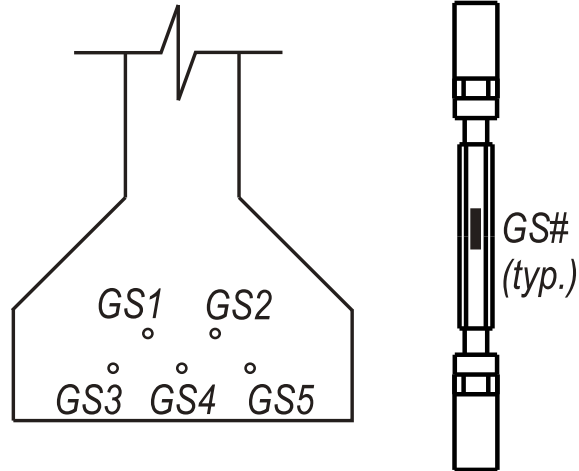


Figure 69–Splice assembly: Coupler strain

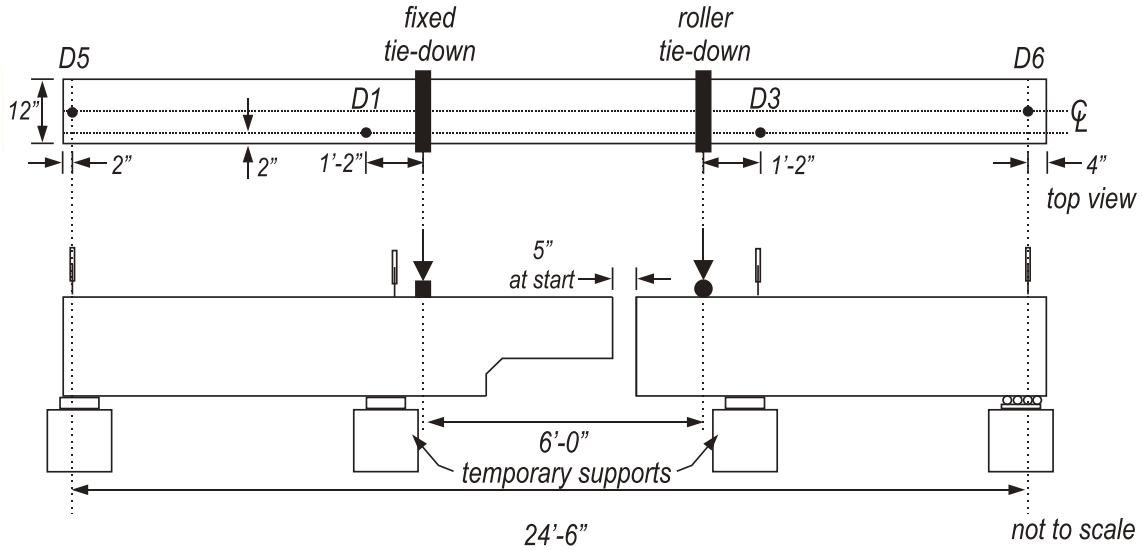


Figure 70–Splice assembly: Vertical displacement gages

The opening at the gap between the two segments was monitored with string-pots. Placement of the string-pots is shown in Figure 71. Relevant dates and ID information for the spliced specimens is given in Table 20. The strand stressing procedure is described in Section 6.4.

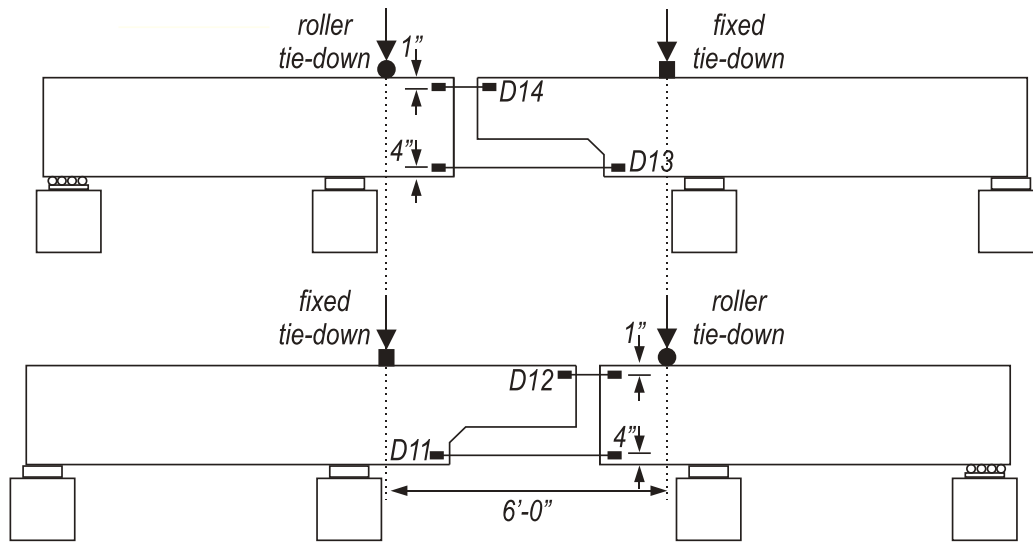


Figure 71–Splice assembly: Longitudinal displacement string-pots

Table 20–Spliced specimens

Specimen	Bonded Segment	Unbonded Segment	Strand Stressed	Closure Poured	Closure Pour Stressed	Deck Pour	Load Test
X1	4b	9u	09/13/2012	09/19/2012	09/26/2012	10/02/2012	10/18/2012
SB	5b	5u	10/19/2012	10/24/2012	10/30/2012	11/06/2012	11/16/2012
SU	9b	7u	11/30/2012	12/04/2012	12/10/2013	12/13/2012	12/20/2012
SU2	8b	4u	01/11/2013	01/16/2013	01/28/2013	01/31/2013	02/08/2013
F1	7b	6u	02/08/2013	02/12/2013	02/19/2013	02/22/2013	03/06/2013
F2	6b	8u	02/27/2013	03/01/2013	03/08/2013	03/21/2013	04/15/2013

## 7.2 Flexure

Four-point bending flexure tests were performed on one control beam with continuous prestressing and one spliced specimen with coupled prestressing strand. The control specimen is referred to as XC; the splice specimen is referred to as X1. A spreader beam was used to create a constant moment region encompassing the spliced region. The specimens were arranged in the test set-up as shown in Figure 72.

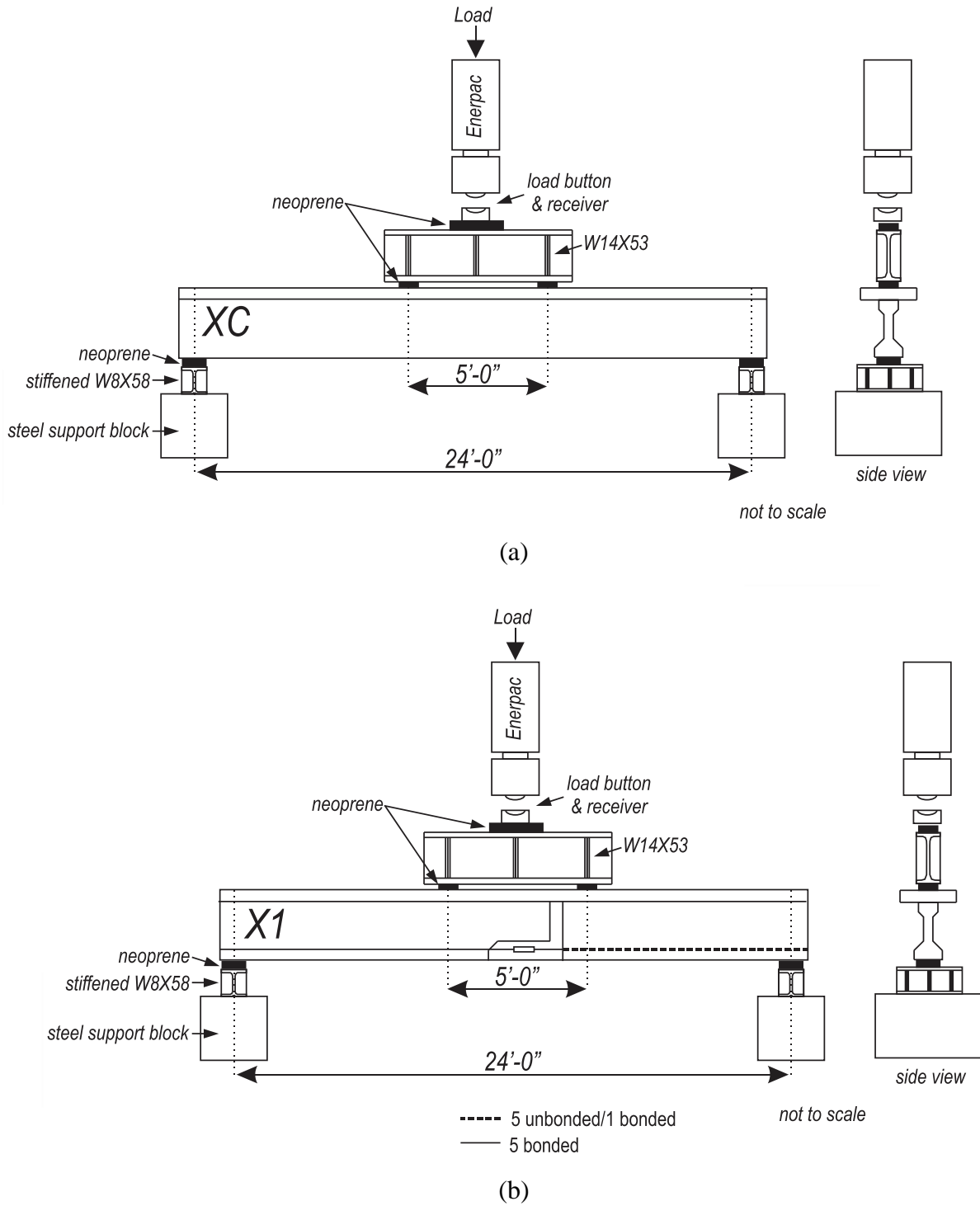


Figure 72–Four-point flexural test set-up: (a) XC and (b) X1

Strain, strand slip, load, and displacement were monitored throughout the test. Seven 200 mm displacement transducers were used to monitor vertical displacement during testing. Two

were placed at either side of the load point of the spreader beam, one was placed at midspan and one was placed over each bearing to measure the support displacement. Six 50 mm displacement transducers were used to monitor out-of-plane displacement during testing. Five strand slip gages were placed on one end of each strand to monitor strand slip. Load application was recorded in conjunction with the strain, strand slip and displacement data. A single vibrating wire gage at midspan was monitored during loading, with readings taken manually at specified load intervals.

Placement of the vertical displacement gages is shown in Figure 73. Placement of the out-of-plane displacement gages are shown in Figure 74.

Specimen X1 had additional instrumentation to monitor splice behavior. Three load cells monitored the prestressing strand load and were placed on the bottom three strands (Figure 75). Four string-pots spanning the closure pour length were also monitored, measuring longitudinal displacement along the beam axis (due to crack opening).

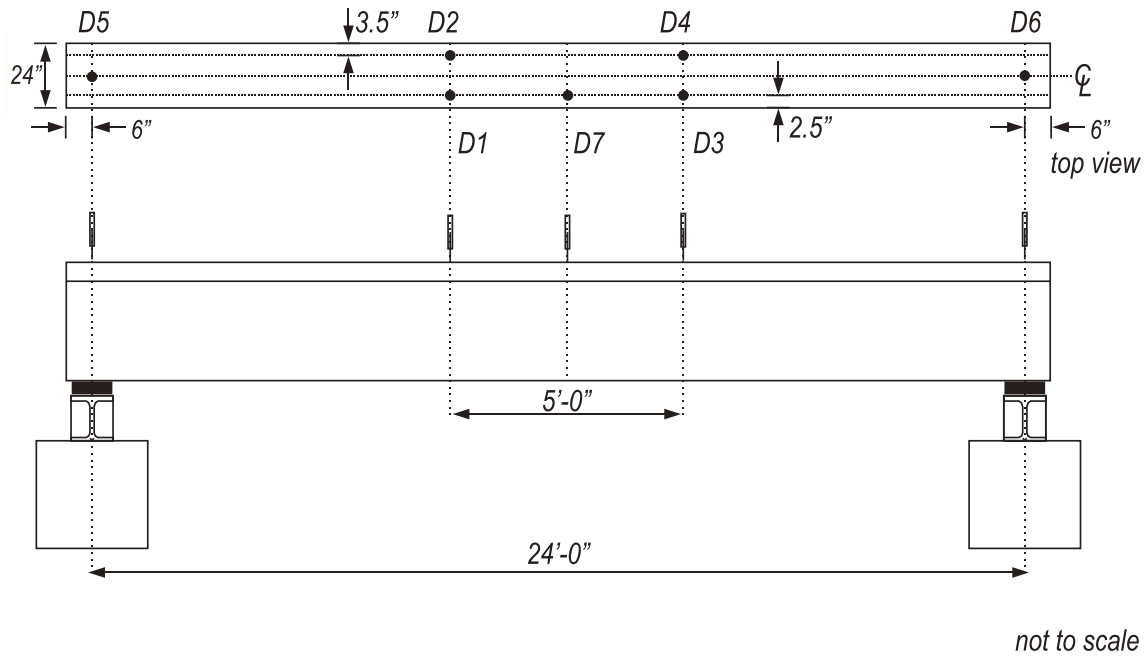


Figure 73–Flexure: Vertical displacement gages

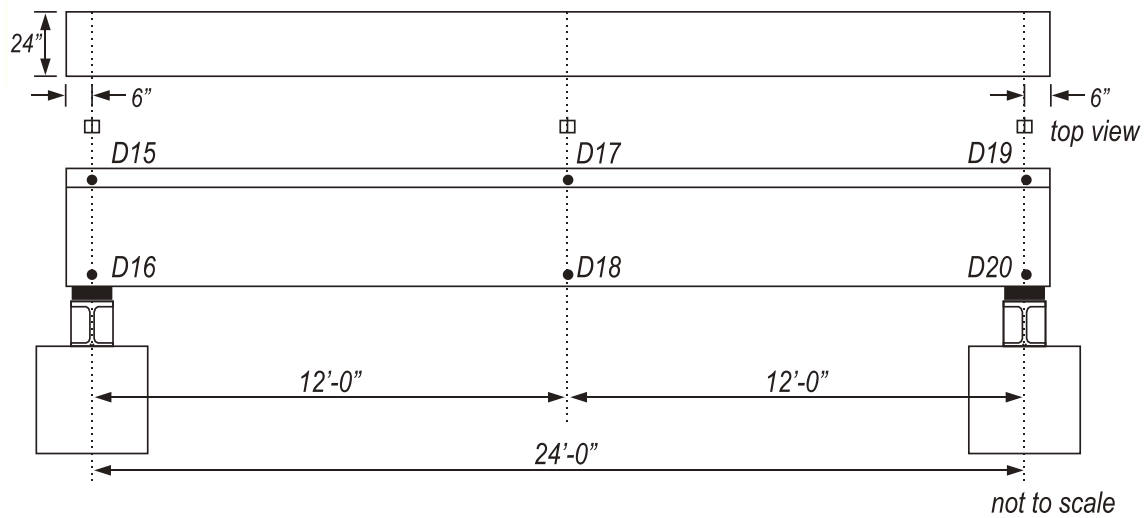


Figure 74–Flexure: Out-of-plane displacement gages

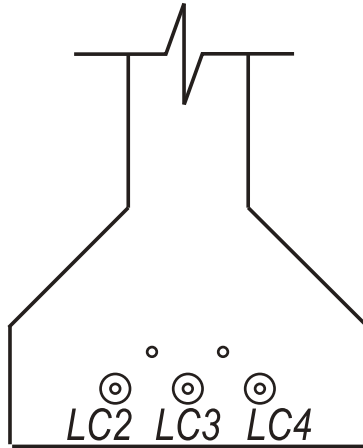


Figure 75–Spliced beams: load cells

In each flexure test, load was applied at 0.2 kip/sec. When cracking was first visually observed, the load was held. The specimen was inspected, and cracks were marked. Load application was then resumed at 0.2 kip/sec until termination of the load test. The test was terminated when either compressive failure occurred in the deck concrete or when excessive deflection of the specimen threatened the instrumentation. In all tests, the flexural capacity (maximum load) was reached prior to end of test.

### 7.3 *Shear*

To investigate the effects of higher shear (lower M/S ratio) on the splice region, three-point bending tests were performed on a shortened span length with a cantilever of 106". Two spliced specimens were tested, flipping the orientation of the splice region and the location of the bonded/unbonded lengths of the specimen. The test set-ups for the spliced specimens are shown in Figure 76.

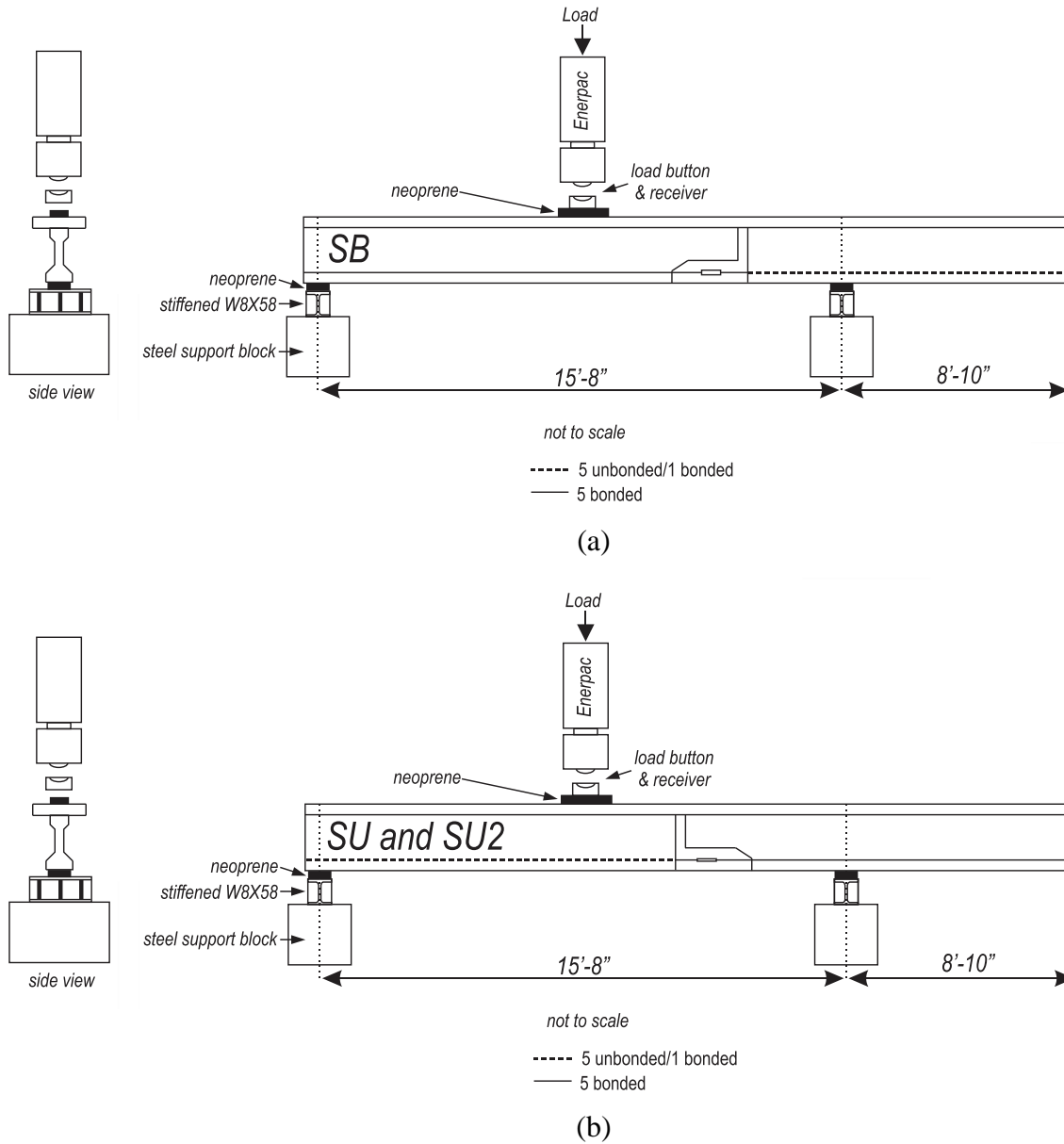


Figure 76–Spliced shear test set-ups for (a) SB and (b) SU and SU2

In each of the test set-ups, the left length of the span—or the tested span—is referred to as the “shear span.”

In the SB test set-up, the segment with five bonded strands (the segment shown to the left in the figure) is placed under the load point, in the shear span. In the SU (and SU2) test set-up, the segment with one bonded strand and five unbonded strands is placed under the load point, in the shear span. In all tests, the test specimen rested on two neoprene pads placed on steel supports which were grouted to the laboratory floor.

Considering the results of these tests, the orientation of the control specimen was determined; the control shear test specimen is shown in Figure 77. The control specimen is referred to as SC. In the chosen orientation, the six bonded strands were within the shear span, in an effort to match the same number of strands in the shear span as in the SU test set-up, which was determined to be the critical orientation for the shear tests. As in the SB tests, the beam rested on two neoprene pads placed on steel supports which were grouted to the laboratory floor.

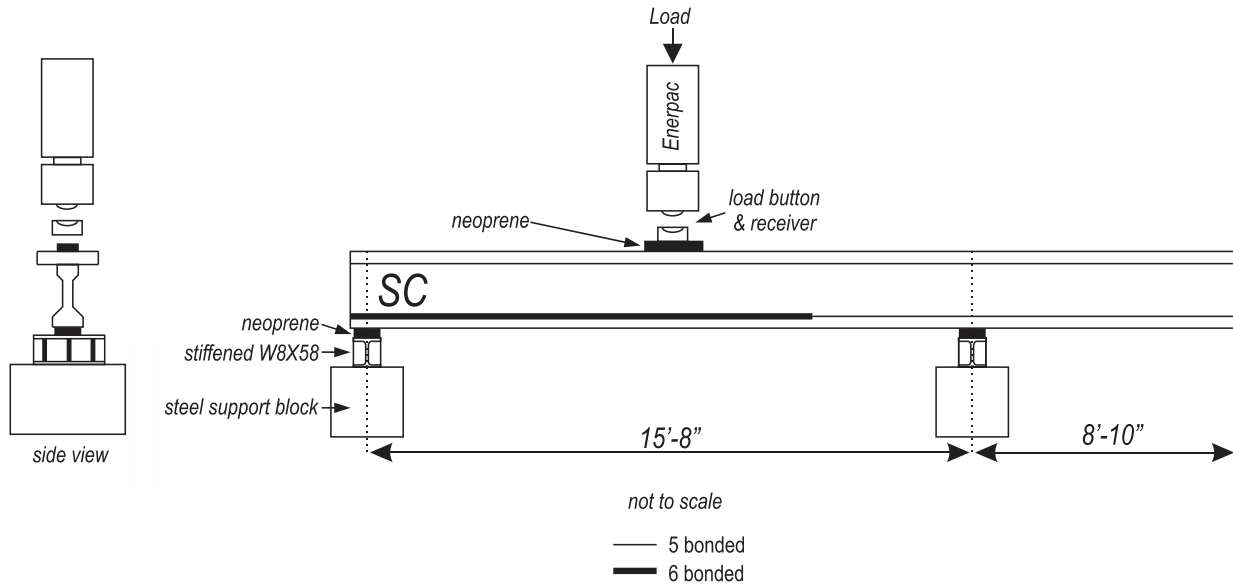


Figure 77–Control shear test set-up

Strain, strand slip, load, and displacement were monitored throughout each test. Four 200 mm displacement transducers were used to monitor vertical displacement during testing. Two were placed at to either side of the load point, and one was placed over each bearing to measure the support displacement. Five strand slip gages were placed on one end of each strand to monitor strand slip. Load was recorded in conjunction with the strain, strand slip and displacement data. A single vibrating wire gage (VWSG) at midspan was monitored during loading, with readings taken manually at specified load intervals. In the spliced specimens, load cells on three of the spliced strands were monitored.

Placement of the vertical displacement gages are shown in Figure 78.

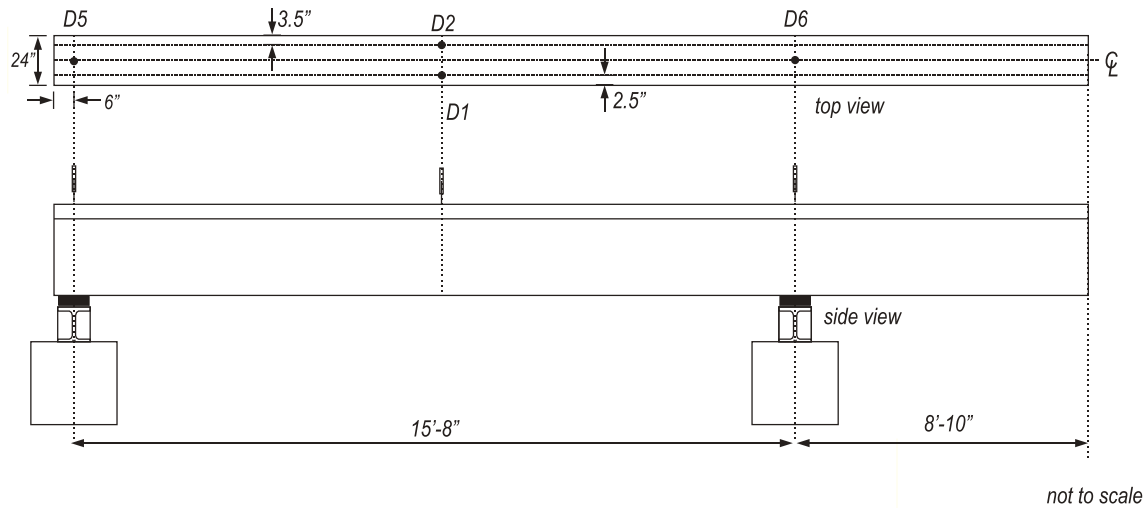


Figure 78–Shear: Vertical displacement gages

All of the spliced specimens had additional instrumentation to monitor splice behavior. Three load cells monitored the prestressing strand load and were placed on the bottom three strands (Figure 75). In the SU and SU2 specimens, five strain gages placed on the flat face of the couplers' turnbuckle (and cast into the closure pour) were monitored; these can be seen in Figure 69.

In each shear test, load was applied at 0.2 kip/sec. When cracking was first visually observed, the load was held. The specimen was inspected and cracks were marked. Load application was then resumed at 0.2 kip/sec until the peak load was reached. The test was terminated when significant load (greater than 10 kip) drop occurred without recovery or when excessive deflection of the specimen threatened the instrumentation.

#### 7.4 Fatigue

Four-point bending fatigue tests were performed on one control beam with continuous prestressing and on two spliced test specimens with coupled prestressing strand. The control beam is referred to as FC; the spliced specimens are referred to as F1 and F2. A spreader beam was used to create a constant moment region encompassing the spliced region. Each specimen was arranged in the test set-up as shown in Figure 79.

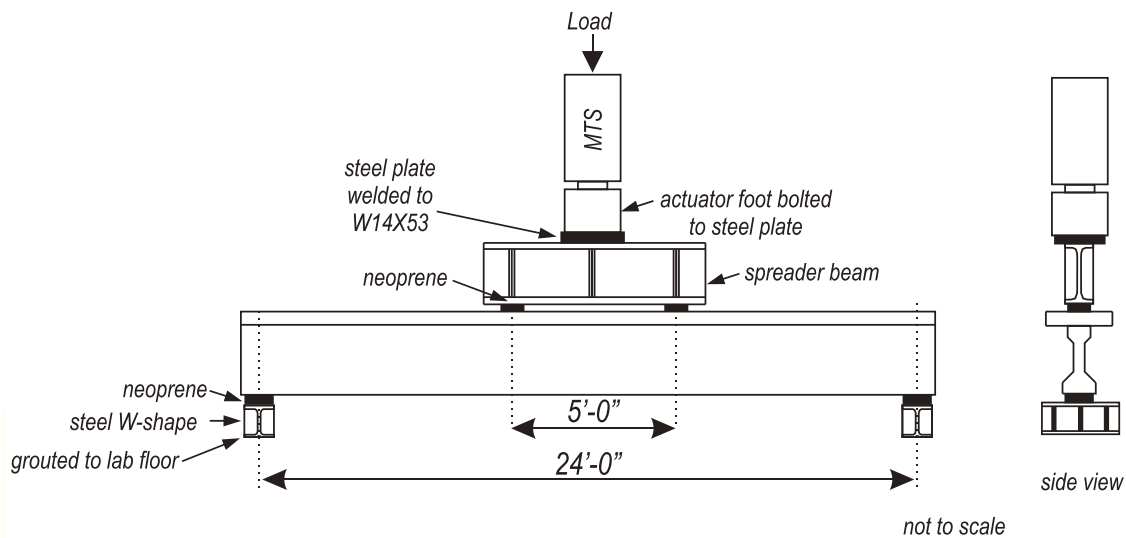


Figure 79–Fatigue test set-up

To reduce the effects on the test set-up during the cyclic loading, several precautions were taken to reduce movement within the set-up and supports. To reduce movement of the supports during the test, the steel W-shapes were grouted to the laboratory floor. To prevent the spreader from walking off the beam, it was welded to a plate which was then bolted to the actuator foot. Measured deflections are, therefore, reflective of displacement of the test specimen and the neoprene pads.

Strain, load, and displacement were monitored throughout the test. Four laser gages were used to monitor vertical displacement during testing. Two were placed at to either side of the spreader beam at midspan and one was placed over each bearing to measure the support displacement. The lasers were pointed toward a white fabric tape target on the surface of the deck. Applied load was recorded in conjunction with the strain, strand slip and displacement data. A single vibrating wire gage at midspan was monitored during loading, with readings taken manually at specified load intervals.

Placement of the vertical displacement gages is shown in Figure 73.

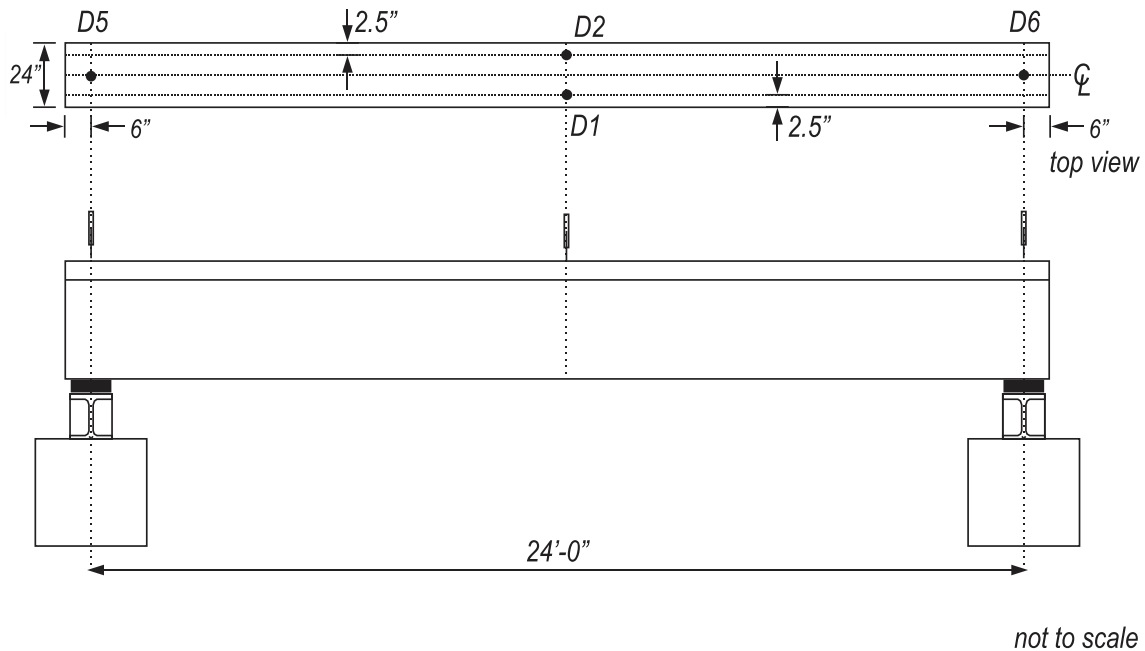


Figure 80–Fatigue: Vertical displacement gages

All of the spliced specimens had additional instrumentation to monitor splice behavior. Three load cells monitored the prestressing strand load and were placed on the bottom three strands (Figure 75) and five strain gages placed on the flat face of the couplers’ turnbuckle (and cast into the closure pour) (Figure 69).

The general load procedure for each specimen is outlined in Table 21 and is best described as occurring in four stages: precracking, decompression (or crack opening tests), fatigue loading and ultimate testing.

Table 21–Fatigue specimen load procedure

Load Procedure	Type	Load Rate	Load Range	# of cycles
Precracking	Static	0.2 kip/sec	0 kip-cracking	1
Decompression	Static	0.2 kip/sec	0 kip-decompression	2-4
Fatigue	Cyclic	2 Hz	40 kip -cracking	2 million
Ultimate	Static	0.2 kip/sec	0 kip–failure	1

## 8 Prestress Losses

Prestress losses were measured with the use of VWSGs; gage locations are covered in Figure 66. The spliced specimens contained two VWSGs—one in the bonded precast segment and one in the middle of the closure pour; for the discussion of prestress losses, only the VWSGs located within the closure pour of each spliced specimen are discussed. The control specimens contained a VWSG in the corresponding location; these gages are used to compute the effective prestress force for each control specimen.

Figure 81 shows the prestress in each specimen for both the precast control specimens and the spliced specimens versus the age of the concrete. For the VWSG in the precast concrete, a jacking prestress level of  $0.6f_{pu}$  was assumed; this jacking prestress was verified with the precast yard's stressing records. To determine the jacking prestress of the splice region of the spliced specimens, the average value of the strand force measured by the three strand load cells was assumed to act at each strand. The x-axis represents the age of the concrete in which the VWSG was encased; this was either the precast concrete or the closure pour for the control and spliced specimens, respectively.

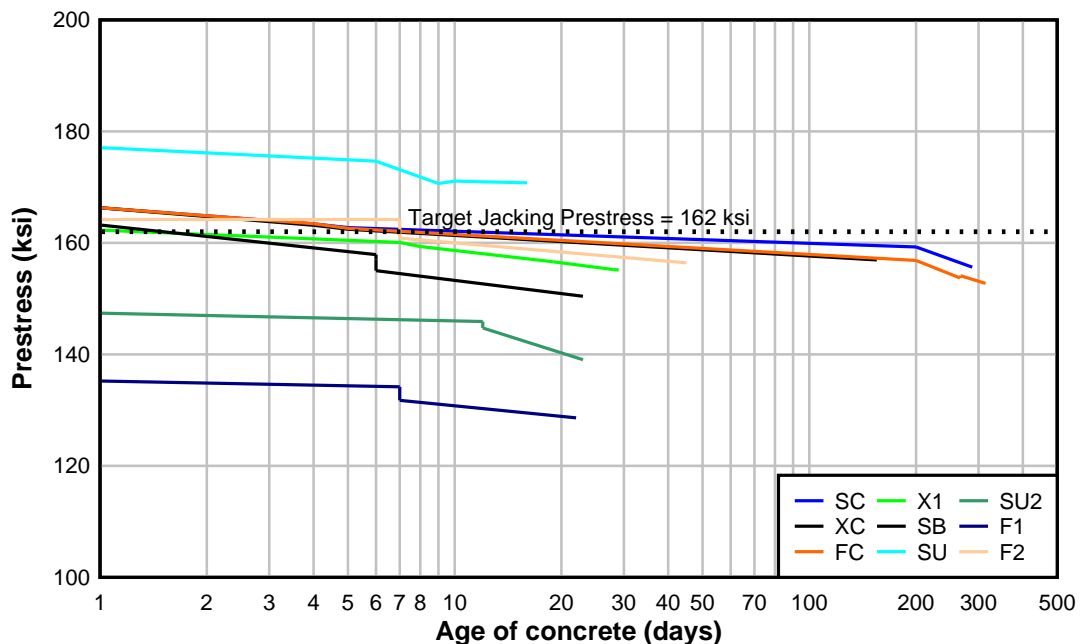


Figure 81—Prestress force

The control specimens exhibited similar prestress losses. All three control specimens were assumed to have the same prestress at jacking, 166.3 ksi. At prestress transfer (day 4), all three control specimens experienced an elastic loss of approximately 3 ksi. Between transfer and the load tests, the three specimens experienced similar long-term losses, as demonstrated by the similarity of the line slope.

The spliced specimens exhibited two interesting behaviors: prestress loss prior to release of the tie-downs and introduction of the prestress force in the closure pour; and decreasing elastic losses with concrete age. For each spliced specimen, the prestress force was introduced into the closure pour approximately 6-7 days after the pour was completed (except for specimen SU2, which was prestressed at day 12). During this time period (prior to prestress of the closure pour), the jacking load was locked off and held in the actuators, resisted by the anchorage at the free end of the unbonded segment. This held force resulted in some creep of the precast segments. Prior to prestress of the closure pour, some prestress was lost as the concrete of the precast segments crept under the load. Additionally, the effect of the concrete age at the time of the closure pour prestressing was evident: the younger concrete had higher elastic losses. Following this trend, specimen SU2—with the longest cure prior to release—had the least elastic losses of the spliced specimens.

The VWSG mounted at the centroid of the spliced prestressing strands was used to determine the prestress losses at key points during the spliced beams' construction and life until load testing. For the precast control specimens, the jacking force was determined from the calibrated monostrand jack used to stress each strand, as recorded in the stressing records from the precaster. For the spliced specimens, the jacking force was considered to be the prestress force present at tightening of the lock-nut. This prestress force was calculated as the average measurement of the load cells instrumenting the three bottom strands acting in all five strands. The prestress forces at jacking are presented in Table 22.

Due to concern regarding the reliability of the load cell readings, later splice assemblies included strain gages on the flat face of the turnbuckle of each coupler—these readings were used to indirectly determine the strand force. Calibration of the strain gage readings to equivalent force was done in separate tensile tests. Based on the calibration, the strand force was also indirectly determined for each strand. The average of these readings is also provided in Table 22. In general, these measurements were taken as a redundant check of the strand force, to

prevent overstressing the strand during the splice assembly process. The strand force according to the calibrated strain gages is reported here for comparison; all calculations of prestress losses and strand force utilize the measurements from the strand load cells.

Table 22-Jacking prestress

Specimen	Average Total Force by Load Cell (kip)	Average Total Force by Calibrated Strain Gage (kip)	Average Strand Stress (ksi)
SC	127.2	n/a	166.3
XC	127.2	n/a	166.3
FC	127.2	n/a	166.3
X1	124.2	n/a	162.3
SB	123.1	117.4	161.0
SU	135.5	116.4	177.1
SU2	112.8	120.2	147.4
F1	105.7	116.6	138.2
F2	125.6	125.8	164.1

The initial prestress force is considered the jacking prestress force minus the elastic losses. For all specimens, it was calculated based on prestress losses measured by the VWSGs at the time of prestress transfer, based on the differential strain readings from the VWSG and the Young's modulus of the strand. For the precast control specimens, prestress transfer occurred when the strands were cut free from the bed. For the spliced specimens, the initial force was considered to be the prestress force present just after release of the tie-downs, when the prestress force was imparted to the splice region, causing an immediate elastic loss in the closure pour. Elastic losses between the jacking and the prestress transfer are then revealed. Table 23 shows the initial prestress force for each completed specimen.

Table 23–Measured initial prestress

Specimen	Average Total Force by VWSG (kip)	Average Strand Stress (ksi)
SC	125.0	163.4
XC	124.8	163.2
FC	125.0	163.4
X1	122.5	160.1
SB	118.5	155.0
SU	133.6	174.7
SU2	110.7	144.8
F1	100.8	131.8
F2	123.1	160.9

Table 24 presents the effective prestress for all specimens, calculated as the force present at the time of the load test (for the fatigue specimens, the time of the first load test was used) based on the differential strain readings from the VWSG and the Young’s modulus of the strand. Long-term losses, such as due to creep and shrinkage, between the jacking and the time of the load test are then revealed.

Table 25 presents the measured prestress losses; both initial and time-dependent losses were calculated as a percentage of the jacking prestress (measured as described above).

Table 24–Measured effective prestress

Specimen	Average Total Force by VWSG (kip)	Average Strand Stress (ksi)
SC	119.0	155.6
XC	120.1	156.9
FC	116.8	152.7
X1	118.7	155.2
SB	115.0	150.4
SU	130.7	170.8
SU2	106.4	139.1
F1	98.4	128.6
F2	119.7	156.4

Table 25–Measured prestress losses

Specimen	Initial losses (%)	Concrete age at release (days)	Long-term losses (%)	Total prestress loss (%)	Concrete age at load test (days)
SC	1.7	4	4.7	6.4	288
XC	1.9	4	3.7	5.6	155
FC	1.7	4	6.4	8.2	314
X1	1.4	7	3.0	4.4	29
SB	3.7	6	2.8	6.6	23
SU	1.4	6	2.2	3.6	16
SU2	1.8	12	3.8	5.7	23
F1	4.7	7	2.3	6.9	22
F2	2.0	7	2.7	4.7	45

Prestress losses affect structure serviceability; therefore, accurate prediction of the anticipated losses for spliced specimens is important. The measured prestress losses compare well with typical 25-50 ksi (12-25% of a specimen stressed to  $0.75f_{pu}$ ) of prestress losses (due to all immediate and long-term effects) observed in typical prestressed concrete sections (PCI 2004). The measured losses for all specimens were at the lower end of this range.

Predicted prestress losses were also computed for comparison using the PCI method (Zia et al. 1979) –though the prediction methods are intended only for pretensioned girders consisting of normal weight concrete and 270 ksi prestressing strand. Though the spliced specimens do not fall into this category, the estimates were calculated and are provided for general reference. The specified concrete strength at transfer and the specified 28-day strength was used to estimate the modulus of elasticity at transfer as 4630 ksi and at time of loading as 5500 ksi (per ACI,  $E = 33000w_c^{1.5}\sqrt{f'_c}$ ). Relative humidity was assumed to be 75%. Table 26 presents these predictions.

Figure 82 compares the measured and PCI predicted losses. In all cases, the PCI predicted prestress loss is greater than the measured loss. Overestimation of prestress losses by PCI has been observed by other researchers (Onyemelukwe et al. 2003).

For comparison, a crack opening test was performed on some specimens to determine the effective prestress level; the losses calculated using the decompression method were also determined. The crack opening tests are covered in the next section.

Table 26–PCI prestress losses

Specimen	Elastic losses (ksi)	Long-term losses (ksi)	Total prestress loss (ksi)	Total prestress loss (%)
SC	3.8	10.2	14.0	8.4
XC	3.8	10.2	14.0	8.4
FC	3.8	10.2	14.0	8.4
X1	3.7	9.7	13.5	8.3
SB	3.7	9.6	13.3	8.3
SU	4.1	11.4	15.5	8.8
SU2	3.3	8.3	11.7	7.9
F1	3.1	7.5	10.6	7.7
F2	3.8	10	13.7	8.3

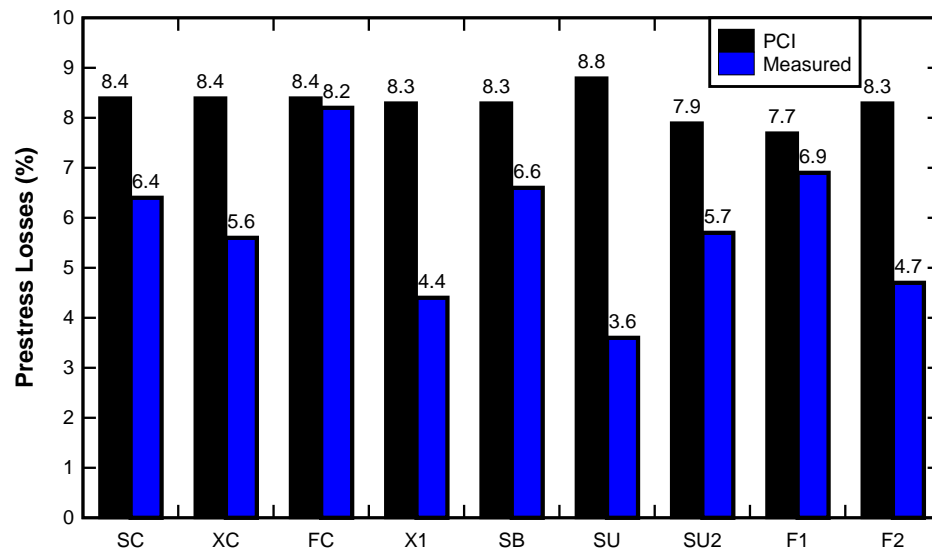


Figure 82–Measured prestress losses vs. PCI

Decompression - or crack opening - tests were also performed on some test specimens as an alternate measure of the effective prestress force. For each of the decompression tests, the specimen was placed in the four-point bending test set-up shown in Figure 72.

While the specimen was loaded, the load-deflection plot and the beam were monitored for cracking. At first crack, the load was held and the crack location was identified and marked. The load was then removed from the beam and two strain gages were placed on opposite sides of, and perpendicular to, the crack, longitudinal to the beam axis (Figure 83). Load was then reapplied to the specimen. When the crack re-opened, the slope of the load-strain plot changed,

indicating that the pre-compression caused by the prestress force had been overcome. This method has been described by Pessiki et al. (1996).

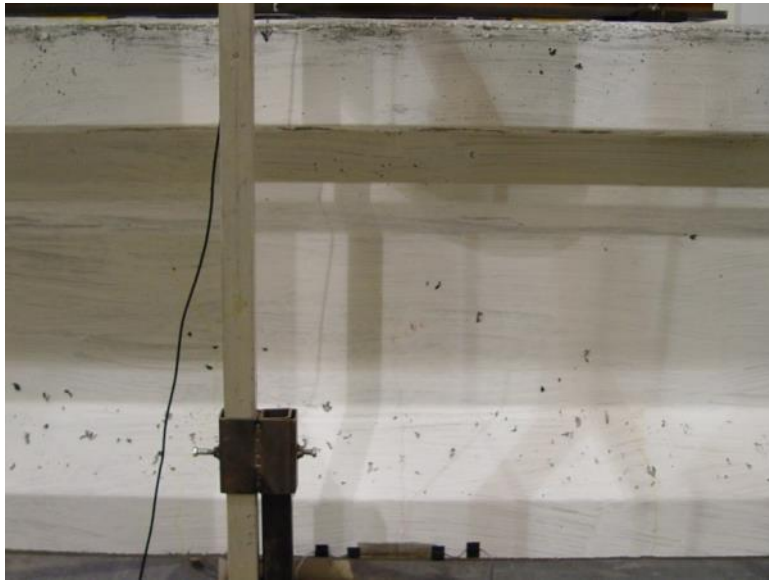
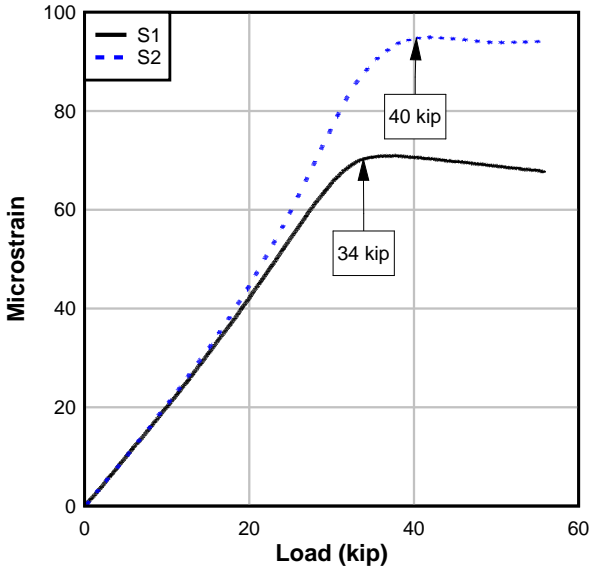


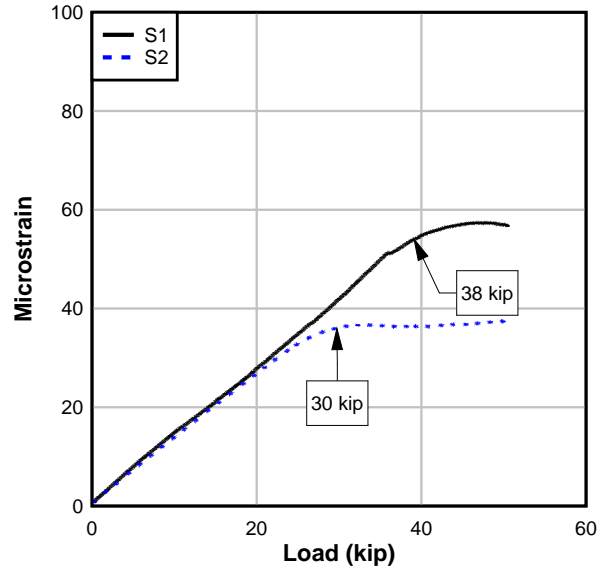
Figure 83–Decompression strain gages

When the initial cracking load was removed, the prestress forced the crack closed and returned the beam section to full uncracked section properties. The decompression load is defined as the average of the two loads at which the strain load curve reaches a plateau. Figure 84 shows a plot of the strain data from the gages applied adjacent to the first visible crack on the control fatigue specimen and on the first spliced fatigue specimen.

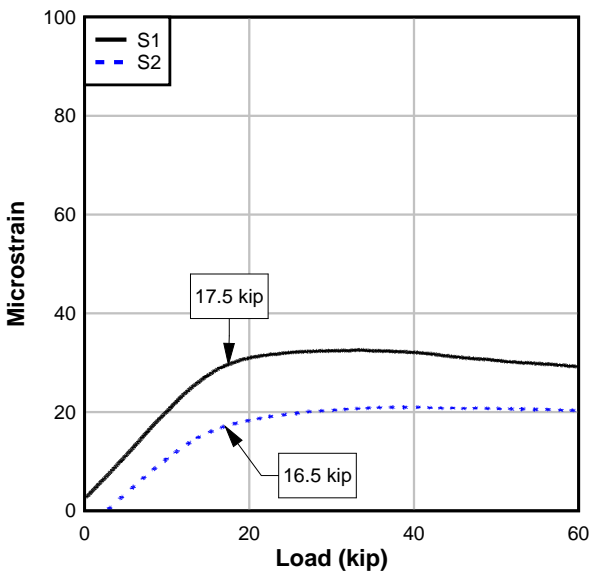
Assuming the decompression load corresponds to zero stress at the bottom of the beam, the effective prestress can be calculated from the applied load required to reach decompression. To calculate the effective prestress, the compression caused by the prestress force and its eccentricity are equated to the tensile stress induced to reach the decompression load using uncracked gross section properties. The effective prestress, as determined with this approach, is given in Table 27.



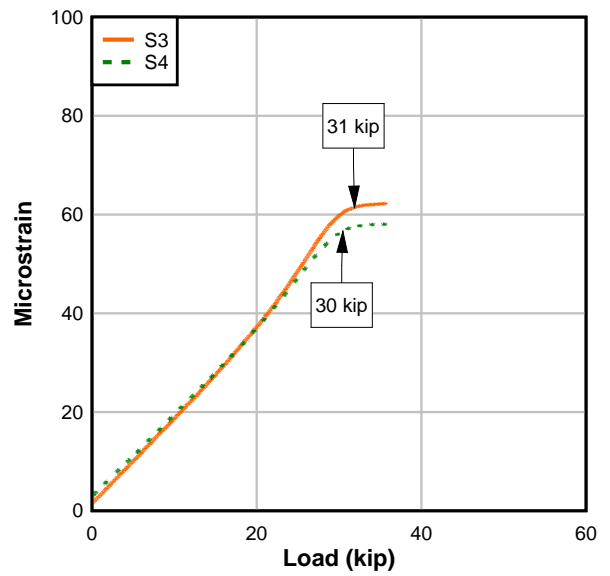
(a)



(b)



(c)



(d)

Figure 84–Decompression: (a) FC; (b) F1; (c) F2-joint and (d) F2-crack

Table 27–Effective prestress force by decompression

Specimen	Average Decompression Load (kip)	Calculated Total PS Force (kip)	Calculated Strand Stress (ksi)	$f_{se}$ per Decompression/ $f_{se}$ per VWSG
FC	37	97.9	128	0.84
F1	34	91.8	120	0.93
F2–joint	16	57.4	75	0.47
F2–crack	30	82.6	108	0.67

Decompression tests were performed on one control beam and two spliced beams. Because of the location of the constant moment region, only the test of the control beam could be used to evaluate the effective prestress induced at the precast yard. The effective prestress calculated from the decompression test of this control specimen corresponded to later test results: the effective prestress was lower than the anticipated prestress (based on the precast yard’s stressing records minus the measured prestress losses). Based on this method, XC’s strands had 19.6 kip/strand vs. the 23.4 kip/strand as determined by the stressing records and VWSG measurements—approximately 16% less prestress force.

Two measurements of decompression were taken of specimen F2. The first ‘crack’ which occurred and was instrumented was an opening of the vertical interface between the closure pour and the bonded segment; this is referred to as F2-joint. This location exhibited much less precompression, indicated by the low load at which the joint reopens. The first true crack—located at the bottom of the bottom flange in the middle of the closure pour—was also instrumented and is referred to as F2-crack. This region exhibited higher precompression, indicating that the closure pour was successfully precompressed by the splicing procedure.

The decompression tests performed on the two spliced beams, based on the location of the crack, were indicative of the effective prestress force in the splice region of the beam. The calculated strand force based on the results of these tests closely matched the strand load as measured by the load cells for specimen F1. For example, for F1, the ratio of the calculated PS strand force per the decompression test/measured strand force per the load cells was 0.93. On the other hand, specimen F2’s measured strand load via the load cells did not correspond well to the calculated strand force, based on the decompression test. The decompression method has been shown to be not wholly accurate (O’Neill and Hamilton 2009), but the results corresponded

to the observed low cracking loads in the control specimens, suggesting that the initial prestress force in the precast segments was indeed lower than specified.

## 9 Splice Assembly Results and Discussion

Figure 85 shows the average strand load versus time for the splice assembly procedure of specimen X1. Also labeled are the jack pressures at each load hold. The shown plot is typical of the splice assemblies and will be used for discussion; all other splice assembly load-history plots are included in Appendix F–Splice Assembly Plots.

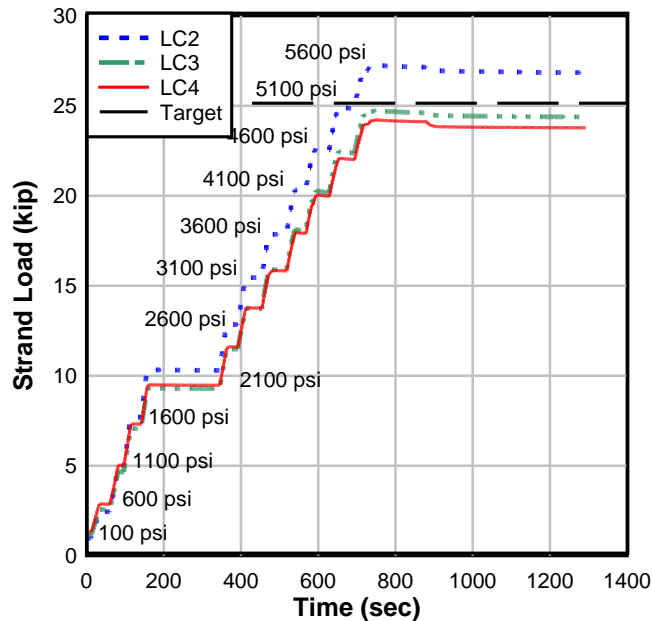


Figure 85–Load history of X1

During the splice assembly procedure, a pair of hydraulic jacks was pressurized in a series of steps, with holds every 500 psi of additional pressure. This was done due to repeatedly check that the manual nature of the stressing procedure (using hand jacks) was stressing the strands synchronously. At each hold, the corresponding jack pressure is labeled in the plot.

As the jacks were pressurized, the generated compression force was resisted by tension in the strands, which elongated as the stress increased, opening the gap between the precast segments. Figure 86 shows the general concept.

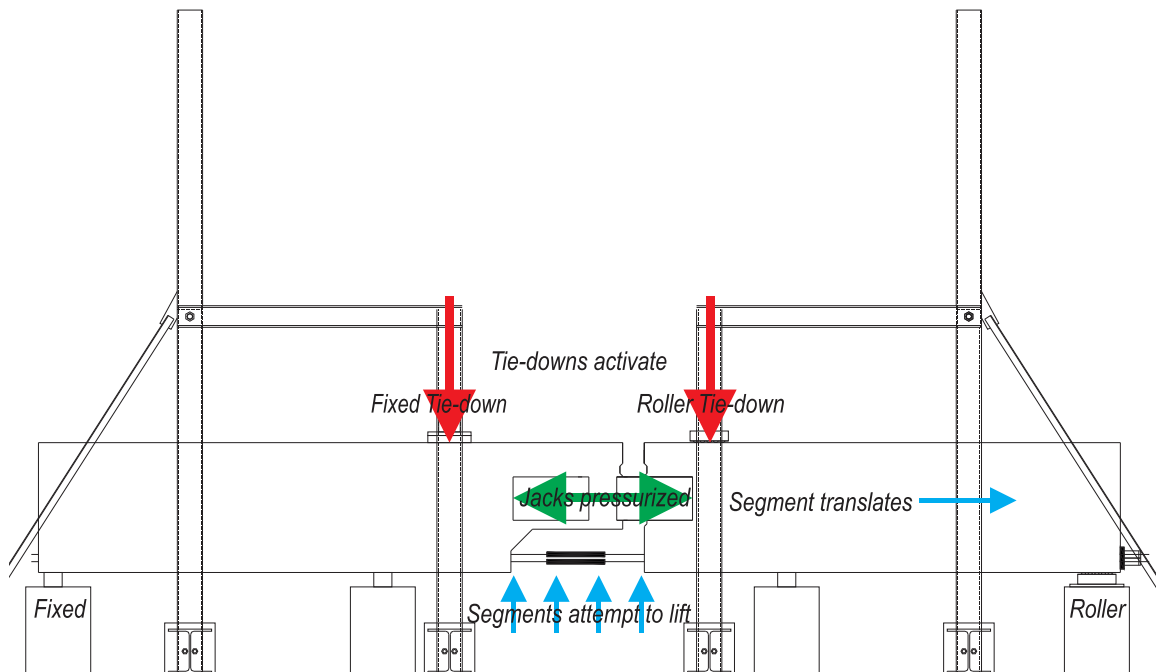


Figure 86–Stressing procedure

Metallic creaking noises were heard during the pressurization of the jacks, as the connections in the tie-down frame system resisted the applied force. The amount of noise heard was a function of how tightly each set-up was cinched down prior to the stressing procedure.

Figure 87 shows the average strand load (calculated as the average of the three hollow load cells on the bottom row of prestressing strands) versus the gap opening during the splice assembly of SB and SU. Gap opening was measured at four locations: at two locations on the top flange and two locations on the bottom flange at the approximate location of the strand centroid. The predicted elongation of the strand (per PL/AE) was 1 in., assuming a target strand load of 25 kip, an unbonded length of (gage length) of 174 in. and a 7-wire 1/2 dia. 270 ksi lo-lax strand. Using the calibration charts provided by Enerpac for the CLL504 jack, the pressure required in each jack to achieve 25 kip/strand was 5690 psi/jack. The target elongation value (1 in.)—corresponding to  $0.6f_{pu}$  prestress force in the strand - is shown on the plot for reference.

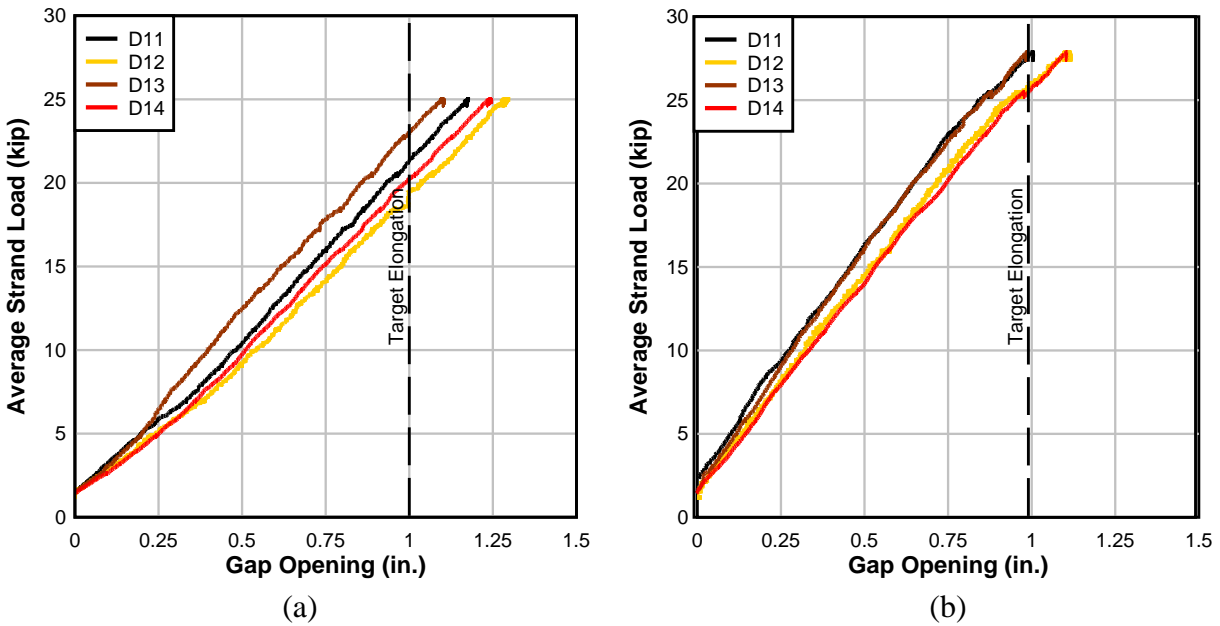
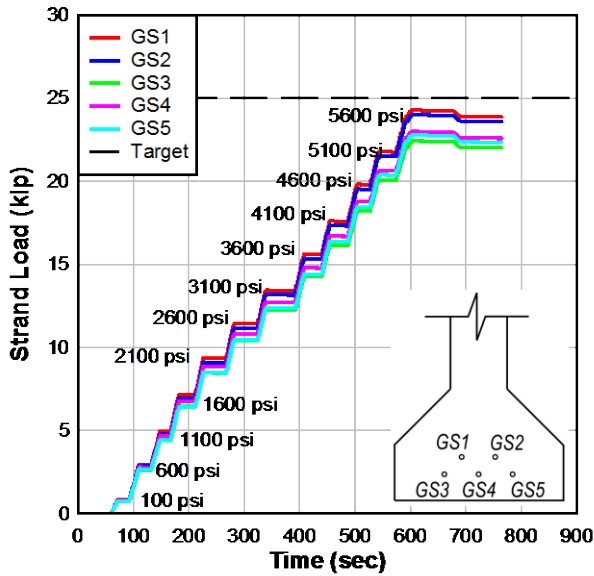


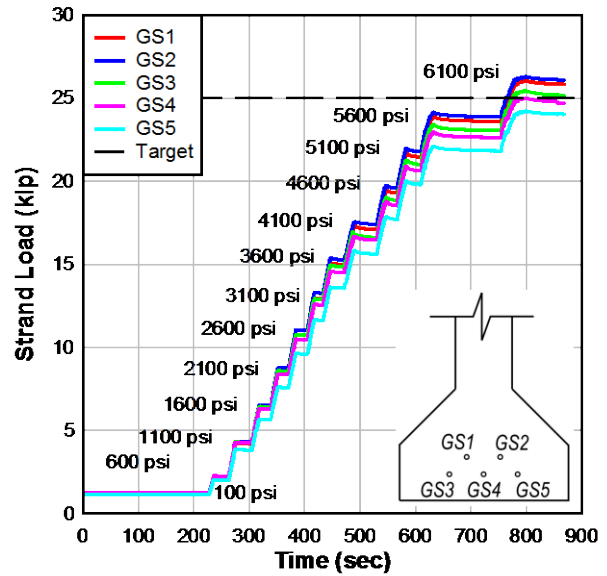
Figure 87–Strand load for (a) SB and (b) SU

In the shown plot, as the jack pressure increased, the prestressing strand load increased and the gap between the precast segments opened in a linear fashion—indicating that the strand was stressing linear-elastically. This relationship was shown to exist in every splice assembly.

In general, due to the moment generated by the eccentricity between the jack force and the coupled strands, the top of the gap “opened” more than the bottom. The difference between the top opening and the bottom opening at the final stressed position was approximately 1/4-1/8 in. and was affected by the tightness of the system, i.e., how well the channels were tied down to the precast segments prior to the stressing of the strand. The moment generated caused the top strands to typically develop more prestress force than the bottom row strands; this relationship is also seen in the strand load as measured by strain gages on the couplers. Figure 88 shows the calculated strand force, based on a calibrated strain gage versus time.



(a) SU2



(b) F2

Figure 88–Strand load history based on calibrated coupler strain for (a) SU2 and (b) F2

The magnitude of these vertical movements was affected by the conditions at each restraint. In each case, the roller tie-down—which consisted of a steel Hilman roller displaced upward more than the fixed tie down—which consisted of a neoprene pad and a load cell. An example is shown in Figure 89. The slackness of the rollers in the roller tie-down allowed more vertical movement than the neoprene of the fixed tie-down.

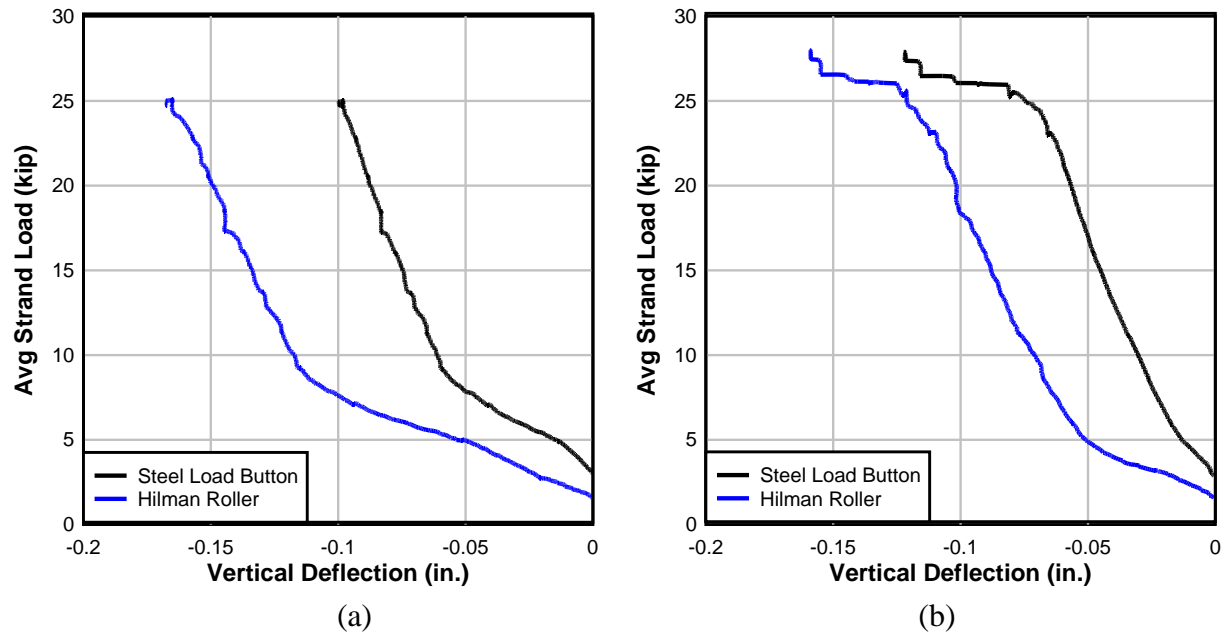


Figure 89–Tie-down deflections: (a) SB and (b) SU

The effect of the moment generated by the applied jacking force and the induced strand tension can also be seen in the vertical displacement at the tie-down and support locations. While the LVDT gages placed at the two tie-downs indicate an upward movement of the precast segments, the LVDT gages at each of the supports indicate downward movement, indicating that the segments were slightly rotating as the strands were stressed. An example of the support deflections is shown in Figure 90.

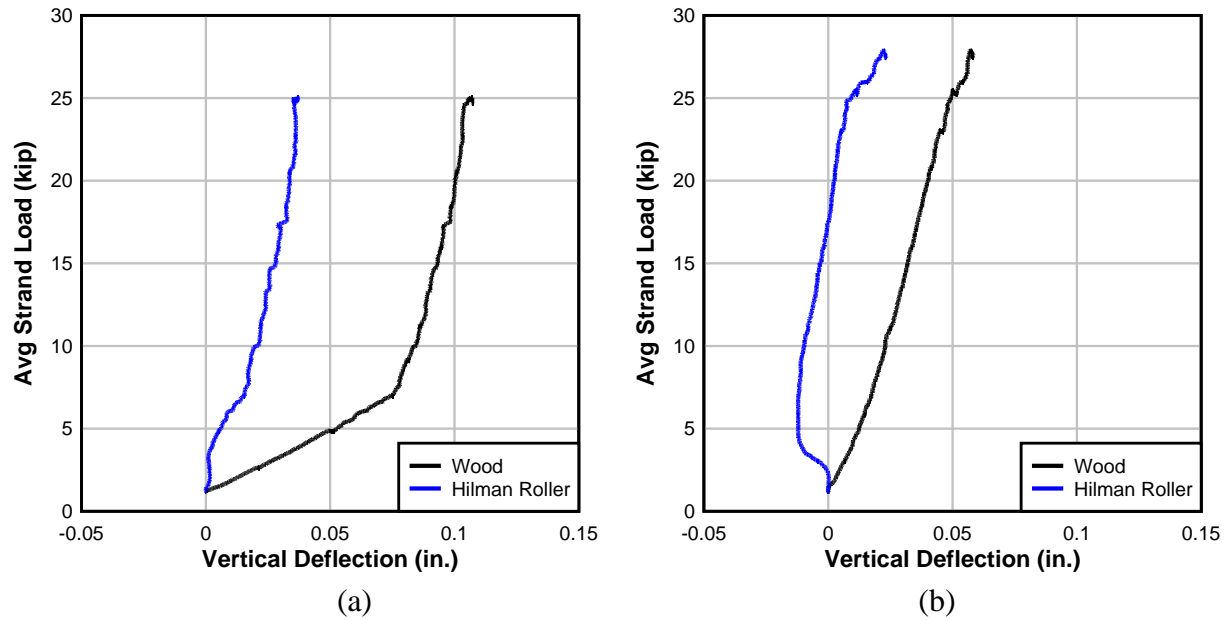


Figure 90–Support deflections: (a) SB and (b) SU

The bottom string pot readings were used to determine the cut-off point for the splice stressing procedure. The strand was stressed until gages D11 and D13 measured approximately 1 in.–corresponding to 1 in. of strand elongation or approximately 25 kip/strand. The string-pots were chosen as the critical criteria over the load cells as a safety consideration; because there was some concern of inaccuracies in the load cells, the strand elongation was considered the safer approach.

At approximately 1 in. of gap opening at the bottom flange, the stressing procedure was halted and a locking-ring on each jack was used to mechanically hold the achieved prestress force. Table 28 shows the strand loads for each of the splice assemblies as measured by the three load cells. The assumed prestress force is based on the average of the three load cells.

Table 28–Spliced specimens: strand loads per load cell

Spliced Specimen	LC2 (kip)		LC3 (kip)		LC4 (kip)		Average Strand Load (kip)	
	Preload	Final	Preload	Final	Preload	Final	Preload	Final
X1	0.98	26.73	1.10	24.23	1.27	23.55	1.12	24.84
SB	1.16	22.35	0.94	24.40	1.59	27.13	1.23	24.63
SU	0.82	23.27	0.91	23.07	1.83	34.97	1.19	27.10
SU2	1.44	22.74	1.00	20.60	0.89	24.33	1.11	22.56
F1	1.37	23.06	1.16	16.46	1.32	23.92	1.28	21.15
F2	0.36	22.95	1.23	22.82	1.92	29.57	1.17	25.11

The reinforcement near the bracket attachment in the splice region was based on a strut-and-tie model. Instrumentation was installed in key areas to verify the design assumptions and consisted of strain gages placed in the assumed tie and compressive strut locations. These measurements were taken more to evaluate the behavior during the stressing procedure in a general sense on a global level than to assess the measurement magnitudes or local strains.

Figure 91 shows the simplification of the strut-and-tie model used to determine the reinforcement in the end of the precast segment required to resist the tensile stresses induced during the application of force to the bracket.

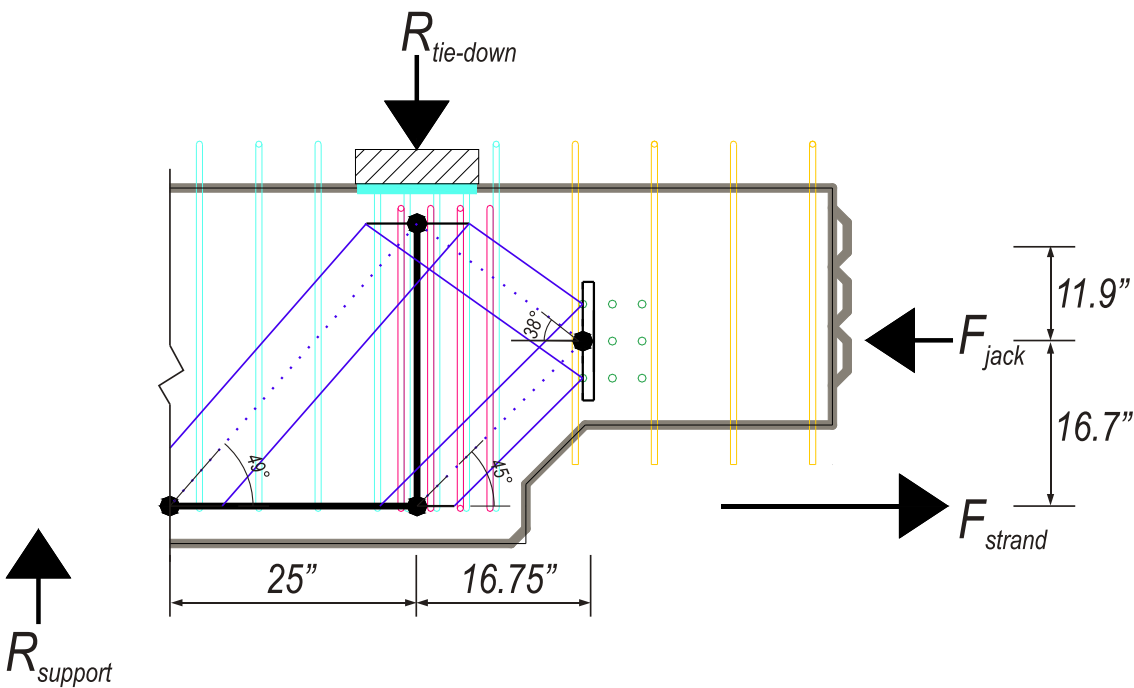


Figure 91–STM: assumed dimensions

The strut-and-tie model assumed application of an external compressive load due to the jack at the bolt group centerline, where the bracket transfers load to the precast segment (labeled  $F_{\text{jack}}$ ). This compressive force is resisted by a tensile force in the prestressing cables; this force was assumed to act at the centroid of the strand pattern (labeled  $F_{\text{strand}}$ ). Due to the eccentricity between the two loads, the segment attempts to lift; the movement is resisted by a reaction at the tie-down ( $R_{\text{tie-down}}$ ) and at the support ( $R_{\text{support}}$ ).

The location of these external forces and reactions determined the general geometry of the assumed strut-and-tie model. A compressive strut was assumed to form from  $F_{\text{jack}}$  up to the tie-down, or  $R_{\text{tie-down}}$ . Another compressive strut was assumed to extend to a tie at the centroid of the prestressing strand. Finally, another tie was assumed to form directly under the tie-down force. At this assumed tie location, additional stirrups were detailed.

Two stirrups were instrumented with strain gages (S01 and S02) and placed within the precast segments during construction as described in Section 7.1. An external strain gage (S25) was also placed on the concrete surface of the precast segments prior to the splice assembly procedure at the same location along the beam length. This gage was used to verify the readings of the stirrup gages and to check the assumption of perfect bond between the rebar and the precast concrete. Based on the perfect bond assumption, the strain measured in the concrete should be approximately equivalent to the strain in the ties. Figure 92 shows the measured strain for the three strain gages versus the average strand load for the stressing of specimens X1 and SU. The gage locations are shown in Figure 68.

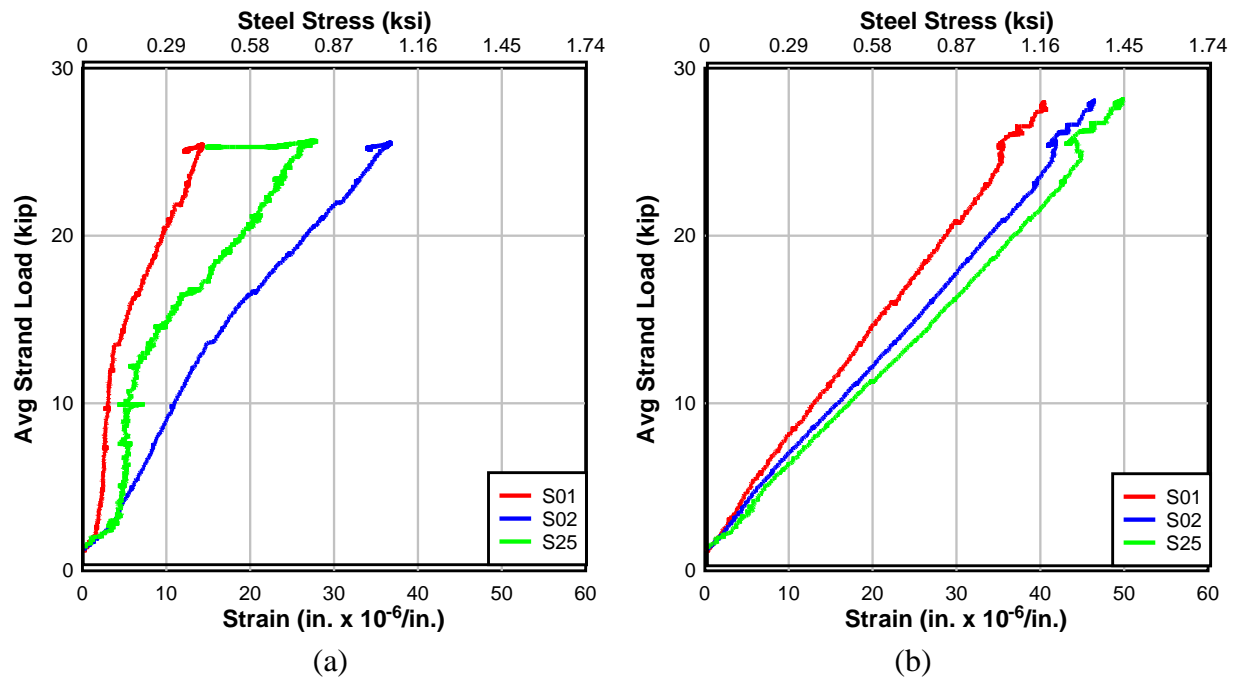


Figure 92–Tie strain (a) X1 and (b) SU

In each case, the measured strain in the tie region is tensile - as predicted by the strut-and-tie model - and increases linearly as the strand load increases. The measured rebar strain (gages S01 and S02) is approximately 10-50 microstrain—a corresponding stress of 0.3-1.2 ksi less than the cracking strain of the concrete. Similar measurements of tensile concrete strain were measured by the surface foil gage S25, which measured within 10 microstrain of the rebar gages. All gages recorded strains less than 100 microstrain, i.e., less than the typical concrete tensile strain at cracking. Though the strut-and-tie model did not form (cracking to reveal the reinforcement did not occur), its approximate location appears to be in this region.

Figure 93 shows a plot of the strain measured by gages along the beam top flange versus the average strand load. Also shown in the figure are the gage locations and the assumed strut-and-tie model. This field of strain gages was placed to approximately determine the node location of the compressive strut, i.e., the location of the compressive strut node nearest the tie-down. Because the angle of the strut is assumed and unknown, these measurements were taken to simply visualize the region affected by the compressive strut introduced during the stressing procedure.

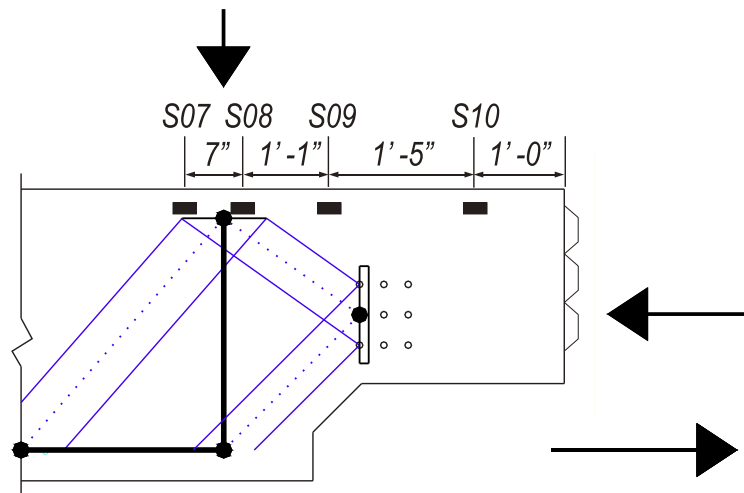
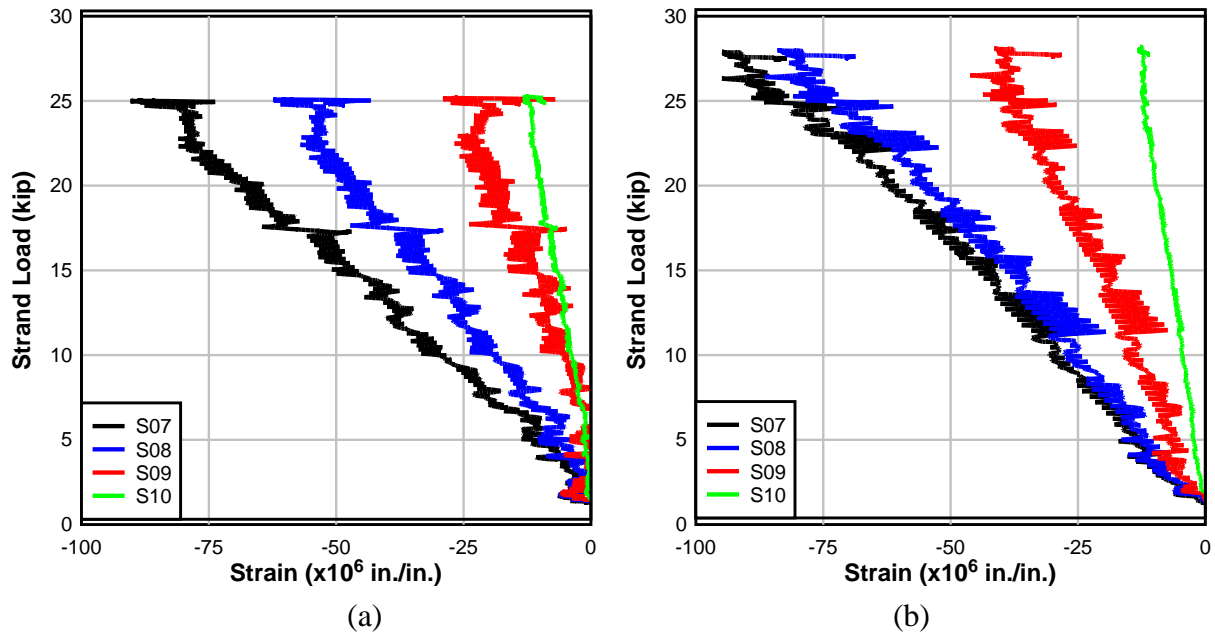
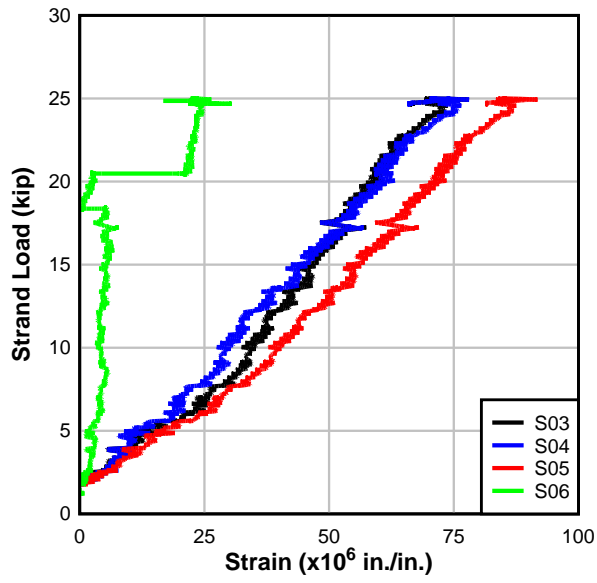
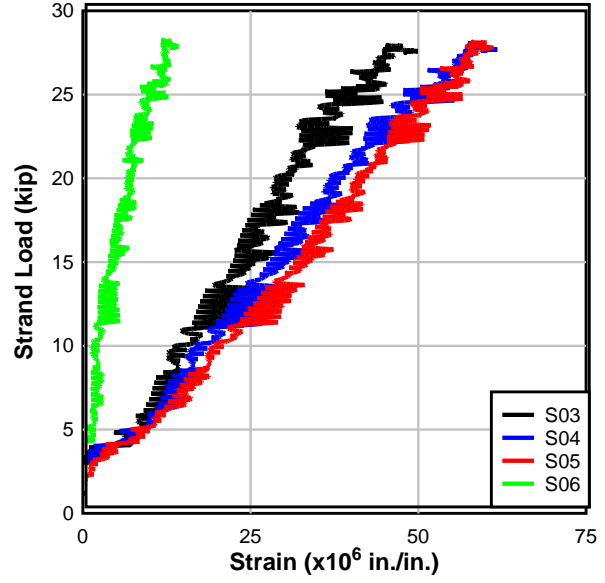


Figure 93–Strain in top flange for (a) SB (b) SU

Finally, strain gages were placed on the concrete surface along the bottom flange of the beam, at the approximate height of the tendon centroid (Figure 94). The strain measured by these gages captures the tensile strain imparted into the bottom flange of the beam as the prestressing strand was stressed. In general, however, this is an area of complicated force interaction; tension applied to the concrete via the stressed strand was not directly measurable with the strain gages, due to the interaction of the incoming compressive strut. Figure 94 shows the strain in this region versus the average strand load.



(a)



(b)

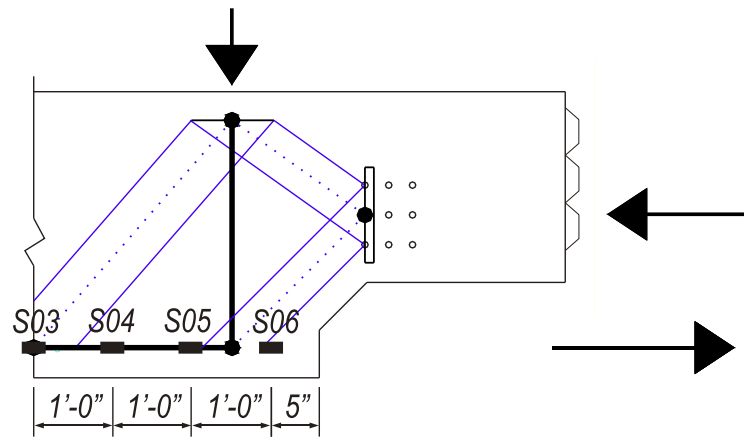


Figure 94—Transfer length strain (a) SB (b) SU

## 10 Flexural Results and Discussion

Two specimens were tested in four-point bending to evaluate flexural behavior: one control specimen (XC) and one spliced specimen (X1). This chapter presents and discusses the results. The test set-up and procedure are described in Section 7.2.

### 10.1 Flexure—XC

Figure 95 shows the load-displacement plot of the control flexure test specimen XC. The XC specimen correlates to precast segment 2 of pour 1 (Figure 43). As load was applied, XC exhibited linear-elastic behavior up to a cracking load of approximately 77 kip.

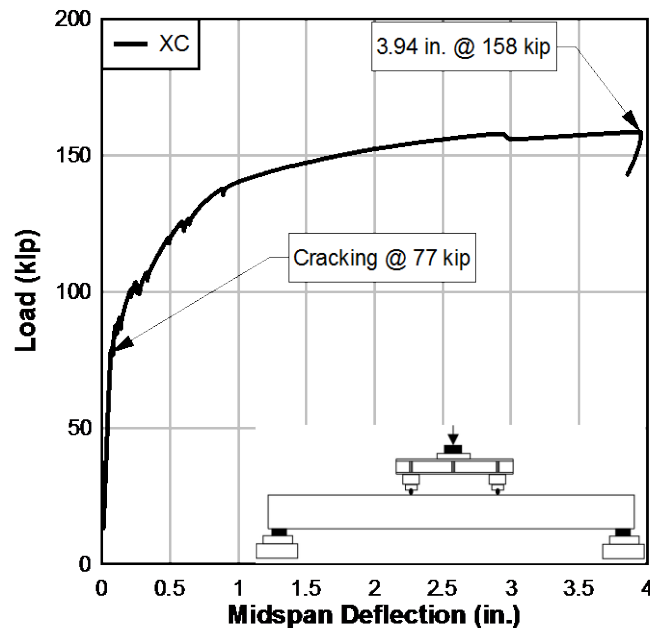


Figure 95–XC: Ultimate

At approximately 80 kip, a single crack extending from the bottom flange into the web was visually observed at midspan. The load was held and the crack was measured; the crack was 0.015 in. wide at approximately 3 in. from the bottom of the beam (point 1) and 0.005 in. wide at point 2, as shown in Figure 96.

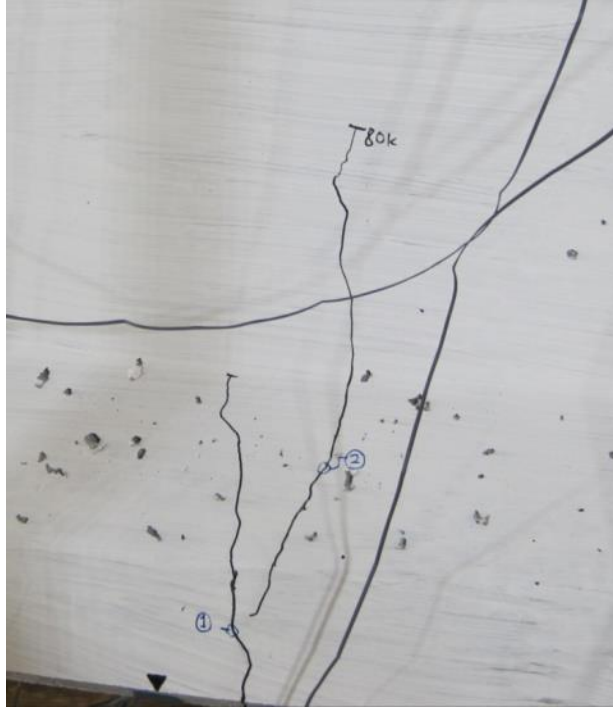


Figure 96–XC: First crack at midspan

As XC was loaded beyond cracking, sudden minor load decreases occurred periodically until the midspan deflection reached just less than 1 in. These decreases indicated flexural crack formation and were confirmed with audible cracking sounds and visual observations. Although the peak load had not been reached, the test was terminated at a deflection of approximately 4 in. (maximum load of 158 kip) to avoid damage to instrumentation. After the applied load was removed from the beam, a permanent set of 2.38 in. was measured at midspan (Figure 97).



Figure 97–XC: Permanent set

Measured compressive concrete strains in the top of the deck at midspan were near 0.003 at termination of the test and the load-deflection plot was nearly flat, indicating that the prestressing strands were yielding and that the specimen's actual flexural strength would not have been significantly higher than the peak load of 158 kip (Figure 98). The strain gage at the top of the deck at midspan also indicates a change in slope at 77 kip, corresponding to the cracking load indicated by the load-displacement plot.

Inspection of the strain load-strain plot of the gage on the bottom flange at midspan suggests that cracking of the section was predicated by microcracking (beginning at 73 kip).

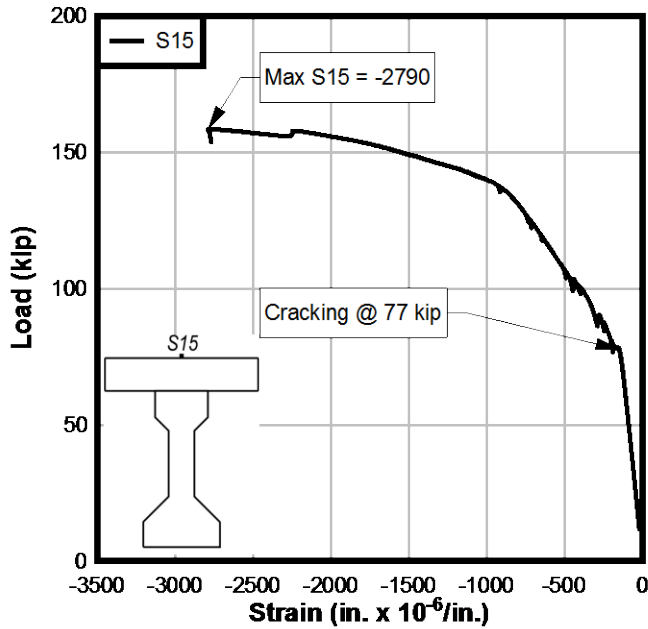


Figure 98–XC: Compressive concrete strain at midspan

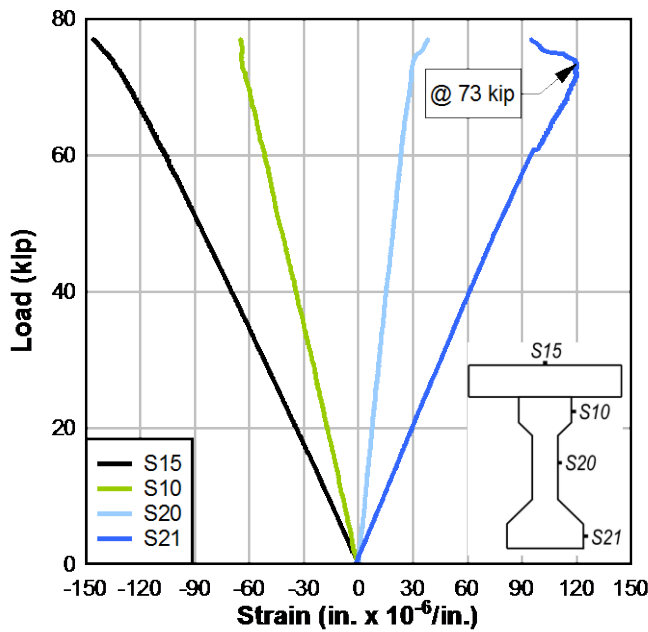


Figure 99–XC: Midspan strain profile

Out-of plane displacement was also monitored; very little out-of-plane movement occurred during the load test. No significant strand slip was recorded during the load test (the maximum was 0.0003 in.), indicating that the load points were far enough away from the supports to ensure a flexural failure mode under the area of interest.

## 10.2 Flexure–X1

Figure 100 shows the load-displacement plot of the spliced flexure test specimen X1. X1 was a spliced specimen constructed of segments 4b (from pour 1) and 9u (from pour 2) (Figure 43). The plot indicates that as load was applied, X1 exhibited linear-elastic behavior up to an applied load of approximately 64 kip.

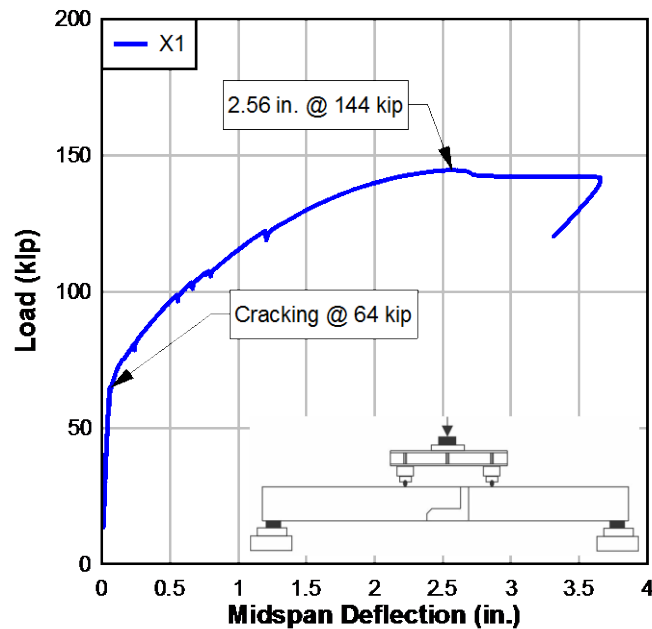


Figure 100–X1: Ultimate

At 68 kip, a single crack was visually observed at the vertical interface of the unbonded precast and the closure pour (Figure 101). Note that this was the only crack at this load; other inconsistencies in the white-wash seen in the figure are from incomplete white-wash application or rough surfaces of the concrete. Prior to 68 kip, only superficial cracks where the closure pour overlapped the precast concrete were noted (Figure 102).

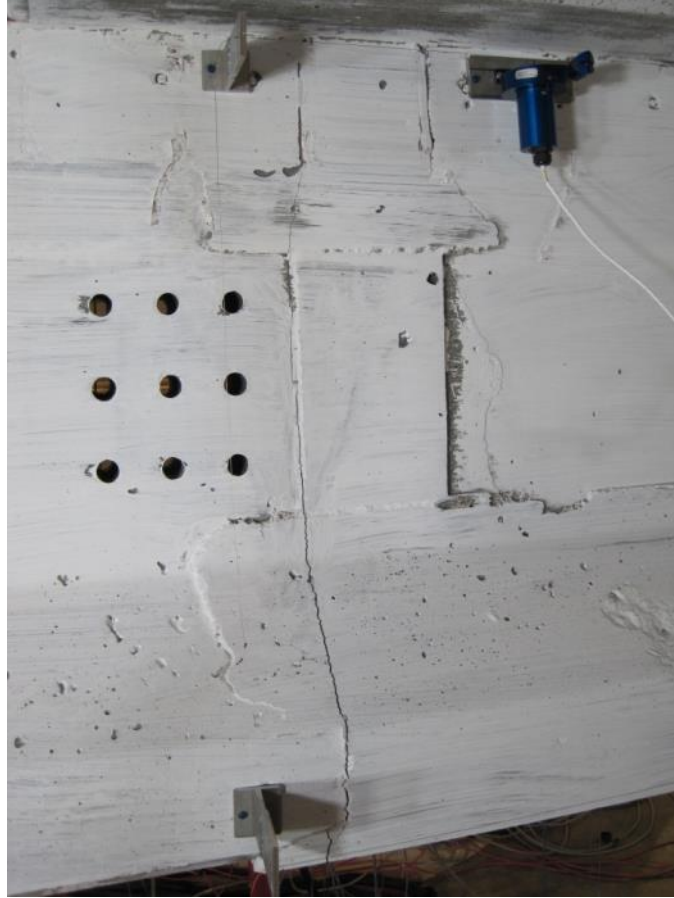


Figure 101-X1: Vertical crack at interface



Figure 102-X1: Superficial cracks at overlap

After cracking, X1's behavior became inelastic, indicated by the nonlinearity of the load-deflection plot as stiffness decreased. As additional load was applied, the single vertical crack

continued to open, until approximately 80 kip, when flexural cracks began to develop in the bonded section of the specimen. From approximately 80 to 120 kip, sudden minor load decreases occurred periodically until the midspan deflection reached approximately 1.25 in. These decreases indicated flexural crack formation and were confirmed with audible cracking sounds and visual observations. Figure 103 shows the cracks after termination of the load test.

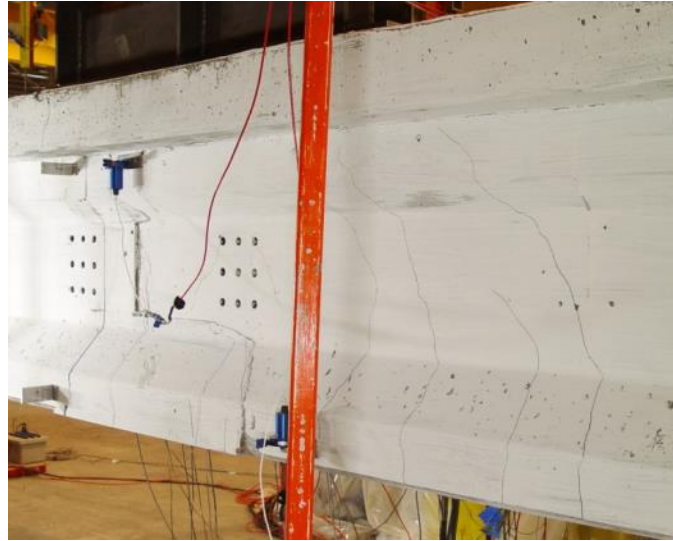


Figure 103–X1: Flexural cracking

At 144 kip, the peak load was reached as X1 deflected 2.56 in. at midspan. Following a load drop of approximately 2 kip, the specimen continued to deflect without resisting additional load. Failure of X1 occurred when the deck above vertical interface crushed; the failure was accompanied by pronounced vertical deflection of the specimen prior to deck failure. Figure 104 shows the measured deck strain at midspan (gage S15) and near the location of deck crushing (S16); the maximum compressive strain of approximately 0.002 was measured nearest the crushed concrete.

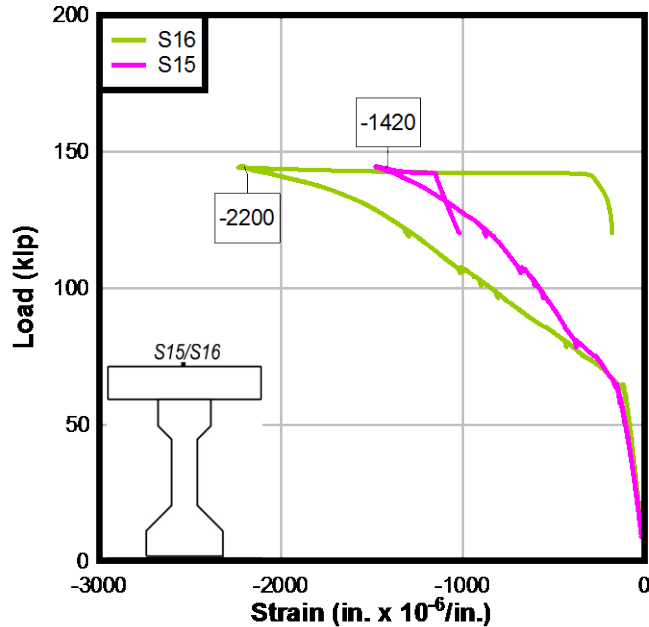


Figure 104-X1: Deck strain

No significant strand slip was recorded (the maximum was 0.004 in.) during the load test, indicating that the load points were far enough away from the supports to ensure a flexural failure mode in the area of interest.

### 10.3 Service and Cracking Behavior

To highlight the flexural service behavior, Figure 105 shows the load-displacement plot of XC and X1 up to a midspan deflection of 0.3 in. The secondary y-axis shows the ratio of the calculated bottom fiber stress to  $\sqrt{f'_c}$  (psi). The bottom fiber stress is calculated assuming the effective prestress level calculated for XC based on the initial prestress reported in the stressing records minus the prestress losses measured by the vibrating wire strain gages. The load level corresponding to the extreme fiber tensile stress at the splice location for the Service III limit state in the prototype FIB96 is shown for reference ( $5.3\sqrt{f'_c}$  (psi)).

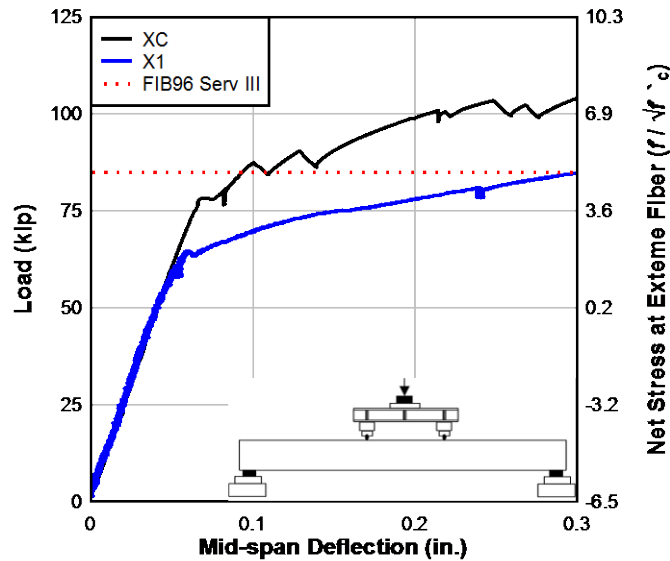


Figure 105–XC and X1: Elastic behavior

As shown in the plot, both test specimens exhibit either cracking or joint opening (in the case of X1) prior to both the prototype FIB96 Service III stress ( $5.3\sqrt{f'_c}$  (psi)) and the predicted cracking load. Assuming that cracking occurs when the extreme bottom fiber tensile stress reaches  $7.5\sqrt{f'_c}$ (psi), the predicted cracking load was calculated to be approximately 105 kip for both specimens, based on the measured effective prestress. The XC specimen cracked at an applied load of 77 kip, while the spliced X1 specimen developed a joint opening at 64 kip. These applied loads corresponds to an approximate bottom fiber stress of  $3.8\sqrt{f'_c}$ (psi) and  $2.2\sqrt{f'_c}$ (psi) in XC and X1, respectively.

Potential causes for the low cracking load were investigated, including the low specified jacking prestress of  $0.6f_{pu}$  (vs. the more typical  $0.75f_{pu}$ ), the achieved initial prestress level at lock-off, and measured prestress losses. For the following discussion of the cracking load, the control specimen XC is considered.

The lower-than-usual specified prestress was investigated as a potential cause of the low cracking load caused by a longer than anticipated transfer length. Research done by Kaar et al. on beams prestressed with 7-wire 1/2-in. diameter 270 ksi prestressing strand with lower than typical effective prestress indicate that at lower levels of effective prestress, the measured transfer length is consistently less than the transfer length as calculated by AASHTO-LRFD (Kaar et al. 1963; AASHTO 2007). Similar trends have been reported by others. Further, research by Kaar et al. (1963), and Zia and Mostafa (1977) indicate that a gradual release of

prestress, as was performed during the construction of the test specimens, reduces the transfer length.

Inspection of the precast yard stressing records confirms that the prestressing strand was tensioned to the specified  $0.6f_{pu}$  and that temperature effects were considered. Due to the atypical specification of  $0.6f_{pu}$ , careful attention was paid by the precaster and UF personnel during the stressing operation. It is assumed that the specified initial jacking prestress was achieved and is not the cause of the low cracking load.

Excessive prestress losses were also investigated and dismissed as a potential cause of the low cracking load. Prestress losses were measured with vibrating wire strain gages at the approximate height of the strand pattern centroid. VWSG measurements of the differential strain change over time indicated a prestress loss of approximately 6% in both the XC and in the bonded segment of the spliced specimen X1 (location of X1's first crack).

The prestress loss measured with the VWSG corresponded well with the prestress loss predicted by PCI, which predicts an approximate loss of 8%. (A table of estimated prestress losses for all specimens based on the PCI method is included in Chapter 8.) As a further check of the VWSG reliability, VWSG strain measurements were compared with strain measurements of external foil strain gages at low applied loads (before cracking) while the test specimen was behaving elastically. Figure 106 shows the strain measurements of both the VWSG and the external foil strain gage at the midspan of XC, at approximately the same height. During the load test, VWSG measurements were recorded manually every 10 kip, while the foil gage measurements were recorded continuously by the DAQ. The VWSG readings have been corrected for batch and temperature effects. The gages correlate well, confirming the VWSG readings; it can be assumed that VWSG were reading properly.

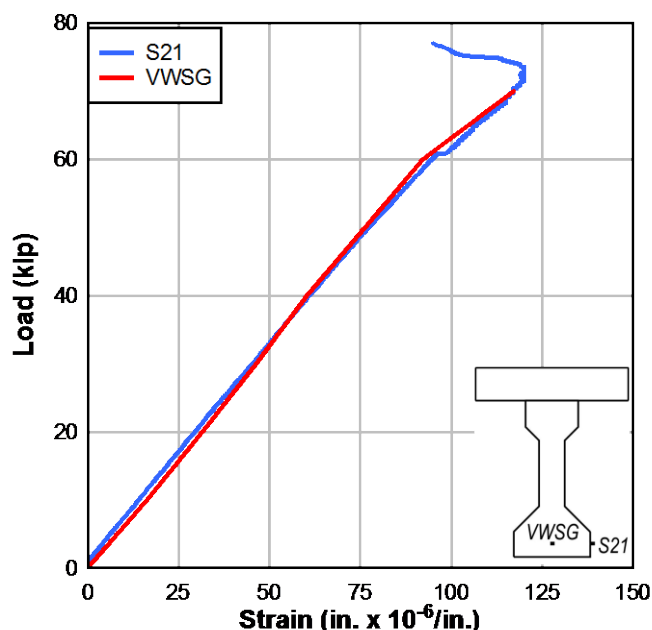


Figure 106–XC: VWSG vs. bottom flange strain gage

O’Neill and Hamilton (2009) observed the trend that girders with lower effective prestress force exhibit lower bottom fiber stresses ( $6.1\sqrt{f'_c}$  (psi) to  $7.6\sqrt{f'_c}$  (psi)) while the same girder section with higher effective prestress cracked at higher bottom fiber tensile ( $12.1\sqrt{f'_c}$  (psi) and  $14\sqrt{f'_c}$  (psi)); however in all cases, the measured cracking stresses were within the anticipated range of  $6-7.5\sqrt{f'_c}$  (psi). The general trend (of lower than expected cracking load) may be seen in the experimental data, but it cannot be stated definitively, given that the magnitude of the cracking stresses is so low.

No cause of the low cracking load was identified; however, because the segments used to construct the spliced beams were constructed in the same manner during the same period and, in the case of the bonded segments, simultaneously, the cracking load of the control beam is used as a benchmark for further comparison with the spliced specimens. Whatever the mechanism, because all the specimens cracked at a low load, and based on the decompression/crack opening tests to back-calculate the induced prestress, it must be assumed that the prestress level in each of the precast segments is less than the effective prestress predicted by the specified value minus the measured prestress losses.

X1 cracked at a lower load than XC, as can be seen in the plot; consideration of the location of the initial crack, and the early crack development, explains this discrepancy. As in the case of a typical prestressed beam, XC cracks when the applied load overcomes the initial

precompression of the beam and the modulus of rupture of the concrete; in the case of XC, the beam cracks when the bottom fiber stress is approximately  $4\sqrt{f'_c}$  (psi). At the cracking moment, a flexural crack developed midway between the load points. X1's first crack, however, occurred at the vertical face of the closure pour (Figure 107).

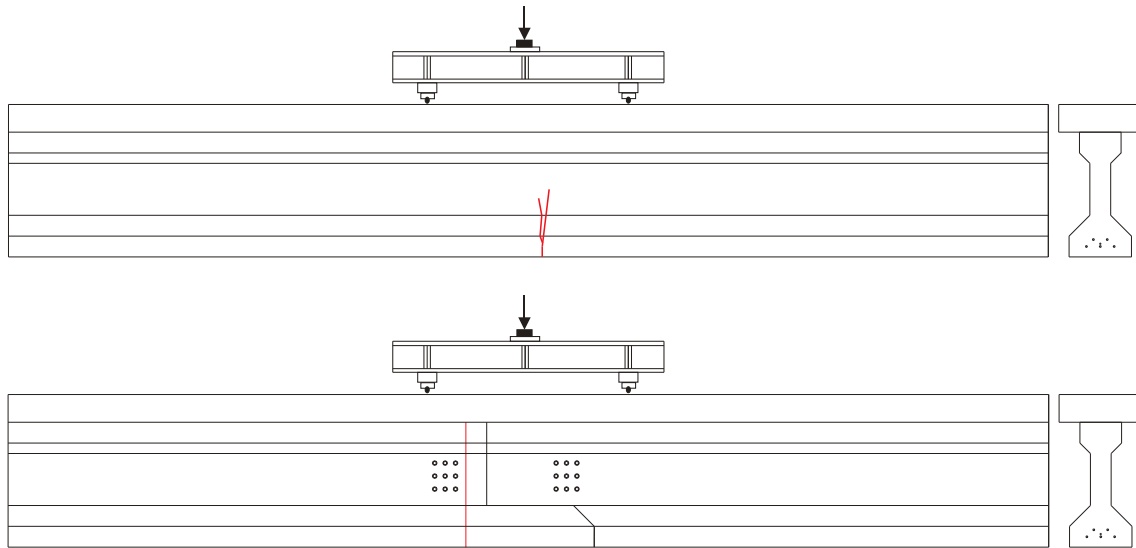


Figure 107–XC vs. X1: first crack

The abrupt change in stiffness noted in the load-displacement plot of X1 is not a cracking load, but rather the load required to overcome bond at the dry joint between the precast segment and CIP splice concrete. Consequently, a lower load - slightly greater than that required to reach the decompression moment—is required to open the joint (at approximately  $2.2\sqrt{f'_c}$  (psi)). In contrast with XC, the “crack” occurred at a pour interface, and was dependent on the bond between the precast concrete and the closure pour concrete. This joint opening mechanism is confirmed by post-failure inspection of the pour interface. As shown in Figure 108, the concrete pours separated almost directly down the interface, with little break-off of either concrete - evidence of little bonding of the two segments.

It can also be observed from Figure 108 that the shear keys exhibited little damage, indicating that the keys had sufficient strength to transfer shear across the interface.

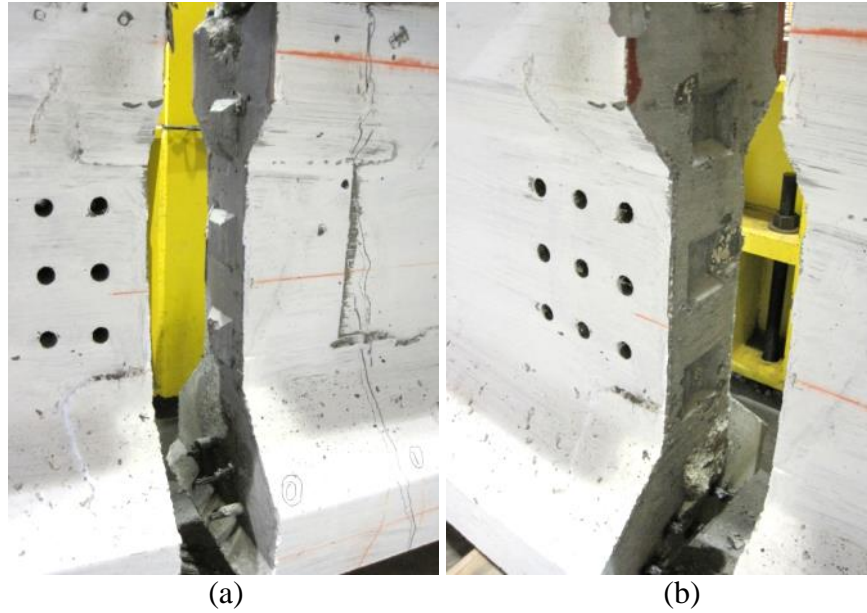


Figure 108–Dry joint interface post-demolition, looking at (a) the closure pour, (b) the precast

As loading progressed, XC cracks were noted to be uniformly distributed between the load points, which is typical of bonded prestressed beam behavior (Figure 109). Conversely, X1 behaved more like an unbonded, prestressed beam: the crack pattern focused around a single crack at the end of the unbonded length with some flexural cracks in the bonded segment.

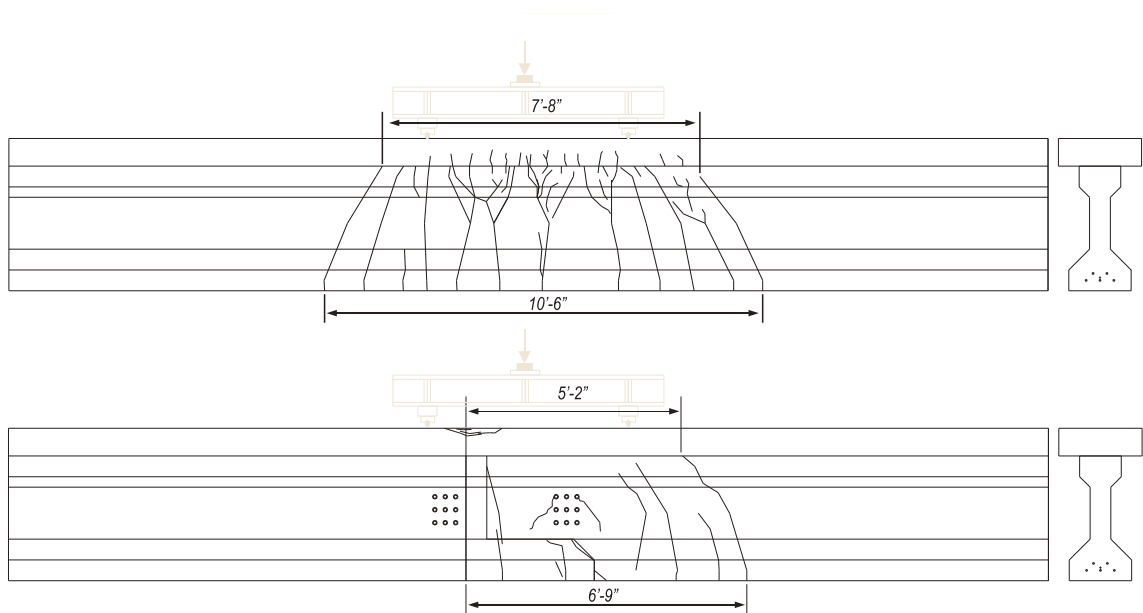


Figure 109–XC vs. X1: final cracking patterns

In XC, flexural cracks formed frequently as the load increased from 77 kip to approximately 135 kip as indicated by sudden minor drops in load (Figure 105). Furthermore, beyond 135 kip, XC resisted little additional load as the deflection increased. Formation of X1's first crack (at the vertical interface), however, occurred at 64 kip with no additional cracks forming until approximately 80 kip. This delay is reflected in the plot—no load drops are apparent from 64 to 80 kip. During the same load range in XC, several load drops and audible cracking were observed. Like in segmental bridge beams with unbonded tendons, the primary crack of X1 formed at the joint. After cracking, this primary crack continued to open with additional applied load, while the adjacent unbonded segment remained uncracked.

Figure 110 shows the displacement measured across the closure pour at the top and bottom of the precast section. Gages D11 and D13 measured the opening at mid-height of the bottom flange; gages D12 and D14 measured opening near the top of the top flange.

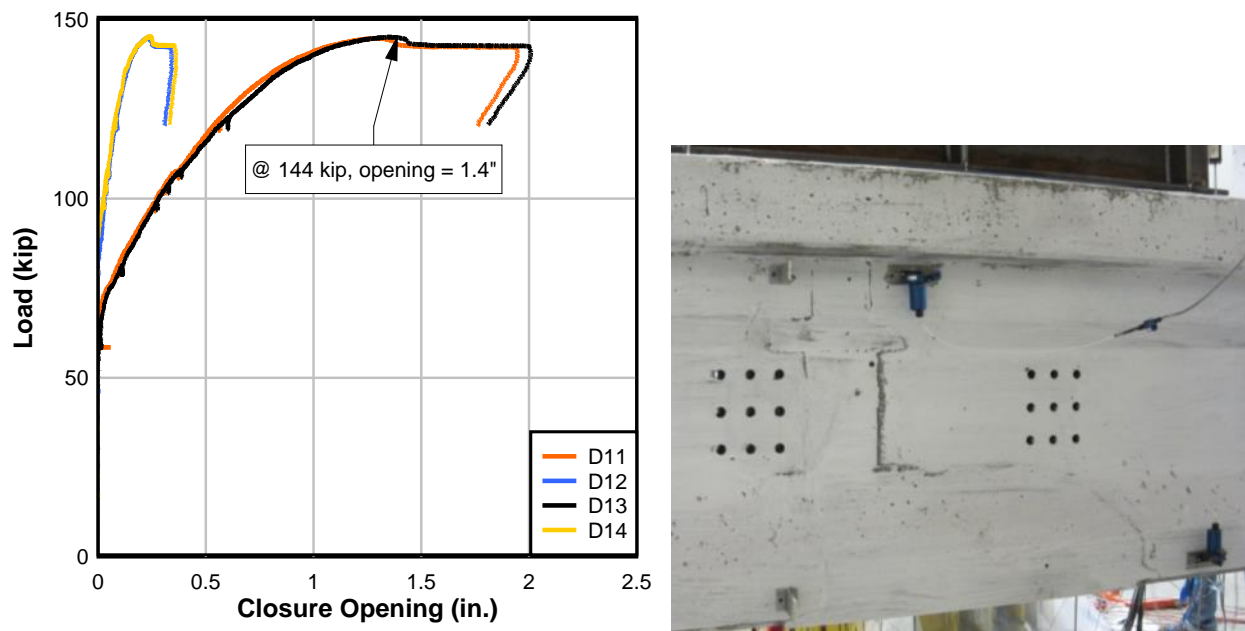


Figure 110–X1: String-pots across closure

At the maximum load, the four cracks contained in the interface opened a combined amount of approximately 1.4 in. at the mid-height of the bottom flange. As shown in Figure 111, most of the crack opening occurred at the joint.



Figure 111-X1: Opening at joint during test

There was some concern that out-of-plane movement of the splice specimen would be greater than normal, due either to the variable section stiffness along the beam's length or slight variation in the precast segment alignment due to the splice assembly process. To compare, out-of-plane displacement was monitored during load testing of XC and X1 (Figure 112). Both XC and X1 exhibited little out-of-plane displacement indicating that X1 behaved, at least longitudinally, like a homogenous, prismatic member under vertical load.

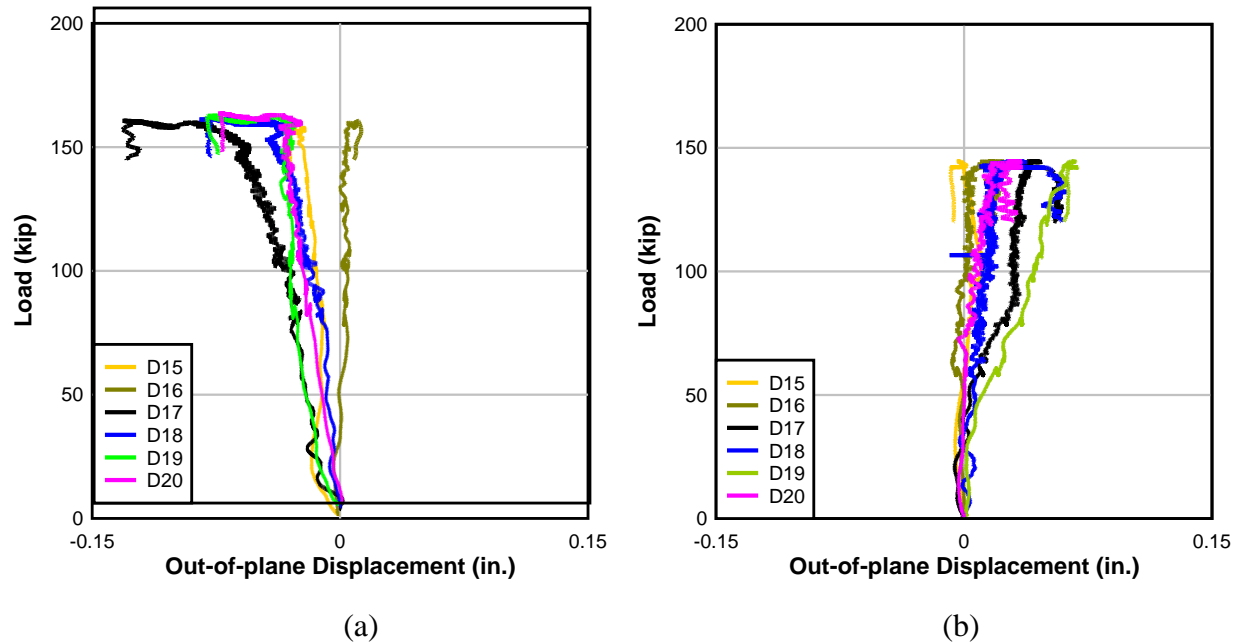


Figure 112–Out-of-plane displacement: (a) XC (b) X1

#### 10.4 Comparison of Flexure Strength

The computed flexural strength is compared to their respective load-displacement plots in Figure 113. The strength was computed in accordance with AASHTO-LRFD using specified materials of 4.5 ksi deck concrete and 270 ksi prestressing steel. The predicted bonded moment capacity at 0.003 concrete compressive strain was 631 kip-ft, which corresponds to an applied load of 123 kip. For both XC and X1, the peak load exceeded the predicted design strength of a bonded prestressed member. Considering the cracking behavior and failure mode of the spliced specimen X1, the AASHTO-LRFD capacity was also calculated assuming the steel strands were unbonded. The calculated moment strength, assuming all five strands were unbonded, was 589 kip-ft, which corresponded to an applied load of 114 kip. X1 exceeded the anticipated capacity of an unbonded section.

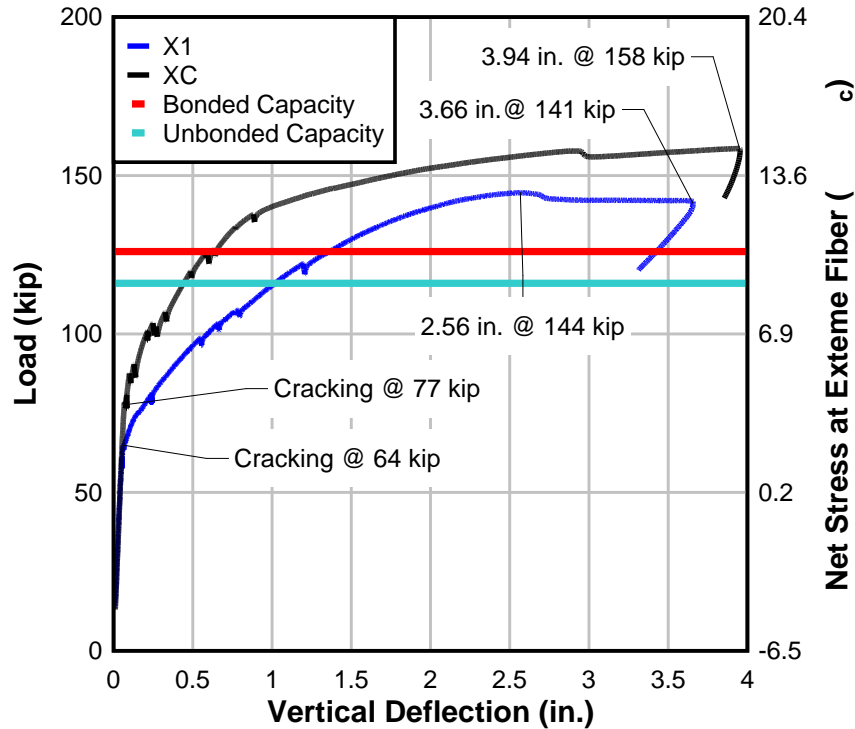


Figure 113–Flexural strength: XC and X1

The flexural capacity of X1 was approximately 144 kip; compared with XC’s capacity of 158 kip. This is only a difference of approximately 8%. Both specimens exhibited significant vertical deflection at midspan under maximum load. The displacement ductility of X1 was of interest in evaluating the influence of the coupler on the overall beam behavior. In preliminary strand-in-air tests of the couplers with strand, the wedge of the couplers caused the strand to rupture prior to yield. In the test of X1, however, the opening of the joint at the vertical interface (away from the coupler) prevented flexural cracking from occurring at or adjacent to the coupler and the strand yielded prior to the compressive failure of the deck. It appears the closure pour concrete contributed to the overall anchorage of the strand at the coupler, holding the coupler in place. Another possibility is that the concrete surrounding the anchor wedges intruding into the wedges during pour of the closure. The wedges were thereby unable to slip at higher loads, preventing stress concentrations on the strand and thus delaying rupture.

At the maximum applied load of 145 kip, the beam continued to deflect without resisting additional load. The midspan deflection at the maximum applied load was approximately 2.6 in. with a permanent set 0.75 in. upon load removal. X1 exhibited a tension-controlled flexural failure as the deck concrete crushed (Figure 114).

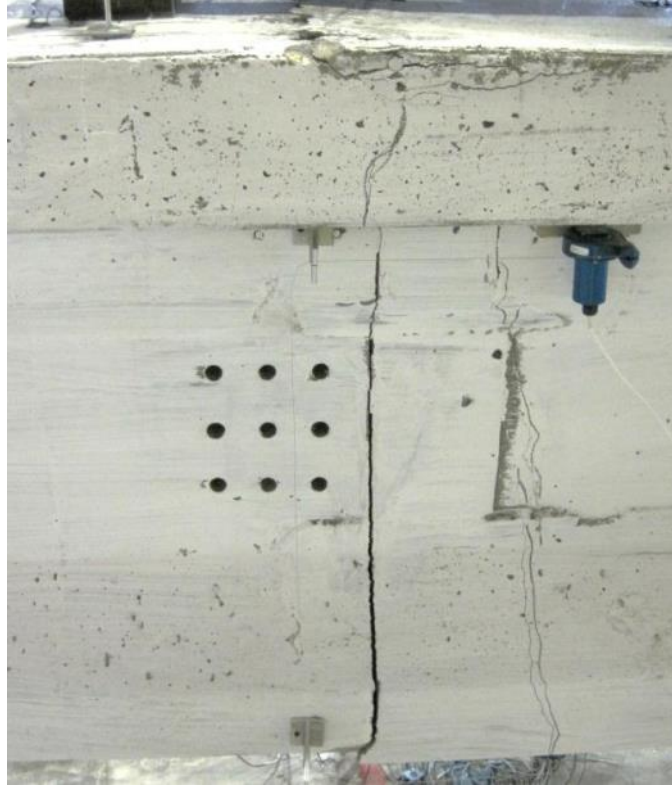


Figure 114—Damage to X1 following testing with spalled concrete in compression zone and wide, permanent crack

Evidence of strand yielding can be seen in the strand load during and after the flexural load test (Figure 115). At the start of the load test, each strand had approximately 25 kip of prestressing force. Until the specimen cracked at approximately 64 kip of applied load, the prestressing strand showed little increase in force. After cracking, the strand load increased until the test was terminated. After unloading the specimen upon completion of the load test, the load cells read approximately 5 kip per strand—the loss in load indicating that the strand had yielded. Further, strand-in-air testing of the prestressing strand used in the specimen indicated that the yield strength (defined as 1% elongation) of the strand was approximately 39.2 kip (Appendix E—Precast Yard and Material Reports); every strand was loaded beyond this predicted yield point. In fact, the ultimate tensile strength of the strand was approximately 43.7 kip.

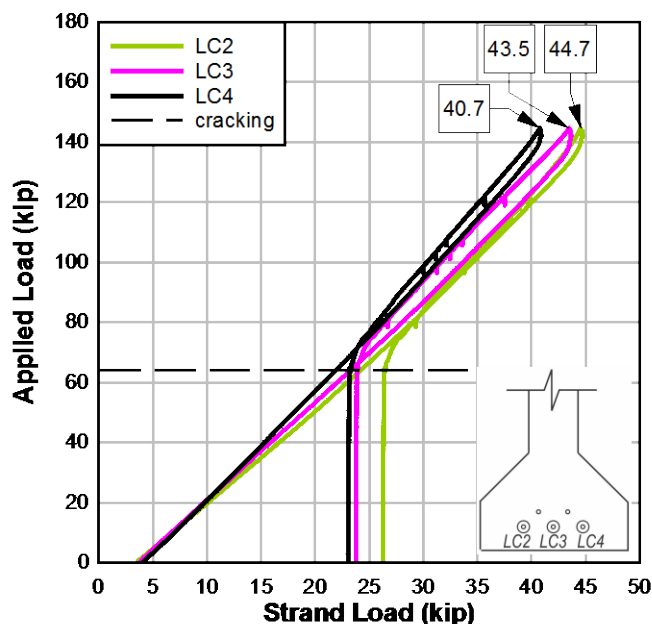


Figure 115-X1: Strand load

Despite concerns that the coupler would cause premature rupture of the strand prior to yield, the strand went well into its yield plateau prior to the compression failure of the deck concrete. Evidence of strand yielding is in the incomplete closure of the main crack after complete unload (Figure 114), in the reduction of the readings of the strand load cells (Figure 115) and in the permanent deflection of the beam (Figure 97).

An interesting comparison of capacity can be quantified by comparing the observed failure moment and reserve capacity (if applicable) to the predicted cracking moment. XC reached its peak (and ultimate) load at 2.1 times its cracking load; X1 reached its peak load at 2.3 times its cracking load. After achieving peak load, X1 continued to carry approximately 98% of the peak load, deflecting nearly 1 in. prior to a crushing of the deck. Even taking into consideration that the control load test (XC) was stopped to protect the instrumentation prior to ultimate load, based on strain measurements both specimens exhibited nearly similar capacity prior to failure.

For purposes of design, it appears that, based on the performance of the spliced specimen, the flexural capacity of the splice region can be conservatively predicted by assuming bonded prestressing strands. A more conservative approach would be to assume unbonded strands in the splice region.

## 11 Shear Results and Discussion

Four specimens were tested in a three-point set-up to evaluate shear behavior: one control specimen (SC) and three spliced specimens (SB, SU, and SU2). This chapter presents and discusses the results. The test set-up and procedure are described in Section 7.3.

### 11.1 Shear–SC

Figure 116 shows the load-displacement plot of the shear control test specimen (SC)—a continuously prestressed precast beam. SC was precast segment 1 from pour 1 (Figure 43). The orientation of the SC load test was chosen to compare behavior with the SU and SU2 spliced specimen load tests. The plot indicates that as load was applied, SC exhibited linear-elastic behavior up to a cracking load of approximately 128 kip.

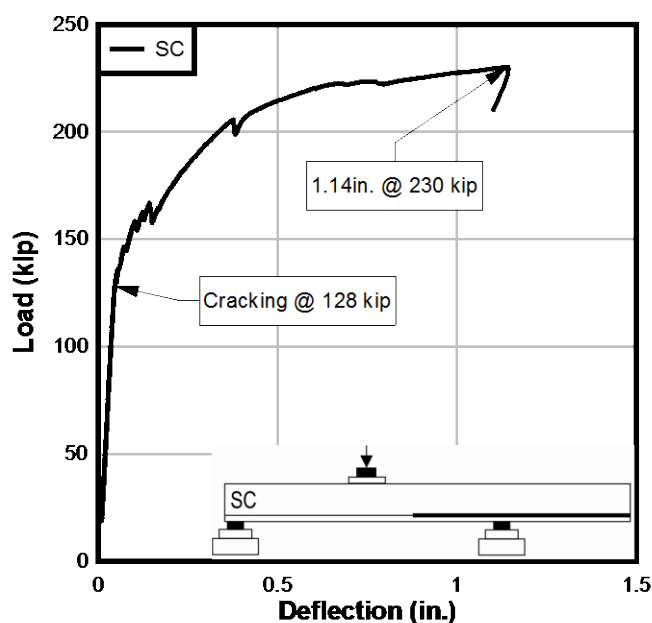


Figure 116–SC: Ultimate

The first visible crack was a flexural crack which occurred at 128 kip. It formed approximately under the load point (Figure 117). While SC is a homogenous precast specimen, the location of what would be the closure pour in a spliced beam has been sketched onto the beam to provide a reference for discussion.

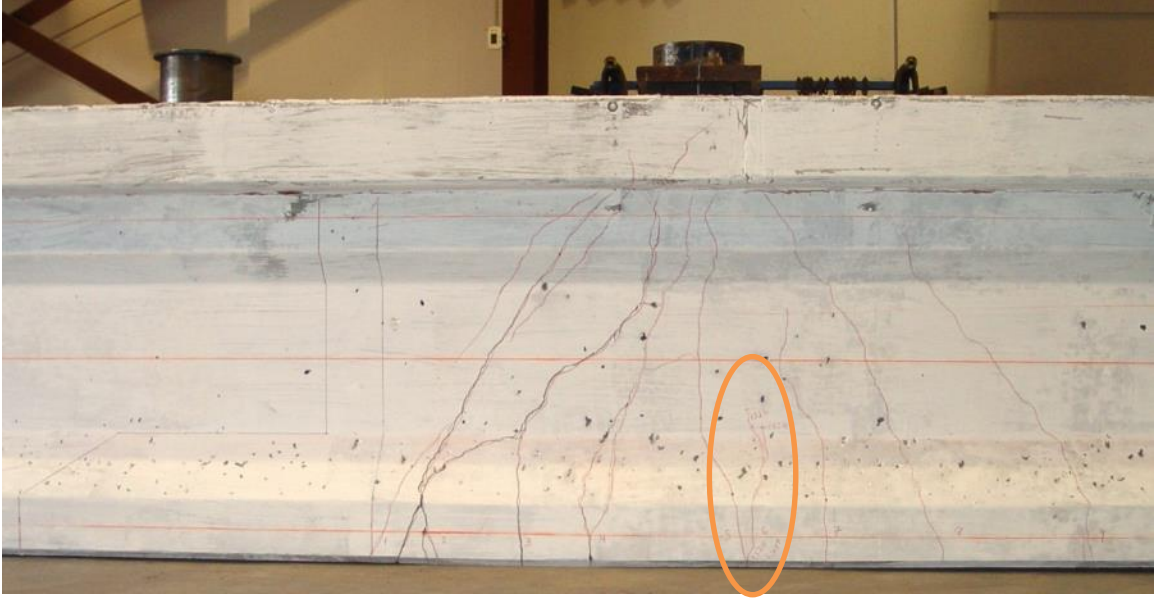


Figure 117-SC: Crack pattern

As SC was loaded beyond cracking, sudden minor load decreases occurred periodically until the midspan deflection was approximately 0.4 in. These decreases indicated flexural crack formation and were confirmed with audible cracking sounds and visual observations of the crack development. At the peak load of 230 kip, the specimen deflected approximately 1.1 in. at the load point. A flexural failure mode was observed as the deck concrete crushed under the load point. A permanent set at the load point of 0.4 in. was measured after the load was removed.

Compressive strain measured in the deck strain at the load point reached approximately 0.003 (Figure 118). The strain gages become erratic prior to the peak load, indicating local cracking of the concrete in the top of the deck.

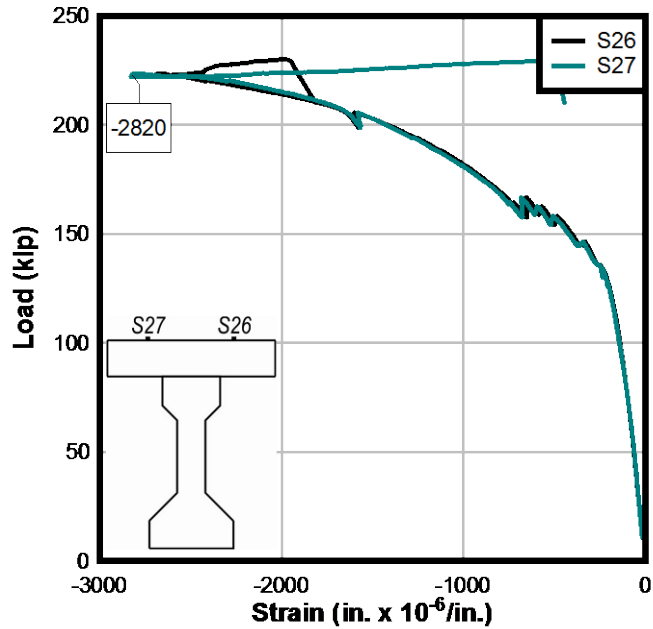


Figure 118-SC: Strain at load point

## 11.2 Shear-SB

Figure 119 shows the load-displacement plot of the spliced test specimen loaded with the load applied to the bonded segment. This is referred to as specimen SB - the spliced specimen constructed of bonded segment 5b and unbonded segment 5u (Figure 43). The plot indicates that, as load was applied, SB exhibited linear-elastic behavior up to a cracking load of approximately 120 kip; a crack was visually observed at this load.

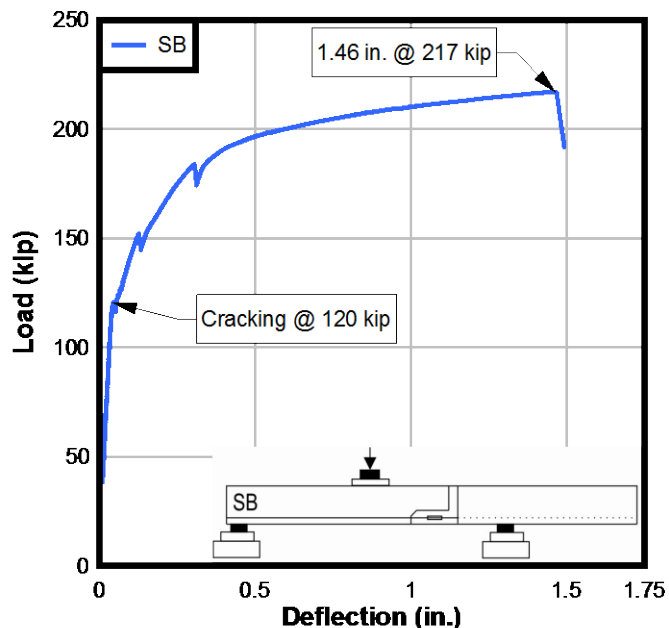


Figure 119–SB: Ultimate

The first visible crack was a flexural crack located approximately under the load point. The load was held at 120 kip and the crack was marked. The first crack is circled in Figure 120.

As the specimen was loaded beyond cracking, two load decrease events occurred—one at 145 kip and again at 183 kip. The load dropped was approximately 8 and 10 kip, sequentially. These load decreases correspond to slight changes in the strand slip gages (Figure 121); the magnitude of the strand slip readings suggest that the gages were jostled by the cracking of the beam, not strand slippage.

The peak load was approximately 217 kip when the deck failed in compression under the load point (Figure 122); a maximum deflection of 1.5 in. occurred at the load point at the ultimate load.

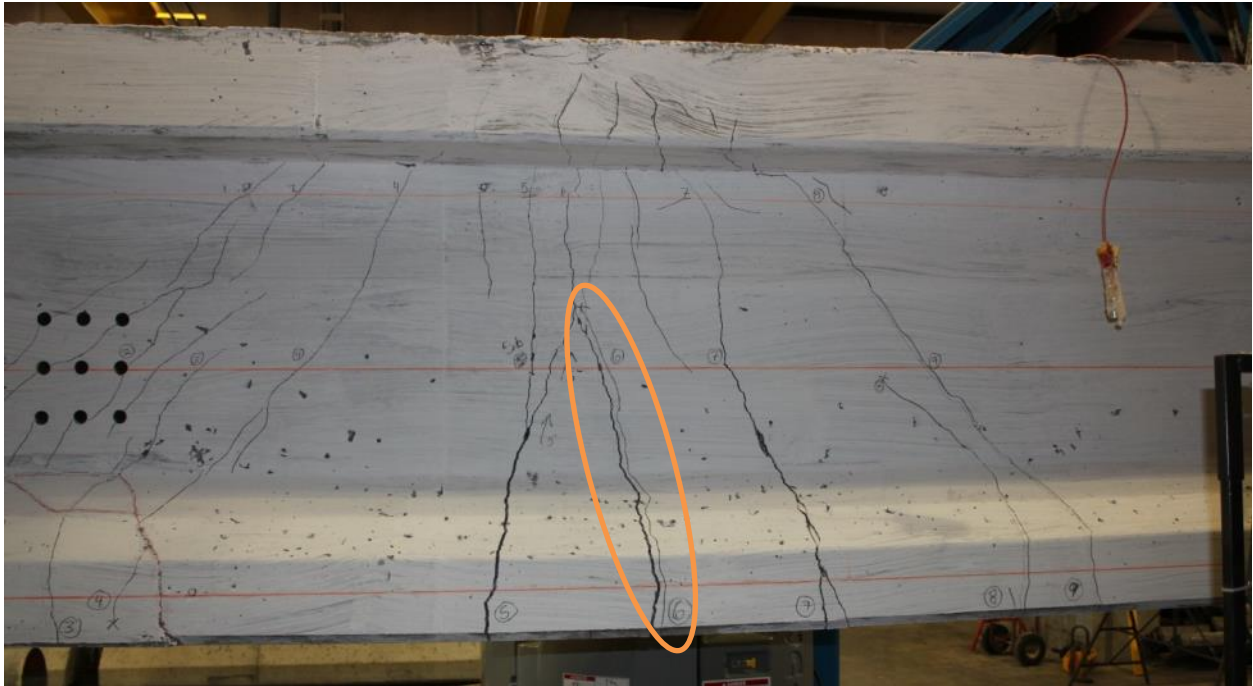


Figure 120-SB: First crack

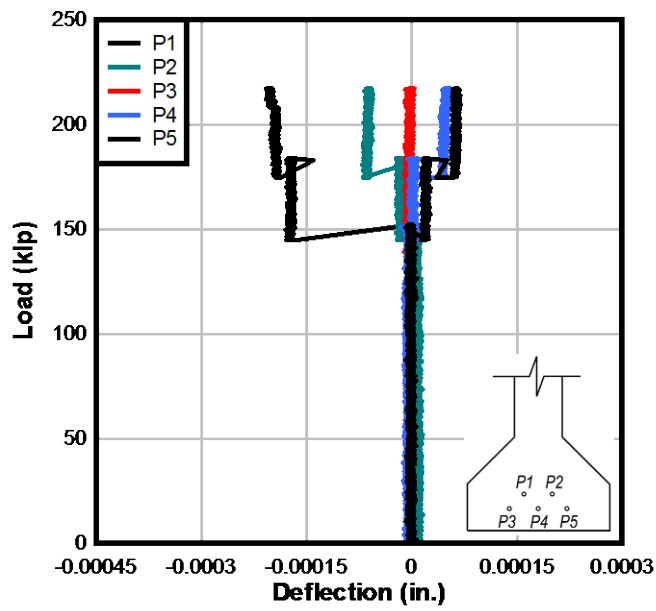


Figure 121-SB: Strand slip



Figure 122–SB: Deck at failure

Compressive strains at the top of the deck near the load point maxed out around 0.0035 at a load of approximately 208 kip (prior to the peak load); the plot is shown in Figure 123. From 208 to 217 kip, the deck concrete experienced local crushing around the concrete, indicated by the strain reversal measured by the gages.

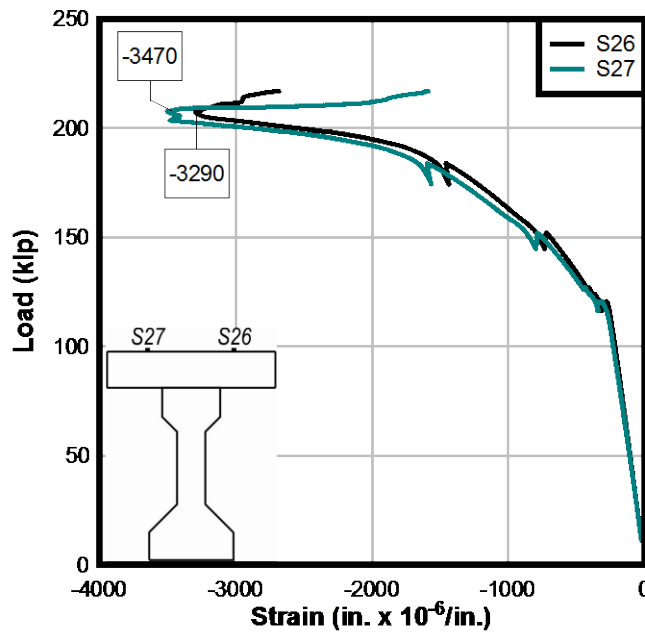


Figure 123–SB specimen: Strain at load point

### 11.3 Shear–SU

Figure 124 shows the load-displacement plot of SU with the load applied to the unbonded segment. SU was the spliced specimen constructed of bonded segment 9b and unbonded

segment 7u (Figure 43). The plot indicates that, as load was applied, SU exhibited linear-elastic behavior up to a cracking load of approximately 125 kip.

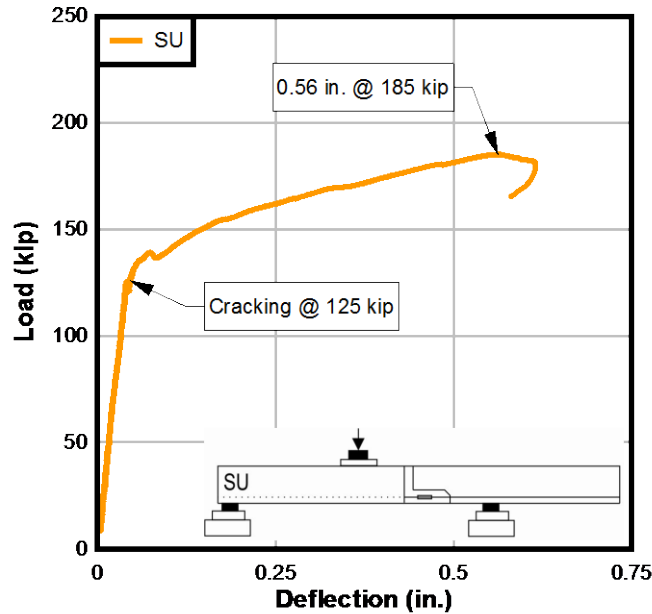


Figure 124–SU: Ultimate

The first visible crack was a web shear crack forming across the joint in the splice area (Figure 125).

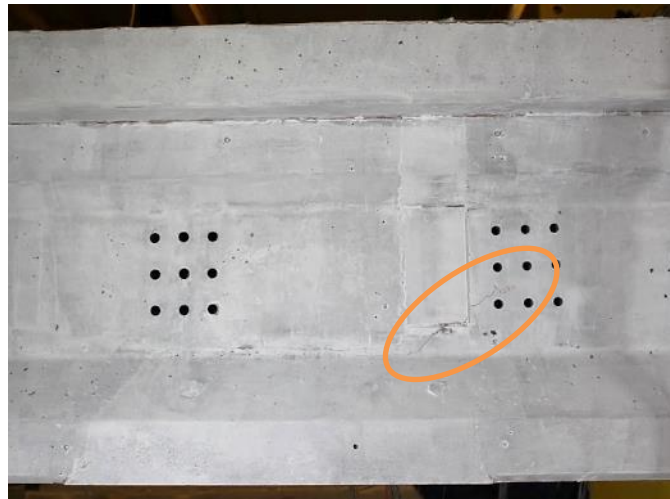


Figure 125–SU: First crack

As load application continued, the cracks propagated diagonally toward the load point. At 130 kip, an opening of the joint was observed at the vertical interface between the closure pour and the unbonded segment. SU exhibited a slightly reduced stiffness, until approximately 140 kip. Where a crack crossed a joint interface, the crack changed direction to follow the path

of least resistance, i.e., the dry joint. From 140 kip to 185 kip, the load-deflection nearly plateaued, revealing marked reduction in specimen stiffness. Once the compression concrete was lost (through cracking of this region), the unbonded segment suddenly slipped downward. At the peak load of 185 kip, SU deflected approximately 0.6 in. at the load point. A shear failure mode was observed as the crack at the vertical interface propagated until a slip occurred between the closure pour and the unbonded precast segment. A torsional rotation of the top flange away from the bottom flange was observed. Figure 126 shows the spliced region cracking after failure.

Compressive strain measured in the deck concrete at the load point did not reach 0.003 (Figure 127).

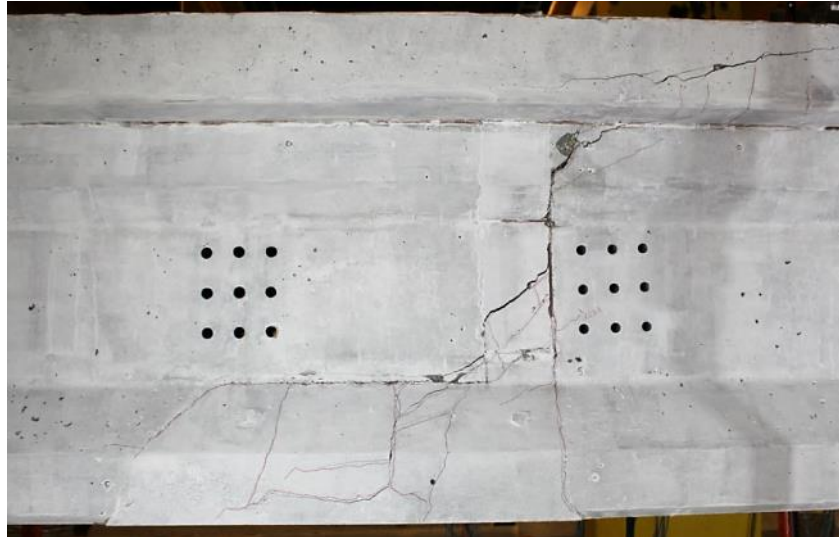


Figure 126-SU: Joint at failure

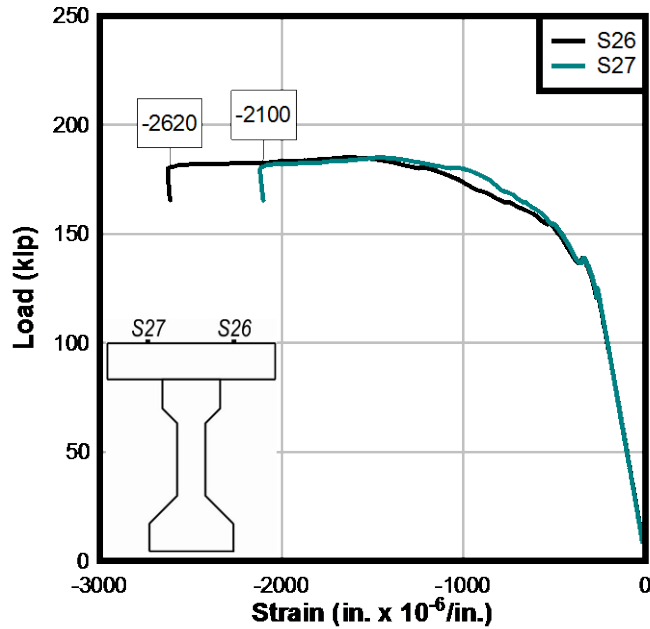


Figure 127–SU specimen: Strain at load point

#### 11.4 Shear–SU2

Figure 128 shows the load-displacement plot of the second spliced test specimen—hereafter referred to as SU2—with the load applied to the unbonded segment. SU2 was the spliced specimen constructed of bonded segment 8b and unbonded segment 4u (Figure 43). This load test was performed to verify the behavior of the first SU test. The plot indicates that as load was applied, SU2 exhibited linear-elastic behavior up to a cracking load of approximately 123 kip.

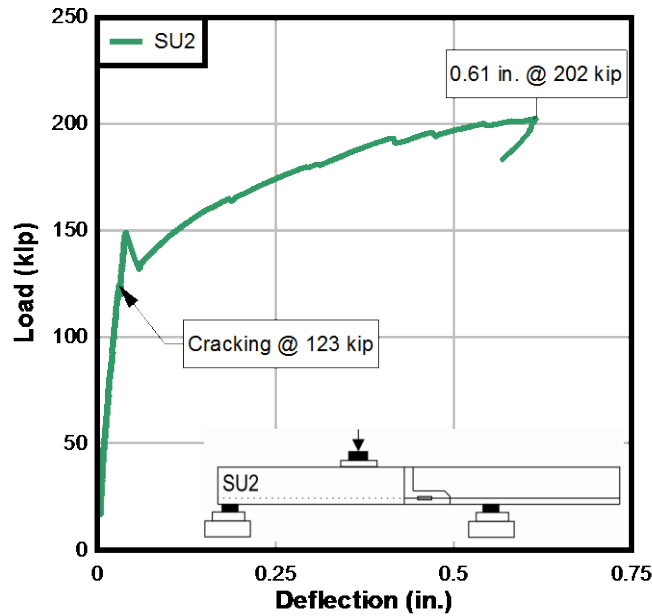


Figure 128–SU2: Ultimate

The first visible crack was a web-shear crack which formed in the precast concrete near the joint (Figure 129). At the cracking load, the crack affected only the precast concrete, halting at the closure pour.

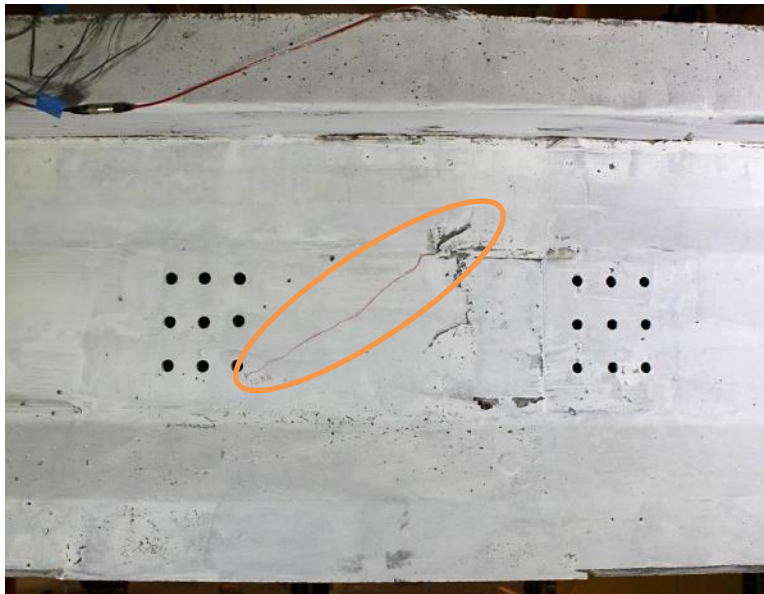


Figure 129–SU2: First crack

As additional load was applied, SU2 exhibited reduced—but nearly equal- stiffness, until approximately 149 kip. At 149 kip, a major load decrease of approximately 18 kip occurred when a flexural crack formed directly under the load point (Figure 130).



Figure 130–SU2: Flexural crack at 149 kip

At the peak load of 202 kip, SU2 deflected approximately 0.6 in. at the load point. A combined flexural-shear failure mode was observed as the main flexural crack under the load point continued to open and the web-shear crack (the first crack) propagated diagonally toward the load point; slip between the two segments at the vertical interface of the closure joint was again observed, similar to the test of the SU specimen (Figure 131).

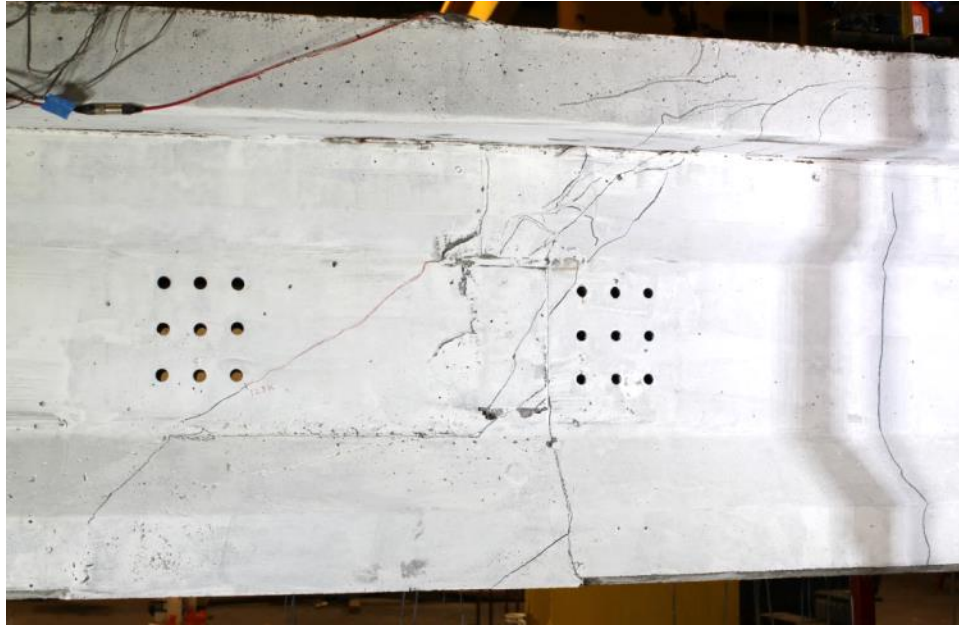


Figure 131-SU2: Joint at failure

Compressive strain measured in the deck strain at the load point exceeded 0.003 (Figure 132), corresponding with observed crushing of the deck concrete at the load point.

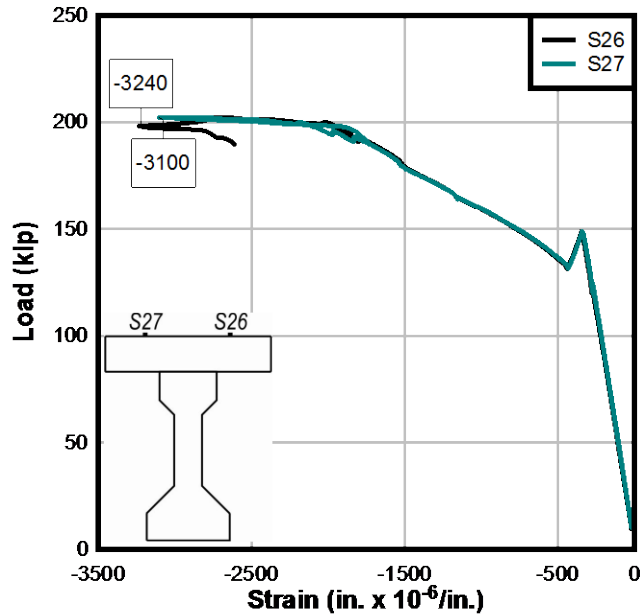


Figure 132-SU2: Strain at load point

### 11.5 Comparison of Service and Cracking Behavior

To aid the discussion of the shear specimens' service and cracking behavior, Figure 133 compares the test set-ups of the SC, SB and SU specimens and provides each specimen's bond pattern. As illustrated in the figure, several spliced specimens were tested, varying the orientation of the bond pattern to encompass the behavior of each side of the spliced beam. A single control specimen—with continuously prestressed, bonded strand—was oriented in the direction of most interest, based on the spliced specimen results. The chosen orientation of the control specimen (SC) placed the end with five bonded strands under the load point similar to the load tests of SU and SU2. The orientation of SC matched the quantity of strands in the shear span, but not the bonding pattern, to SU and SU2.

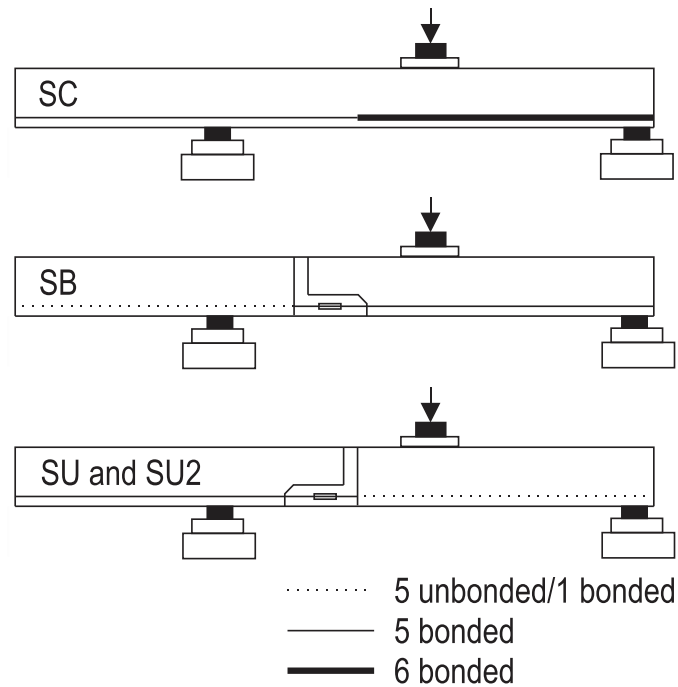


Figure 133–Bond patterns of shear tests

To highlight the elastic behavior the shear specimens, Figure 134 shows the load-displacement plot up to a deflection of 0.2 in.

Each specimen behaved linear-elastically up until cracking. Specimen SU2 exhibited slightly stiffer behavior than SC, SB, or SU. The cracking loads are given in Table 29.

SC had the highest cracking load at an applied shear of 128 kip; all of the spliced specimens cracked within 10 kip of this value. Consideration of the location and type of crack is relevant.

Figure 135 shows the first crack location of each shear specimen. The first crack is shown as a thick red line.

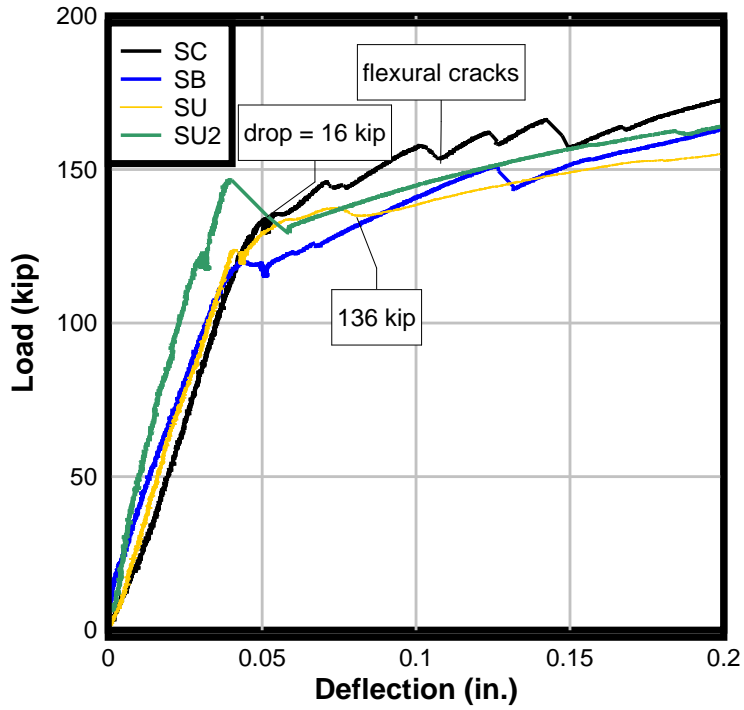


Figure 134–Shear comparison: Elastic behavior

Table 29–First crack of shear specimens

Specimen	Crack Type	Cracking load (kip)
SC	Flexure	128
SB	Flexure	120
SU	Web-shear	125
SU2	Web-shear	123

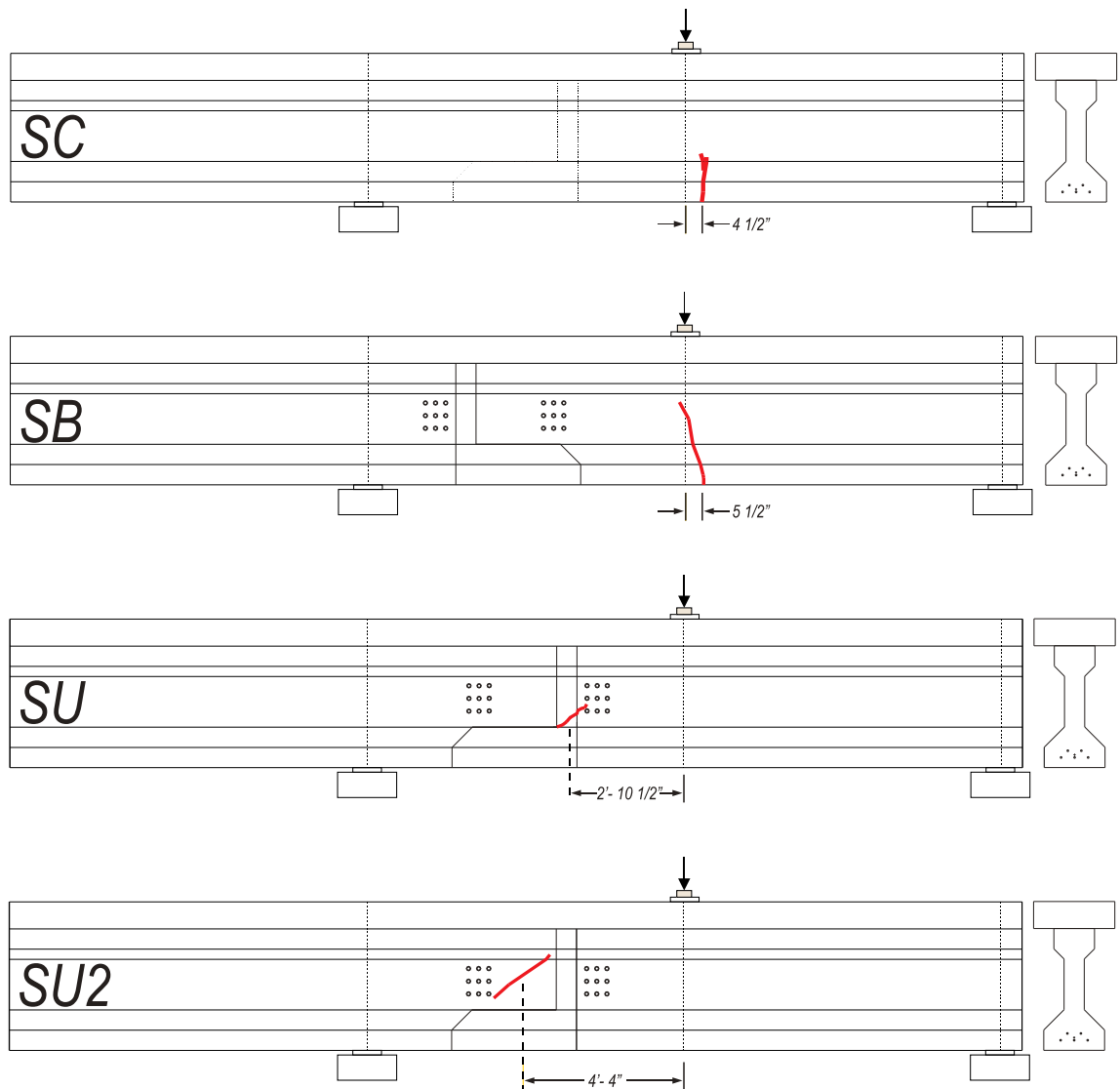


Figure 135–Shear specimens: First crack locations

The first crack in the SC and SB specimens was a flexural crack and occurred in nearly the same location—approximately under the load point. Based on the effective prestress, as determined from the stressing records and the VWSGs, and the applied load, the bottom fiber stress at cracking of the SC and SB specimens was  $4.1\sqrt{f'_c}$  (psi) and  $3.6\sqrt{f'_c}$  (psi), respectively .

Both SU specimens exhibited similar service level shear behavior. In both the SU and SU2 beam, the first crack formed as a web-shear crack near the joint. In the SU beam, the web-shear crack crossed the interface between the precast concrete and the closure pour concrete. The formation of the SU crack in this location—crossing the pours—indicates composite action between the precast and closure pour. On the other hand, its development within the joint

indicates a possible weak area of the splice, where the smaller size of the aggregate in the closure pour provides less aggregate interlock to resist shear and where the increased spacing of the stirrups has reduced contribution to the shear capacity. In contrast, the first crack of the modified SU2 affected only the precast concrete of the spliced specimen. The use of the epoxy bonding agent appears to have strengthened the joint region, forcing the first crack formation away from the joint.

As the crack development progressed after first crack, the specimens continued to exhibit very different behavior. The SC and SB specimens developed multiple flexural cracks, well-distributed under the load point, in the fan-like formation typical of crack patterns seen in three-point bending tests of bonded prestressed beams.

The SB specimen developed cracks across a larger portion of the span, especially around the pipe inserts. Two possibilities for the prevalence of cracks in this area exist: the pipe inserts may have inhibited the consolidation of the concrete in this area during the precast pour, or the splice stressing procedure caused unnoticed cracking to occur at this location. SB did develop a few cracks along the closure pour interface, though those that did form followed the direction of the compressive strut under the load and continued in a diagonal direction toward the load point. Though the splice region appears to have affected some of the crack development, in general, the crack pattern is much like that of SC.

Specimens SU and SU2 exhibited behavior more commonly associated with unbonded prestressed beams. Figure 137 shows the final crack pattern of the SU and SU2 specimens.

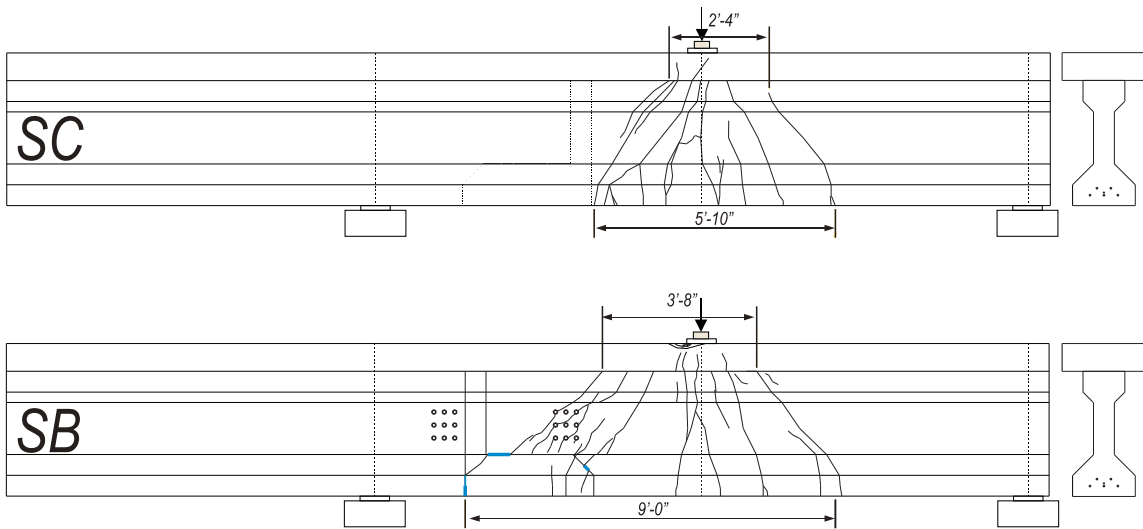


Figure 136–SC vs SB: Crack pattern

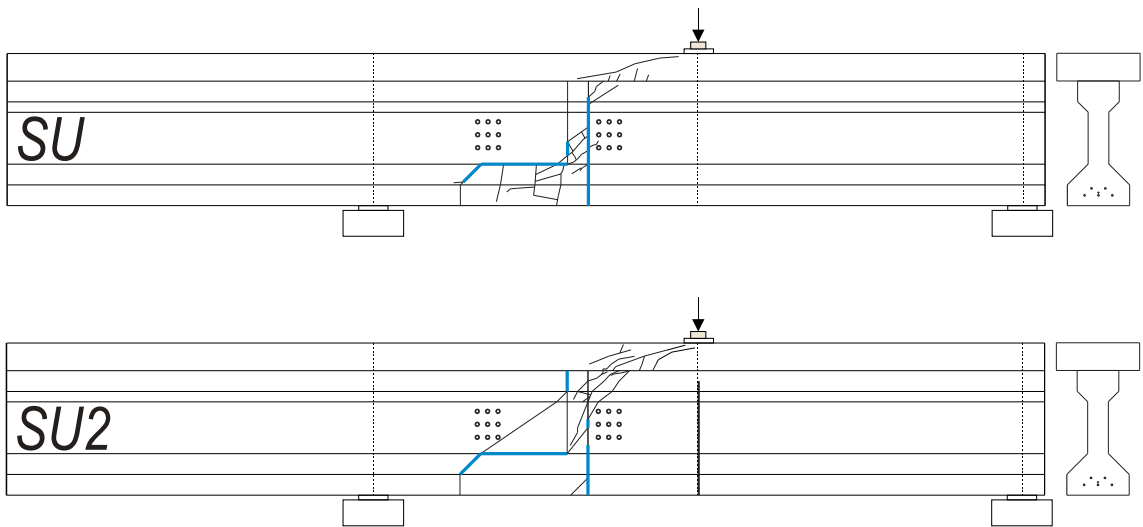


Figure 137–SU vs SU2: Crack pattern

While the SC and SB beams developed a well-distributed fan pattern of flexural and flexural-shear cracks under the load point, the SU and SU2 specimens, on the other hand, developed flexural-shear and shear cracks concentrated toward the joint and the bonded segment of the shear span. In both the SU and SU2 specimens, all cracks initiated either at an interface between concrete pours, or within the splice concrete, except for the single vertical crack under the load point in SU2. Except for this crack, the unbonded segments of the span remained uncracked, except in the top flange, where cracks propagated as the load test neared its

termination. Unlike the SB specimen, cracking around the pipe inserts did not occur in the SU or SU2 specimens.

In SU and SU2, crack opening occurred principally at the main vertical crack. From the vertical crack's first visual appearance until peak load, most crack width growth was visually observed to occur at this location in both specimens.

In the SU2 specimen, the main vertical crack formed directly under the load point, in the unbonded segment, and did not occur until approximately 149 kip—after the development of much of the flexural cracking in the splice region. Strain gages on the bottom flange at this location registered the crack formation at 149 kip (Figure 138).

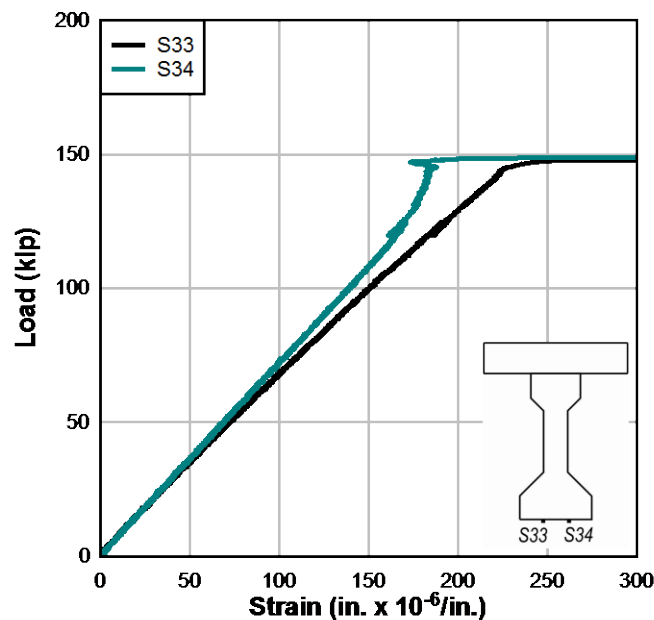


Figure 138–SU2: Bottom strain at vertical crack location

The formation of the vertical crack under the load point in SU2 marked a significant change in its behavior. The location of the crack—in the unbonded segment—exposed the entire unbonded tendon length to the load induced stress. As load was applied beyond 149 kip, the prestressing strand load increased beyond the prestress level. Figure 139 shows a plot of the load cells on three of the prestressing strands vs. the applied load. A reference line is provided at 149 kip, indicating when the vertical crack formed. A separate reference line is provided at 123 kip—formation of the first crack. Note that this crack did not cause increased strand load.

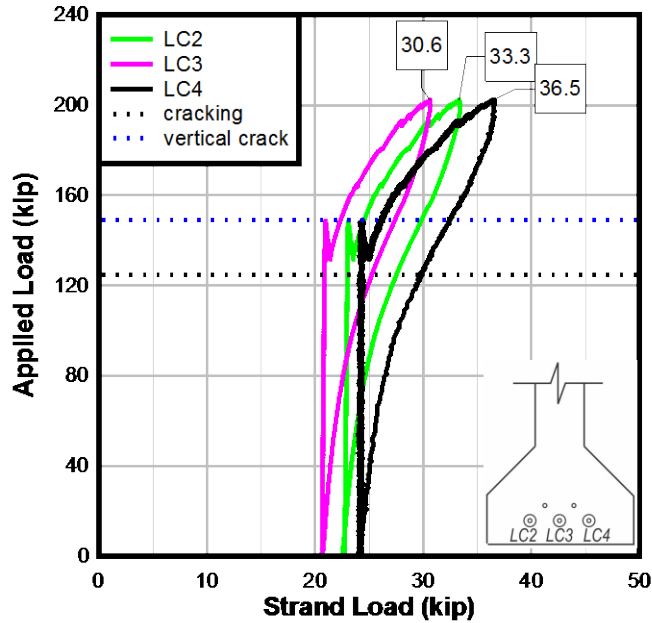
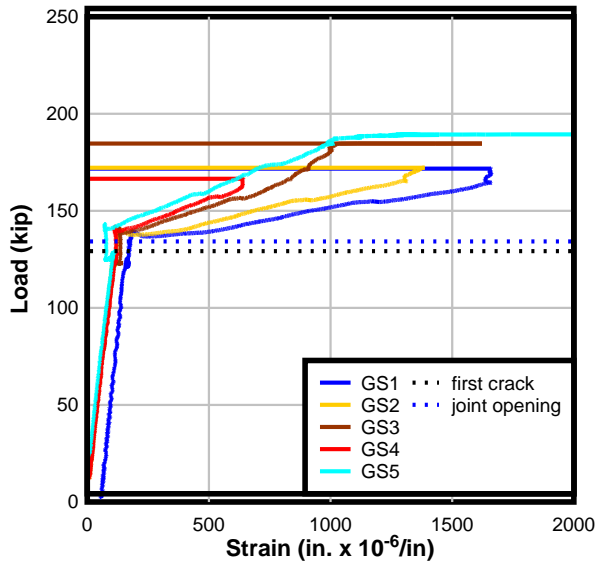


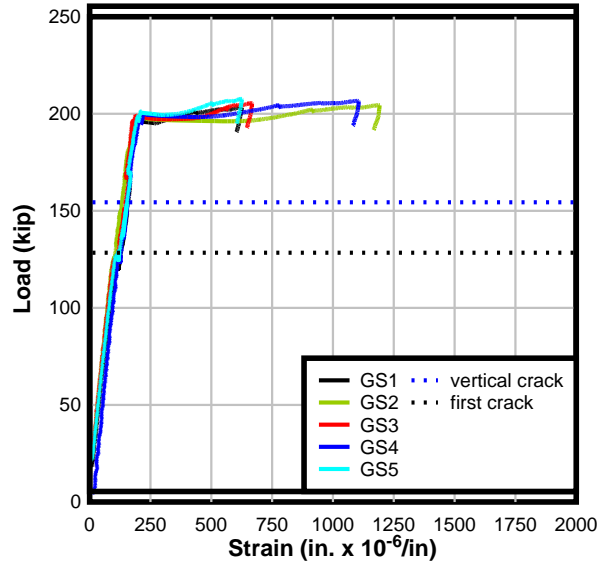
Figure 139-SU2: Strand load

Figure 140 shows the load-strain plots for the strain gages placed on the faces of the couplers for SU and SU2. These strain gages (hereafter referred to as GS gages) were placed during the splice assembly and were cast within the closure pour. Figure 140(a) shows the applied load vs. the strand load for SU. Reference lines are provided at 123 kip and 130 kip, the load at which the first crack and the joint opening, respectively, were visually observed. Figure 140(b) shows the applied load vs. the strand load for SU2. Reference lines are provided at 125 kip and 149 kip, the load at which the first crack and the vertical crack at the load point, respectively, were visually observed.

Unlike the SU2 load cells, the SU2 GS gages do not measure a significant change in slope when the vertical crack forms. Instead, the SU2 gages indicate a linear relation of a single slope from zero applied load until peak load, with only small jags in the data (corresponding the crack events). Based on this trend, it can be surmised that the couplers remain bonded to the concrete through the duration of the SU2 test. Near peak load, the gages indicate a significant increase in strain, suggesting that the couplers were finally exposed. If the strand debonded such that the couplers—and therefore the GS gages—were part of the unbonded length of strand, we would see a change in slope at some point during the test.



(a) SU



(b) SU2

Figure 140–Coupler strain gages: (a) SU and (b) SU2

In specimen SU, the formation of the joint opening at the vertical interface was visually observed at approximately 130 kip, after the formation of two web-shear cracks in the closure pour. In contrast to the effect of cracking on SU2, the joint opening in SU did not have the same immediate effect on the prestressing strand load.

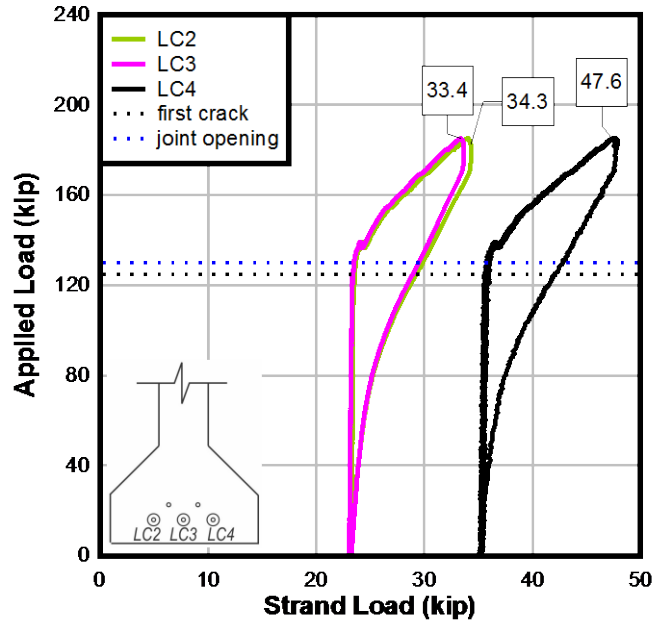


Figure 141-SU: Strand Load

Based on the delay between the vertical crack formation and the gain in the strand load, it can be surmised that the crack at the interface did not expose the prestressing strand immediately. Inspection of the closure pour concrete after demolition of the specimen shows some bonding between the closure pour concrete and the precast concrete around the single bonded strand at this location (Figure 142). The bonding in this area may have slowed the exposure of the prestressing strand until approximately 139 kip, when Figure 141 indicates that the prestressing strand began to pick up load.



Figure 142–Post-test: End view of unbonded segment

In both Figure 136 and Figure 137, the thick blue lines indicate locations where the cracks developed along the interface. It can be seen that in both the SU and SU2 cases, cracks tended to follow the interfaces between two pours. The cracks were drawn to the weakest areas— or the joint areas—where the relatively weak bond between the two concrete pours serves as a crack development path. Cracks of this type are absent (understandably) from the control beam and only occur for short lengths in the SB specimen. The lower shear stress on the splice region, particularly the vertical interface of the joint, may contribute to their relative absence from the SB specimen.

Once a crack initiated at an interface, the crack progressed along it, with little bond between the new and old concrete, the crack formation path was predictable. The shear keys did not resist the “crack opening”, instead the segments simply separated.

In general, shear resistance of a reinforced concrete beam is provided by the concrete of the compressive chord, aggregate interlock, the steel stirrups and dowel action of the longitudinal (prestressing) steel (though this is minimal). In the splice region, the aggregate interlock is reduced because of the smaller aggregate of the self-consolidating concrete. Steel contribution to the shear resistance is mainly provided by the stirrups, which have an increased spacing in the

splice region to accommodate the congestion caused by the couplers. The coupled prestressing strand provides some, albeit limited, dowel action.

Based on observations of the SU tests, modifications were made to the splice design to increase the shear resistance at the joint. An additional stirrup—centered in the closure pour—was provided to provide additional resistance in the closure concrete, in an attempt to prevent crack formation in the vertical column of the joint. Additionally, an epoxy bonding agent was applied to all of the precast faces to provide additional bond to the closure pour. The expectation was that the epoxy would delay or prevent crack formation at the interfaces. (A full description of the modifications is provided in Section 6.6.)

The effects of these modifications are evident when considering the crack development during the load test of SU2. The first crack in SU2 formed in the web of the bonded segment's precast, whereas, in SU, it had formed in the web of the closure pour.

### *11.6 Comparison of Shear Strength*

The load-deflection plot of the four shear tests up to ultimate strength is shown in Figure 143. For discussion purposes, SC and SB are presented together in Figure 143(a) and SU and SU2 are shown in Figure 143(b). For reference, the applied load required to reach the AASHTO-LRFD calculated moment capacity (assuming bonded strands) is shown at 171 kip. Each specimen had a different shear capacity, due to different spacing of the stirrups in the splice region. AASHTO-LRFD shear capacities are calculated for each specimen and given in Table 30. All calculations were performed assuming the section and specified material properties given in Chapter 5.

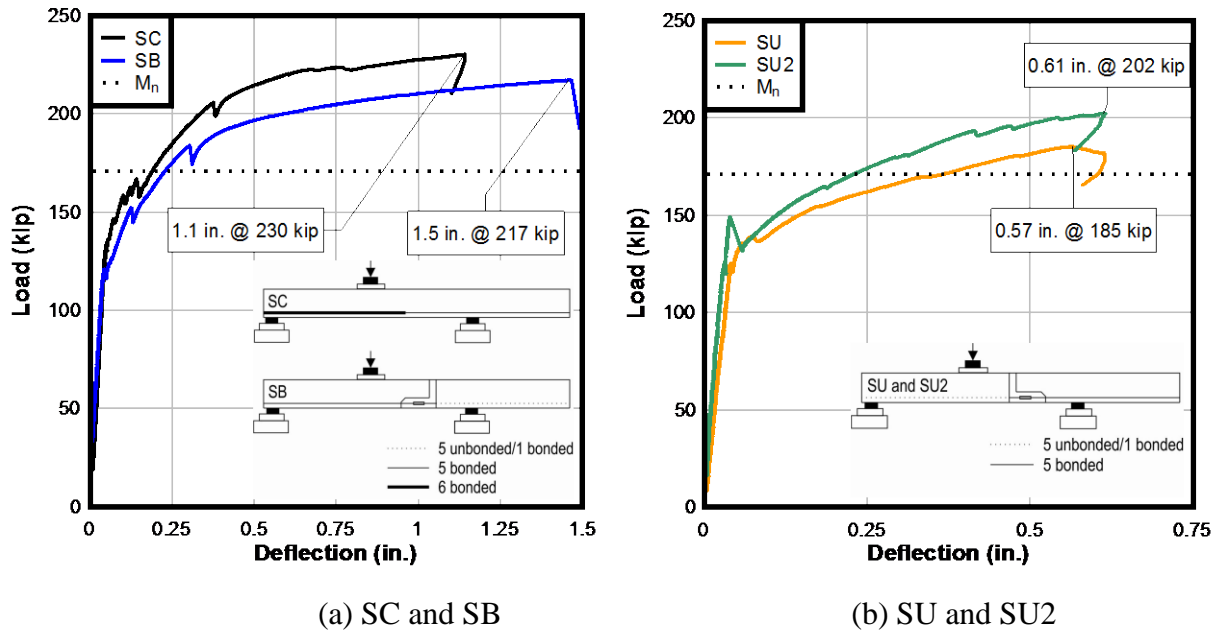


Figure 143–Ultimate behavior: (a) SC and SB and (b) SU and SU2

The experimental flexural capacity of all shear specimens—including the control and all spliced beams—was greater than the AASHTO-LRFD calculated design values (regardless of whether or not the strands were considered bonded).. Specimen SC reached the highest load and deflection at its ultimate state, when it failed in flexure as the deck crushed. Similarly, SB reached peak load when the deck under the load point crushed. Measured strain at this location indicated that the deck strain had exceeded 0.003 for both SC and SB. The failure mode can best be characterized as a tension-controlled flexural failure.

Figure 139 and Figure 141 show the strand load as the applied load was removed at the end of the test. In both SU and SU2, the strand load completely recovered the prestress force present at the start of the test, indicating that the strand had not yet begun to yield in either test. The failure of SU is best characterized as a shear failure, occurring when the segments slipped apart when the cracks propagated diagonally towards the load point and compromised the deck. The failure of SU2 is best characterized as a compression-controlled flexural failure because the concrete crushed at ultimate, but the strand had not yet begun to yield.

Table 30 compares the ultimate behavior of the splice region of specimens SC, SB, SU and SU2 to the AASHTO-LRFD calculated design values at the location of interest: the vertical interface of the closure pour. Figure 144 shows the location of interest corresponding to the

values given in Table 30.  $M_n$  was calculated in accordance with AASHTO-LRFD Article 5.7.3.  $V_n$  was calculated in accordance with AASHTO-LRFD Article 5.8.3.4.2 at the location of least shear resistance, the vertical column of the closure pour. A stirrup spacing of 12 in was assumed for the spliced specimens without the additional stirrup; 6 in. was assumed when the additional stirrup was used. The applied  $V_x$  and  $M_x$  are also given at this location. All calculations were performed assuming the section and specified material properties given in Chapter 5. Self-weight is included.

Table 30–Shear specimens’ ultimate behavior at vertical interface

Specimen	Deflection at load point, in.	$M_x$ (kip-ft)	$M_n$ Bonded (kip-ft)	$M_n$ Unbonded (kip-ft)	$V_x$ (kip)	$V_n$ (kip)	$M_x/M_n$ Bonded	$M_x/M_n$ Unbonded	$V_x/V_n$
SC	1.14	270	631	n/a	120	189	0.43	n/a	0.63
SB	1.46	254	631	589	113	92	0.40	0.43	1.22
SU	0.56	485	631	589	95	92	0.77	0.82	1.03
SU2	0.61	531	631	589	104	141	0.84	0.90	0.74

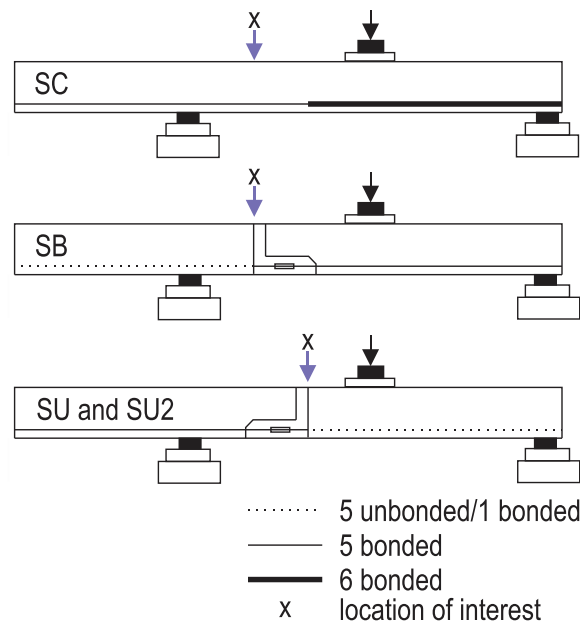


Figure 144–Shear location of interest

Again, the ultimate behavior of the control specimen (SC) and the bonded specimen (SB) are more alike than the two unbonded specimens (SU and SU2). However, due to the different stirrup spacing in each specimen, as well as the different bonding pattern placement in the tested shear span, it is most useful to compare each specimen's applied shear at ultimate to the AASHTO-LRFD calculated design capacity, instead of attempting to compare the specimens to each other.

SC:

- Stirrup spacing at location of interest: 4 in.
- Greatest applied shear at ultimate load, but also the greatest capacity (due to shortest stirrup spacing).
- Flexural compression failure at load point. The applied shear to shear capacity ratio was 0.63 while the applied moment to moment capacity was 0.43. The flexural failure mode was as designed.

SB:

- Stirrup spacing at location of interest: 12 in.
- Flexural compression failure at load point. The applied shear to shear capacity ratio was 1.22; despite the applied load surpassing the design capacity, the specimen exhibited a flexural failure mode. The applied moment to moment capacity was 0.40. This was the same ratio as seen in specimen SC.

SU:

- Stirrup spacing at location of interest: 12 in.
- Shear failure. The segments slipped at the vertical interface. The applied shear to shear capacity ratio was 1.03; in this specimen (unlike SB), the application of shear beyond capacity resulted in a shear failure.

SU2:

- Stirrup spacing at location of interest: 6 in.
- Flexural compression failure at load point. Also observed slip at vertical interface. The applied shear to shear capacity ratio was 0.74. The applied moment to moment capacity was 0.84.

The service and ultimate improvement in performance of specimen SU2 over specimen SU can be attributed to the two modifications made to the splice design: the epoxied joint,

instead of a dry joint, as well as the additional stirrup. The concentrated rotation and deflection at a dry joint opening is reduced with the use of epoxy, allowing the specimen to achieve a greater ultimate load and deflection. This phenomenon has been noted by other researchers (Saibabu et al. 2013). The additional shear resistance contributed by the additional stirrup also contributed to SU2's improved ultimate behavior. Specimen SU—tested in the same set-up as SU2—had an anticipated additional 50 kip of shear capacity at the location of interest (the vertical column of the closure pour). The applied shear at ultimate load of SU2 was indeed greater, yet did not result in the shear failure seen in SU.

The chosen shear test set-up creates a lower-bound solution for the shear behavior and capacity of the splice. This was intentional: considering that the actual moment-to-shear ratio could not be achieved with the test specimen length, the load and support locations were chosen to maximize the shear effects on the splice region. The resulting shear test set-up creates a lower  $M/V$  (3.7) than would be seen in the FIB96 prototype design (32.9). In other words, the loading situation tested is unlikely in an actual design; however, the tests provided a chance to examine the shear behavior and capacity of the splice region. Based on observed behavior during these tests, modifications were made which positively affected the service-level behavior of the splice region, and which increased the shear capacity of the splice region.

## 12 Fatigue Results and Discussion

This chapter covers the fatigue testing of control specimen (FC) and two spliced specimens (F1 and F2) to determine the effect of fatigue cycling on the splice connection. Initially, the specimens were statically loaded to crack the specimen and to determine the stiffness prior to initiating the fatigue cycling. This initial cracking load was followed by several static loads to conduct decompression testing to aid in estimating the effective prestress force. These load cycles are covered in the *Static Conditioning* sections. The specimen was then loaded in fatigue for up to 2 million cycles at the selected load range; results and observations related to fatigue testing are covered in the *Fatigue Loading* sections. Finally, the specimens were tested to their ultimate strength following the fatigue loading; this load testing is described in the *Ultimate Strength Test* sections. The test set-up and procedure are described in Section 7.4.

### 12.1 Specimen FC

FC was precast segment 3 from pour 1, shown in Figure 43.

#### 12.1.1 Static Conditioning

Figure 145 shows the load-displacement plot of the initial static loading of the control specimen FC. The trend is linear with some initial variation from 0 to approximately 20 kip attributed to the sensitivity of the laser gages and the inherent roughness of the deck surface, as well as take-up in the test fixtures. At 74 kip, the load-displacement plot shows a significant change in slope, indicating crack formation. This was confirmed by visual observation of two cracks at 76 kip (Figure 146).

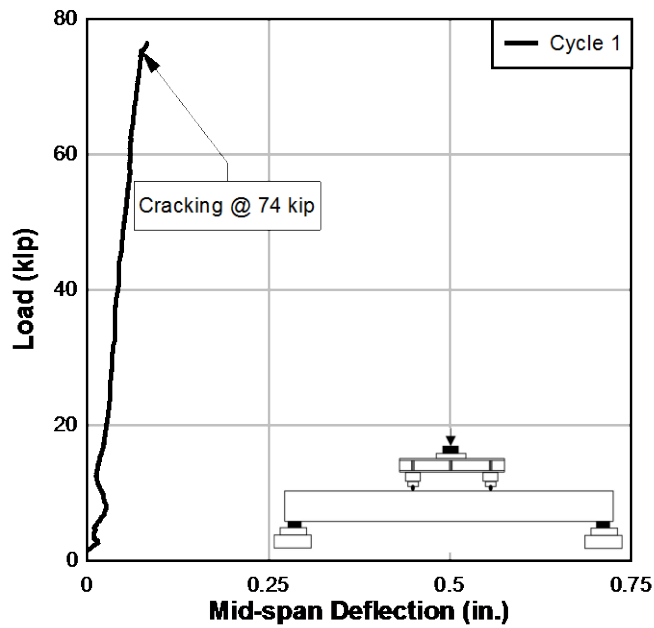


Figure 145-FC: Static conditioning

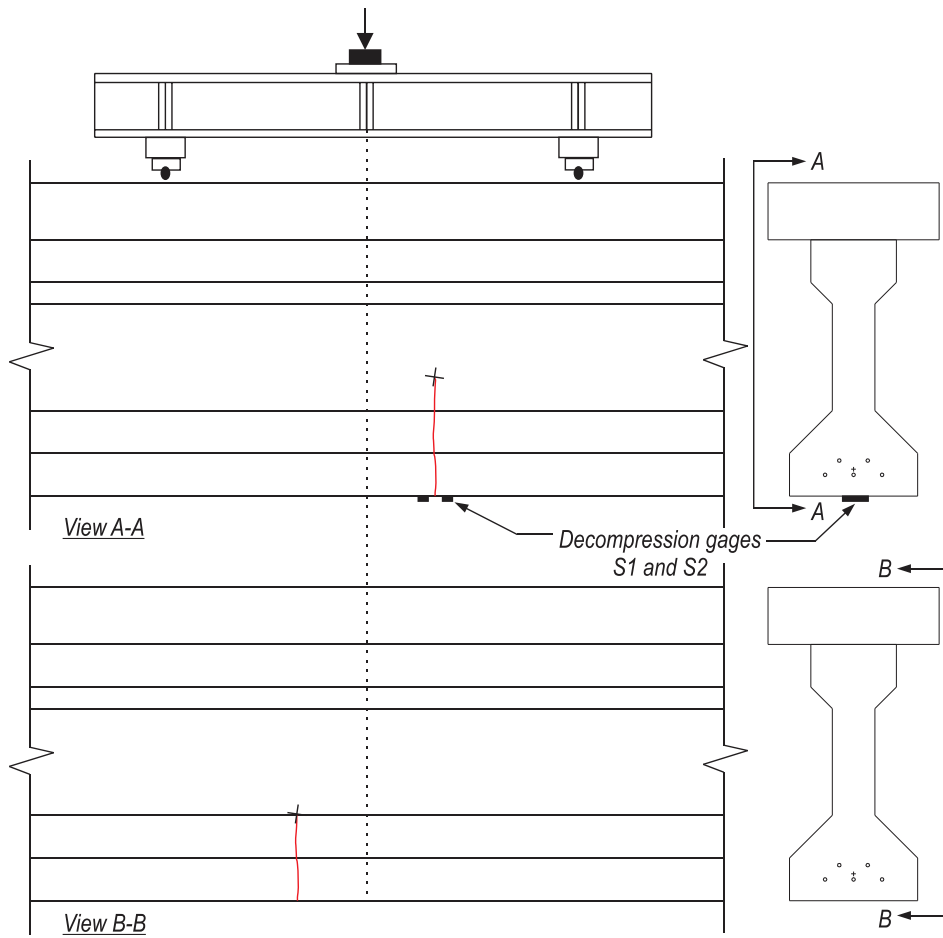


Figure 146-Specimen FC: First cracks

After precracking, decompression tests were performed on one of the FC cracks to determine the effective prestress. Figure 147 shows the load-displacement plots for the three load cycles of this procedure. (Multiple load cycles were performed to ensure the repeatability of the strain readings used for determination of the effective prestress.)

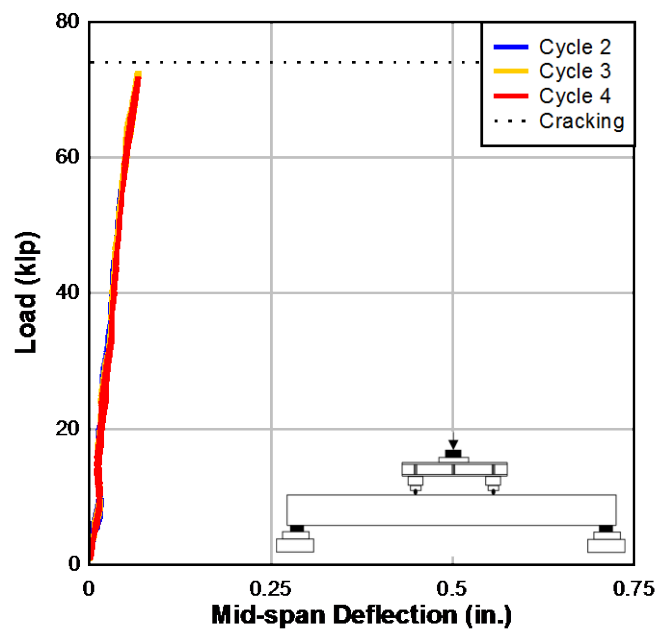


Figure 147–FC: Decompression load cycles

For the second load cycle (cycle 2), the specimen was loaded to 56 kip. In subsequent load cycles, the specimen was loaded to 72 kip. In all cases, the intent was to observe crack opening at the crack locations, which occurred at a load corresponding to a change in the strain readings of gages placed adjacent to the crack. No additional cracking of the specimen was observed during these load cycles.

Figure 148 shows the plot of strain versus applied load for the three decompression load cycles. In each of the load cycles, the strain gages S1 and S2 both gages change slope at an applied load of approximately 37 kip.

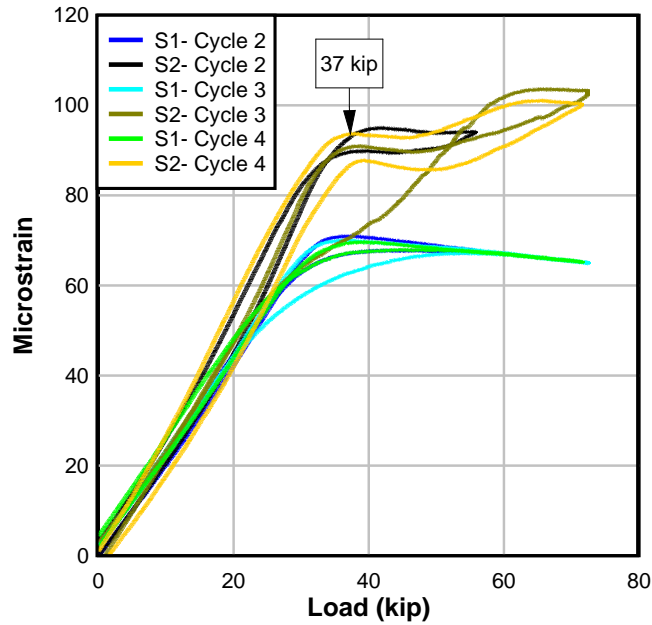


Figure 148–FC: Decompression strain readings

### 12.1.2 Fatigue Loading

FC was cycled at 2 Hz between 40 kip and 72 kip for 518,000 cycles. At the start of the test, this load range resulted in deflections from 0.034 in. to 0.071 in. Figure 149 shows a selection of load-unload cycles, recorded as the test progressed. The cycles shown were selected at intervals to demonstrate the degradation of the beam as the fatigue loading approached the end of the test.

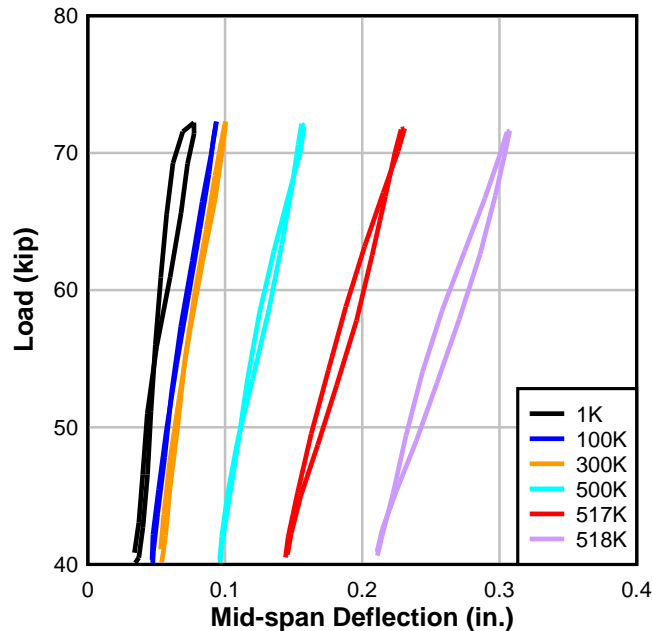


Figure 149-FC: Fatigue

Visual inspection of the specimen at approximately 80,000 cycles revealed the development of additional hairline cracks on one side of the beam. Cracks were observed at the bottom flange of the specimen at the location of each load point. The result of continued crack growth can be observed in the plot, which shows steady degradation of the specimen stiffness over time. Crack development continued throughout the test, as existing cracks lengthened and new cracks formed.

Between 517,000-518,000 cycles, the specimen began to rapidly degrade. Finally, at approximately 518,000 cycles, a severe change in specimen stiffness triggered the preset interlocks on the MTS, causing the cyclic load application to stop.

The beam was unloaded and inspected for damage. The primary crack was observed to remain open under beam self-weight. Flexural cracks in the constant moment region had propagated toward and had nearly reached the deck. Though degradation of the specimen was obvious by visual inspection and in the load-displacement plots, the beam fatigue test was restarted. The specimen began to rapidly degrade, with increasing permanent deflections and after approximately 1000 cycles, the test was terminated to prevent instrumentation and equipment damage.

The strand stress ranges experienced in FC were predicted by calculation rather than direct measurement. The strand stress range was determined by the assumed strand strain due to

effective prestress, the differential strain induced by loading (assuming the cracked moment of inertia), and the constitutive model of the prestressing strand, as determined with strand-in-air tests of the prestressing strand. The strand stress range at the crack location was approximately 20.5 ksi, or 7.6% of  $f_{pu}$ .

### 12.1.3 Ultimate Strength Test

Figure 150 shows the load-displacement plot of the ultimate strength test of FC. Before initiating the load test, the specimen had several cracks, which extended from bottom to top of the precast; the cracks did not appear to extend into the deck. These cracks were located within the constant moment region of the test set-up and can be seen in Figure 151(a).

As load was applied, the specimen exhibited early nonlinear behavior. Pre-existing cracks were observed to re-open, with the largest openings occurring in the cracks formed during static conditioning. Crack growth was only observed to occur in the pre-existing cracks; all cracks were located within the constant moment region.

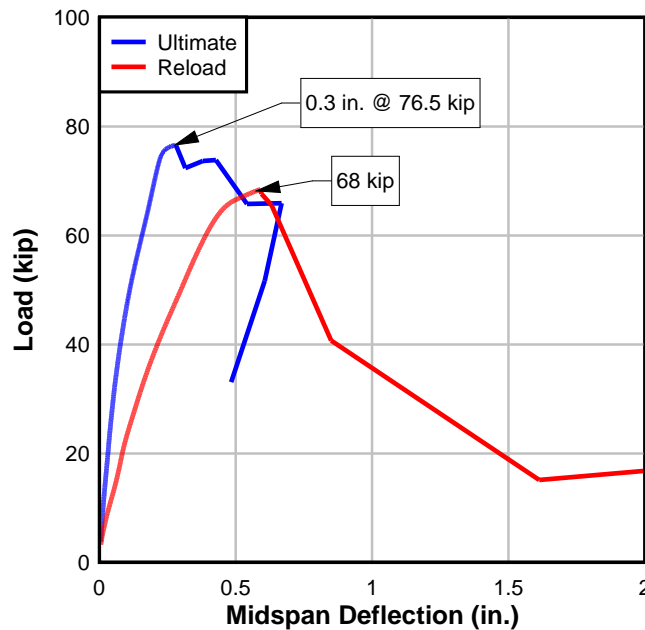
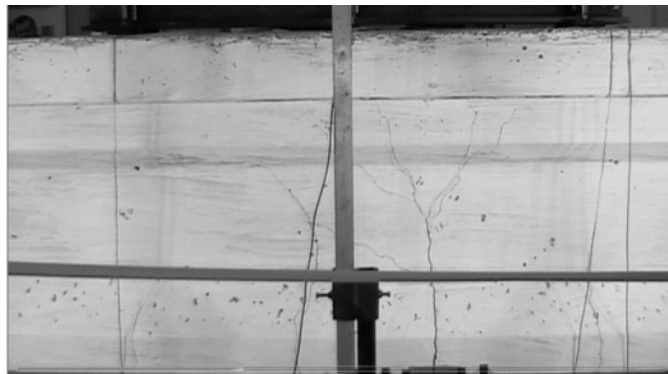


Figure 150–FC: Ultimate



(a)



(b)



(c)

Figure 151–FC crack progression at (a) no load; (b) ultimate (c) second loading

At approximately 77 kip, several loud reports were heard, indicating that prestressing wires had fractured. A load loss of more than 15 kip triggered the preset MTS interlock, and load application was halted. Ultimate load was approximately 77 kip and occurred at a beam

midspan deflection of approximately 0.3 in. Upon removal of the load, the beam continued to carry its own self-weight (Figure 151(b)), but exhibited a permanent set of 0.25 in.

The interlocks were removed and the specimen was reloaded, achieving a maximum load of 68 kip. At 68 kip, more reports were heard and the specimen hit the floor. Figure 151(c) shows the specimen after termination of the second loading.

Ultimate strength was controlled by the rupture of prestressing strand, which was reached before compressive failure of the deck. The load-strain plots of gages on the top of the deck (Figure 152) confirms that strain was well below the ultimate compressive strain of 0.003 when peak load was reached, indicating that the deck crushing occurred as the specimen settled after strand rupture.

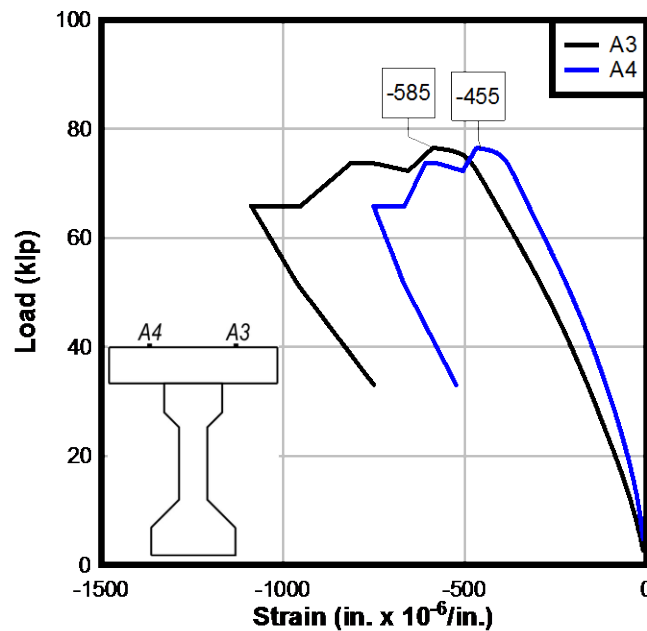


Figure 152-FC: Ultimate

Ruptured strands were inspected with a JEOL SEM-6400 scanning electron microscope for signs of fatigue wear. Many of the strands exhibited ductile failure surfaces such as shown in Figure 153(b). A number of strands, however, were noted to have varying degrees of fatigue cracking as shown in Figure 153(a). The crack initiation site (indicated by the arrow) is typically a point of contact either with an adjacent wire (center or outer wire) or reinforcing bar. Evidence

of fatigue wear is noted in the beach-mark wear, characteristic of gradual crack formation during cyclic loading.

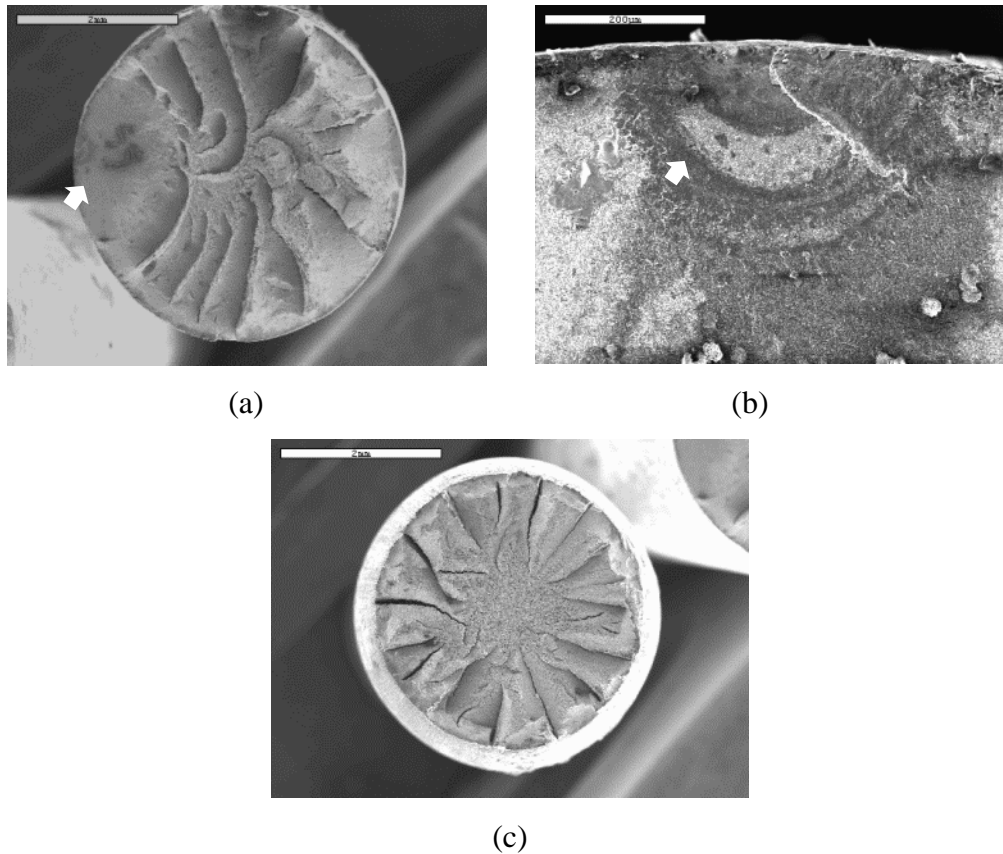


Figure 153–FC strand showing (a) fatigue (20X) (b) fatigue (200X) (c) yield (20X)

## 12.2 Specimen F1

F1 was the spliced specimen constructed of bonded segment 7b (from pour 1) and unbonded segment 6u (from pour 2), as shown in Figure 43.

### 12.2.1 Static Conditioning

Figure 154 shows the load-displacement plot of the initial static loading of F1. The trend is initially linear with some variation due to take-up in the test fixtures. At 54 kip, the load-displacement plot shows a slight change in slope, indicating a change in the specimen stiffness. This was confirmed by visual observation of the first ‘crack’ at 55 kip on one side of the beam (location shown in Figure 155). While the crack did occur in the area of greatest bending stress,

it is best described as an opening or separation of the bond at the closure interface. A similar opening was not observed on the opposite side of the beam.

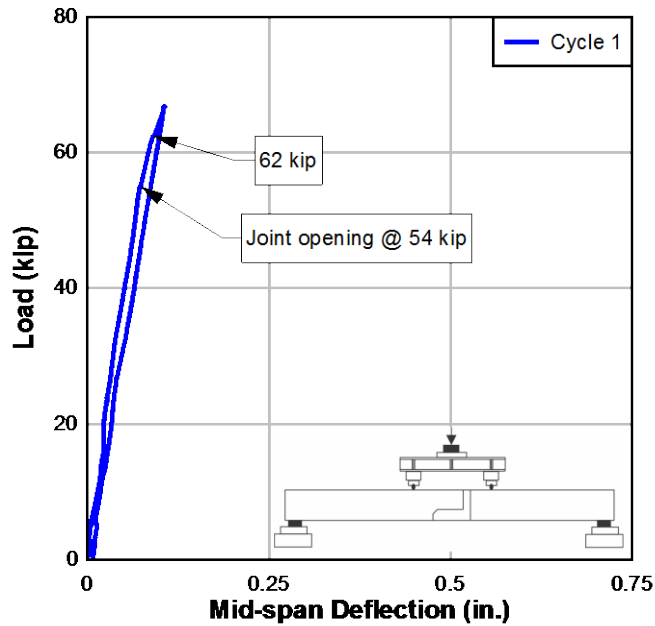


Figure 154-F1: Static conditioning

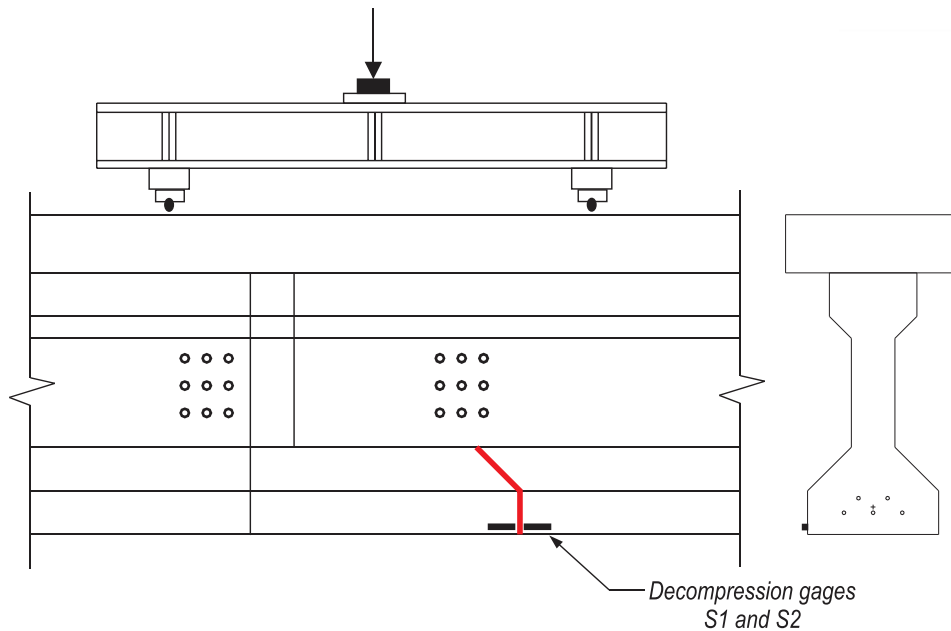


Figure 155-F1: Joint opening

Evidence of the joint opening can be seen in the plot of the coupler strain versus applied load (Figure 156). At 54 kip, the strain gages on the couplers located toward the opening side of the beam (GS1, GS3 and GS4) indicated a ‘crack’ had formed. The gages on the opposite side of

the beam remained linear-elastic until 62 kip, indicating that the opening formed unsymmetrically as the load was increased and that—at 62 kip - the opening had propagated entirely through the width of the beam. Load application was continued until approximately 67 kip to develop the joint opening.

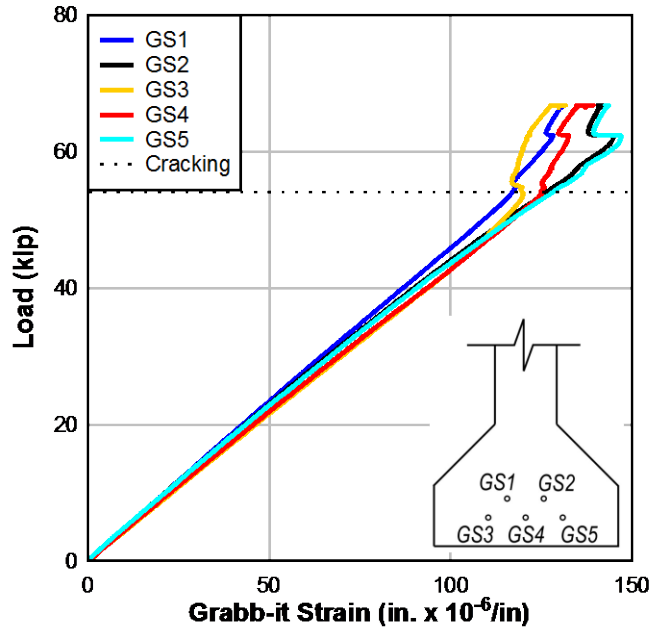


Figure 156–F1: Coupler strain

After precracking, decompression tests were performed on the joint opening of F1 to determine the effective prestress; gages were placed on either side of the first crack, as indicated in Figure 155. Figure 157 shows the load-displacement plots for the two decompression load cycles.

The specimen was loaded to 70 kip and 50 kip in successive load cycles. The intent was to observe crack opening at the first ‘crack’ location, which corresponded to a change in the strain readings of gages placed adjacent to the joint opening (gage locations shown in Figure 155). Figure 158 shows the strain vs. applied load plots for the second load cycle; strain data from the first load cycle was questionable and is not shown in the figure. The gages were replaced for cycle 3. Multiple load cycles were performed to ensure the repeatability of the strain readings used for determination of the effective prestress.

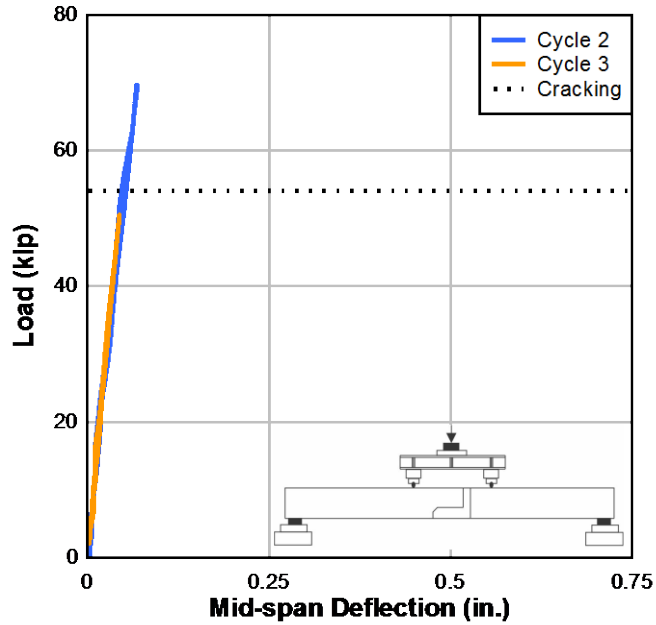


Figure 157-F1: Decompression load cycles

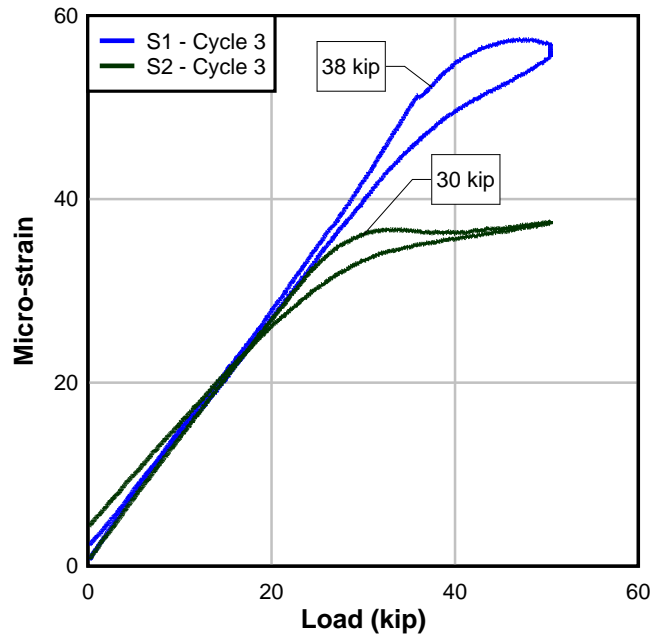


Figure 158-F1: Decompression strain readings

### 12.2.2 Fatigue Loading

F1 was cycled at 2 Hz between 40 kip and 54 kip for 2 million cycles. At the start of the fatigue loading, this applied load range resulted in deflections from 0.036 in. to 0.049 in. Figure

159 shows a selection of load-unload cycles, occurring at different times during the test. The cycles shown were selected at intervals to demonstrate the degradation of the specimen through the 2 million load cycles. At two million cycles, the specimen had only slightly decreased stiffness compared to the initial stiffness; at the end of the test, the specimen deflected between 0.054 in. and 0.070 in. at 40 kip and 54 kip, respectively.

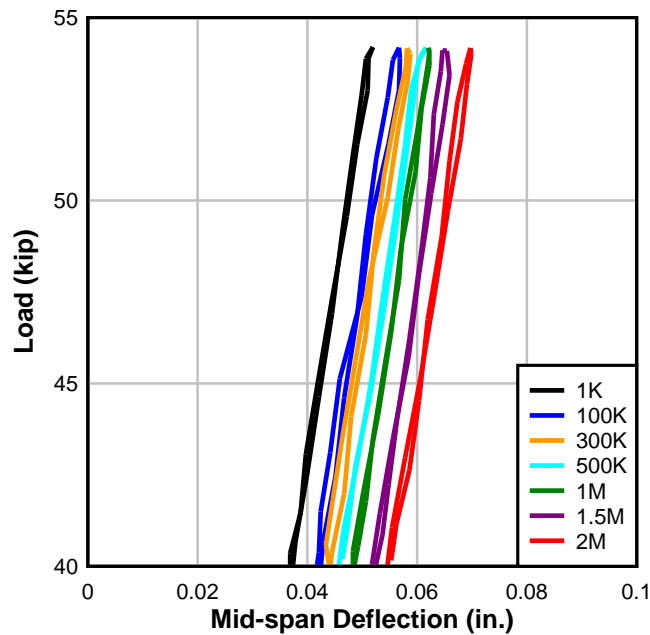


Figure 159-F1: Fatigue

The specimen was inspected after the 2 million cycles to evaluate crack growth; no additional cracking of the specimen was found. Propagation of the first crack was not observed.

The strand stress ranges experienced in F1 were predicted by calculation for later comparison with direct measurement. The strand stress range was determined by the assumed strand strain due to effective prestress, the differential strain induced by loading (assuming the cracked moment of inertia) and the constitutive model of the prestressing strand, as determined with strand-in-air tests of the prestressing strand. The strand stress range at the crack location was approximately 9 ksi, or 3.3% of  $f_{pu}$ .

### 12.2.3 Ultimate Strength Test

Figure 160 shows the load-displacement plot of the ultimate strength test of F1 after completion of fatigue cycling. The ultimate load test was performed in the four-point bending test set-up (Figure 38) used to precrack the specimen. The plot indicates that as load was

applied, the specimen exhibited linear-elastic behavior, until approximately 66 kip, when the vertical interface of the closure joint began to open. As loads were applied beyond 66 kip, the vertical opening propagated up toward the deck, allowing the specimen to significantly deflect under increasing load.

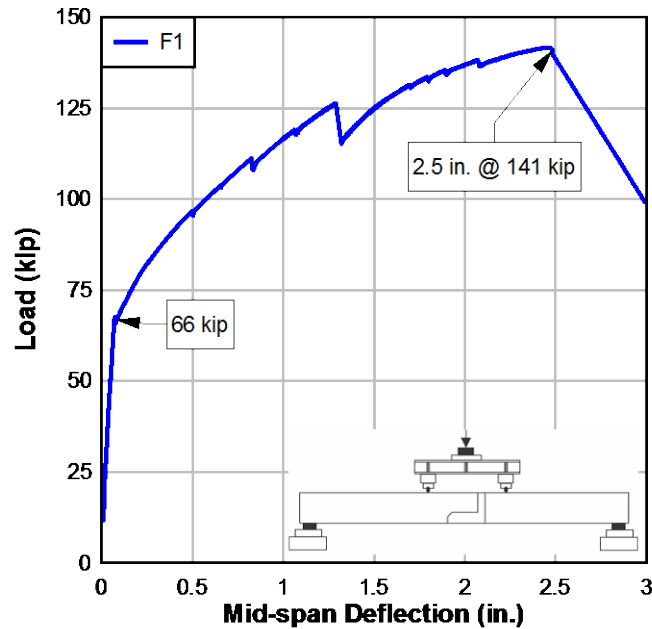
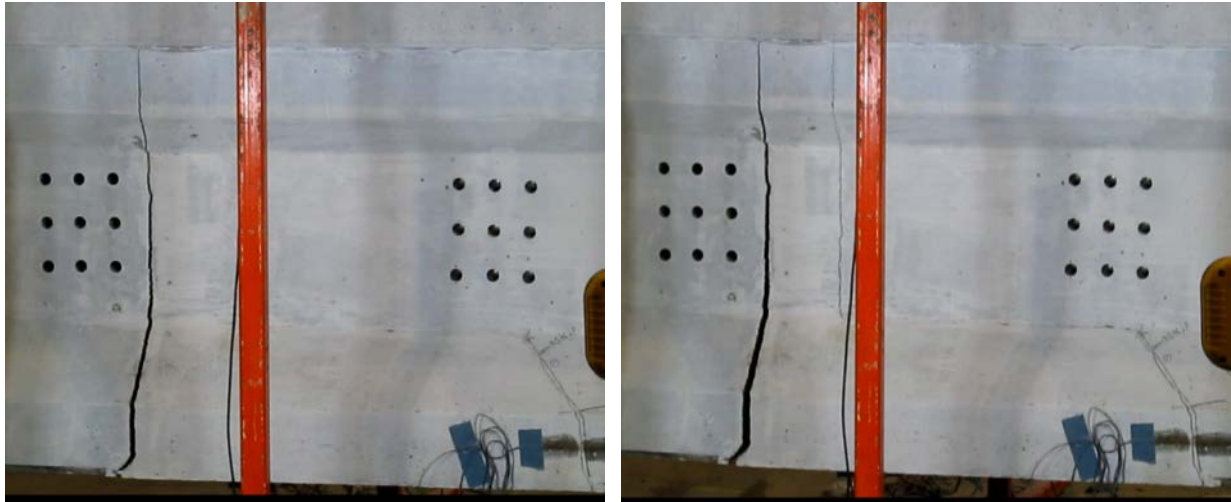


Figure 160–F1: Ultimate

Beyond 66 kip, the load-deflection plot reveals a change in specimen stiffness. At approximately 110 kip, several small load drops occurred, corresponding to audible cracking, which indicated the formation of additional cracks. At 125 kip, a significant load drop occurred accompanied by a loud report - likely due to prestressing strand wire or wires rupturing. A sudden opening of cracks around the outline of the closure pour occurred. Figure 161 shows the closure pour just before and just after this event. Several flexure-shear cracks were also observed to develop outside of the constant moment region.

At approximately 141 kip, the specimen reached ultimate load when strands ruptured near the first crack and the beam hit the floor. At failure, the principal flexural crack closed indicating that the couplers provided anchorage for the unbonded tendons to remain stressed. Figure 163 shows F1 after failure.



(a)

(b)

Figure 161–F1: Crack pattern at (a) 125 kip, prior to strand rupture (b) after load drop

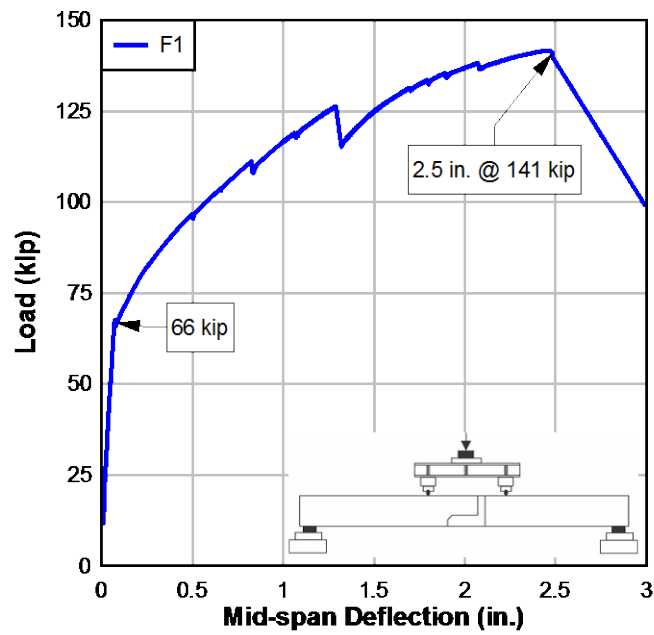


Figure 162–F1: Ultimate



Figure 163–F1: Post-failure

Fracture of the strand predicated compression failure in the deck. The maximum measured compressive strain in the constant moment region of the deck was approximately 0.0016 (Figure 164).

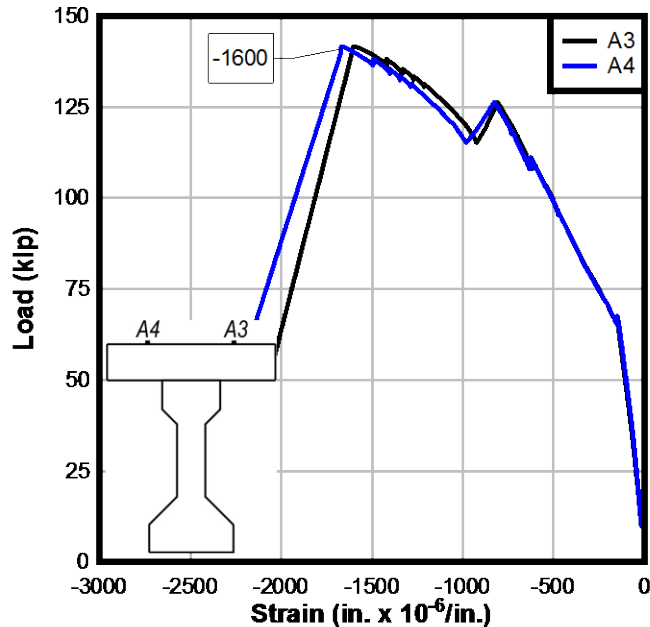
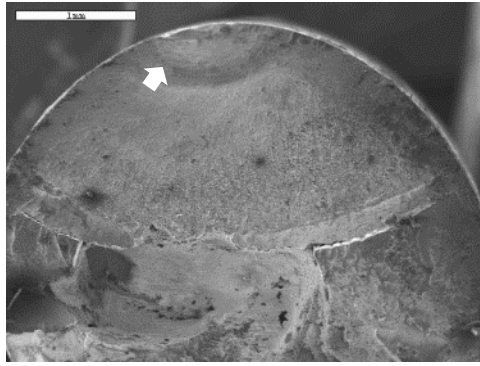
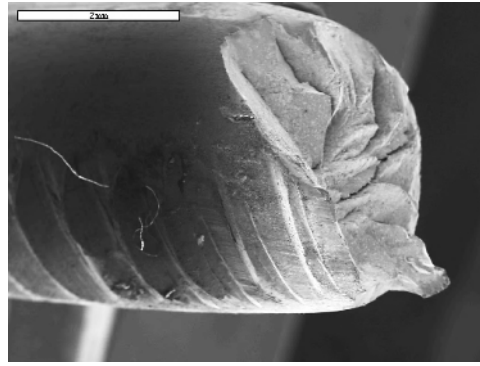


Figure 164-F1: Deck strain

Broken strands were inspected with a JEOL SEM-6400 scanning electron microscope for signs of fatigue wear. Inspection revealed most strands had yielded; some strands indicated fatigue wear. Figure 165 shows several examples of the strand failure surfaces. The crack initiation site (indicated by the arrow) was typically a point of contact either with an adjacent wire (center or outer wire) or reinforcing bar, though as shown in Figure 165(b), the crack initiation site in one of the top strands was within the coupler wedge, and occurred where the teeth bit into the strand. In post-failure inspection, it was observed that the wedge had improperly seated at this location (Figure 165(c)). This observed strand failure mode was unique to the F1 specimen. Additional discussion of observations is covered in Section 12.4.1.



(a) F1TW5



(b) F1TE3



(c)

Figure 165–F1: (a) top strand showing fatigue (40X ) (b) failure at teeth (20X)  
(c) misaligned wedges

### 12.3 Specimen F2

F2 was the spliced specimen constructed of bonded segment 6b (from pour 1) and unbonded segment 8u (from pour 2), as shown in Figure 43.

#### 12.3.1 Static Conditioning

Figure 166 shows the load-displacement plot of the initial static loading of F2. The trend is initially linear with some variation due to take-up in the test fixtures. A crack was visually observed at 63 kip which formed in the bonded precast segment and was associated with a change in slope of the load displacement plot. The crack was within the constant moment region, but outside of the closure pour, extending underneath the beam and visible on both sides (Figure 167).

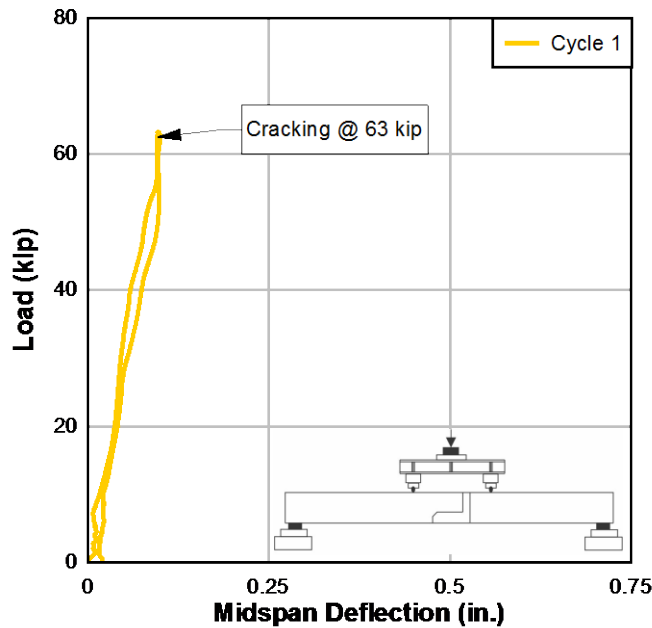


Figure 166-F2: Precrack

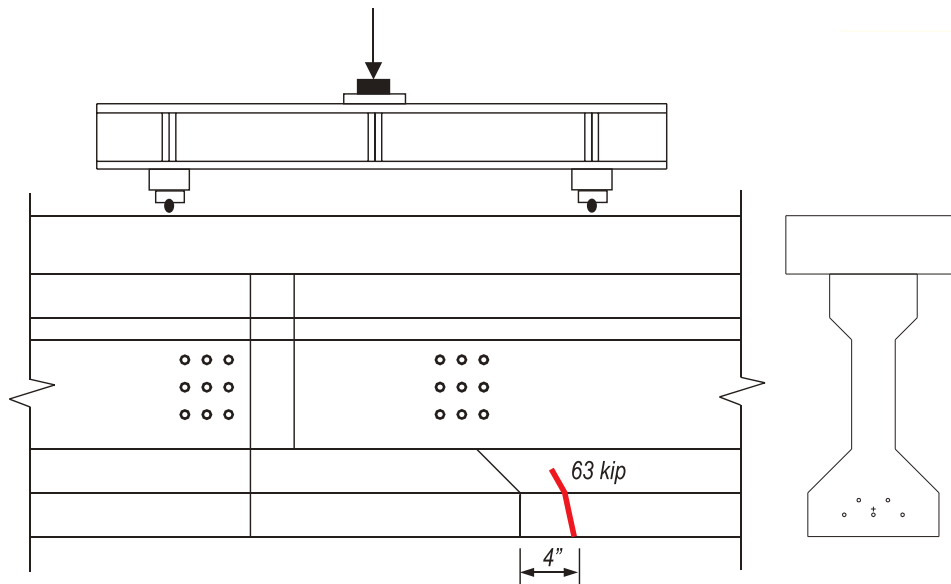


Figure 167-F2: First crack

Coupler strain (Figure 168) indicated possible micro-cracking prior to the observed cracking load. At 57 kip, the strain gages on the coupler located closest to the first crack (GS3) indicated cracking had initiated. At loads beyond 57 kip, the other gages (GS1,GS2, GS4, GS5) remained nearly linear-elastic up to cracking which occurred at 63 kip.

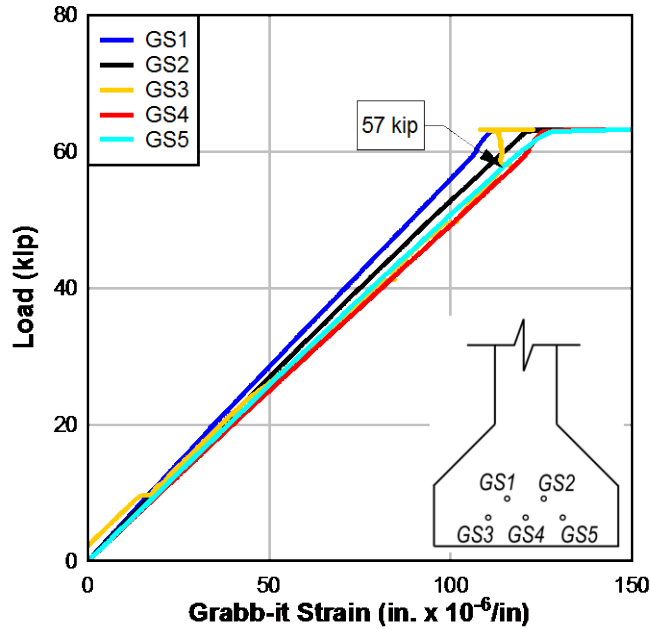


Figure 168-F2: Precrack coupler strain

After precracking, decompression tests were performed at two different cracks. Gage and crack locations are shown in Figure 169. Initially, three load cycles were applied with the strain gages mounted at the crack that formed in the bonded precast segment; the load-deflection plot is shown in Figure 170(a). Upon loading the specimen to 72 kip during the third static load cycle, a second crack formed at the specimen midspan, within the closure pour. Two strain gages were placed on either side of this new crack and an additional three cycles were applied. The load-deflection plot for these three load cycles are shown in Figure 170(b).

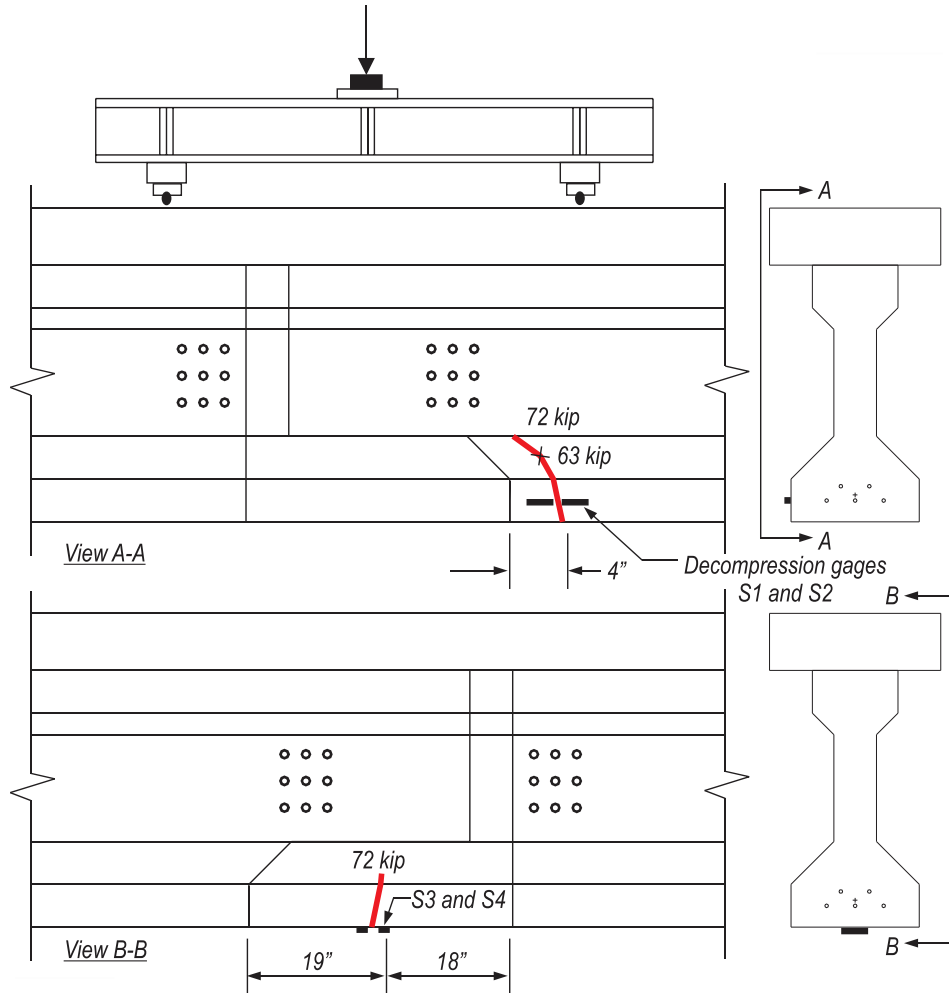
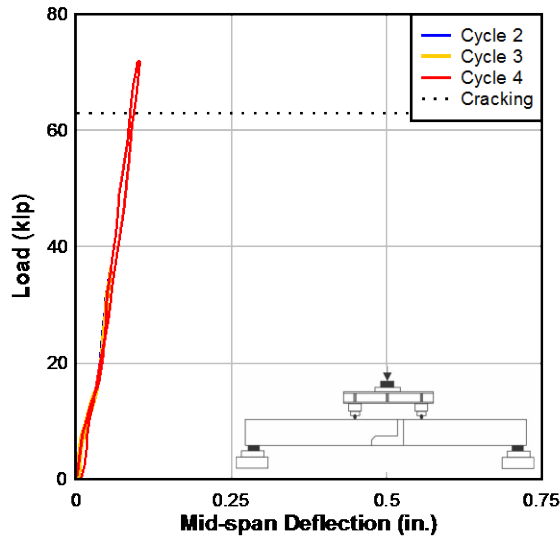
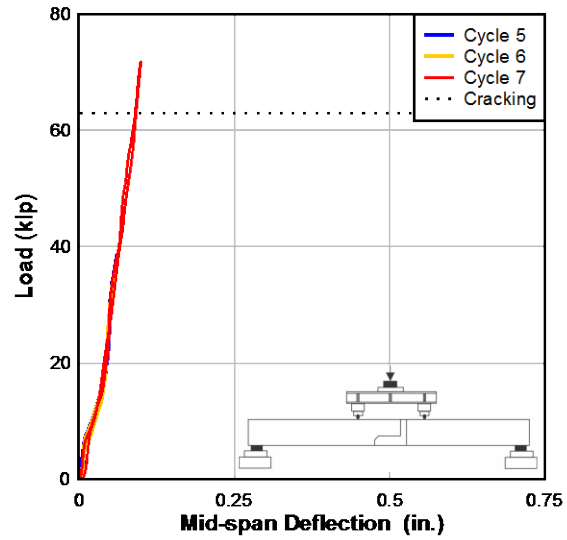


Figure 169-F2: First cracks with strain gages



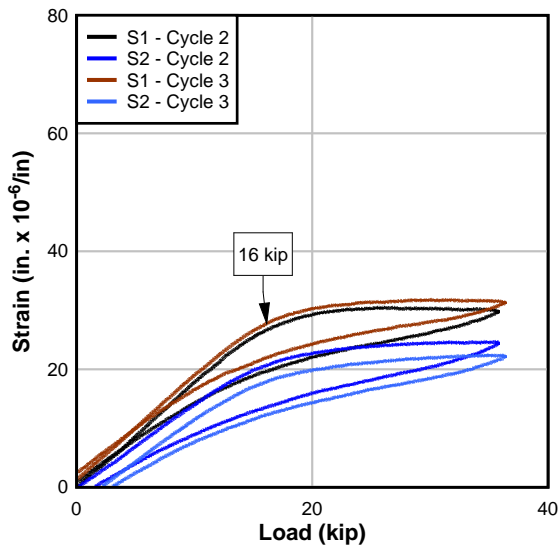
(a)



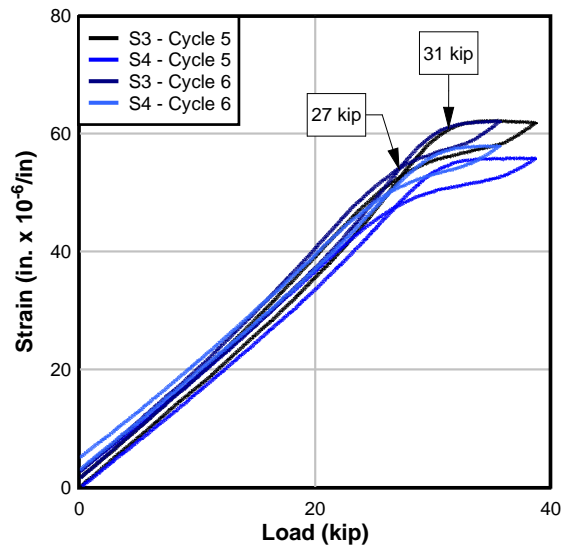
(b)

Figure 170–F2: Static load cycles (a) 2-4 and (b) 5-7

Figure 171(a) shows the strain for the first two cycles and Figure 171(b) shows the measured strain for cycles 5-6 which were taken on the second crack that formed. Because the cracks were located in different segments of the spliced specimen, different decompression moments were measured as indicated in the two plots.



(a) Cycles 1-2



(b) Cycles 4-5

Figure 171–F2: Decompression strain readings

### 12.3.2 Fatigue Loading

F2 was cycled at 2 Hz between 40 kip and 72 kip for 2 million cycles. At the start of the test, this load range resulted in midspan deflections from 0.035 in. to 0.056 in. Figure 172 shows a selection of load-unload cycles, occurring at different times during the test. The cycles shown were selected at intervals to demonstrate the degradation of the specimen over the 2 million load cycles. The bilinear slope of each cycle indicates that the section is exhibiting a change in stiffness, i.e., the crack is opening and closing. Between 1.5 million and 2 million cycles, the specimen exhibits a significant change in the cracked stiffness of the section, indicating degradation of the section due to fatigue. At the end of the test, the specimen deflected between 0.070 in. and 0.12 in. at 40 kip and 72 kip, respectively.

The specimen was inspected throughout the 2 million cycles for crack propagation. Cracks were observed to grow, and new cracks formed. Most notably, an opening of the vertical interface of the closure pour was observed at approximately 1.7 million cycles. The cracks were marked as they propagated and can be seen in Figure 173.

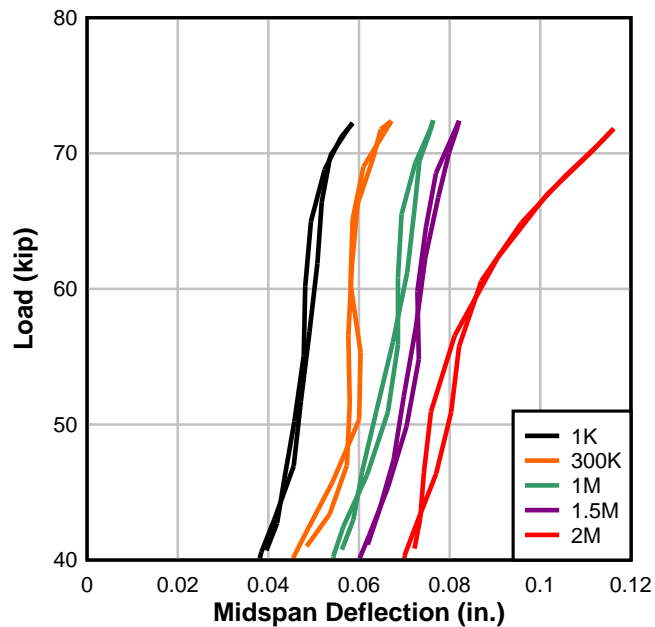


Figure 172–F2: Fatigue

The strand stress ranges experienced in F1 were predicted by calculation for later comparison with direct measurement. The strand stress range was determined by the assumed strand strain due to effective prestress, the differential strain induced by loading (assuming the cracked moment of inertia) and the constitutive model of the prestressing strand, as determined

with strand-in-air tests of the prestressing strand. The strand stress range at the crack location was approximately 20.5 ksi, or 8% of  $f_{pu}$ ; this strand stress range matched that of the control specimen, FC.



Figure 173–F2: Cracking after 2 million cycles

### 12.3.3 Ultimate Strength Test

Figure 174 shows the load-displacement plot of the static failure of F2. The plot indicates that, as load was applied the specimen exhibited linear-elastic behavior until 76 kip, when a stiffness change occurred. As load was applied beyond 76 kip, most crack propagation occurred at the vertical crack at the closure pour interface. After the vertical crack reached the deck, propagation of the first crack—occurring in the bonded segment—began to occur more rapidly. This crack also propagated up toward the deck.

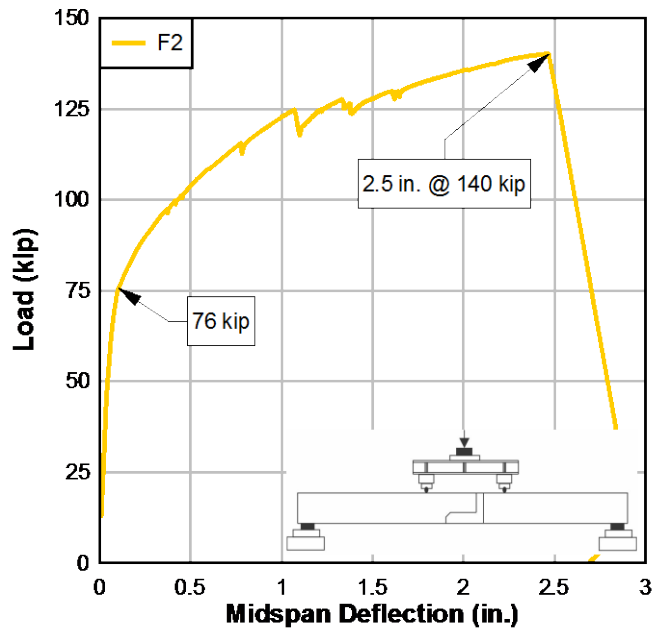


Figure 174–F2: Ultimate

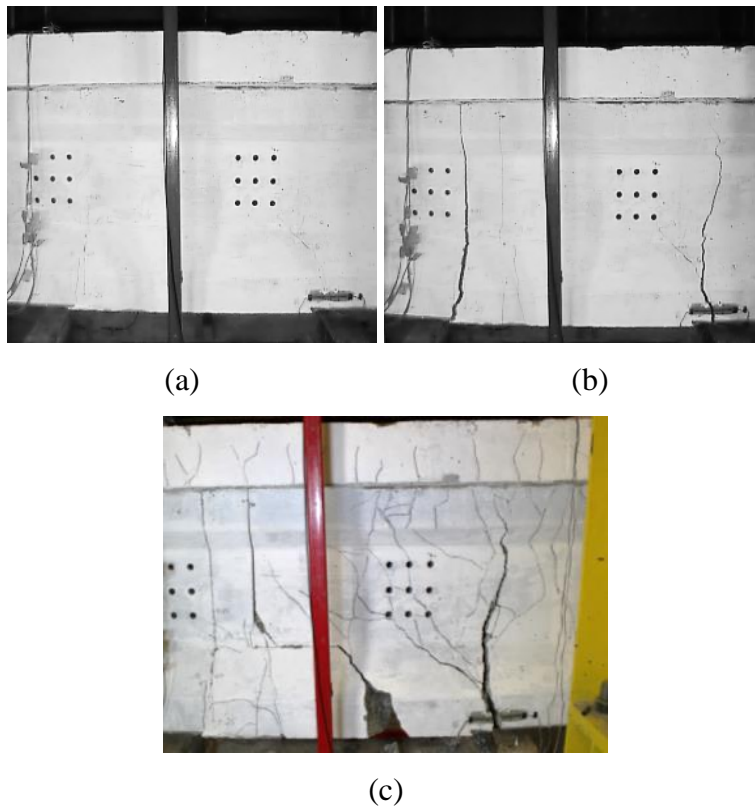


Figure 175–F2 crack progression at (a) 70 kip, (b) 137 kip, and (c) ultimate (cracks marked)

From 115 to 130 kip, several sudden load drops occurred, indicating the formation of new cracks. These load drops were accompanied with audible and visible cracking of the concrete. A major load drop occurred at approximately 125 kip, though a new crack was not visually observed. A load drop at 130 kip corresponded to a shear-flexure crack observed in the bonded segment, outside of the constant moment region.

As ultimate load was approached, the opening at the vertical interface widened significantly—about 1 in. at the bottom—with an apparent hinge just below the deck (Figure 175). As load application continued, the significant flexural crack at the vertical interface of the closure pour (which had opened around 1.7 million fatigue cycles) propagated up to the deck and allowed the specimen to experience significant vertical deflection. The vertical interface crack opened more than 1 in. as the specimen approached the ultimate load. At approximately 140 kip of load and 2.5 in. of displacement, the specimen reached ultimate strength, and several strands fractured. Strand fracture was audible and was visually confirmed by inspection of the specimen post-failure.

Fracture of the strand predicated compression failure in the deck. The maximum measured compressive strain in the constant moment region of the deck was approximately 0.002 and occurred near a load point (Figure 176).

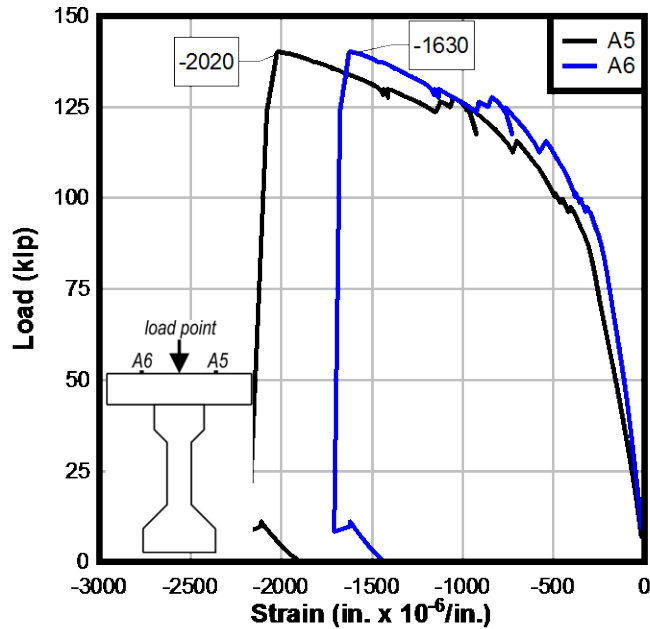
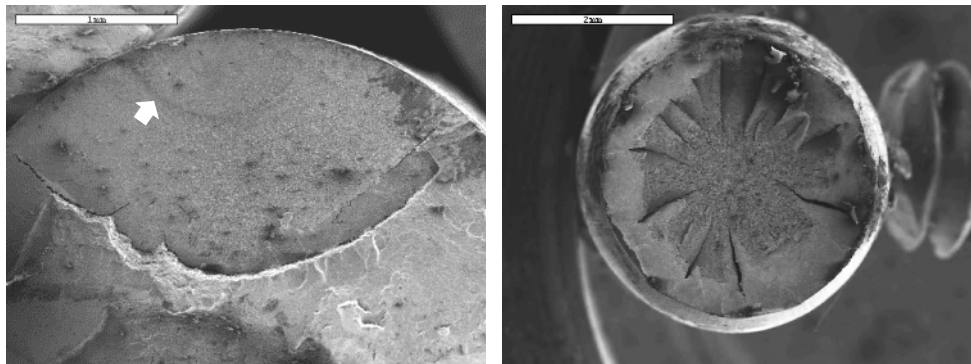


Figure 176-F2: Deck strain

Broken strands were inspected with a JEOL SEM-6400 scanning electron microscope for signs of fatigue wear. Inspection revealed that most strands had yielded; some strands indicated fatigue wear. All strands remained engaged by the couplers; strand rupture, if it occurred, was located outside of the splice. Figure 177 shows the wire failures and several examples of the strand failure surfaces. Additional discussion of observations is covered in Section 12.4.1.



(a)F2BW4

(b)F2TE1

Figure 177-F2: (a) bottom strand showing fatigue (40X) (b) top strand yield (20X)

## 12.4 Discussion and Comparison of Behavior

### 12.4.1 Fatigue

Flexure cracks formed in different locations in spliced specimens F1 and F2. Fatigue of strands occurred near those locations during the cyclic loading, eventually becoming the location of strand rupture during the ultimate load test.

Figure 178 shows F1's first crack and bonding pattern, as it pertains to the discussion which follows.

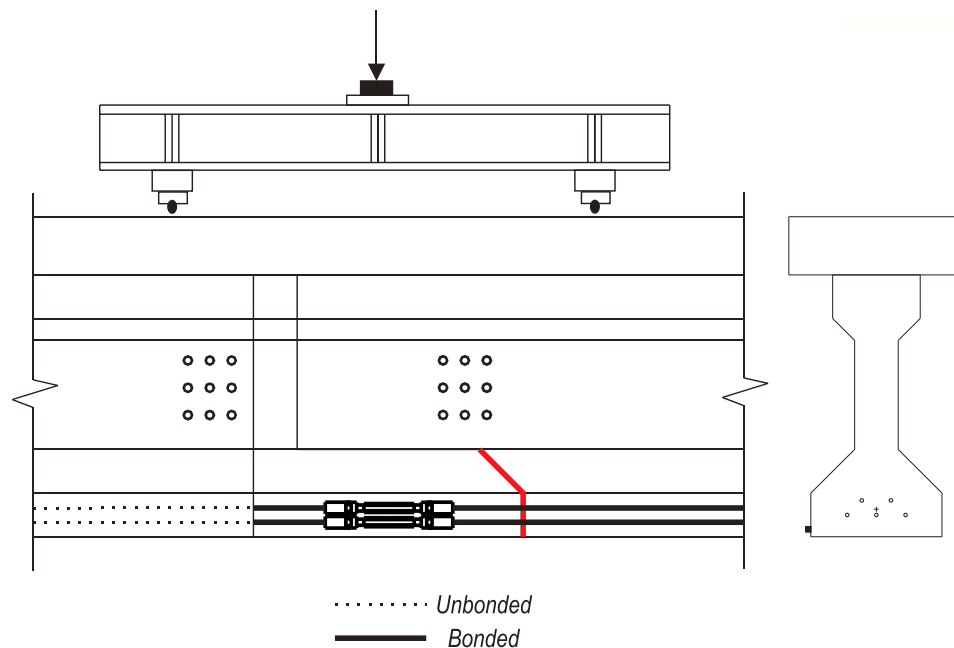


Figure 178–F1: Cracks at start of fatigue

F1's strands were fatigued at the notch interface. At this location, the strands were bonded to both the precast and the closure pour. Because the strand was bonded in this location, the free length of strand that was stressed during each cycle was only as wide as the crack, resulting in a high stress concentration on the strand. F1's theoretical strand stress range at the crack location (calculated based on cracked moment of inertia and the differential strain induced by loading) was approximately 9 ksi, or 3.3% of  $f_{pu}$ . This is ultimately where the strands failed in the F1 specimen during the static ultimate load test. As shown in Figure 165(a), the strands exhibited fatigue wear at this location.

The fatigue stress range introduced on the strand is restricted to the crack length; this can also be seen in the load cell and coupler strain gage measurements. The load cells on F1 measured the strand stress range in the unbonded portion of the tendon; the coupler strain gages

measured the coupler stress range (Table 31). (The measured stress range in the threaded portion of the coupler was calculated using the minimum net section of the threaded portion of the coupler.)

The load cells measure a strand stress range of only approximately 100 psi—a negligible measurement—indicating that the unbonded length of strand is not being fatigued during the load cycle. The magnitude of each measured strand stress range indicates that the length of strand between the coupler (which acts as an anchorage) and the chuck at the end of the unbonded length is not being fatigued by the cyclic loading. Meanwhile, the couplers—which are bonded within the closure pour—undergo a stress range comparable with that expected of an uncracked section subject to the applied cyclic load. The calculated stress range in the strands assuming gross section properties (an uncracked specimen) and a modulus of elasticity of 4776 ksi is approximately 0.88 ksi. The coupler strain gages measure a stress range of approximately 1 ksi. A VWSG located near the couplers at the approximate height of the strand centroid measured a similar stress range of approximately 0.78 ksi in the second load cycle. These measurements indicate that the couplers are experiencing a stress range expected in an uncracked section—reaffirming the idea that the cyclic loading is only affecting/fatiguing the strands at the crack at the notch interface.

Table 31–F1: Stress ranges measured during fatigue cycling

Strand	Cycle	Strand (ksi)	Coupler (ksi)
1	1,000	n/a	1.03
	2,000,000	n/a	0.975
2	1,000	n/a	1.07
	2,000,000	n/a	1.05
3	1,000	0.103	1.02
	2,000,000	0.127	1.00
4	1,000	0.151	1.06
	2,000,000	0.163	1.00
5	1,000	0.124	1.02
	2,000,000	0.113	1.06

Table 31 also shows stress ranges near the beginning and end of the fatigue load cycling. The stress range experienced by each strand is approximately the same (within a couple psi) at 1000 cycles as the stress range experienced at 2 million cycles. This was true for all strands in F1. Similarly, the coupler stress range at the start of the test was approximately equal to the

stress range experienced at 2 million cycles. Because the stress range does not appear to change throughout the test, it can be inferred that the specimen's moment of inertia was not affected by the fatigue test.

The occurrence of strand rupture at ultimate load—and the evidence of fatigue wear seen through the scanning electron microscope—indicates that the strand located at the initial crack must have experienced a significant stress range during the cyclic loading. The strand stress range at the crack location, based on calculations assuming a cracked moment of inertia, was approximately  $0.03f_{pu}$ .

Figure 179 shows F2's first two cracks (which formed during static conditioning) and bonding pattern, as it pertains to the discussion which follows. F2's first crack - which was stressed by the fatigue loading - was located in the bonded precast segment, near where F1 was fatigued. At the start of the test, The F2 strand stress range at the first crack location, based on calculations assuming a cracked moment of inertia, was approximately  $0.08f_{pu}$ . A second crack (also shown in Figure 179) across the coupler exposed the coupler to fatigue loading.

Table 32 shows the stress ranges experienced by the F2 strands and the couplers at both the start of the test and the end of the test. Similar to the first crack of F1, F2's first crack creates a high stress concentration at the exposed bonded strand at that location. Because the second crack (Figure 179) exposes the couplers, all of the F2 couplers were subject to a higher stress range than the stress range predicted assuming an uncracked section (2 ksi). Neither crack exposed the unbonded length. Evidence of this can be seen in the load cell measurements: because the unbonded length was initially not subject to the cyclic load, the strand stress range measured by the load cells was very low—only a couple hundred psi.

Table 32–F2: Stress ranges measured during fatigue cycling

Strand	Cycle	Strand (ksi)	Coupler (ksi)
1	1,000	n/a	5.96
	2,000,000	n/a	3.6
2	1,000	n/a	12.08
	2,000,000	n/a	8.36
3	1,000	0.543	2.84
	2,000,000	2.27	1.8
4	1,000	0.27	8.72
	2,000,000	1.15	3.8
5	1,000	0.459	15.7
	2,000,000	1.53	10.6

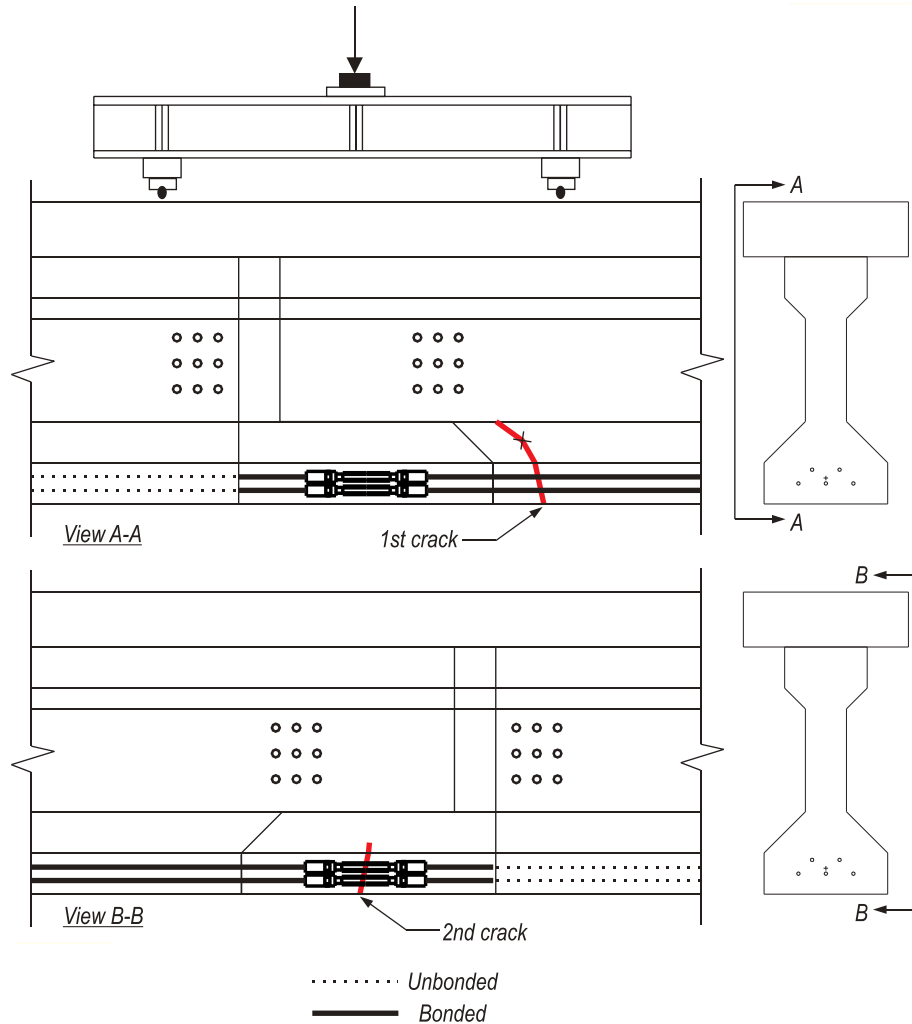


Figure 179–F2: Cracks at start of fatigue

Specimen F2 (subjected to a larger load range), in contrast to F1, did experience fatigue degradation over the duration of the fatigue test. Changes in the measured stress ranges in the strand and the coupler - as well as visually observed crack propagation - reveal the degradation of the specimen. From 1,000 cycles to 2 million cycles, the coupler data indicate a reduction in stress range for all five couplers. Two things are hypothesized: 1) that the coupler experienced strain relief, as cracks forming on either side of the coupler reduced the precompression of the concrete in the closure pour, and 2) local debonding of the strand increased the gage length, reducing the strain. This is unlike what occurred in specimen F1, which did not develop additional cracking over the fatigue testing period. On the other hand, according to the load cell readings, the stress range experienced by each strand at 2 million cycles was greater than the

stress range experienced at 1,000 cycles, indicating that some degradation of the specimen's cross-section/moment of inertia had occurred, increasing the strand stress range when the unbonded length was finally subjected to the fatigue loading. This is assumed to have occurred at approximately 1.7 million cycles, when an opening of the vertical interface was observed. Figure 180 shows the crack pattern at the end of the fatigue test, as well as the hypothesized debonding around the coupler.

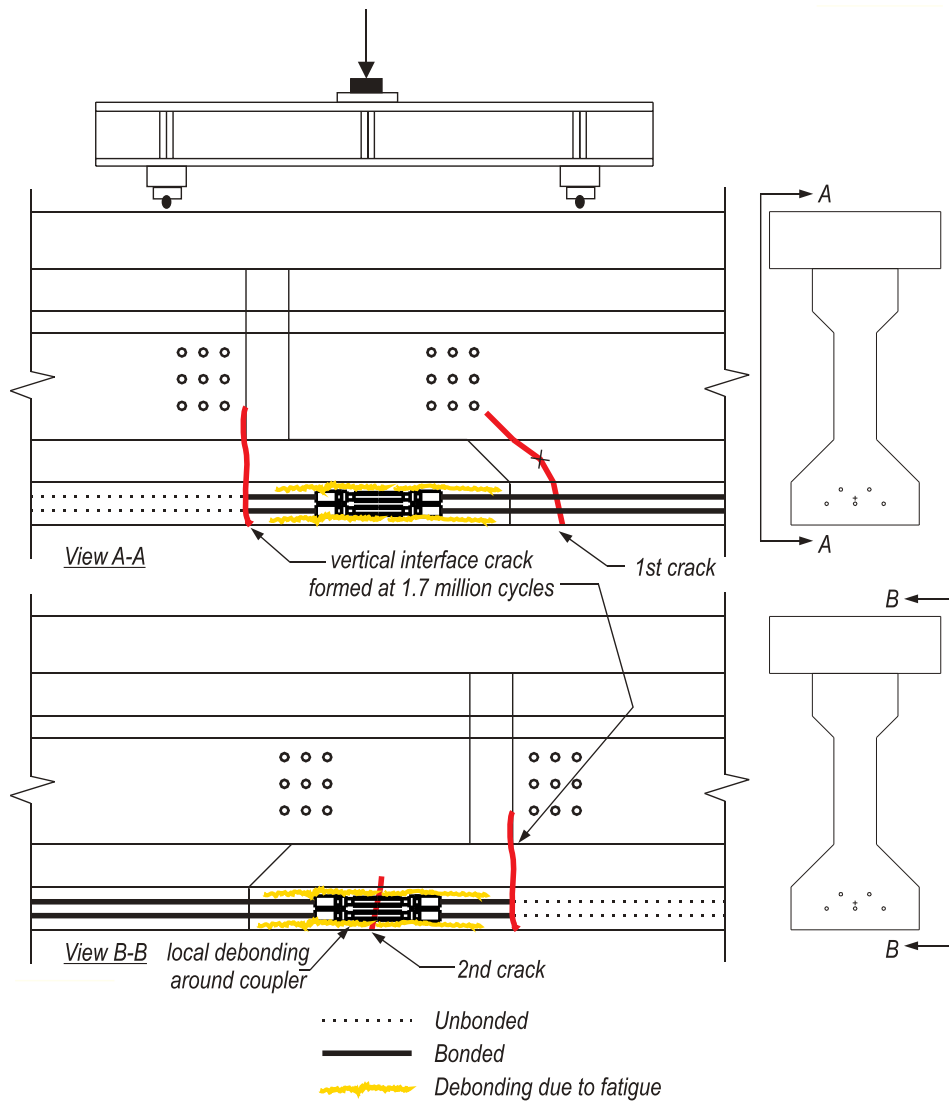


Figure 180-F2: Section degradation due to fatigue

Performance was also evaluated by comparison of the load-deflection plots over time. The plot shows the load vs. midspan deflection for the FC, F1 and F2 specimens at the start and end of fatigue loading. All fatigue tests were conducted in the same test set-up.

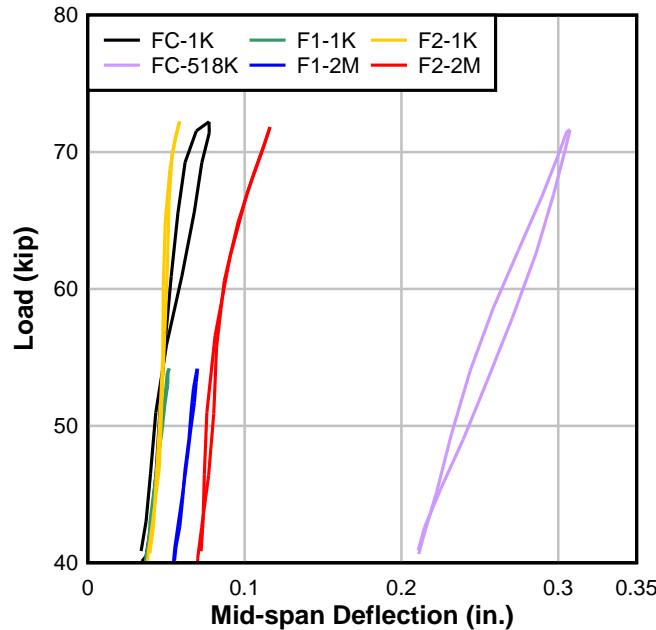


Figure 181–Fatigue: Deflection at start and end of tests

The plotted midspan deflection is the average of the two midspan laser displacement gage readings minus the average support displacement. At the start of each of the fatigue tests, the control FC and the two spliced specimens (F1 and F2) all have the same midspan displacement at 40 kip—approximately 0.04 in. The slopes are also nearly equivalent—indicating that each specimen had approximately the same stiffness at the start of the test.

The effect of the fatigue loading can be seen by comparing the 1,000<sup>th</sup> cycle vs. the last cycle. FC experiences a large loss of ductility and stiffness; that, combined with the sudden deflection change after 518,000 cycles and the reduced capacity when loaded to failure, indicates wires ruptured during fatigue cycling. The midspan deflection of the F1 specimen at 40 kip increases from 0.04 in. to 0.06 in., revealing a loss of ductility over time; though, because the slope does not change, the stiffness of the specimen has remained the same. On the other hand, the FC and F2 specimens exhibit a loss of stiffness (increase in slope) and permanent set (loss of ductility; increase in magnitude of deflection at 40 kip) between the first thousand cycles and the last cycle. Both FC and F2 at their last cycle exhibit bilinear behavior, indicating that the specimen stiffness changes mid-load cycle.

### 12.4.2 Ultimate

Figure 185 shows the load-deflection plot for the ultimate load tests of all three fatigued specimens (FC, F1 and F2). For comparison, the AASHTO-LRFD predicted bonded (123 kip) and unbonded flexural capacities (114 kip) are also shown.

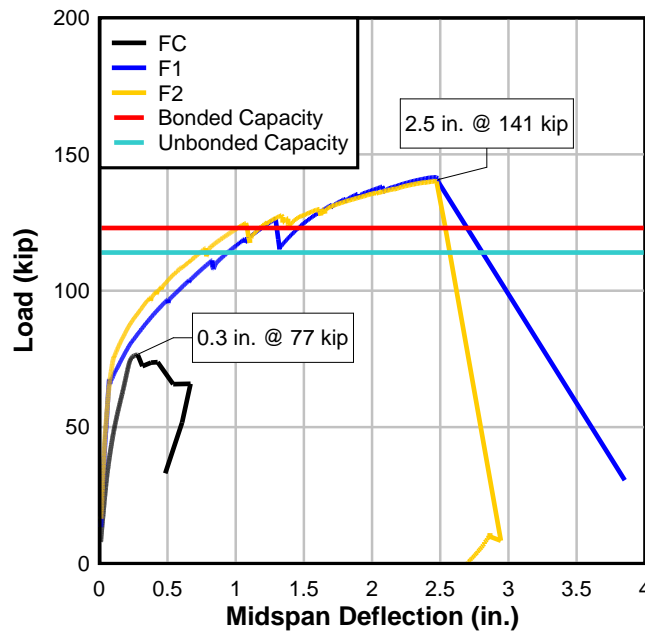


Figure 182 –Post-fatigue Failure: FC, F1 and F2

As can be seen in the plot, both spliced specimens had a higher tested capacity than the control specimen after fatigue loading. It is also worth noting that both specimens survived the 2 million fatigue load cycles, while the control specimen experienced rapid degradation around 518,000 cycles. The ultimate capacity of FC was 77 kip—only slightly larger than the high end of the load cycle (72 kip) and less than the capacity (both bonded and unbonded) as calculated per AASHTO. Meanwhile, both F1 and F2 exceeded the AASHTO-LRFD predicted capacity (both bonded and unbonded) and, though each had been subjected to different load ranges, developed the same ultimate capacity prior to failure. While F2 initially fatigued the strand at a bonded crack, it is hypothesized that bond degradation of the coupler (Figure 180) relieved the stress range on the strand in this area, thus allowing the specimen to reach a greater ultimate strength than FC. FC represented the worst case stress concentration of a bonded strand for a 40-72 kip load range. Though similar bond degradation around the coupler did not appear to occur in F1,

the lower load range reduced the stress range on the bonded strand; the lower load range apparently did not affect the ultimate capacity of F1. Figure 183 shows a comparison of the tested fatigue to the AASHTO-LRFD calculated. The left y-axis compares the applied moment at ultimate to the AASHTO-LRFD bonded design capacity; the right y-axis compares the applied moment at ultimate to the AASHTO-LRFD unbonded design capacity.

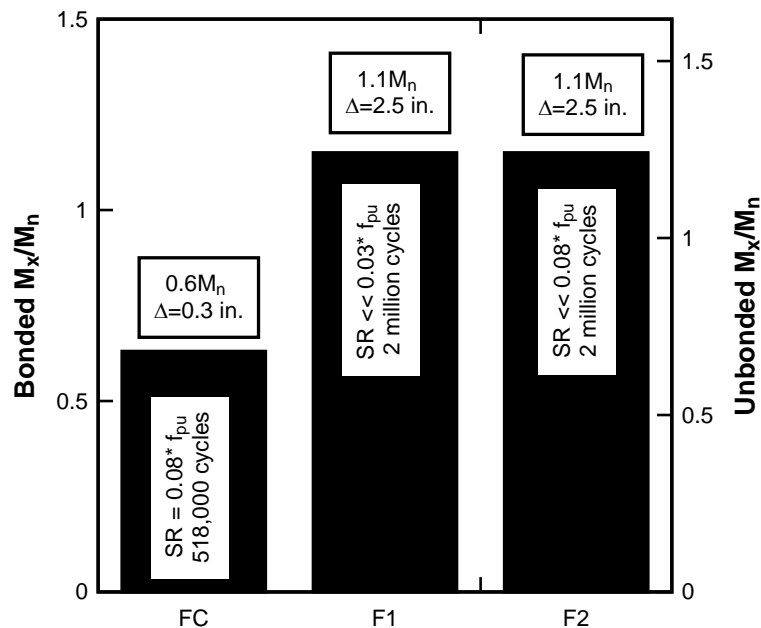


Figure 183–AASHTO: FC, F1 and F2

Figure 183 also presents the strand stress range due to fatigue loading, calculated based on cracked section properties. For bonded specimen FC, the strand stress range was approximately 8% of  $f_{pu}$ . If the spliced specimens had been bonded, the applied stress range was 3% and 8% on F1 and F2, respectively. Due to the lack of bond, the strand stress range was actually much less than either of these calculated values.

Fatigue performance of the spliced specimens FC, F1, and F2 was also evaluated through comparison with the static failure tests. The fatigued specimens were compared against the non-fatigued specimens to evaluate the effect of fatigue loading on the ultimate capacity and deflection at failure. Figure 184 shows the load-displacement plot for XC and FC, including the AASHTO-LRFD predicted bonded and unbonded capacity. Figure 185 compares the ultimate strength test of the non-fatigued spliced specimen X1 to those of the two fatigued specimens F1 and F2.

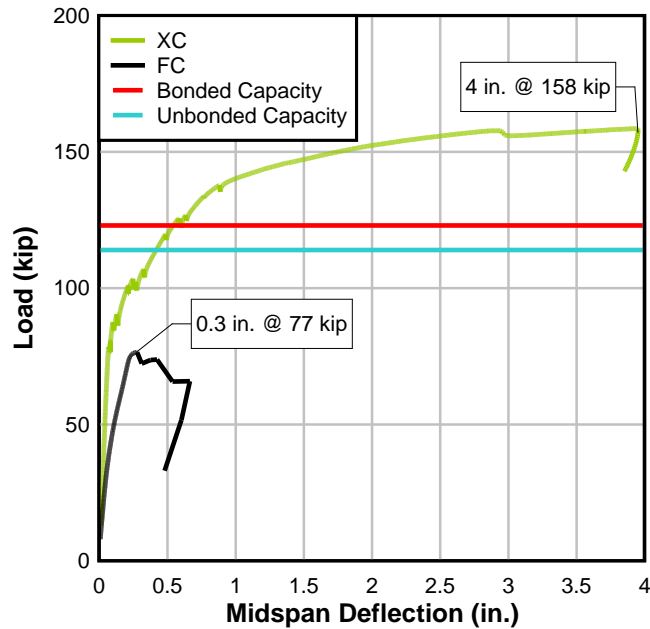


Figure 184—Static vs. Post-fatigue Failure: Control specimens

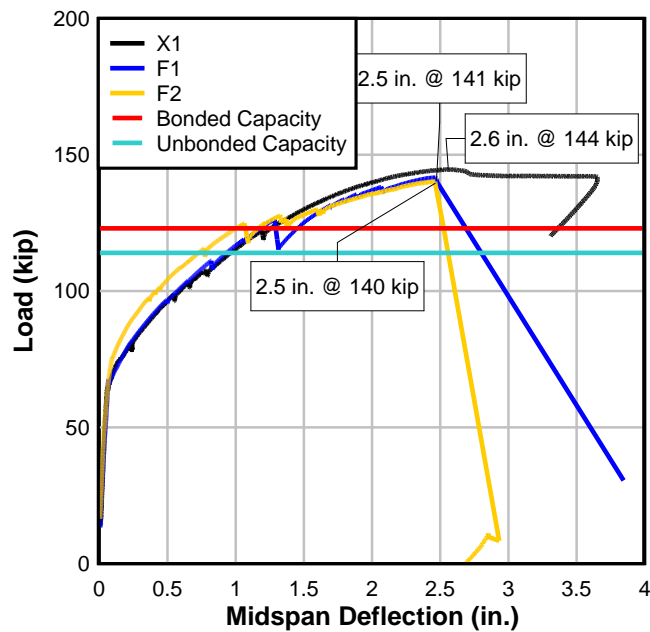


Figure 185—Static vs. Post-fatigue Failure: Spliced specimens

As shown in Figure 184, the ultimate capacity of FC was affected by the fatigue loading, as expected due to the rupture of strand at 518,000 cycles. Both the ductility and the ultimate load were significantly reduced. FC had an ultimate capacity of approximately 77 kip—nearly 50% less capacity than XC. X1 had only a slightly higher ultimate load (144 kip) and midspan deflection (2.6 in.) at failure than that of the F1 and F2, which both failed at approximately 140

kip and 2.5 in. of deflection. Additionally, the spliced specimens reserve capacity—the specimen’s ability to continue carrying load after ultimate—appears to have been affected by the fatigue. After achieving ultimate load, X1 lost some load (approximately 3 kip) but continued to deflect under a load equal to 98% of the ultimate load capacity achieving a maximum deflection of 3.7 in. before the concrete crushed. Conversely, the failures of the fatigued specimens F1 and F2 were sudden and caused by strand rupture; neither spliced specimen carried additional load after ultimate. Furthermore, less than 10% of the ultimate strength remained in load capacity after the peak load was reached. The flexural strength of the spliced beams was not affected by fatigue; the failure mode, however, became brittle and sudden.

Comparison of the ductility ratio  $\mu_{cr}$ , (calculated as the ratio of the mid-span deflection at ultimate to the deflection at cracking) reveals the effect of fatigue on the specimens’ failure mode (Table 33). The FC ductility ratio  $\mu_{cr}$ , calculated as the ratio of the deflection at ultimate to the deflection at cracking, was 4 versus XC, which had a  $\mu_{cr}$  ratio of 60.

Table 33–Ductility ratios

Specimen	Ductility Ratio $\mu_{cr} = \Delta_{ult}/\Delta_{cr}$
XC (static)	60
X1 (static)	43
FC	4
F1	35
F2	25

The ductility ratio similarly reveals the effect of fatigue on the spliced specimens. Once again, the ratio is calculated as the mid-span deflection at ultimate to the deflection at cracking, where cracking was either when the specimen cracked or a joint opened (creating a change in specimen stiffness). X1, F1 and F2 have a ductility ratio of 43, 35 and 25, respectively: while the ultimate flexural strengths of the spliced specimens appear to have been unaffected by the 2 million cycles of fatigue loading, the ductility was affected. Additionally, the general trend appears to be that the specimen ductility is more affected by the higher applied stress range.

The location of the primary crack affected the strand rupture and ductility at ultimate. In the ultimate load test of F1, the crack at the notch interface became the location of strand rupture at ultimate load. In post-failure inspection of F1, it was observed that a single top row strand had slipped completely from the wedge. Post-failure inspection revealed that the wedge had

improperly seated (Figure 187). All but one wire of the other top row strand remained engaged by the coupler; this strand ruptured at the notch crack. The bottom row of strands ruptured at the crack location (Figure 186).



Figure 186-F1: Post-failure



Figure 187-F1: Wedge seating

F2's strand ruptured at the primary crack location shown in Figure 167, approximately 14 in. away from a Grabb-it face. The ruptured strands are seen in Figure 188. It can be observed in the picture that the strand rupture has occurred at a rebar location; inspection of the strand found evidence of fretting between the rebar and the bottom row prestressing strand initiated the fatigue wear at this location (Figure 189).



Figure 188-F2: Post-failure

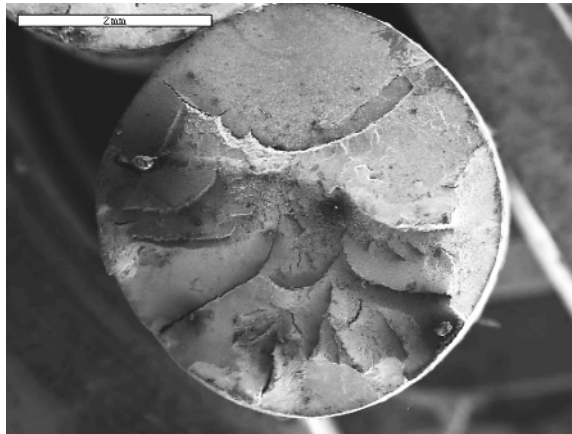


Figure 189-F2: Fatigue wear

In both spliced specimens, the Grabb-its acted effectively as anchorages post-failure, maintaining the prestress force in the unbonded strand. The effectiveness of the Grabb-its as anchorages will now be discussed.

Figure 190 shows the applied load versus the strand load for specimen F1. The plot shows that, after approximately 67 kip, the prestressing strands begin to take on additional load, indicating that the precompression has been overcome. At 126 kip, a drop in the applied load corresponds with the sudden deflection shown in Figure 160 and a loud report, indicated strand

rupture. At ultimate load, the load cells indicated a strand force reduction of approximately 5 kip, indicating that the some but not all of the prestress force had been lost.

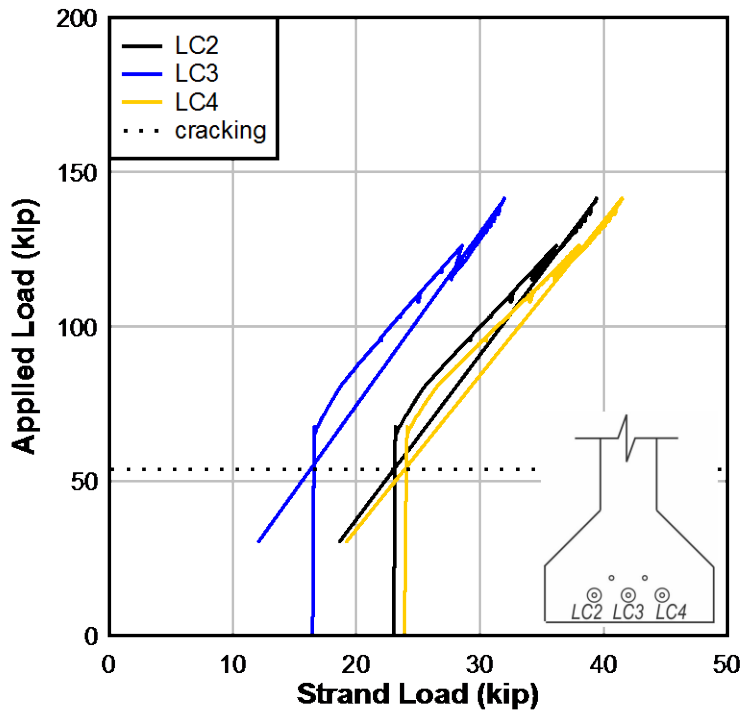


Figure 190-F1: Load cells

Figure 191 shows the applied load versus the strand load for F2. At ultimate load, the load cells indicated a strand force reduction of approximately 8 kip, indicating that the some but not all of the prestress force had been lost.

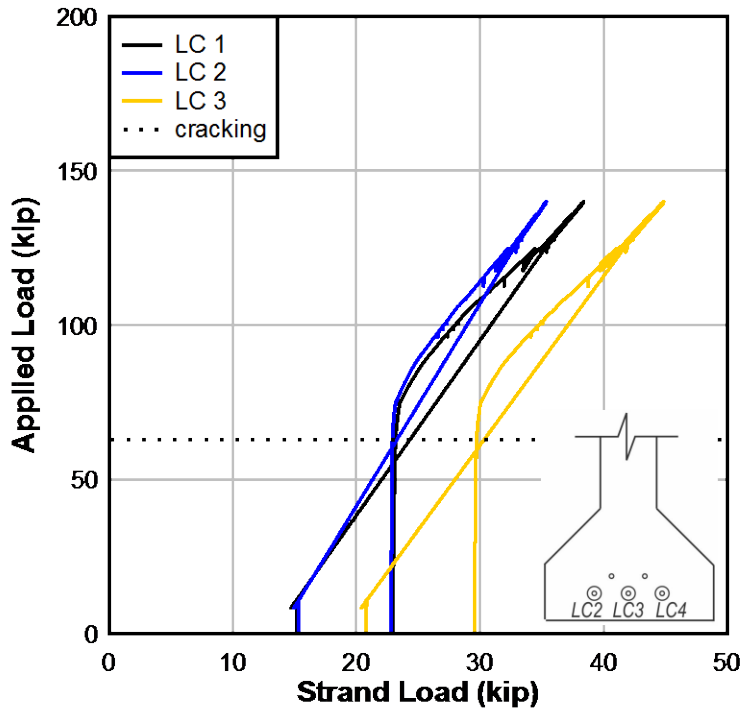


Figure 191-F2: Load cells

Both specimens F1 and F2's load cells indicate partial stress relief of the unbonded strand after ultimate failure of the specimen. In both specimens, when the strand ruptured at ultimate load, the large vertical crack between closure pour concrete and the unbonded segment slammed shut, completely closing the joint opening at the vertical interface of the closure pour (as seen in Figure 175). Because the failure of both specimens occurs at the fatigued crack near the bonded segment, the unbonded segment and closure pour remain prestressed, due to the anchorage action of the coupler.

### 13 Discussion and Observations

Table 34 presents the applied moments, calculated cracking moment, and bottom fiber stress states for each specimen that experienced flexural cracking. Though specimens SC and SB were tested to examine shear response, their exhibited behavior was principally flexural in nature, and so they are presented here. The applied moment was calculated based on the applied load at cracking plus the self-weight moment. The calculated cracking moment was calculated assuming cracking to occur at a bottom fiber tensile stress of  $7.5\sqrt{f'_c}$ , assuming the effective prestress to be that measured by the load cells minus the prestress losses measured by the VWSG. The bottom fiber tensile stress was also calculated based on the measured effective prestress. The ratio of the applied moment to the predicted cracking moment is given for reference.

Table 34–Flexural cracking behavior

Specimen	Crack Type	Calculated $M_{cr}$ (kip-ft)	Applied M (kip-ft)	$f_{bot}/\sqrt{f'_c}$ per LC, ksi	Applied M / Calculated $M_{cr}$
XC	Flexure	542	412	3.8	0.76
X1	Flexure/Bond	538	351	2.2	0.65
SC	Flexure	629	507	4.1	0.81
SB	Flexure	617	476	3.6	0.77
FC	Flexure	534	396	3.6	0.74
F1	Flexure/Bond	489	305	2.3	0.62
F2	Flexure	541	343   389	1.9   3.2	0.63   0.72

Although no reason was identified for the low cracking moment, each specimen was found to crack at a lower load than anticipated. In general, the ratio of the applied moment (including self-weight moment) to the cracking moment was between 0.6 and 0.8.

Table 35 presents the applied shear at cracking and the calculated web-shear resistance (AASHTO-LRFD 5.8.4.4.3) for both specimens. Specimens SU and SU2 exhibited shear behavior, with the first crack developing as a web shear crack. The applied shear was calculated using both the jack load and the shear due to the specimen self-weight. The calculated web-shear resistance was calculated assuming the effective prestress to be that measured by the load cells minus the prestress losses measured by the VWSG. It was also assumed that the concrete strength was equal to the specified 8500 psi. The ratio of the applied shear to the predicted cracking shear is given for reference.

Table 35–Web shear cracking

Specimen	Crack Type	$V_{cw}$ (kip)	Applied V (kip)	Applied $V/V_{cw}$
SU	Web Shear	77	59	0.77
SU2	Web Shear	78	58	0.74

Other post-ultimate test observations pertaining to serviceability, ultimate strength, and construction techniques are commented on in the following sections.

### 13.1 Closure Pour Observations

Several observations of note were made concerning the closure pour, including:

- The use of epoxy improved the closure pour bond. Epoxy was not used in the first three splice assemblies (X1, SB, SU). Figure 192(a) shows the closure after demolition; it can be seen that—for the most part - the closure pour concrete broke away cleanly at the joint. In later specimens (SU2, F1 and F2), an epoxy (Master Builders Concesive Liquid LPL) was used to improve the bond. In post-test inspections of these specimens, the failure planes occurred across the different pours, indicating that the epoxy had some beneficial effect. An epoxied joint can be seen in Figure 192(b).

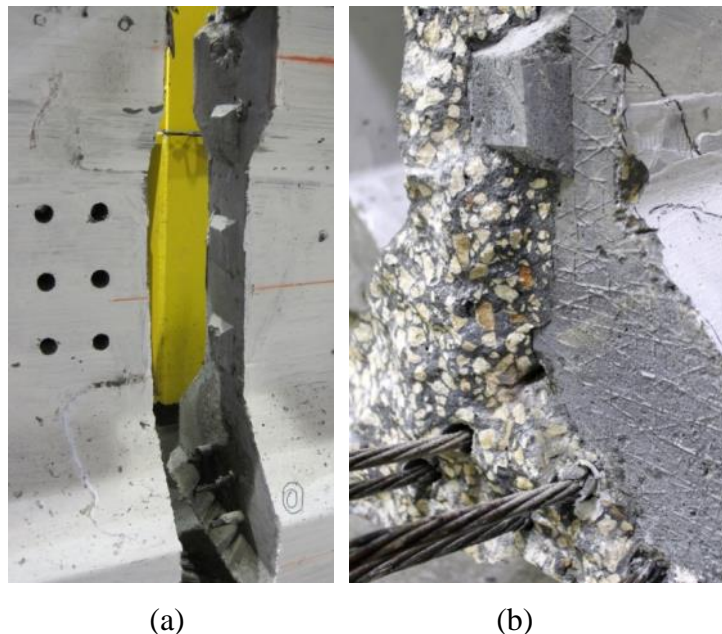


Figure 192–Bond at vertical interface (a) X1 and (b) F2

- Observed evidence of intrusion of the closure pour concrete into the unbonded segment’s PVC sheathing. This indicates that the self-consolidating concrete used in the closure

pour was sufficiently flowable to penetrate and potentially affect the behavior of the unbonded length.



Figure 193–F2: Concrete intruding into unbonded length

- Self-consolidating concrete worked well, with enough flowability to form a voidless pour, so long as the form sides were vibrated using a hand-held vibrator. In one splice assembly (SB), hand-held vibrators were not used, resulting in a void at the reentrant corner of the splice region (Figure 194). The void was repaired prior to testing.



Figure 194–SB: Void at reentrant corner

- Shear keys were observed to be effective when the specimen was tested in a high V/M ratio set-up with the unbonded length under the load point (both tests SU and SU2).



(a)

(b)

Figure 195–Shear keys (a) SU and (b) SU2

- Water transmission was observed along the bonded length of strand approximately ten minutes after the completion of the closure pour. Water was observed to wick the entire bonded length (approximately 13.5 ft) of every strand. Figure 196 shows the end of the bonded precast segment prior to the pour, at 35 minutes, and at 45 minutes after the pour of SU.



(a)

(b)

(c)

Figure 196–SU: (a) Prior (b) 35 minutes (c) 40 minutes

### 13.2 Coupler Observations

Evidence of improper seating of one wedge in specimen F1, perhaps resulting in notching of the strand and affecting the fatigue capacity. Figure 187 shows the coupler from one of the top row strands from specimen F1. The wedge was improperly seated, with concrete slurry holding it in place.

## 14 Summary and Conclusions

This report presents research and development of a new splice technique to lengthen the span of transportable precast prestressed concrete girders. The design and development of the splice focused on an intended application: a simply-supported I-girder with a span length of greater than 200 ft. Utilizing the FDOT's longest spanning I-girder section, the FIB96, a prototype beam design for a 208-ft simply-supported span provided the shear and moment demand on the splice for an example case. The prototype FIB96 was designed in accordance with AASHTO-LRFD 2007 (AASHTO 2007) and the FDOT Structural Design Guidelines (SDG) (FDOT 2010).

A splice design was then developed and integrated into the prototype design, in coordination with the FDOT design office. In the proposed splice design, transportable segments are pretensioned at a precast yard and the strands are cut prior to transport and then spliced on site. Prestressing force is applied to the system by a hydraulic jack on each side of the girder web. External brackets transfer the force from the hydraulic jacks to the precast segments by thru-bolts that pass through the web of the beam. The internal restraint provided by the coupled prestressing strand resists the jacking force, and the prestressing strand is stressed.

To evaluate the splice design assembly procedures and structural behavior, nine specimens were constructed using the AASHTO Type II cross-section; three control specimens and six spliced specimens were fabricated. To accomplish this, fifteen precast prestressed segments were constructed at a precast facility. The precast segments were then transported to the FDOT Structures Research Lab, where six spliced specimens were assembled, splices stressed, and closures poured. The assembly and stressing procedure included instrumentation to evaluate the procedure. Decks were poured on each specimen in preparation for testing. Though labor-intensive, the prestressed splice concept was constructible.

Load testing of the completed specimens was conducted to evaluate flexural, shear, and fatigue behavior. Prestress losses were measured and cracking development was observed to assess service behavior. Additional component testing of the coupler used in the splice design was performed at the State Materials Office.

The following are significant findings from this research:

- Observed prestress losses in the splice region ranged from 5 to 10%, which is less than typical values (10-20%).
- Crack opening occurred primarily at the vertical interface of the closure pour in tests of the spliced specimens.
- Flexural strength of spliced specimens exceeded the AASHTO-LRFD values for bonded strand by 15% and for unbonded strand by 24%.
- Spliced specimen (F1) exhibited greater fatigue resistance than the control specimen (FC) when cycled at the same strand stress range of 0.08fpu. F1 survived 2 million cycles while FC survived 518,000 cycles.
- Fatigue of spliced specimens did not impact the strength or deflection at ultimate load; it did, however, affect ductility and failure mode. All fatigued specimens (FC, F1, F2) collapsed due to strand rupture at peak load.
- At ultimate load, the non-fatigued spliced specimen tested in four-point bending (X1) failed in compression (as the deck crushed); fatigued spliced specimens (F1 and F2) failed when strands ruptured.
- Fatigue cycling reduced displacement capacity when compared to static (non-fatigued) specimens during the ultimate load test. Non-fatigued XC and X1 had ductility ratios of 60 and 43, respectively. Fatigued specimens FC, F1 and F2 had ductility ratios of 4, 35, and 25, respectively.
- Non-fatigued flexure specimen (X1) deflected an additional 1 in. beyond peak load-supporting at least 98% of the peak load.
- The shear test set-up imposed a moment to shear ratio (M/V) ratio of 3.7, which is a higher relative shear than is present in the prototype FIB96 design (32.9). In the one specimen that did exhibit the characteristics of a shear failure, the vertical interface of the dry joint/closure pour was the location of failure and the shear strength of the spliced specimens exceeded the shear strength calculated per AASHTO-LRFD modified compression field theory. All other specimens tested in the shear set-up failed in flexure.
- Shear strength of spliced specimens was shown to be moderately improved (9%) through additional stirrups and epoxy application to the joint.

- Disturbance of the “transfer length” region of the bonded segment occurred during the stressing procedure, resulting in an area susceptible to flexural cracks.
- Couplers did not appear to generate excessive cracking in the closure pour concrete. Coupler congestion did not appear to affect the service performance.
- At ultimate, couplers acted as anchorage points, maintaining a significant portion of prestress force in the strand.

## 15 Recommendations and Future Research

Although similar systems have been tested and used, this particular splice design has not been tested. Consequently, a number of issues were noted during the development and testing of this splice that might be pursued in future testing:

- Increased shear resistance through inclusion of additional reinforcement and splice-region reinforcement is recommended. Use of mechanical shear connectors have been shown to be effective in developing shear resistance in spliced precast beams (Kim et al. 2008).
- Design to force failure away from the couplers and away from the vertical interface of the closure pour.
- Use anchorage devices to reduce the transfer length in the disturbed regions near where strand stressing impacts the strand bond in the precast segments. Because the splice is not at a zero moment location within the span (as commonly found in continuous span designs of precast segmental I-girder bridges), one of the main issues to overcome is the development of adequate prestress force at the splice end of the precast segments. To accommodate this requirement, investigation of a several anchorage devices (intended to shorten the transfer length of the prestress force) is recommended.
- Considering using ultra-high performance concrete instead of prestressing the splice.
- Considering a change to the FIB cross-section at the splice location. The use of a block-out at the splice would allow the inclusion of additional reinforcement and less congestion of splice hardware (couplers, etc).
- Stagger the coupler locations to limit congestion.

Additional recommendations related to the construction and detailing of the splice region:

### Regarding detensioning:

To better control the strand and ensure its integrity (for later splicing), a staged, slow detensioning procedure was coordinated with the precaster. The prestress in each strand was initially slowly released by means of a single strand jack, at the steel bulkhead of the live end. The resulting inequality of force in the bed was only  $0.6 \cdot f_{pu} \cdot 0.153 \text{ in}^2$ , or approximately 25 kips. This force was not of sufficient magnitude to cause the beam segments to shift in the bed.

Following the release at the live end, the strand was torch cut at the dead end, equalizing the force exerted on beams. No movement of the beams was visually observed during this procedure. The strand remained intact at both the live and dead ends of the bed. To speed the cut-down process in the prototype beam, it is recommended that a pair of multi-strand jacks be used to gradually release the prestress force simultaneously at the live and dead end. Gradual release of the force in this manner will not only protect the strand for later splicing, but will reduce the bursting effects caused by the large number of strands in the pattern.

Because a low prestress force was present in the strands, the chance of strand recoil (bird nesting) was mitigated to some degree. If the level of prestress is increased beyond  $0.6f_{pu}$ , or if 0.6-in. dia strand is used, then additional consideration concerning the cut-down procedure is warranted. As it was, the amount of energy present in the test specimen strand was low enough that when torch-cut at the dead end, the strand did not recoil excessively.

Regarding care and handling of the splice region:

Wooden boxes were constructed to form the coped end region of the splice. A fillet at the interior corner was included to reduce stress concentrations, and to aide in the removal of formwork. The wooden box was left in place during curing and storage at the precast plant to protect both the coped end and the protruding strand.

Regarding pipe inserts:

For future projects, the pipe inserts should be on a square grid, to ensure proper orientation. This was handled with the test specimen by marking the top of the pipe insert.

The pipe inserts were prepared prior to precasting. Pipe alignment was maintained by inserting the pipes into a template made of steel plate and tack-welding the pipes to #3 rebar. The steel templates were made by plasma cutting holes in the proper orientation; pipes were inserted through the holes and thus held in place during welding to the #3 rebar. The rebar was used to tie in the pipe insert. Placement of this rebar obstructed the stirrups in at least one insert; the obstructing rebar was removed and field welded in a clear location. To prevent this in the future, take consideration of the reinforcement congestion near the pipe insert and utilize the smallest available rebar.

Regarding concrete consolidation around the pipe inserts: A high slump concrete was used to increase the flowability of the paste around in highly congested area around the pipe

inserts, however during vibration of the concrete, care was taken surrounding the pipe inserts so as not to dislodge them. Issues regarding concrete consolidation in this area may need to be addressed at a later time.

## 16 References

- AASHTO. (2007). AASHTO-LRFD Bridge Design Specifications (4th edition with 2007 interim revisions). American Association of State Highway and Transportation Officials, Washington D.C.
- Abdel-Karim, A. M., and Tadros, M. K. (1992). "Design and Construction of Spliced I-Girder Bridges." *PCI Journal*, 37(4), 114-122.
- Abdel-Karim, A. M., and Tadros, M. K. (1992b). "State-of-the-Art of Precast/Prestressed Concrete Spliced I-Girder Bridges" Precast/Prestressed Concrete Institute, Chicago, IL.
- ACI 318-08. (2008). Building Code Requirements for Structural Concrete (ACI318-08) and Commentary. American Concrete Institute, Farmington Hills, MI.
- ASTM A416. (2006). Standard Specification for Steel Strand, Uncoated Seven-Wire for Prestressed Concrete. West Conshohocken, PA: ASTM International.
- ASTM A1061. (2009). Standard Test Methods for Testing Multi-Wire Steel Strand. West Conshohocken, PA: ASTM International.
- ASTM C39. (2010). Standard Test Method for Compressive Strength of Cylindrical Concrete Specimens. West Conshohocken, PA: ASTM International.
- Castrodale, R. W., and C. D. White. (2004). NCHRP Report 517: Extending Span Ranges of Precast Prestressed Concrete Girders. (Vol. 517). Transportation Research Board, Washington D.C.
- Collins, M. P. and Mitchell, D. (1991). *Prestressed Concrete Structures*. Prentice Hall, City, State.
- FDOT (Florida Department of Transportation). (1999). Gandy Bridge Construction Drawings, FDOT, Tallahassee, FL.
- FDOT (Florida Department of Transportation). (2004). New Directions for Florida Post-Tensioned Bridges: Design and Construction Inspection of Precast Concrete Spliced I-Girders. Vol. 4, FDOT, Tallahassee, FL.
- FDOT (Florida Department of Transportation). (2009). Temporary Design Bulletin C09-01, FDOT, Tallahassee, FL.

FDOT (Florida Department of Transportation). (2009b). Temporary Design Bulletin C09–05, FDOT, Tallahassee, FL.

FDOT (Florida Department of Transportation). (2010). FDOT Structures Manual, FDOT, Tallahassee, FL.

FDOT (Florida Department of Transportation). (2010b). FDOT LRFD Prestressed Beam v 3.2 MathCAD program, FDOT, Tallahassee, FL.

FDOT (Florida Department of Transportation). (2010c). *Bridge Maintenance and Repair Handbook*, FDOT (2010), Tallahassee, FL.

Gerwick, B. C., Jr. (1993). *Construction of Prestressed Concrete Structures*. 2nd Ed. Wiley-Interscience, New York, NY.

Hsu, T.T.C (1993). *Unified Theory of Reinforced Concrete*. CRC Press, Boca Raton, FL.

International Code Council Evaluation Service (ICCES). (2011). Acceptance Criteria for Post-Tensioning Anchorages and Couplers of Prestressed Concrete. Whittier, CA: ICCES.

Jaber, F., Tadros, M. K., Fallaha, S., Chuanbing, S., and Morgan-Girgis, A.F. (2006). "Nebraska Precast Record: 204th Street Bridge Spans Single Point Interchange." *PCI Journal* 51(6), 48-54.

Johnson, Bruce. "RE: Citizen's Representative Office – Customer Entry." (Oregon DOT). Email to Natassia Brenkus. Aug 29 2011.

Joint PCI-PTI Committee on Segmental Construction. (1982) "Recommended Practice for Precast Post-Tensioned Segmental Construction."

Kaar, P.H., LaFraugh, R.W. and Mass, M.A, (1963). "Influence of Concrete Strength on Strand Transfer Length." *PCI Journal*, 8(5), 47-67.

Kim, J., Chung, W. and Kim, J. H. J. (2008) "Experimental Investigation On Behavior Of A Spliced PSC Girder With Precast Box Segment", *Engineering Structures*, 30(11), 3295-3304.

Labia, Y., Saiidi, M., and Douglas, B. (1996). CCEER-96-2 Evaluation and Repair of Full-Scale Prestressed Concrete Box Girders. University of Nevada, Reno, NV.

Lacey, G. C., Breen, J. E. and Burns, N. H. (1971). "State of the Art for Long Span Prestressed Concrete Bridges of Segmental Construction." *PCI Journal*, Sept-Oct 1971, 53-77.

Law Engineering (1990). Tensile test results of Enerpac Precision Sure-lock Grabb-it. Provided by Enerpac (manufacturer). Tests performed by Law Engineering.

Loper, J. H., Marquis, E. L. and Rhomberg, E. J. (1988). "Precast Prestressed Long-Span Bridges." *ASCE Journal of Construction Engineering and Management*, 114(1), 95-103.

Lounis, Z., Mirza, M. S. and Cohn, M. Z. (1997). "Segmental and Conventional Precast Prestressed Concrete I-Bridge Girders." *ASCE Journal of Bridge Engineering*, 2(3), 73-82.

Ministry of Transportation of Ontario. (2011). "Many Innovations Make Light Work: Dingman Drive Bridge Repaired Using a Suite of Cost-Saving Innovations." *Road Talk*, 17(1), 1-2.

Nicholls, J. J., and Prussack, C. (1997). "Innovative Design and Erection Methods Solve Construction of Rock Cut Bridge." *PCI Journal*, 42(4), 42-55.

Nikzad, K., Trochalakis, T., Seguirant, S.J., and Khaleghi, B. (2006). "Design and Construction of the Old 99 Bridge—An HPC Spliced-Girder Structure." *PCI Journal*, Jan-Feb 2006, 98-109.

O'Neill, C. M. and Hamilton, H.R. (2009). "Determination of Service Stresses in Pretensioned Beams." *FDOT Research Report No. 00063967*. FDOT, Tallahassee, FL.

Onyemelukwe, O.U., Moussa Issa, P.E., and Mills, C.J. (2003). "Field Measured Prestress Concrete Losses Versus Design Code Estimates." *Experimental Mechanics*. 43(2), 201-215.

Overman, T.R., Breen, J.E., and Frank, K.H. (1984). "Fatigue Behavior of Pretensioned Concrete Girders." *Research Report No. FHWA/TX-85/39+300-2F*. Texas State Department of Highways and Public Transportation, Austin, TX.

PCI (2004). *PCI Design Handbook: 6th Edition*, Precast/Prestressed Concrete Institute, Chicago, IL.

Pessiki, S., Kaczinski, M. and Wescott, H.H. (1996). "Evaluation of Effective Prestress Force in 28-Year-Old Prestressed Concrete Bridge Beams." *PCI Journal*, 78-89.

Rabbat, B. G., Kaar, P.H., Russell, H. G. and Bruce (Jr), R.N. (1979). "Fatigue Tests of Pretensioned Girders with Blanketed and Draped Strands." *PCI Journal*, July-August 1979, 88-114.

Rabbat, B. G., and Russell, H. G. (1982). "Optimized Sections for Precast Prestressed Bridge Girders." *Journal Prestressed Concrete Institute* 27.4: 88-104.

Ralls, M. L., Aktan, A. E. and Culmo, M. P. (2000). *Concrete Bridges: Transportation in the New Millennium*. Transportation Research Board, Washington D.C.

Rao, C. and Frantz, G.C. (1996) "Fatigue Testing of 27-Year-Old Prestressed Concrete Bridge Girder Box Beams." PCI Journal, Sept-Oct 1996, 74-83.

Roller, J.J., Russell, H.G., Bruce, B.N. and Martin, B.T. (1995). "Long-Term Performance of Prestressed, Pretensioned High Strength Concrete Bridge Girders." PCI Journal, Nov-Dec 1995, 48-59.

Ronald, H.D. (2001). "Design and Construction Considerations for Continuous Post-Tensioned Bulb-Tee Girder Bridges." PCI Journal, May-Jun 2001, 44-66.

Russell, B.W. and Burns, N.H. (1993). "Static and Fatigue Behavior of Pretensioned Composite Bridge Girders Made with High Strength Concrete." PCI Journal, 116-128.

Saibabu, S., Srinivas, V., Sasmal, S., Lakshmanan, N. and Iyer, N. R. (2013) "Performance Evaluation of Dry and Epoxy Jointed Segmental Prestressed Box Girders Under Monotonic and Cyclic loading", Construction and Building Materials, 38, 931-940.

Saidii, M. S., Labia, Y. and Douglas, B. (2000). "Repair and Performance of a Full-Scale Pretensioned Concrete Girder." PCI Journal, Mar-Apr 2000, 92-101.

Seguirant, S. J. (1998). "New Deep WSDOT Standard Sections Extend Spans of Prestressed Concrete Girders." PCI Journal, 92-105.

Shanafelt, G.O. and Horn, W.B. (1980). NCHRP Report 226: Damage Evaluation and Repair Methods for Prestressed Concrete Bridge Members. Transportation Research Board, Washington D.C.

Shanafelt, G.O. and Horn, W.B. (1985). NCHRP Report 280: Guidelines for Evaluation and Repair of Prestressed Concrete Bridge Members. Transportation Research Board, Washington D.C.

Waheed, A. P., Kowal, E. and Loo, T. (2005). Repair Manual for Concrete Bridge Elements. Alberta Infrastructure and Transportation. Province of Alberta, Canada.

Walsh, K.Q. and Kurama, Y.C. (2010). "Behavior of Unbonded Post-Tensioning Monostrand Anchorage Systems Under Monotonic Tensile Load." PCI Journal, Winter 2010, 97-114.

Weigel, J. A., Seguirant, S.J., Brice, R. and Khaleghi, B. (2003). "High Performance Precast, Pretensioned Concrete Girder Bridges in Washington State." PCI Journal, 48(2), 28-52.

Zia, P. and Mostafa, T. (1977). "Development Length of Prestressing Strands." PCI Journal, 22(5), 54-65.

Zia, P., Preston, H.K., Scott, N.L., and Workman, E.B. (1979). "Estimating Prestress Losses." *Concrete International*, 1(6), 32-38.

Zobel, R. S., Jirsa, J.O., Fowler, D.W. and Carrasquillo, R.L. (1997) "Evaluation and Repair of Impact Damaged Prestressed Concrete Bridge Girders." Research Report No. FHWA/TX-97/1370-3F. Texas State Department of Highways and Public Transportation, Austin, TX.

Zobel, R.S. and Jirsa, J.O. (1998). "Performance of Strand Splice Repairs in Prestressed Concrete Bridges." *PCI Journal*, Nov-Dec, 72-78.

## Appendix A–Prototype Design

The dead loads present at release of the prestressing tendons include only the self-weight of the precast segment; in other words,  $w_{\text{beam}}$  of each segment length. The self-weight moment at release acts across the entire precast beam length.

Figure 197 shows the moment and shear diagram for dead loads at release of prestressing tendons for end segments of the beam. Figure 198 shows the moment and shear diagram for the middle segments at release.

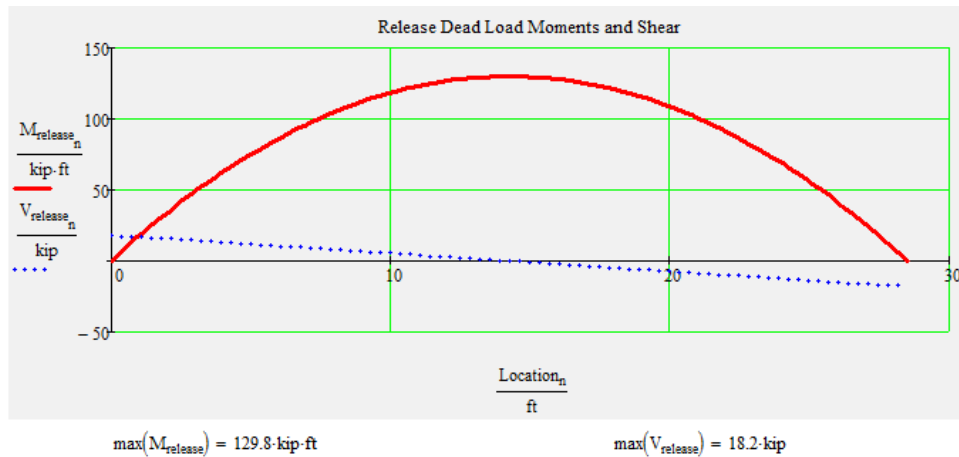


Figure 197–Unfactored Dead Loads at Release on Non-composite End Segments

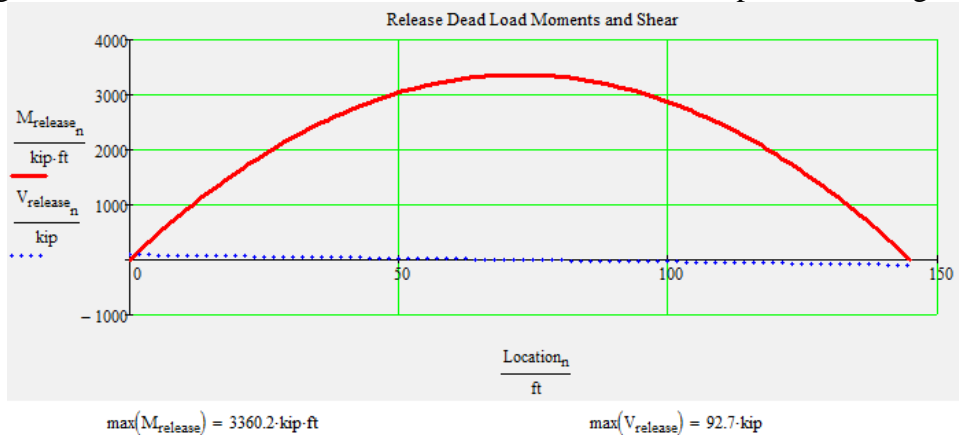


Figure 198–Unfactored Dead Loads at Release on Non-composite Middle Segment

After release of the prestressing strand, the segment cambers up. It is then assumed to rest on a knife edge at the edge of the bearing length.

Figure 199 shows the moment and shear diagram for dead loads prior to deck curing and subsequent development of composite action. The dead loads during this stage include the weights of the beam, deck and formwork (used during deck construction). The loads acting on the beam are assumed to act on a beam (span length) with end cantilevers (the bearing lengths).

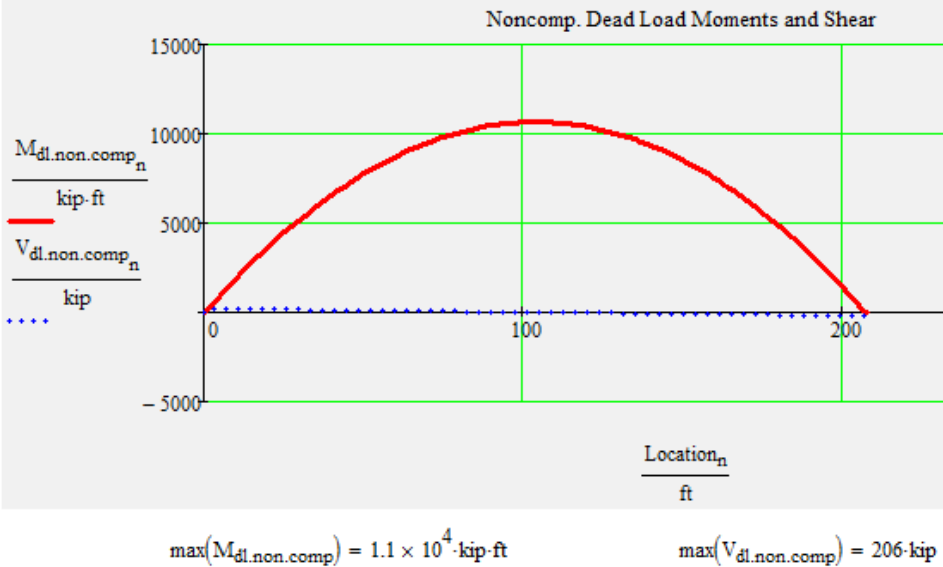


Figure 199–Unfactored Dead Loads on Non-Composite Section–Assembled Length

Figure 203 shows the moment and shear diagram for dead loads on the composite section. The dead loads acting on the composite section include the weight of the deck, beam, barriers, deck formwork and future wearing surface.

Live Load

Figure 200 shows the maximum unfactored moment and shear diagram for legal truck loads due to the HL-93 truck (shown without the dynamic allowance applied):

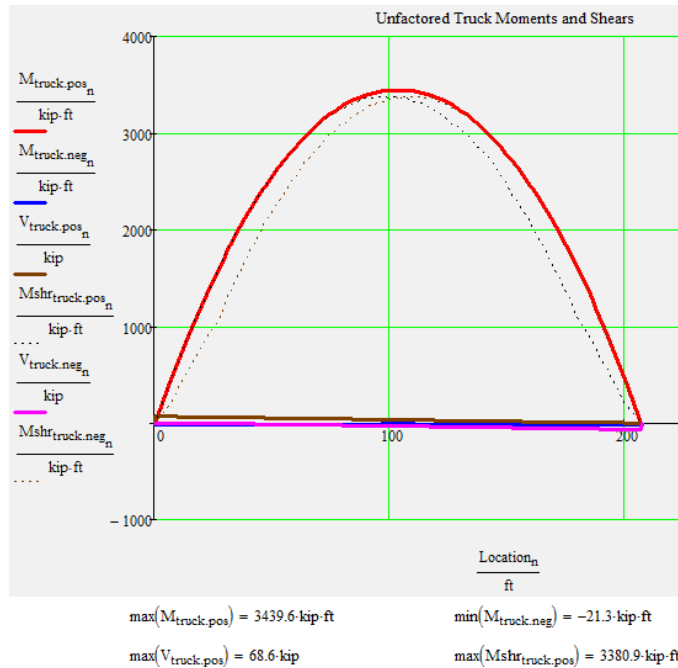


Figure 200–Unfactored Moment and Shear Envelopes due to Legal Truck

Figure 201 shows the maximum unfactored moment and shear diagram for permit loads due to the FL-120 truck. The loads are shown without the dynamic allowance.

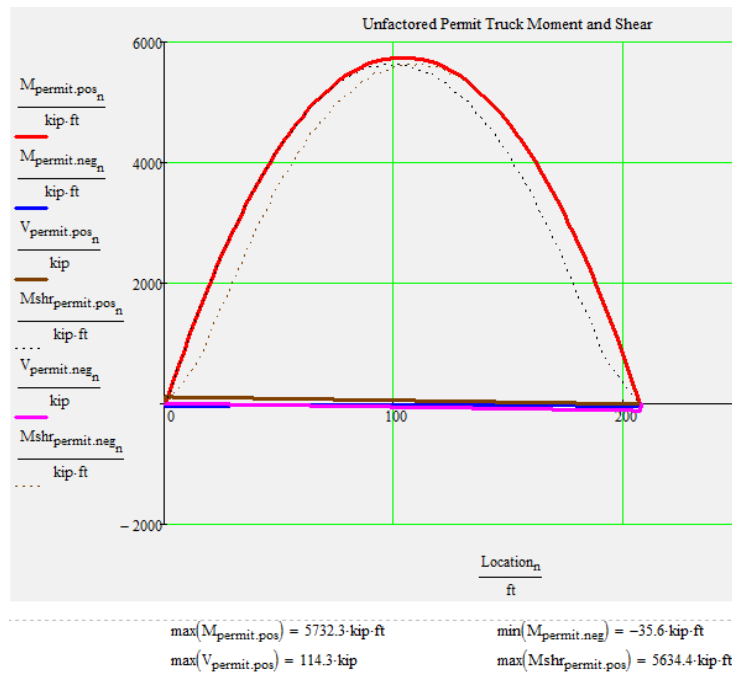


Figure 201–Unfactored Moment and Shear Envelopes due to Permit Truck

Figure 202 shows the maximum unfactored moment and shear diagram due to lane loading.

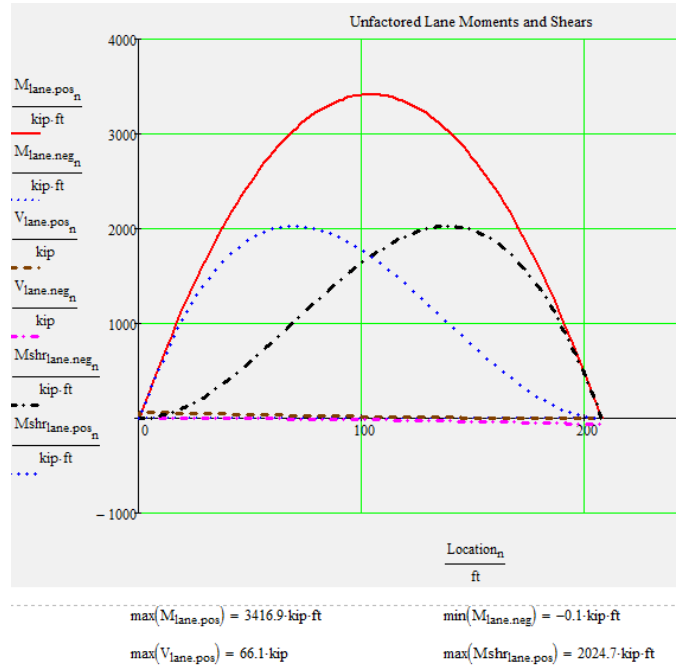


Figure 202–Unfactored Moment and Shear Envelopes due to Lane Loading

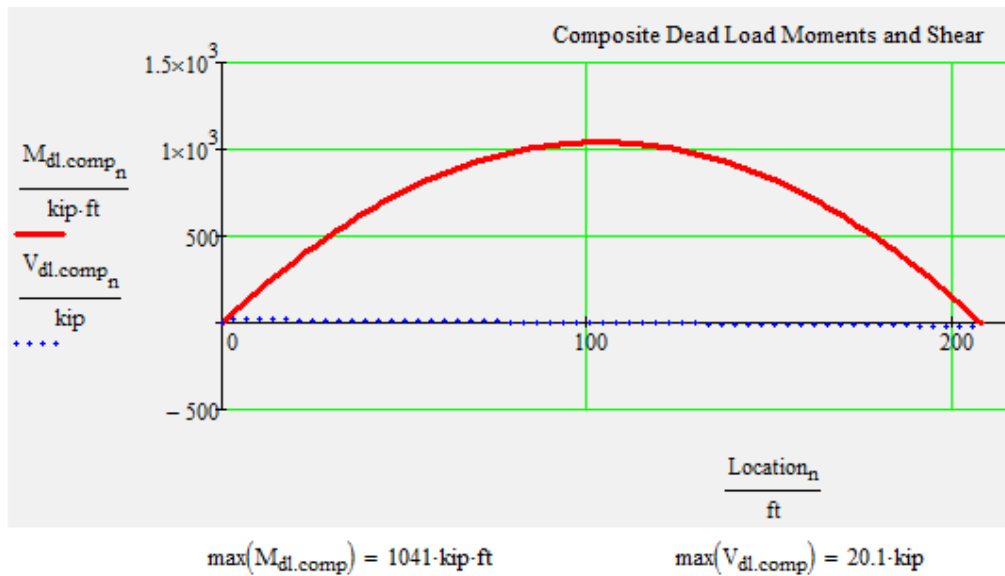


Figure 203–Unfactored Dead Loads on Composite Section

## Appendix B—Splice Concepts

The goal of this research is to develop a localized splice in order to extend the span lengths of I-girder sections. Several design constraints have been taken into consideration during the splice prototype development:

- 1) Elimination of full-length post-tensioning.
- 2) Elimination or reduction of localized post-tensioning.
- 3) Elimination of end block, if possible.

The preliminary splice design concepts investigated herein are intended for long simple span structures where the beam segments are spliced on the ground at the bridge site, and then lifted into place. Splicing of the beams on the ground at the site would eliminate the need for temporary towers. This concept would require sufficient space within the FDOT right-of-way to allow multiple beams to be spliced and stored prior to lifting into place.

### Splice Design A

Splice Design A developed with limited use of post-tensioning at the splice location. Shown in Figure 204, Splice Design A utilizes post-tensioning bar to provide a prestress force to the splice, precompressing the splice concrete.

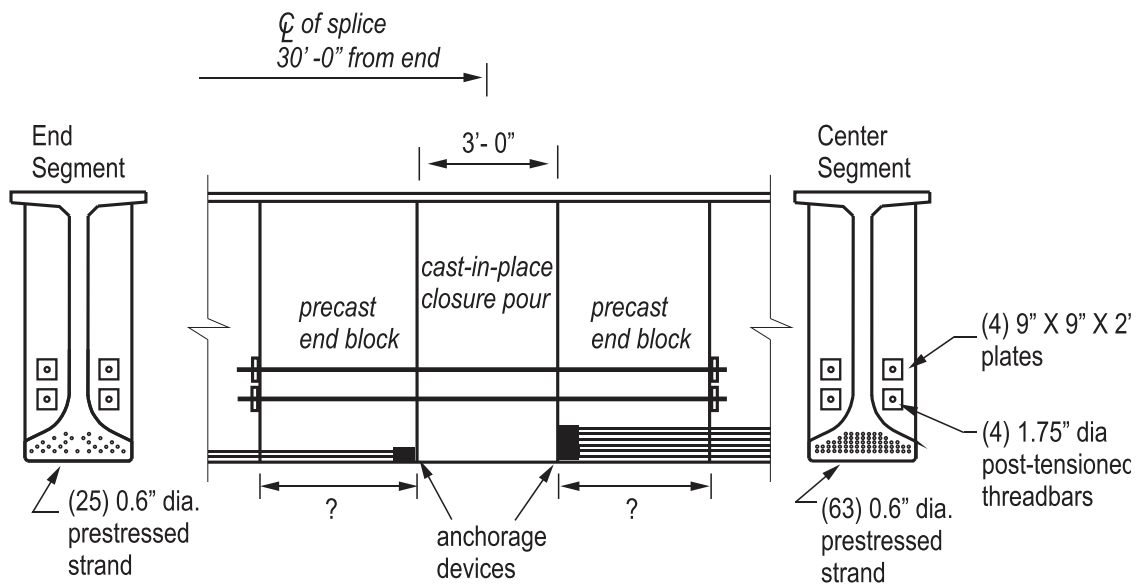


Figure 204—Splice Design A  
(with anchorages)

In Splice Design A, anchorage devices at the end of the precast segments accelerate the development of the prestress force in the precast segment. In this configuration, the anchorage devices must be placed in the precast concrete segments at the precast facility. In the strength limit state, the post-tensioning bars actively prevents against failure.

Design A has the following advantages and disadvantages:

**Advantages:**

- Splice cast-in-place closure pour concrete is cast in a single step.
- Elimination of prestress transfer lengths. (Post-tensioning force is applied beyond the transfer length in the precast segments to ensure a continuous prestress force.)
- Splice concrete precompressed.
- Number of construction steps is minimized.

**Disadvantages:**

- Complicated force transfer between prestressing strand and post-tensioned bar.
- Aesthetic impact and additional cost of rectangular section at splice.
- Post-tensioning equipment and expertise required.
- Beam end block forming is difficult to incorporate into standard beam forms.  
However, if the center segment was standardized or stepped in 5' increments, this would simplify forming.

## ***SPLICE DESIGN B***

Splice Design B, shown in Figure 205, includes anchorage devices within the cast-in-place concrete of the splice, where they act as couplers for the prestressing strands.

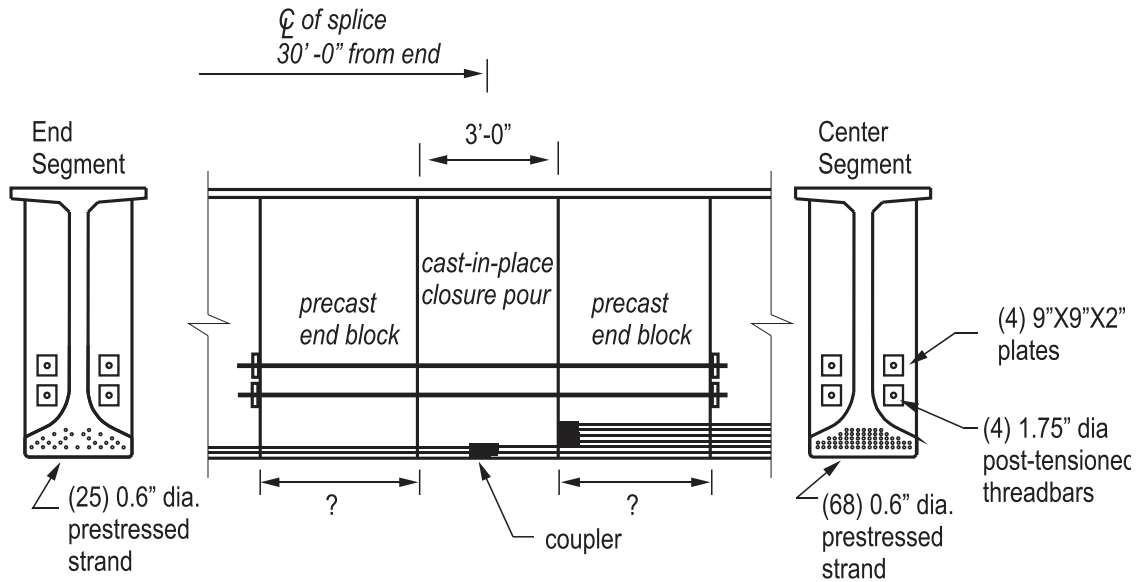


Figure 205–Splice Design B  
(with anchorages and couplers)

In Design B, the prestressing strands extend beyond the end of the precast segments and the coupling device is utilized to mechanically splice the strands prior to the splice concrete pour.

Splice Design B has all of the same advantages and disadvantages at Design A, plus the added advantage of continuity of the prestressing strand. However, the bars may fail prior to mobilizing the coupled strands, especially given the short bar length.

### **SPLICE DESIGN C**

Splice Design C was developed to ensure that the splice concrete is prestressed without the necessity of post-tensioning with bar. In this design, the prestressing strands are spliced together using splice chucks to provide continuity to the prestressing strands continuing from the end segment into the middle segment (Figure 206). Prestress force is then introduced into the splice strand using a flatjack. A single rectangular flatjack is placed in the narrow gap between the webs of the two precast segments. As the flatjack is pressurized, the two segments are forced apart, which induces stress in the strands when the coupling wedges seat. The compressive thrust of the flatjack and the equal and opposite tensile force in the strands form an internal positive moment at the splice. If the pressure in the flatjack is increased such that the self-weight moment of the girder is exceeded, then the girder will lift off of the ground and no further

increase in pressure is possible. Further inflation of the flatjack causes relative rotation of the segments resulting in the formation of a hinging mechanism as illustrated in Figure 207.

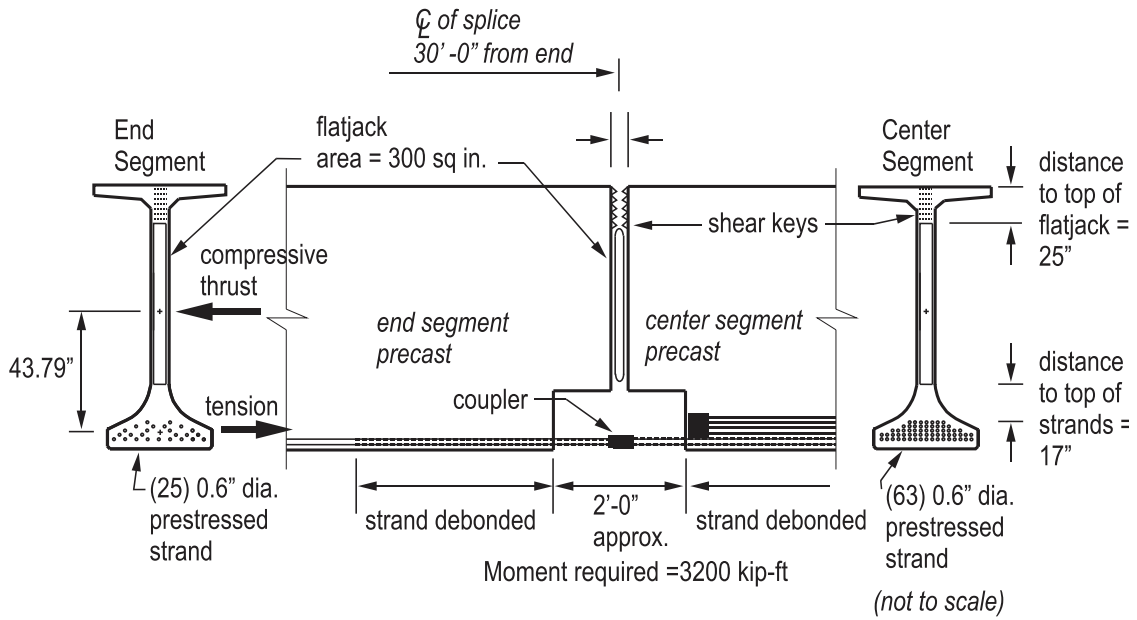


Figure 206–Splice Design C

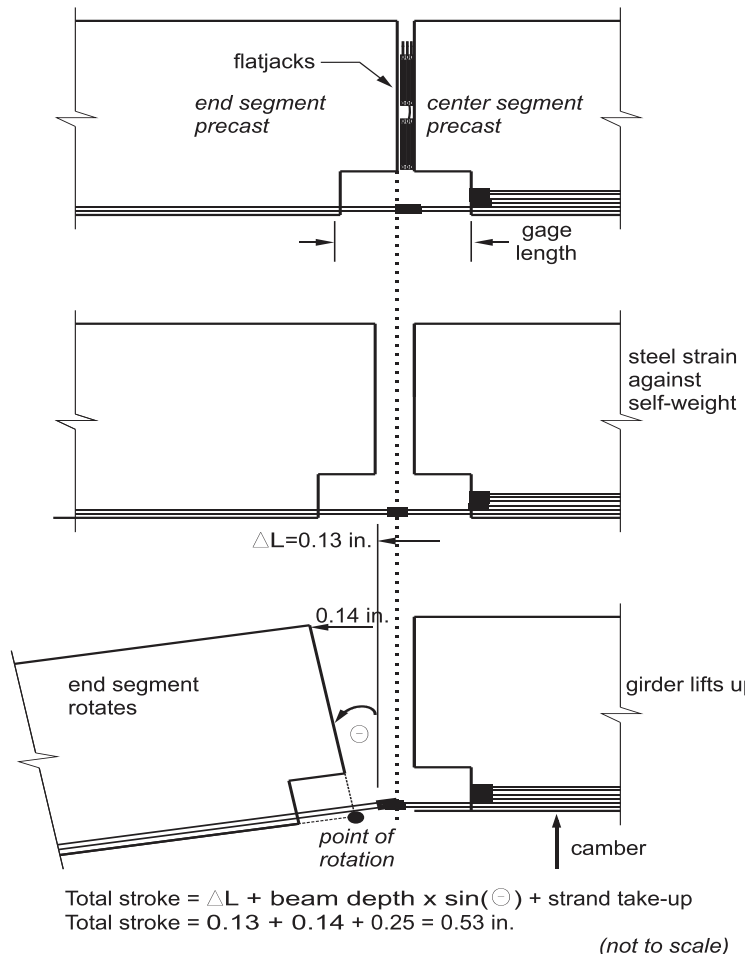


Figure 207–Hinging (and attendant camber) caused by inflation of flatjack. Rotation angle is exaggerated to illustrate mechanism.

To avoid this lift off, the moment arm between the centroid of the flatjack and strands can be adjusted such that the force in the strands is developed without exceeding the girder self-weight. Assuming that the flatjack can be pressurized to approximately 3000 psi and that the target strand stress is  $0.6f_{pu}$ , the flatjack area required is 293 sq in. If the flatjack is assumed to be 7 in. wide, then the moment arm required to generate an internal moment equal to the self-weight moment is approximately 44 in.

As shown in Figure 206 (though not to scale), the flatjack would fit within the web of the FIB96. The size of the required flatjack would allow shear keys in the area above the flatjack, and would not obstruct the notch required at the bottom of the cross-section.

Adequate lateral bracing will be necessary to stabilize the girder in the region around the splice during the jacking procedure. If the segments are jacked such that the applied moments exceeds the self-weight moment, a small rotation of the end segment will result.

Following jacking, concrete can be cast above and below the flatjack to form the portion of the splice concrete that will be prestressed. Release of the flatjack pressure will induce a prestress force that will be equal to the force imposed by the flatjack and located at the flatjack centroid. The flatjack is then removed from the section and an expansive grout or epoxy fill (similar to a segmental joint) can then be placed.

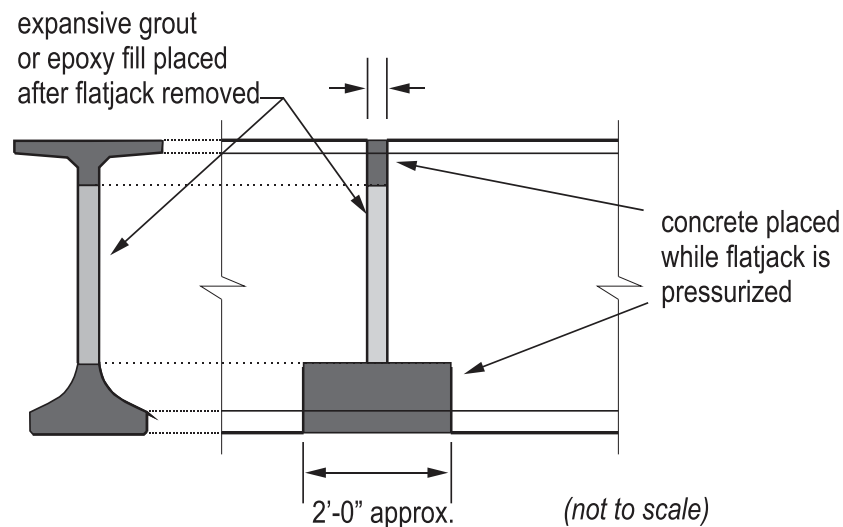


Figure 208–Splice closure pour

Overall camber can be imposed by constructing the splice with the girder segments positioned as shown in Figure 209. The main segment can be supported at a slightly higher elevation than the support locations at the ends of the end segments. This will require adequate site clearance and careful geometry control during fabrication of the splice. Indeed, individual segment camber will be reduced by the positive internal moment caused by the splice jacking. This must be anticipated so that the final total camber is as desired. Furthermore, the splice end of the end segments must be constructed such that the flatjack surfaces are parallel during jacking.

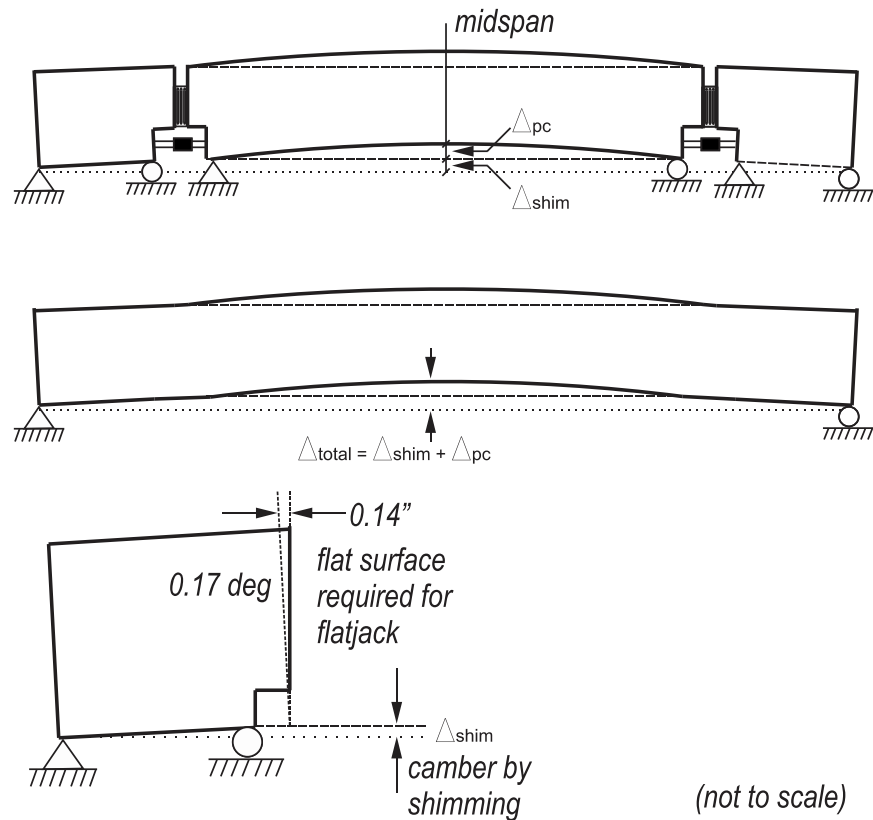


Figure 209–Splice C with canted ends

**Advantages:**

- No change in girder cross-section.
- Desired camber can be introduced during the jacking stage.
- No post-tensioning required.
- Simplified line of action of prestressing force (Compared with Prototypes A and B).
- The flatjack may be removed or left in place.
- precompression of a portion of the splice concrete.

**Disadvantages:**

- Due to geometry of the girder cross-section, limited bearing area is available to the flatjack.
- Prestress force induced in the strand at the splice location is limited by the girder self-weight.
- Bracing for stability and shear near splice location required during jacking.

- Hydraulic fluid replacement process is a delicate procedure, requiring the presence of the flatjack manufacturer.

### ***SPLICE DESIGN D***

To increase the flatjack bearing area, and subsequent thrust force, Splice Design D was developed. As shown in Figure 210, the cross-section of the ends of the precast segments rectangular. This allows the use of commercially available round flatjack envelopes in rectangular embedment blocks.

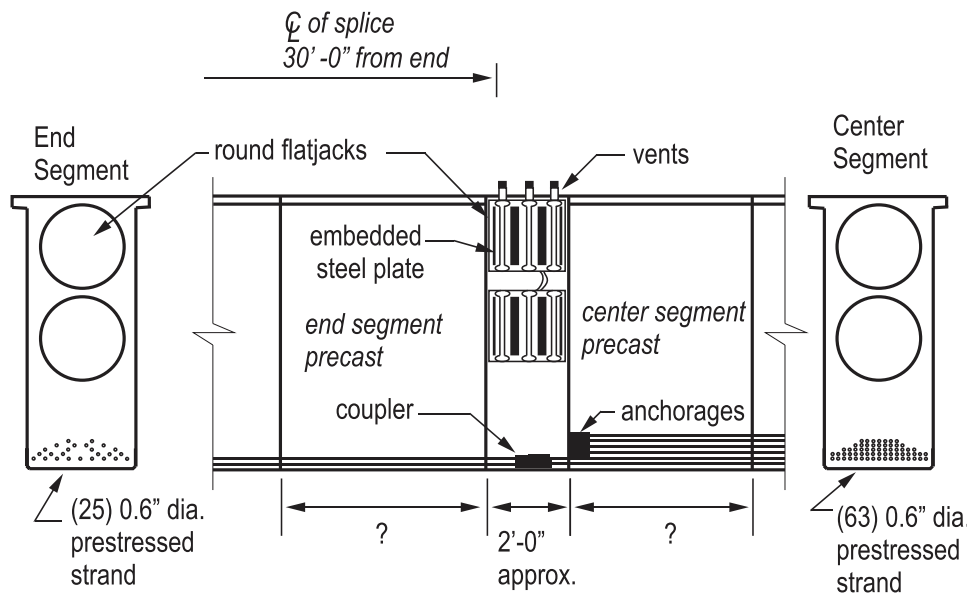


Figure 210—Splice Design D

**Advantages same as Splice Design C, plus:**

- Commercially available flatjack shapes can be used.

**Disadvantages, same as Splice Design C, plus:**

- Aesthetic impact and additional cost of rectangular section at splice.
- Beam end block forming is difficult to incorporate into standard beam forms.

### ***SPLICE DESIGN E***

Splice Design E (Figure 211) involves the use of multiple jacks in order to maintain vertical alignment of the girder segments during the jacking stage. Additionally, Splice Design E

incorporates several concrete pours to complete the splice, with the goal of flatjack removal before the final pour, a similar approach as used in Design C.

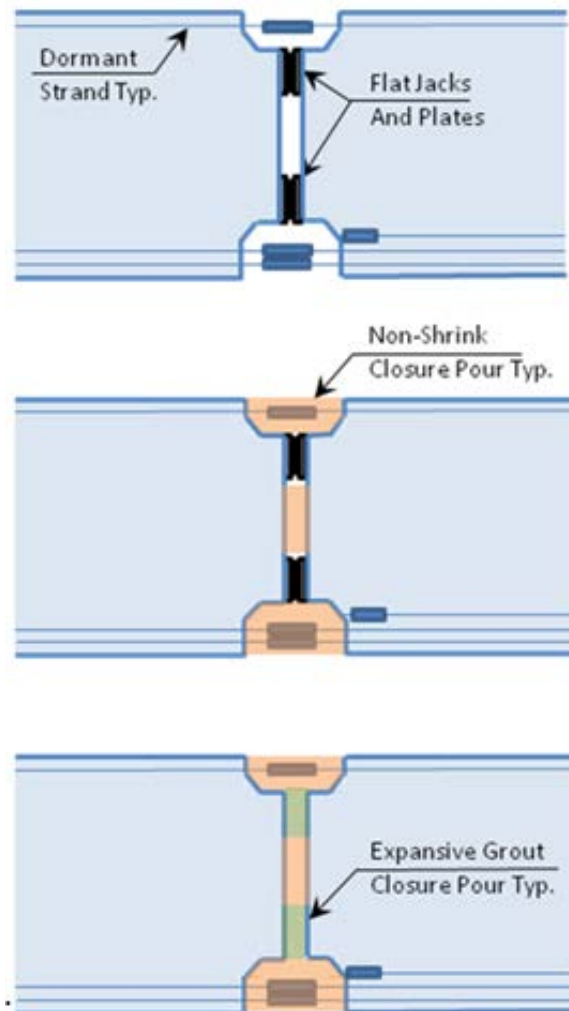


Figure 211–Splice Design E

As currently proposed, the splice design calls for the dormant strand in the top of the cross-section to be coupled prior to jacking. If this strand is coupled, the flatjack placement is dictated by stress-strain compatibility, if the segment faces are not to rotate. To ensure deformation compatibility and avoid rotation of the joint, the stress in the top strands must equal that in the bottom strands. Consequently, the flatjacks must be placed such that the resultant of the jack force is located at the position shown in Figure 212.

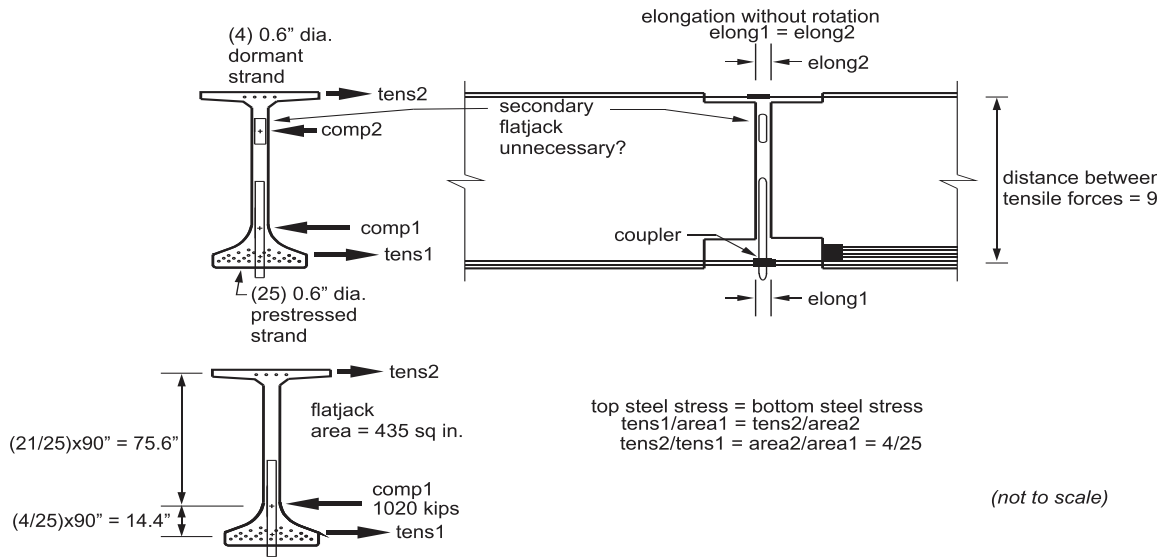


Figure 212–Internal forces in Splice Design E

Assuming a flatjack allowable pressure of 3000 psi, the flatjack must have a contact area of approximately 340 sq. in. to develop the required force. As shown in Figure 212, a flatjack of this size placed with its centroid at the required height would interfere with the strands in the bottom of the section.

**Advantages:**

- No change in girder cross-section.
- No post-tensioning required.
- Simplified line of action of prestressing force (Compared with Prototypes A and B).
- The flatjack need not be left in place, allowing reuse.
- No shear capacity required during jacking, as the beam will not lift.
- Better geometry control than splice designs C and D.

**Disadvantages:**

- As proposed, the flatjack cannot fit into the cross-section.
- Shimming of the precast segments required to introduce camber into the final beam.
- In order to introduce camber through shimming, canted faces of the end segments are required.

- Only the first splice concrete pour is precompressed. Concrete poured after the flatjack is removed is never compressed.

### ***SPLICE DESIGN F***

To eliminate the need for multiple concrete pours to complete the splice, Splice Design F utilizes standard hydraulic cylinder type jacks on the outside of the girder cross-section (Figure 213).

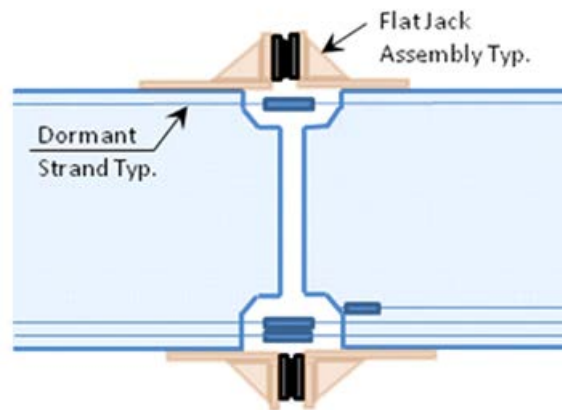


Figure 213–Splice Design F

In this option, steel brackets are mechanically attached to the precast girder segments. Jacks are fit between the assemblies and the precast segments are jacked apart. The brackets could be placed on either side of the girder webs, or on the top and bottom flanges, assuming the precast segments are shimmed up. This option allows for the re-use of the jacks and bracket assemblies.

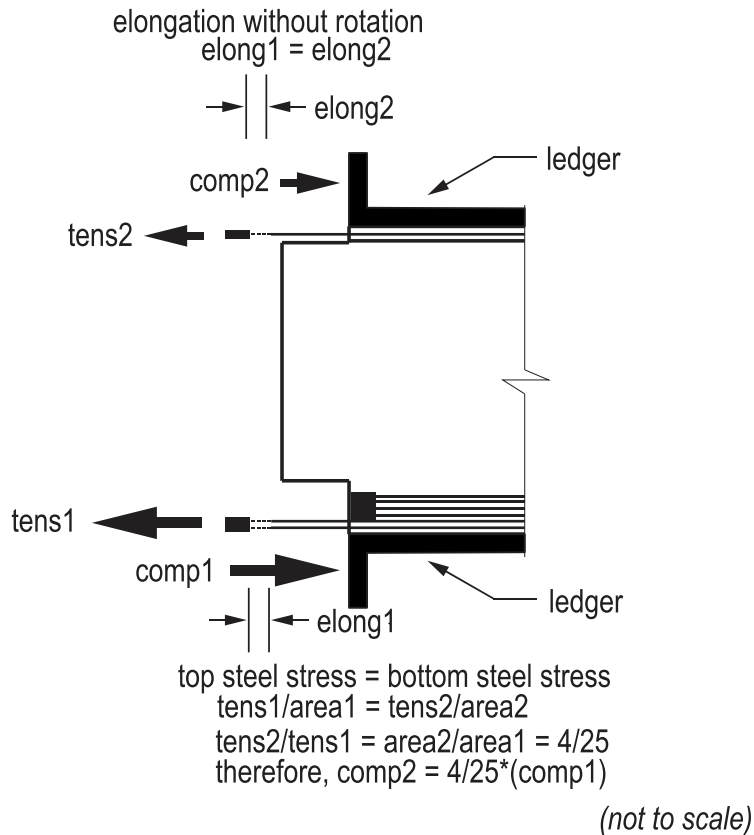


Figure 214—Forces of Splice Design F

The use of brackets as shown above introduces several issues that need to be addressed. The magnitude of the force to be transferred between the jack and the precast segment requires a large number of mechanical fasteners; for example, if 1/2-in. diameter headed studs are used, approximately 105 fasteners would be required in the bottom bracket and 20 fasteners in the top. Consequently, the structural steel bracket would need to be fabricated with sufficient length to accommodate this number of fasteners. Further, installing brackets on the top and bottom of the segment requires shimming of the section to accommodate the bracket on the underside of the segment.

As an alternative, to address these issues, an alteration of the design is proposed. The alternative design, in which the bracket angles are placed on the web face, is shown in Figure 215.

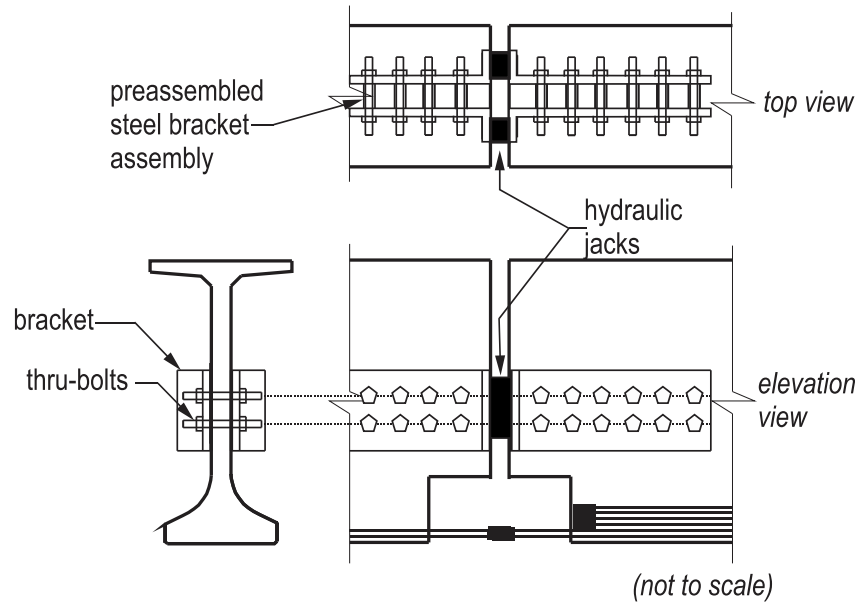


Figure 215–Alternative with side brackets

Advantages of Figure 215, include the ability to accommodate thru-bolts, reducing the number of mechanical fasteners required to transfer the jacking force into the section. To reduce the possibility of spalling at the bolt bearing locations, a preinstalled structural steel assembly could be placed in the precast segment.

**Advantages:**

- No change in girder cross-section.
- Splice concrete is cast in a single step.
- No post-tensioning required.
- Simplified line of action of prestressing force (Compared with Prototypes A and B).
- The flatjack is removable, allowing reuse.
- Splice concrete is completely precompressed if spliced strands are debonded for some length into beam.
- Jack assemblies and details are reusable.

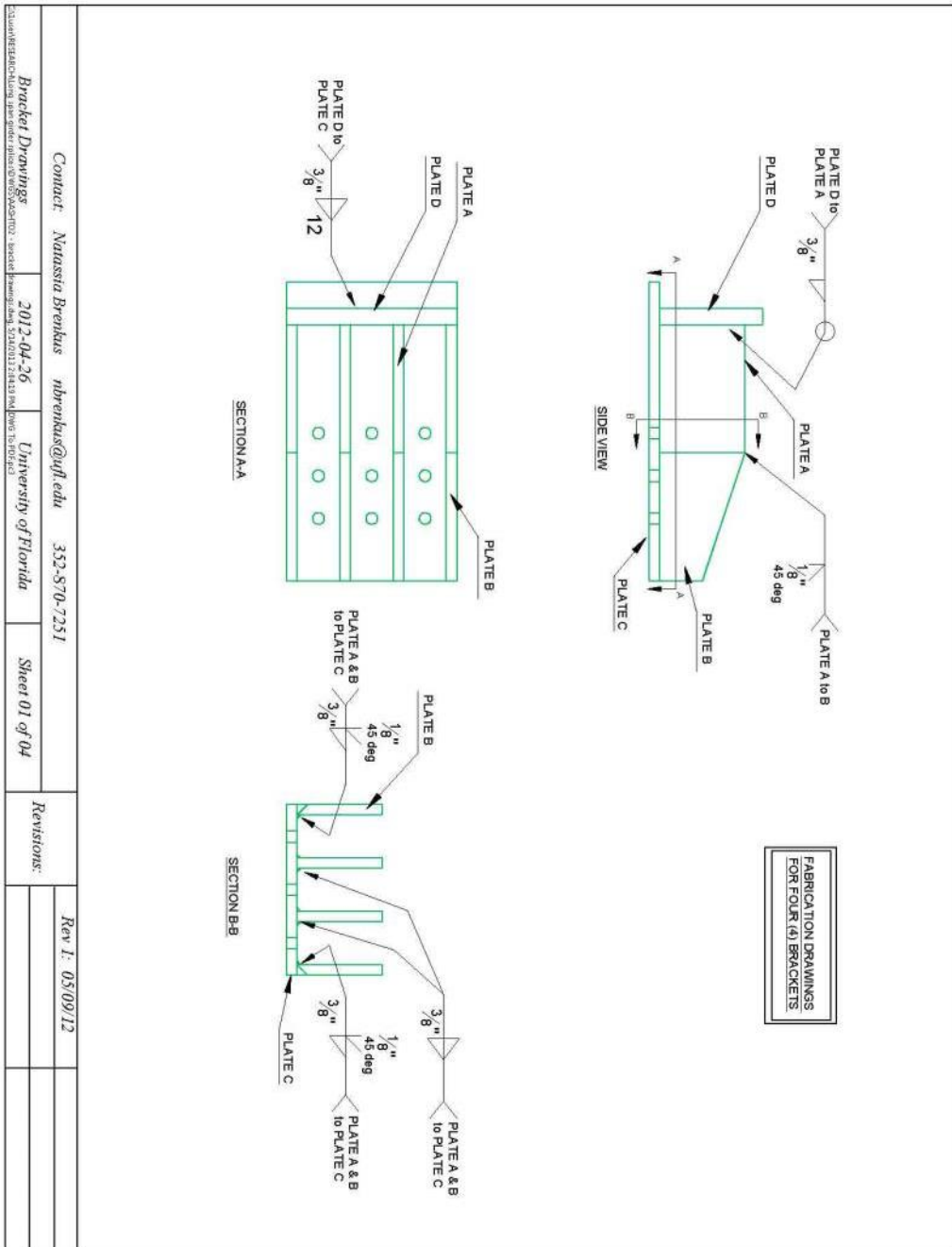
**Disadvantages:**

- Shimming of the beam required to introduce camber.

- Complexity and cost associated with fabrication and installation of embedded splice assembly.

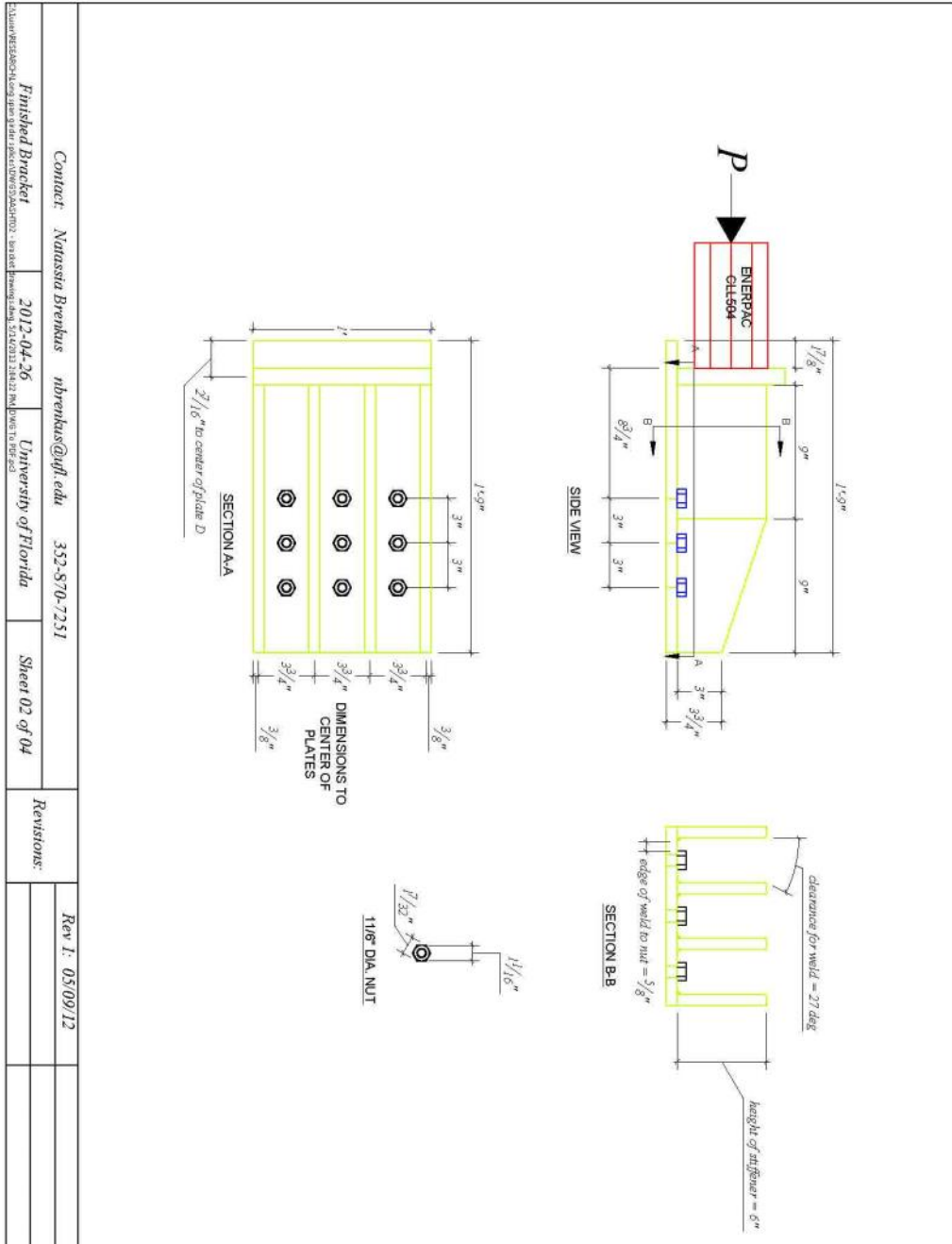
## Appendix C—Bracket Fabrication Drawings

Appendix C - Bracket Fabrication Drawings



Contact: <i>Natassia Breukus</i> <i>nbreukus@ufl.edu</i> 352-870-7251	
Bracket Drawings 2012-04-26 University of Florida	Sheet 01 of 04
Revisions:	Rev 1: 05/09/12

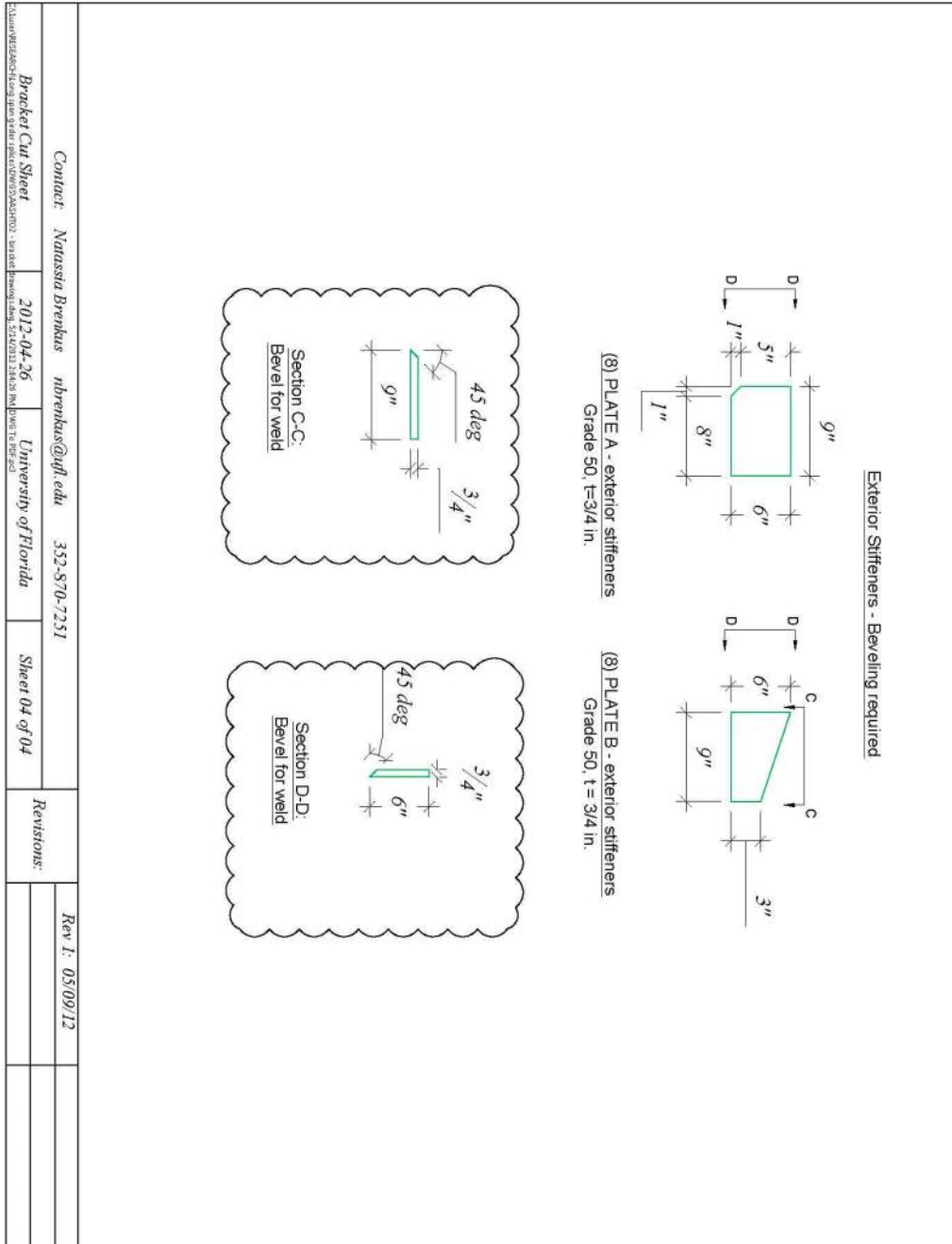
Appendix C - Bracket Fabrication Drawings



<p>Contact: <i>Natassia Brenkus nbrenkus@ufl.edu 352-870-7251</i></p>		<p>Revisions:</p>
<p>Finished Bracket</p>	<p>2012-04-26</p>	<p>University of Florida</p>
<p>21349 RESEARCH CENTER BLDG 3RD FLOOR UNIVERSITY GADSDEN ST GAINESVILLE FL 32611-2134</p>	<p>2012-04-26</p>	<p>Sheet 02 of 04</p>
<p>Rev I: 05/09/12</p>		



Appendix C - Bracket Fabrication Drawings



**Appendix D—Precast Fabrication Drawings**

**General Notes:**

**Materials**

Concrete shall be FDOT class VI  
 f<sub>c</sub> (28 day) = 8500 psi  
 f<sub>c</sub> (release) = 6000 ksi

The same concrete batch(s) shall be used for all three beams

Mild reinforcement shall be ASTM A815 grade 80 (fy 80 ksi)

Prestressing strand shall be ASTM A416 270 ksi Lo-Lax

Fabricator shall provide data sheets from concrete, strand, and rebar suppliers.

Fabricator shall provide report of strand stressing

Fabricator shall provide material samples to UF/FDOT as follows:

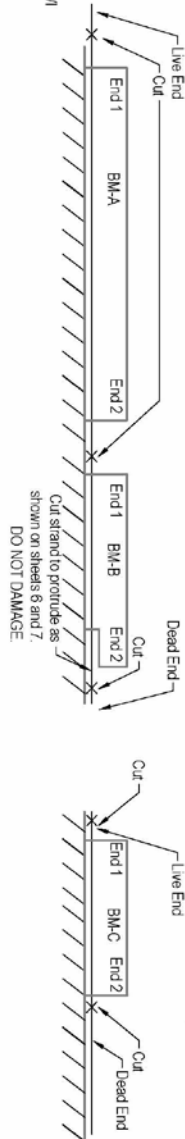
- (8) 4" dia x 8" cylinders from each concrete batch
- (4) cylinders cure with grid
- (4) lab cure
- (8) 36" pieces of prestressing strands free from sand, dust, etc
- Samples taken directly off of reel
- (2) 36" pieces of rebar from each reel

**Schedule**

Start of fabrication is requested by March 19. Shipping is anticipated within 2 months of end of fabrication.

Contact Natassia Brenkus at UF at least (1) week prior to stressing, casting, detensioning, and shipping. 352.870.7251 or nbrenkus@ufl.edu

Allow 24 hours minimum between rebar placement and pour to allow for placement of instrumentation.  
 Allow 24 hours minimum between removal of the formwork and detensioning to allow for placement of research instrumentation.  
 Beams shall be fabricated in two pours. Beam BM-A and Beam BM-B shall be poured first. Beam BM-C shall be poured next.



**Research Instrumentation**

UF/FDOT will provide and install research instrumentation in each of the concrete girders in coordination with the fabricator. Internal instrumentation will be mounted to prestressing strands and rebar prior to casting concrete.

Rebar and bearing plates receiving instrumentation will be noted with an "\*" on the plans. These pieces shall be provided to UF for installation of instrumentation prior to placement of the pieces in the girder.

**Other**

Fabricator will transport girders from the fabrication facility to:  
 FDOT Structures Research Center  
 2007 East Paul Dirac Drive  
 Tallahassee, FL 32310

Delivery time to be coordinated with FDOT.

Unless otherwise noted, fabrication of girders shall follow typical procedures and practices for FDOT bridge girders.

Cover beams with heavy tarp during curing.

Realign top of beams.

Inspections will be provided by on-site FDOT personnel and by UF.

No patch-work or finishing is required.

Special care must be taken to protect protruding strand after detensioning. Carefully coordinated cut-down required. Strands must not be damaged.

Production: Contact Natassia Brenkus (352) 870-7251 at least 1 week prior to stressing, casting, detensioning, and shipping.

Quantities  
 Mark A: 3 pcs  
 Mark B: 6 pcs  
 Mark C: 6 pcs

148 DWGS 03-02-12

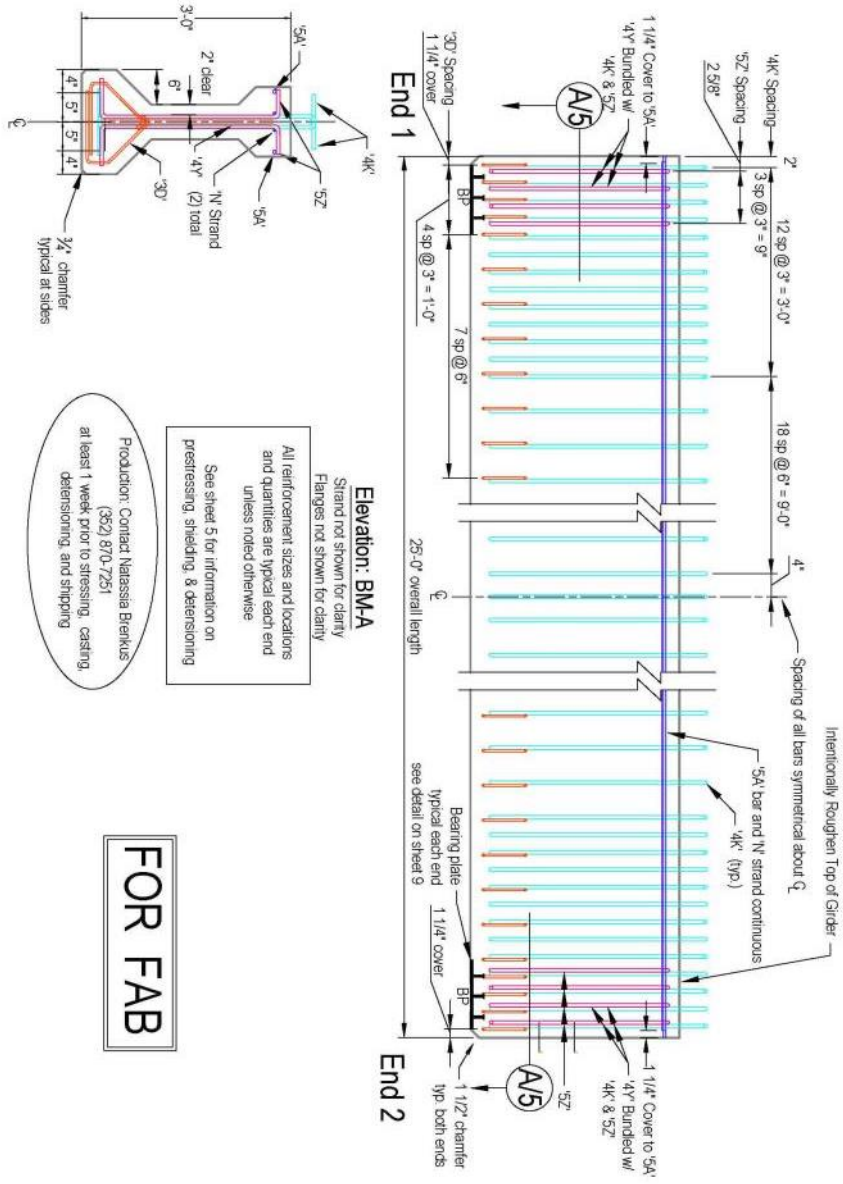
J:\SERVIBRENKUS\DOCUMENTS\RESEARCH\WORK WEEK MAR 12-MAR 16\AASHTO2-Tab drawings.dwg, 3/15/2012 11:46:10 AM, DWG

**FDOT Research**  
 Spliced long-span girders

**University of Florida**  
 Dept. of Civil and Coastal Engineering  
 352.870.7251

**General Notes**  
 Sheet 1 of 11

1



**Elevation: BM-A**  
 Strand not shown for clarity  
 Flanges not shown for clarity  
 All reinforcement sizes and locations  
 and quantities are typical each end  
 unless noted otherwise  
 See sheet 5 for information on  
 prestressing, shielding, & detensioning

Production: Contact Natassia Brenkus  
 (352) 970-7251  
 at least 1 week prior to stressing, casting,  
 detensioning, and shipping

**FOR FAB**

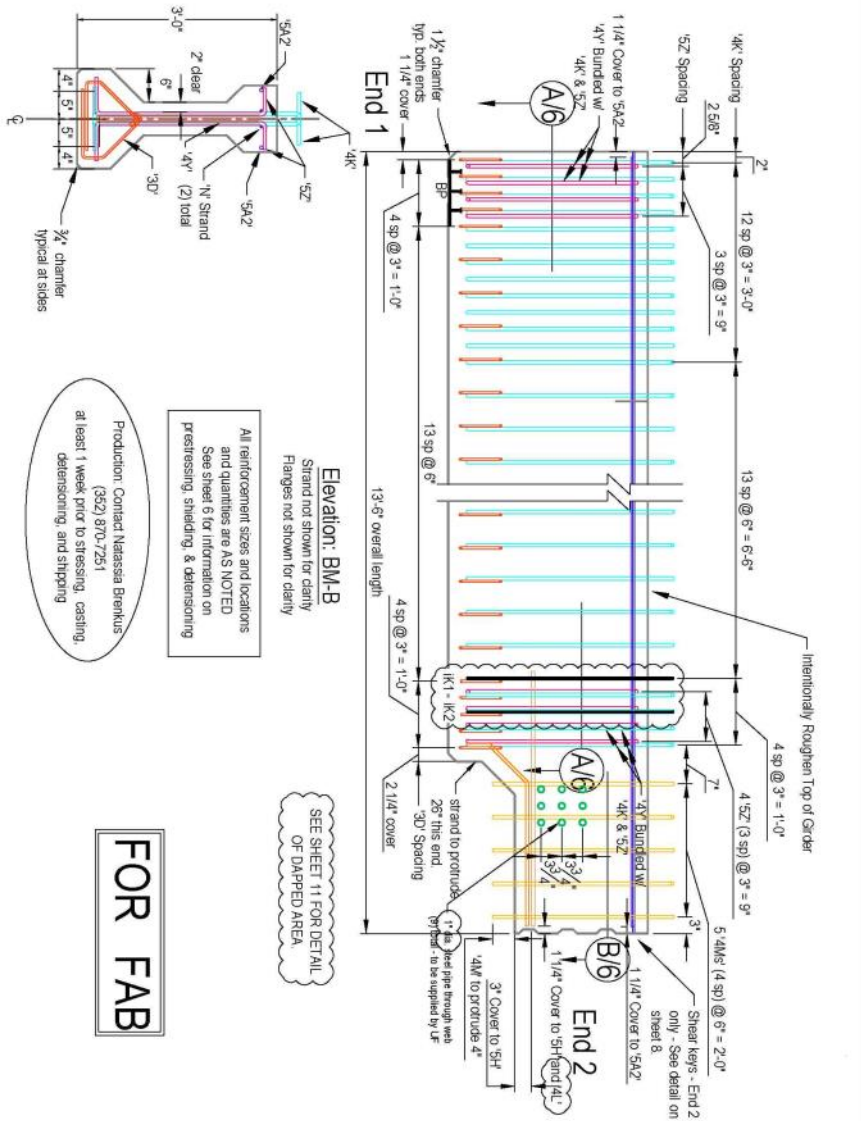
**2**

BM-A: AASHTO II Elevation, End Sections  
 Sheet 2 of 11

University of Florida  
 Dept. of Civil and Coastal Engineering  
 352.870.7251

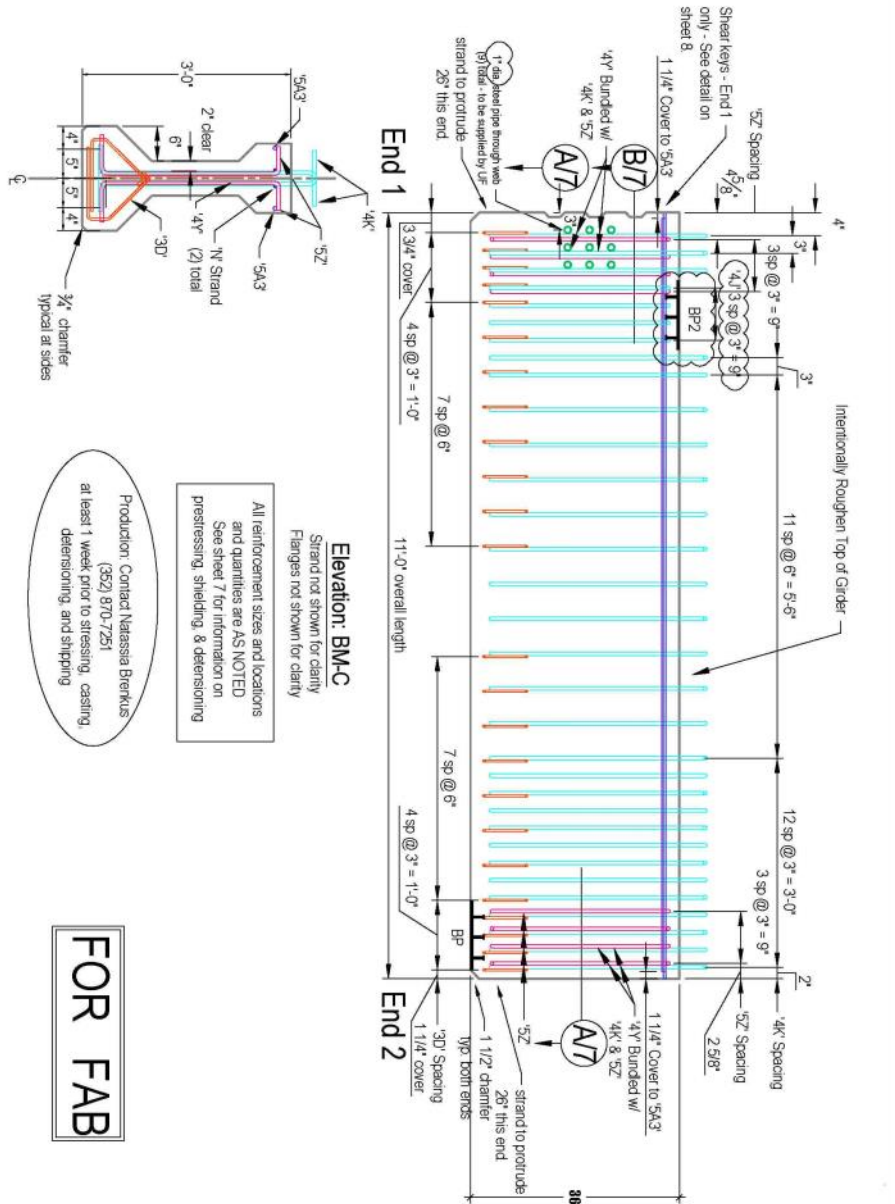
FOOT Research  
 Spliced long-span girders

C:\Users\mbrenkins\Documents\RESEARCH\Work Week Mar 12-Mar 16\AASHTO2 - fab drawings.dwg, 3/15/2012 11:46:18 AM, DWG 11



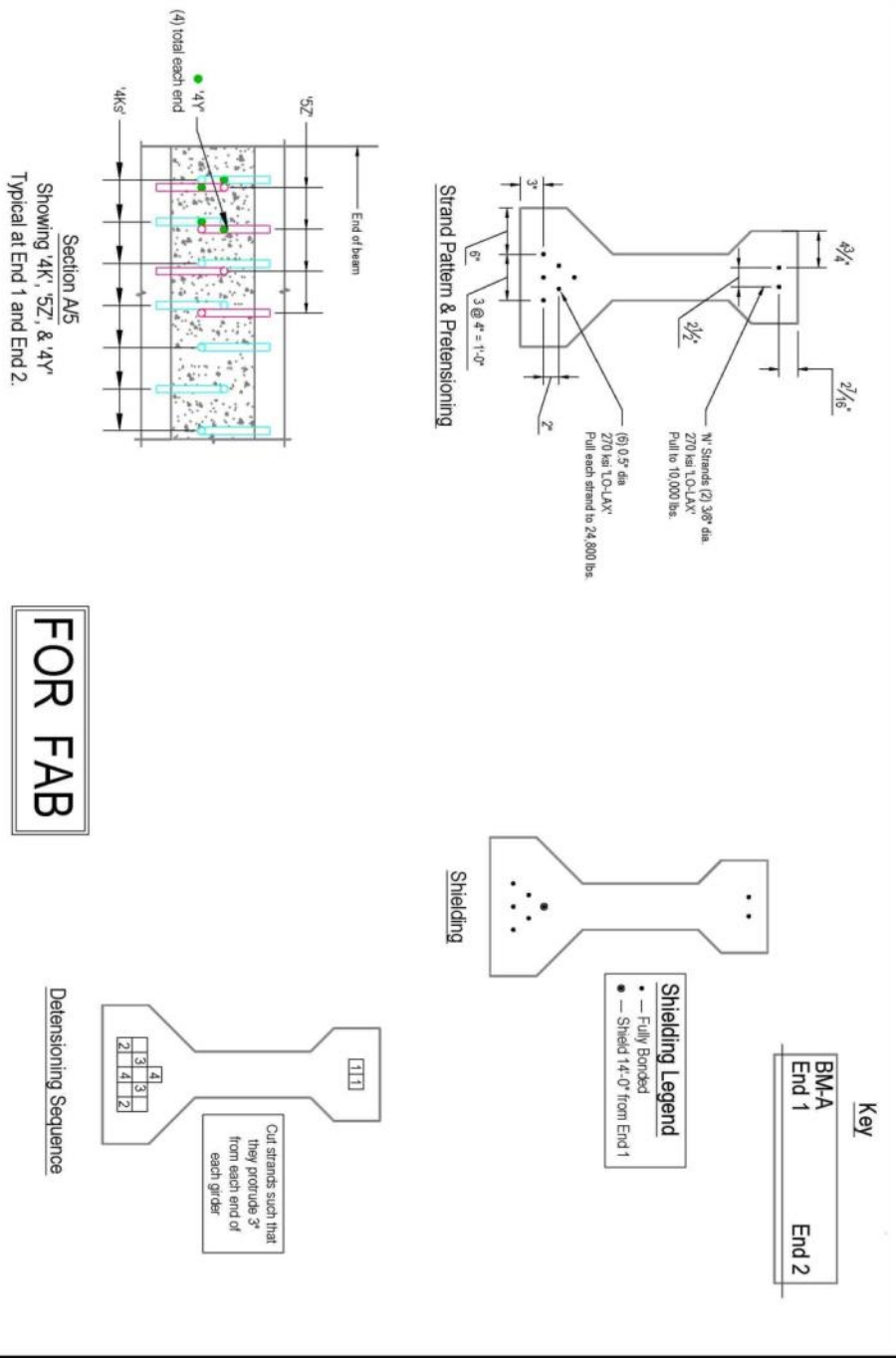
<b>3</b>	BM-B: AASHTO II Elevation, End Sections Sheet 3 of 11	University of Florida Dept. of Civil and Coastal Engineering 852.870.7251	FDOT Research Spliced long-span girders
----------	--	---	--

C:\Users\mbrenkus\Documents\RESEARCH\work week mar 12-mar 16\AASHTO2 - fab drawings.dwg, 3/15/2012 11:46:23 AM, DWG T



<b>4</b>	<b>BM-C: AASHTO II Elevation, End Sections</b> Sheet 4 of 11	University of Florida Dept. of Civil and Coastal Engineering 352.870.7251	<b>FOOT Research</b> Spliced long-span girders
----------	---	---	---

C:\Users\mbrenkus\Documents\RESEARCH\work week mar 12-mar 16\AASHTO2 - fab drawings.dwg, 3/15/2012 11:46:28 AM, DWG T



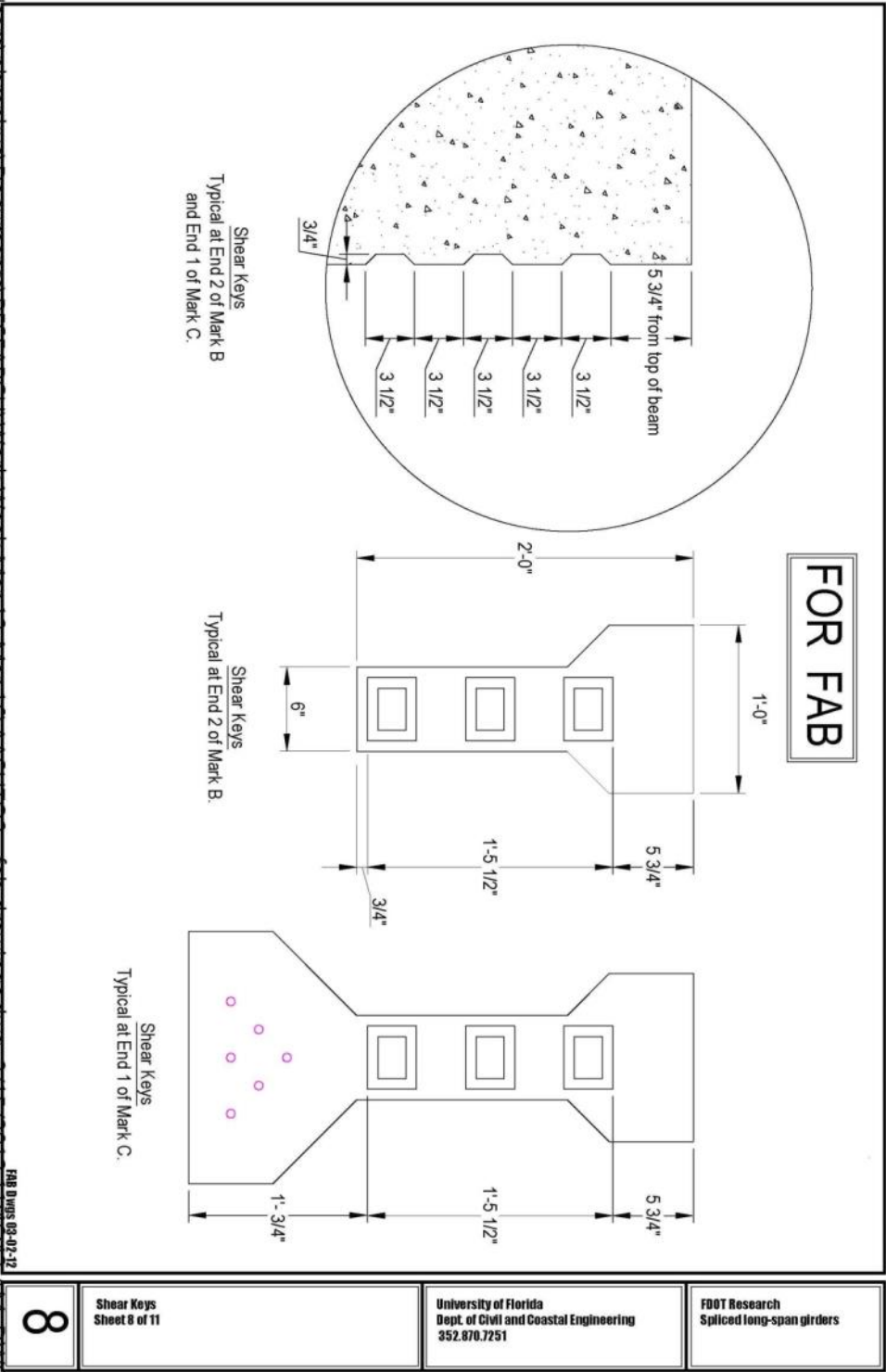
**FOR FAB**

<p>5</p>	<p>BM-A: Details and Delimiting Sequence Sheet 5 of 11</p>	<p>University of Florida Dept. of Civil and Coastal Engineering 352.870.7251</p>	<p>FBOT Research Spliced long-span girders</p>
----------	--	--	--





C:\Users\mbrenkus\Documents\RESEARCH\work week mar 12-mar 16\AASHTO2 - fab drawings.dwg, 3/15/2012 11:46:43 AM, DWG T



8

Shear Keys  
Sheet 8 of 11

University of Florida  
Dept. of Civil and Coastal Engineering  
352.870.7251

FBOT Research  
Spliced long-span girders

C:\Users\mbrenkus\Documents\RESEARCH\WORK week mar 12-mar 16\AASHTO2 - fab drawings.dwg, 3/15/2012 11:46:48 AM, DWG T

Bill of material: BM-A

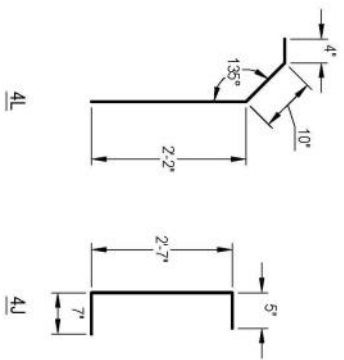
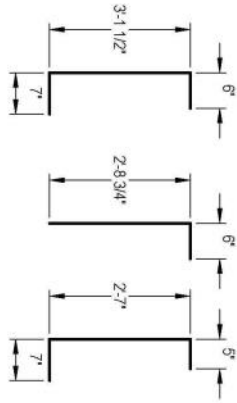
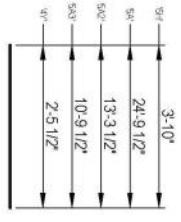
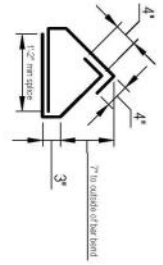
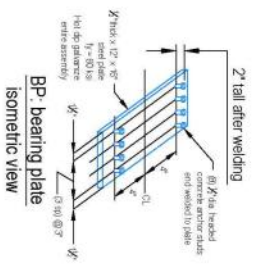
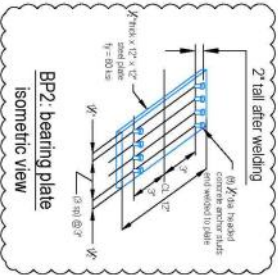
Piece	Size	Qty.	Length	Notes
5A	#5	2	24'-9 1/2"	30" splice (top)
3D	#3	24	3'-8"	12" min. splice (top)
4K	#4	63	4'-2 1/2"	
4Y	#4	8	2'-5 1/2"	
5Z	#5	8	3'-7"	
BP	-	2		

Bill of material: BM-B

Piece	Size	Qty.	Length	Notes
5A2	#5	2	13'-3 1/2"	30" splice (top)
3D	#3	22	3'-8"	12" min. splice (top)
4K	#4	30	4'-2 1/2"	
4Y	#4	8	2'-5 1/2"	
5Z	#5	8	3'-7"	
4M	#4	5	3'-2 3/4"	
5H	#5	2	3'-10"	
4L	#4	2	3'-4"	
BP	-	1		

Bill of material: BM-C

Piece	Size	Qty.	Length	Notes
5A3	#5	2	10'-9 1/2"	30" splice (top)
3D	#3	24	3'-8"	12" min. splice (top)
4K	#4	28	4'-2 1/2"	
4J	#4	4	4'-2 1/2"	
4Y	#4	8	2'-5 1/2"	
5Z	#5	8	3'-7"	
BP	-	1		
BP2	-	1		



Bar Bending  
all bars bend  
around 1/2" dia pin  
all bars bend  
around 2" dia pin  
all bars bend  
around 2 1/2" dia pin  
All sizes are full-size

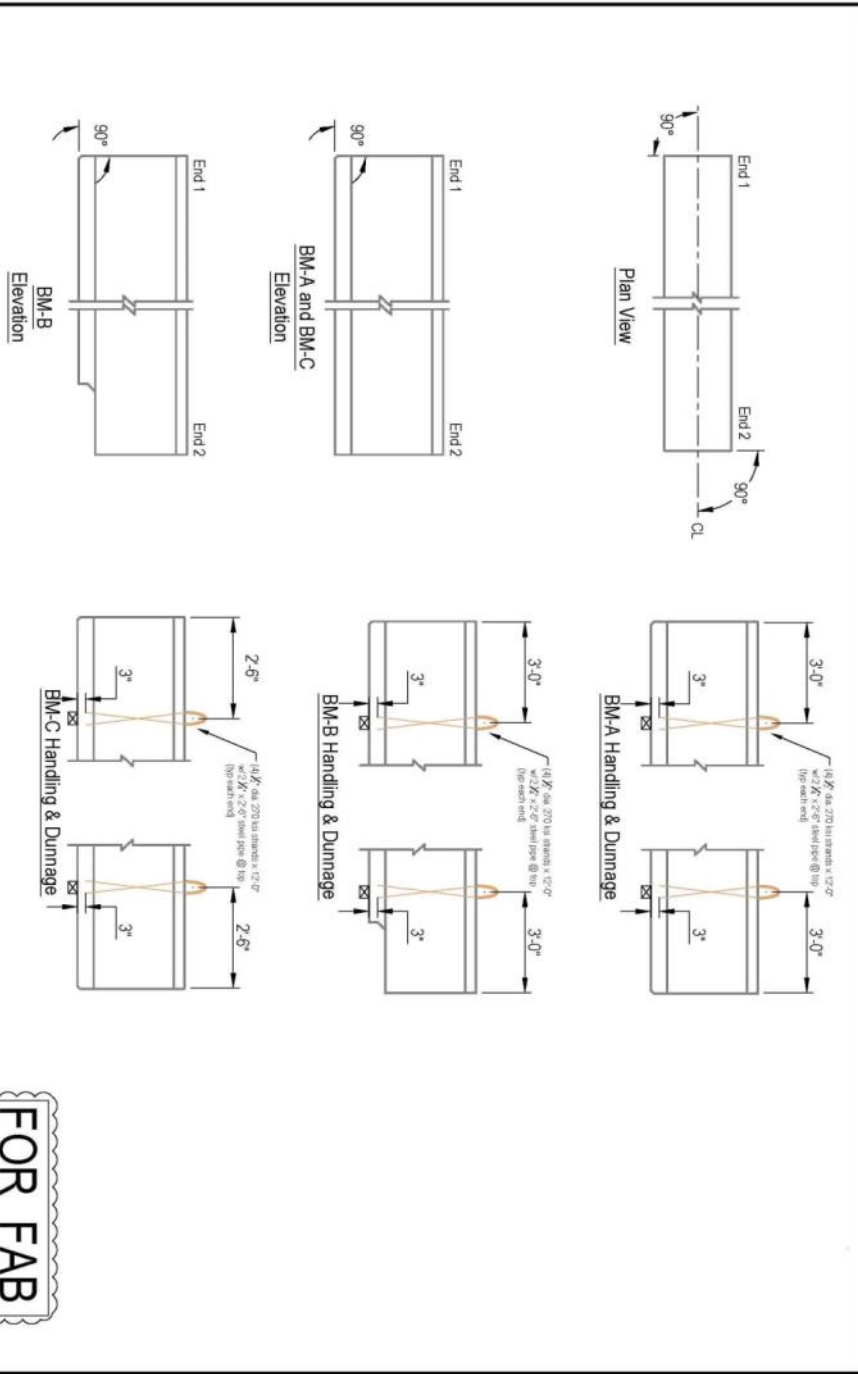
**FOR FAB**

Bar Bend Diagrams and Bills of Materials  
Sheet 6 of 11  
**9**

University of Florida  
Dept. of Civil and Coastal Engineering  
352.870.7251

FOOT Research  
Spliced long-span girders

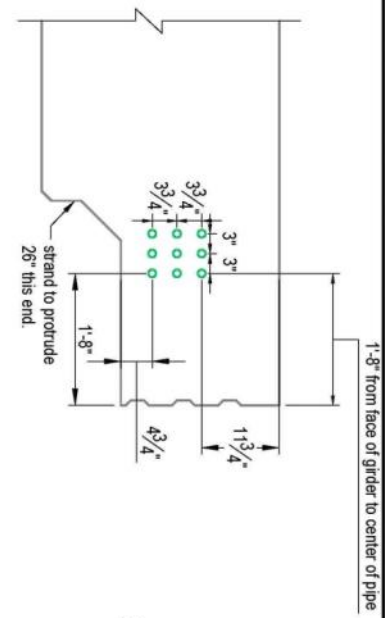
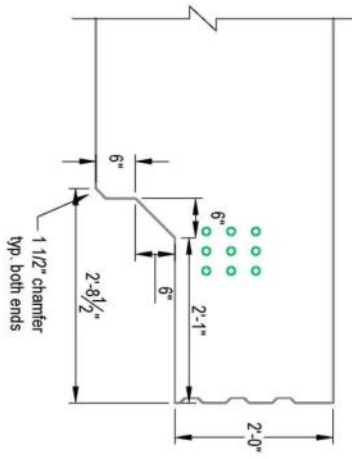
C:\Users\mbrenkus\Documents\RESEARCH\WORK Week 11-12-Mar 16\VAASHTO2 - fab drawings.dwg, 3/15/2012 11:46:53 AM, DWG T



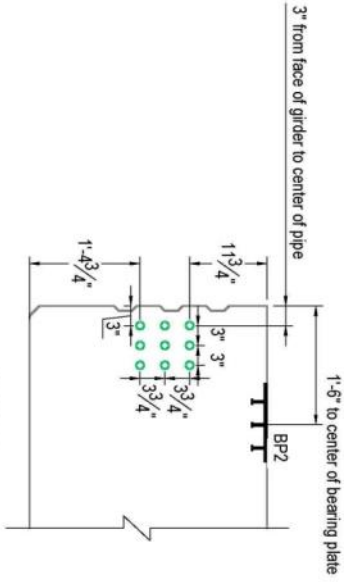
<p><b>10</b></p>	<p>Handling and Dunnage Diagrams Sheet 10 of 11</p>	<p>University of Florida Dept. of Civil and Coastal Engineering 352.870.7251</p>	<p>FBOT Research Spliced long-span girders</p>
------------------	---	--	--

C:\Users\mbrenkus\Documents\RESEARCH\work week mar 12-mar 16\AASHTO2 - fab drawings.dwg, 3/15/2012 11:46:58 AM, DWG T

BM-B  
End 2



BM-C  
End 1



FOR FAB

10	Handling and Dunnage Diagrams Sheet 11 of 11	University of Florida Dept. of Civil and Coastal Engineering 352.870.7251	FBOT Research Spliced long-span girders
----	---	---	--

**Appendix E—Precast Yard and Material Reports**

Pour 1

## WORKSHEET CHECK LIST

<input type="checkbox"/>	TABLE SHEET	JOB #	B1540
<input type="checkbox"/>	STRESS	MARK#	3@BMA, 6@BMB
<input type="checkbox"/>	D.R.O.	SERIAL #	NB1-NB9
<input type="checkbox"/>	PREPOUR	ITEM TYPE	TYPE II
<input type="checkbox"/>	BATCH TICKETS	BED#	42S
<input type="checkbox"/>	CASTING DIAGRAM	MIX DESIGN	05-1366
<input type="checkbox"/>	REBAR/SPIRAL		

3/22/12

Check Off!

Entered in Database

KA

Entered in GSX Database

N/A

Entered in LIMS (initials)

N/A

READY TO FILE

KA

PC6A001~~0~~

0

0

Pour 1

REBAR REPORT  
[Type the document title]

DATE: \_\_\_\_\_

JOB# B1540

BED# 425

MARK# 3 BMB 6AMB

TYPE OF BEAM: Test

BAR SIZE: 3 HEAT: BR1110509801

BAR SIZE: 4 HEAT: BR1110405901

BAR SIZE: 5 HEAT: DL1110663601

BAR SIZE: \_\_\_\_\_ HEAT: \_\_\_\_\_

Stress 1

STRESS INFORMATION SLIP

F.D.O.T. PROJECT

YES

NO

(CIRCLE ONE)



DATE 3-20-12

NUM. OF

INITIAL TENSION 5000

University of  
JOB# B-1540  
B-1540

STRAND

6

FINAL TENSION 24,800

BED# 425

JACK#

PAK# OR COIL# 1302461112055

1302461112057

LIST MARK#S

③ BM-A

④ BM-B

PRODUCT TYPE II-Girders

TYPE OF CABLE .05 1/2 Galax

MUST BE SIGNED BY PERSON FILLING OUT SLIP: Mike B

WILL NOT BE PROCESSED WITHOUT ALL PROPER INFORMATION AND SIGNATURE!

crooked

73k

78k

$\sim 4\sqrt{f'_c}$

calculated

Stress Done



Pour 1

PREPOUR PRODUCTION SHEET

JOB# B1540		PRODUCT_TYPE II				
F.D.O.T.# _____		0			BED# 42S	
CAST DATE <u>3-22-12</u>		MIX # 05-1366				
COMMENT KEYS / = OK, O = ACCEPTABLE, X = NOT ACCEPTABLE						
SERIAL #S	NB1	NB2	NB3	NB4	NB5	NB6
MARK #S	BMA	BMA	BMA	BMB	BMB	BMB
DATE:	3-19-12					
INSPECTOR:	Scott					
WIDTH	/	/	/	/	/	/
LENGTH	/	/	/	/	/	/
HEIGHT	/	/	/	/	/	/
CAPEE HOLES	/	/	/	/	/	/
T BAR HOLES	/	/	/	/	/	/
CHAMFER	/	/	/	/	/	/
SKREW	/	/	/	/	/	/
INSERTS	-	-	-	-	-	-
BLOCK OUTS	-	-	-	-	-	-
FORM CLEANNESS	/	/	/	/	/	/
PLATES FORM FACE	-	-	-	-	-	-
COMMENTS						
STEEL	NB1	NB2	NB3	NB4	NB5	NB6
MARK #S	BMA	BMA	BMA	BMB	BMB	BMB
DATE:	3-22-12					
INSPECTOR:	Scott					
REINFORCEMENT	/	/	/	/	/	/
STEEL SPACING	/	/	/	/	/	/
PLATES	/	/	/	/	/	/
CLEARANCE	/	/	/	/	/	/
LINER	/	/	/	/	/	/
LIFTING LOOPS	/	/	/	/	/	/
SHREATHING	/	/	/	/	/	/
COMMENTS						
INSPECTOR:	3-22-12					
DATE:	Scott					
DROP IN PLATES	-	-	-	-	-	-
BLOCK OUTS	-	-	-	-	-	-
INSERTS	-	-	-	-	-	-
HEADERS	/	/	/	/	/	/
LENGTH	/	/	/	/	/	/
FORMS	/	/	/	/	/	/
COMMENTS						

Pour 1

PREPOUR PRODUCTION SHEET

JOB# B1540	PRODUCT _____ TYPE II				
F.D.O.T.# 0	BED# 42S				
CAST DATE 3-22-12	MIX # 05-1366				
COMMENT KEYS / = OK, 0 = ACCEPTABLE, X = NOT ACCEPTABLE					
SERIAL#	n87	n88	n89	0	0
MARKINGS	BmB	BmB	BmB	0	0
DATE	3-19-12				
INSPECTOR	Scott				
WIDTH	/	/	/		
LENGTH	/	/	/		
HEIGHT	/	/	/		
CABLE HOLES	/	/	/		
REBAR HOLES	/	/	/		
CHAMFER	/	/	/		
SKEW	/	/	/		
INSERTS	/	/	/		
BLOCKOUTS	/	/	/		
FORM CLEANNESS	/	/	/		
PLATES FORM FACE	/	/	/		
COMMENTS					
STEEL #VALUE	n87	n88	n89	0	0
KG/S	0	BmB	BmB	0	0
INSPECTOR	3-21-12				
REINFORCEMENT	Craig	/	/	/	
STEEL SPACING	/	/	/		
PLATES	/	/	/		
CLEARANCE	/	/	/		
LINER	/	/	/		
BEARING LOOPS	/	/	/		
SHEATHING	/	/	/		
COMMENTS					
INSPECTOR	Scott				
DATE	3-22-12				
DROP IN PLATES	/	/	/		
BLOCKOUTS	/	/	/		
INSERTS	/	/	/		
HEADERS	/	/	/		
LENGTH	/	/	/		
FORMS	/	/	/		
COMMENTS					

Appendix E - Precast Yard and Material Reports

PROJECT NO. B1640 BEAM TYPE: \_\_\_\_\_ TYPE II BED NUMBER: 425 INSPECTOR: Self DATE CAST: 3-22-12

FOOT# 0 DESIGN MIX NO. 05-1366 SAMPLE NUMBER \_\_\_\_\_ POSITIVE TEST LOAD NO(s): 0 TOTAL YARDS: 14.82 COVERED:  CUR. COMPOUND:

SERIAL NO	MARK NO.	NB1	NB2	NB3	NB4	NB5	NB6	NB7	NB8	NB9
		BMA	BMA	BMA	BMB	BMB	BMB	BMB	BMB	BMB
		25	25	25	13.500	13.5	13.5	13.500	13.5	13.5

FDOT# 0 ENVIRONMENTAL CLASSIFICATION: RNA



Appendix E - Precast Yard and Material Reports

Pour 1

DURA-STRESS INC.

PLANT NO.: 11-013  
 DELIVERED TO: 42 (Type II)  
 ADDRESS: CHL.110 3-8-2012  
 F.D.O.T. PROJECT NUMBER: B1540

DATE: 3/22/2012  
 TICKET: 1

TRUCK NUMBER 0	D.O.T. CLASS Class VI (8500 PSI)	D.O.T. MIX NUMBER 05-1366	BATCH SIZE 6.00 yards
TIME LOADED 13:57	ARRIVED	DISCHARGED	TODAY'S QTY 6.00 yards

Product Name	ALLOWABLE JOBSITE WATER ADDITION GALLONS	MIXING REVOLUTIONS:		%MC
		AT PLANT	AT JOBSITE	
SAND	PIT NO. 36-491	Actual		4.3
67 Rock	Pit No10-645	6,500	lbs	2.7
Fly Ash	RRG Flyash	9,400	lbs	0.0
Cement 2	Cemex Cement	1,050	lbs	0.0
WATER		4,770	lbs	0.0
MB-AE 90	MBAE90	1,123	lbs	0.0
Delvo	DELVO	12	fluid ozs	
Glenium 7710	GLENIUM 7710	154	fluid ozs	
		424	fluid ozs	

Actual W/C Ratio: 0.28

USING CENTRAL MIXER AND TUCKER BUILT TRANSPORT  
 ISSUANCE OF THIS TICKET CONSTITUTES CERTIFICATION  
 TO THE ACCURACY OF THE ABOVE RECORDED INFORMATION  
 AND COMPLIANCE WITH CURRENT SPECIFICATIONS.

WATER ADDED BY RECEIVER OF CONCRETE: \_\_\_\_\_ GALS.

RECEIVED BY: \_\_\_\_\_

DATE: \_\_\_\_\_

Ref: 43

TIN# B62645463      TIN# H23542575      TIN# T65682853

Appendix E - Precast Yard and Material Reports

Pour 1

DURA-STRESS INC.

PLANT NO.: 11-013  
 DELIVERED TO: 42 (Type II)  
 ADDRESS: CHL. 110 3-8-2012  
 F.D.O.T. PROJECT NUMBER: B1540

DATE: 3/22/2012  
 TICKET: 2

TRUCK NUMBER 0	D.O.T. CLASS Class VI (8500 PSI)	D.O.T. MIX NUMBER 05-1366	BATCH SIZE 6.00 yards
TIME LOADED 14:24	ARRIVED 2:32	DISCHARGED 2:42	TODAY'S QTY 12.00 yards

Product Name	ALLOWABLE JOBSITE WATER ADDITION GALLONS	MIXING REVOLUTIONS:		%MC
		AT PLANT	120 SECONDS	
SAND	PIT NO. 36-491	Actual		4.2
67 Rock	Pit No10-645	6,440	lbs	2.7
Fly Ash	RRG Flyash	9,440	lbs	0.0
Cement 2	Cemex Cement	1,050	lbs	0.0
WATER		4,790	lbs	0.0
MB-AE 90	MBAE90	1,127	lbs	0.0
Delvo	DELVO	12	fluid ozs	
Glenium 7710	GLENIUM 7710	152	fluid ozs	
		472	fluid ozs	

Actual W/C Ratio: 0.28

USING CENTRAL MIXER AND TUCKER BUILT TRANSPORT  
 ISSUANCE OF THIS TICKET CONSTITUTES CERTIFICATION  
 TO THE ACCURACY OF THE ABOVE RECORDED INFORMATION  
 AND COMPLIANCE WITH CURRENT SPECIFICATIONS.

WATER ADDED BY RECEIVER OF CONCRETE: \_\_\_\_\_ GALS.

RECEIVED BY: \_\_\_\_\_

DATE: \_\_\_\_\_

Ref: 46

TIN# B62645463    TIN# (H23542575)    TIN# T65682853

*2 sub*

Appendix E - Precast Yard and Material Reports

Pour 1

DURA-STRESS INC.

PLANT NO.: 11-013  
 DELIVERED TO: 42 (Type II)  
 ADDRESS: CHL.110 3-8-2012  
 F.D.O.T. PROJECT NUMBER: B1540

DATE: 3/22/2012  
 TICKET: 3

TRUCK NUMBER 0	D.O.T. CLASS Class VI (8500 PSI)	D.O.T. MIX NUMBER 05-1366	BATCH SIZE 6.00 yards
TIME LOADED 14:47	ARRIVED 2:50p	DISCHARGED 3:04p	TODAY'S QTY 18.00 yards

Product Name	ALLOWABLE JOBSITE WATER ADDITION GALLONS	MIXING REVOLUTIONS:		%MC
		AT PLANT	120 SECONDS AT JOBSITE	
SAND	PIT NO. 36-491	Actual		4.3
67 Rock	Pit No10-645	6,480	lbs	2.6
Fly Ash	RRG Flyash	9,380	lbs	0.0
Cement 2	Cemex Cement	1,050	lbs	0.0
WATER		4,760	lbs	0.0
MB-AE 90	MBAE90	1,127	lbs	0.0
Delvo	DELVO	12	fluid ozs	
Glenium 7710	GLENIUM 7710	152	fluid ozs	
		468	fluid ozs	

Actual W/C Ratio: 0.28

USING CENTRAL MIXER AND TUCKER BUILT TRANSPORT  
 ISSUANCE OF THIS TICKET CONSTITUTES CERTIFICATION  
 TO THE ACCURACY OF THE ABOVE RECORDED INFORMATION  
 AND COMPLIANCE WITH CURRENT SPECIFICATIONS.

WATER ADDED BY RECEIVER OF CONCRETE: \_\_\_\_\_ GALS.

RECEIVED BY: \_\_\_\_\_

DATE: \_\_\_\_\_

Ref: 51

TIN# B62645463    TIN# (H23542575)    TIN# T65682853

*3 sites*

# WORKSHEET CHECK LIST

Pour 2  
Pour 2

- TABLE SHEET
- STRESS
- D.R.O.
- PREPOUR
- BATCH TICKETS
- CASTING DIAGRAM
- REBAR/SPIRAL

JOB # B1540  
MARK# 6@11  
SERIAL # NB10-NB15  
ITEM TYPE TYPE II  
BED# 42S  
MIX DESIGN 05-1366

3/27/12

Check Off!

Entered in Database

YW

Entered in GSX Database

N/A

Entered in LIMS (initials)

N/A

READY TO FILE

YW

PC6A002Q

0

0

~~200888~~

2

REBAR REPORT

[Type the document title]

DATE :

JOB#

BED#

42

MARK#

BM-C

TYPE OF BEAM:

11

BAR SIZE:

3

HEAT:

BR1110509801

BAR SIZE:

4

HEAT:

BR1210092301

BAR SIZE:

5

HEAT:

DL1110663501

BAR SIZE:

HEAT:

*[Handwritten signature]*  
Stress 2

STRESS INFORMATION SLIP



F.D.O.T. PROJECT

YES

NO

(CIRCLE ONE)

DATE 3-26-12 NUM. OF

INITIAL TENSION 5000

JOB# B-1540 STRAND 6

FINAL TENSION 24,800

BED# 42<sup>S</sup> JACK#

PAK# OR COIL# 1302462112839

LIST MARK#S Ⓟ B-C

PRODUCT TYPE II-TEST

TYPE OF CABLE 1/2 270<sup>K</sup>

MUST BE SIGNED BY PERSON FILLING OUT SLIP:

*[Handwritten signature]*

WILL NOT BE PROCESSED WITHOUT ALL PROPER INFORMATION AND SIGNATURE!

Stress Done

Stress 2

**DURA-STRESS INC.**  
**STRAND STRESS REPORT**

DATE: 3/26/2012      ITEM NO'S: 6-BC

PROJECT NO. B1540

PRODUCT II TEST

BED NO. 42S

NO. OF CABLE: 6

TECHNICIAN: DT

DATE: 3-26-12

JACK CAL DATES: 10-3-11

AMBIENT TEMP: > 8

JACK #: 7-12

CABLE TYPE: 1/2 7W 270 LR ASTM A416

FINAL TENSION 25405

+ 2.5% 26040

24770

FINAL ELONGATION 17 1/2

+ 2.5% 17 15/16

- 2.5% 17 1/16

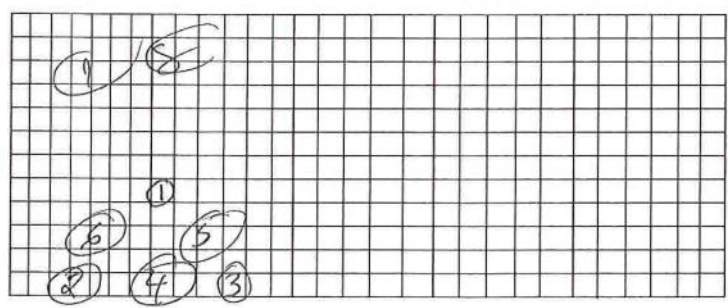
AASHTO MAX = 33048

IF TARGET = AASHTO ELONGATION MAY NOT WORK

CHUCK SLIPPAGE	
LIVE	DEAD
N/A	N/A
AVERAGE:	AVERAGE:
TOTAL:	TOTAL:

GAUGE	ELO	GAUGE	ELO	GAUGE	ELO	GAUGE	ELO	GAUGE	ELO	GAUGE	ELO	GAUGE	ELO	GAUGE	ELO
1	25450	12		23		34		45		56		67			
2	15000	13		24		35		46		57		68			
	15000	14		25		36		47		58		69			
4	13000	15		26		37		48		59		70			
5	15000	16		27		38		49		60		71			
6	15000	17		28		39		50		61		72			
7	10000	18		29		40		51		62		73			
8	10000	19		30		41		52		63		74			
9		20		31		42		53		64		75			
10		21		32		43		54		65		76			
11		22		33		44		55		66		77			

$\frac{7}{16} = \frac{3}{16}$



2.6  
15,000  
All in p.p.a

CHUCK SLIP BOOK

ENTRY LOG

JOB BOOK

42S

Appendix E - Precast Yard and Material Reports

Stress 2

3/26/2012 13:42

JOB#:	B1540		PRODUCT
DATE:	3/26/2012		II TEST
BED #:	42S		w-βC
JACK #			0
STRAND SIZE	1/2 7W 270 LR ASTM A416		0
COIL/PACK/REEL #	1302462112839	0	
	0	0	
	0	0	
	0	0	
BED LENGTH (L):	3818.0625	0	
STRAND SIZE: (A)	0.153	0	
FINAL TEN. (P)	24800	0	
PRE TEN. : (Pi)	5000	0	
M.O.E. (E):	29.00	0	
		0	
		0	

CORRECTION INFO.	
Number of cable #	6
Exp. Conc temp @ Placement:	85
Ambient temperature(at):	70
Abutment rotation (ar):	N/A
Live end seating (les):	0.1875
Dead end slippage (des):	0.125
anchorage movement:	0.5

ELONGATION  
 $\Delta a.t (P \times db / P_b) = 0$   
 $\Delta t. ( P_i \times L ) / ( A \times E ) = 4.3025$   
 $\Delta t'a'b. ( P \times L ) / ( A \times E ) = 17.038$   
 $\Delta t'a'b \text{ shortning} ( b_s / 2 ) + ( b_s / \# \text{strand} ) = 0.3333$

FORCE ADJUSTMENTS  
 $P_b ( P - P_i ) = 19800$   
 $P_t (=) = 0$   
 $P_{ar} ( a_r \times A \times E ) / ( L ) = 0$   
 $P_{les} ( l_{es} \times A \times E ) / ( L ) = 217.8952$   
 $P_{des \text{ no adj. required}} = 0$   
 $P_{bs} ( d_{bs} \times A \times E ) / ( L ) = 387.3305$   
 TOTAL FORCE ADJ. = 605.2257  
 ADJUSTED FORCE = 20405.2257

GROSS ELONG. 17.684

JACKING FORCE = 25405

NET ELONG.	17 1/2
------------	--------

TOTAL ADJ. FORCE	25405
------------------	-------

RANGE + 2.5%	17 15/16
RANGE - 2.5%	17 1/16

AASHTO MAX =	33048
RANGE +2.5% =	26040
RANGE -2.5% =	24770

42S

Pour 2

PREPOUR PRODUCTION SHEET

JOB# B1540		PRODUCT_TYPE II				
F.D.O.T.# _____ 0		BED# 42S				
CAST DATE <u>3-27-12</u>		MIX # 05-1366				
COMMENT KEYS / = OK, O = ACCEPTABLE, X = NOT ACCEPTABLE						
SERIAL #S	NB10	NB11	NB12	NB13	NB14	NB15
MARK #S	BC	BC	BC	BC	BC	BC
DATE:	3-26-12					
INSPECTOR:	Scott					
WIDTH	/	/	/	/	/	/
LENGTH	/	/	/	/	/	/
HEIGHT	/	/	/	/	/	/
CABLE HOLES	/	/	/	/	/	/
"L" BAR HOLES	/	/	/	/	/	/
CHAMFER	/	/	/	/	/	/
SKEW	/	/	/	/	/	/
INSERTS	-	-	-	-	-	-
BLOCK OUTS	-	-	-	-	-	-
FORM CLEANNESS	/	/	/	/	/	/
PLATES FORM FACE	-	-	-	-	-	-
COMMENTS						
STEEL:	NB10	NB11	NB12	NB13	NB14	NB15
MARK #S	BC	BC	BC	BC	BC	BC
DATE:	3-27-12					
INSPECTOR:	Dan					
REINFORCEMENT	/	/	/	/	/	/
STEEL SPACING	#	/	/	/	/	/
PLATES	-	-	-	-	-	-
CLEARANCE	/	/	/	/	/	/
LINER	/	/	/	/	/	/
LIFTING LOOPS	/	/	/	/	/	/
SHEATHING	/	/	/	/	/	/
COMMENTS						
INSPECTOR:	Scott					
DATE:	3-27-12					
DROP IN PLATES	0	0	0	0	0	0
BLOCK OUTS	-	-	-	-	-	-
INSERTS	-	-	-	-	-	-
HEADERS	/	/	/	/	/	/
LENGTH	/	/	/	/	/	/
FORMS	/	/	/	/	/	/
COMMENTS						
During the Pour one Pipe was for side on NB11 moved because of vibration						

Appendix E - Precast Yard and Material Reports

Power 2

PROJECT NO.	B1540	BEAM TYPE:	TYPE II	BED NUMBER:	425	INSPECTOR	Scott	DATE CAST	3-27-12
FDOT#	0	SAMPLE NUMBER	PC6A002Q	TEST LOAD NO(S)	0	TOTAL YARDS	1	COVERED	<input checked="" type="checkbox"/>
DESIGN MIX NO.	05-1366							CUR. COMPOUND	<input type="checkbox"/>

SERIAL NO	MARK NO.	NB10	NB11	NB12	NB13	NB14	NB15
	BC	BC	BC	BC	BC	BC	BC
	11	11	11	11	11	11	11

ENVIRONMENTAL CLASSIFICATION	#N/A
------------------------------	------



Appendix E - Precast Yard and Material Reports

Pour 2

DURA-STRESS INC.

PLANT NO.: 11-013  
 DELIVERED TO: 42 (Type II)  
 ADDRESS: CHL.110 3-8-2012  
 F.D.O.T. PROJECT NUMBER: B1540

DATE: 3/27/2012  
 TICKET: 2

TRUCK NUMBER 0	D.O.T. CLASS Class VI (8500 PSI)	D.O.T. MIX NUMBER 05-1366	BATCH SIZE 2.50 yards
TIME LOADED 14:43	ARRIVED 2:54	DISCHARGED 3:00	TODAY'S QTY 8.50 yards

ALLOWABLE JOBSITE WATER ADDITION  
 \_\_\_\_\_ GALLONS

MIXING REVOLUTIONS:  
 AT PLANT 120 SECONDS  
 AT JOBSITE

Product Name		Actual		%MC
SAND	PIT NO. 36-491	2,720	lbs	4.4
67 Rock	Pit No10-645	3,920	lbs	2.7
Fly Ash	RRG Flyash	445	lbs	0.0
Cement 2	Cemex Cement	2,055	lbs	0.0
WATER		462	lbs	0.0
MB-AE 90	MBAE90	5	fluid ozs	
Delvo	DELVO	64	fluid ozs	
Glenium 7710	GLENIUM 7710	200	fluid ozs	

Actual W/C Ratio: 0.28

USING CENTRAL MIXER AND TUCKER BUILT TRANSPORT  
 ISSUANCE OF THIS TICKET CONSTITUTES CERTIFICATION  
 TO THE ACCURACY OF THE ABOVE RECORDED INFORMATION  
 AND COMPLIANCE WITH CURRENT SPECIFICATIONS.

WATER ADDED BY RECEIVER OF CONCRETE: \_\_\_\_\_ GALS.

RECEIVED BY: \_\_\_\_\_

DATE: \_\_\_\_\_

Ref: 60

TIN# B62645463      TIN# H23542575      TIN# T65682853

*2 3/27/12*

Appendix E - Precast Yard and Material Reports

Pour 2

DURA-STRESS INC.

PLANT NO.: 11-013  
 DELIVERED TO: 42 (Type II)  
 ADDRESS: CHL.110 3-8-2012  
 F.D.O.T. PROJECT NUMBER: B1540

DATE: 3/27/2012  
 TICKET: 1

TRUCK NUMBER 0	D.O.T. CLASS Class VI (8500 PSI)	D.O.T. MIX NUMBER 05-1366	BATCH SIZE 6.00 yards
TIME LOADED 14:06	ARRIVED	DISCHARGED	TODAY'S QTY 6.00 yards

Product Name	ALLOWABLE JOBSITE WATER ADDITION GALLONS	Actual	MIXING REVOLUTIONS:		%MC
			AT PLANT	AT JOBSITE	
SAND	PIT NO. 36-491	6,480	lbs	120	4.3
67 Rock	Pit No10-645	9,400	lbs	120	2.8
Fly Ash	RRG Flyash	1,045	lbs	120	0.0
Cement 2	Cemex Cement	4,765	lbs	120	0.0
WATER		1,079	lbs	120	0.0
MB-AE 90	MBAE90	12	fluid ozs		
Delvo	DELVO	152	fluid ozs		
Glenium 7710	GLENIUM 7710	472	fluid ozs		

Actual W/C Ratio: 0.28

USING CENTRAL MIXER AND TUCKER BUILT TRANSPORT  
 ISSUANCE OF THIS TICKET CONSTITUTES CERTIFICATION  
 TO THE ACCURACY OF THE ABOVE RECORDED INFORMATION  
 AND COMPLIANCE WITH CURRENT SPECIFICATIONS.

WATER ADDED BY RECEIVER OF CONCRETE: \_\_\_\_\_ GALS.

RECEIVED BY: \_\_\_\_\_

DATE: \_\_\_\_\_

Ref: 58

TIN# B62645463      TIN# H23542575      TIN# T65682853

**NUCOR**  
**NUCOR STEEL BIRMINGHAM, INC.**

SOLD TO: DURA STEEL INC  
 PO BOX 90779  
 TO: LEESBURG, FL 34749

SHIP TO: DURA-STRESS INC  
 11325 COUNTY RD 44  
 TO: LEESBURG, FL 34788

**CERTIFIED MILL TEST REPORT**

Ship from:  
 Nucor Steel Birmingham, Inc.  
 2060 Avenue A  
 KISSIMMEE, FL 34758  
 321-219-0191

Date: 1-Mar-2012  
 B.L. Number: 407717  
 Load Number: 104282

Appendix E - Precast Yard and Material Reports

LOT # HEAT #	DESCRIPTION	PHYSICAL TESTS			CHEMICAL TESTS														
		YIELD P.S.I.	TENSILE P.S.I.	ELONG % IN 8"	BEND	WT% DEF	C	Ni	Mn	Cr	P	Mo	S	V	Si	Cb	Cu	Sn	Ca
ALL BUNDLES MUST HAVE TAGS ALL MATERIAL MUST BE CLEAN/NO PITTING/NO RUST DOT INSPECTION AS TRUCK ARRIVES ALL DELIVERIES B/4 3:00 FRIDAYS B/4 NOON																			
PO# => BR1210067801 BR12100678	Nucor Steel - Birmingham Inc 19/#6 Rebar 40' A615M GR 420 (Gr60) ASTM A615/A615M-09b GR 60[420] AASHTO M31-07	63,200 436MPa	101,000 696MPa	16.0%	OK	-4.1% .042	.38 .15	1.22 .19	.026 .035	.056 .007	.23 .003	.34 .016							
PO# => DL1110542202 DL11105422	Nucor Steel - South Carolina 16/#5 Rebar 40' A615M GR 420 (Gr60) ASTM A615/A615M-09b GR 60[420] AASHTO M31-07	66,000 455MPa	108,000 745MPa	12.0%	OK	-4.1% .044	.47 .08	1.29 .09	.005 .010	.028 .005	.15 .005	.30							
PO# => DL1110663801 DL11106638	Nucor Steel - South Carolina 16/#5 Rebar 40' A615M GR 420 (Gr60) ASTM A615/A615M-09b GR 60[420] AASHTO M31-07	65,000 448MPa	106,000 731MPa	13.0%	OK	-6.0% .045	.44 .10	1.15 .15	.024 .020	.050 .005	.17 .003	.40							
PO# => DL1110663801 DL11106638	Nucor Steel - South Carolina 16/#5 Rebar 40' A615M GR 420 (Gr60) ASTM A615/A615M-09b GR 60[420] AASHTO M31-07	68,000 469MPa	109,000 752MPa	13.0%	OK	-3.2% .039	.43 .10	1.23 .13	.013 .020	.050 .005	.17 .004	.36							

NBMG-08 January 1, 2012

Material Safety Data Sheets are available at www.nucorbar.com or by contacting your inside sales representative.

I hereby certify that the material described herein has been manufactured in accordance with the specifications and standards listed herein and that it satisfies those requirements.  
 1) Weld repair was not performed on this material.  
 2) Melted and Manufactured in the United States.  
 3) Mercury, Radium, or Alpha source materials in any form have not been used in the production of this material.

*George F. McLaughlin*

QUALITY ASSURANCE:

**NUCOR**  
**NUCOR STEEL BIRMINGHAM, INC.**

DURA-ST, -SS INC  
 PO BOX 490779  
 TO: LEEBSBURG, FL 34749-

DURA-STRESS INC  
 11325 COUNTY RD 44  
 TO: LEEBSBURG, FL 34788-

**CERTIFIED MILL TEST REPORT**

Ship from:  
 Nucor Steel Birmingham, Inc.  
 2060 Avenue A  
 KISSIMMEE, FL 34758  
 321-219-0191

Date: 6-Feb-2012  
 B.L. Number: 406800  
 Load Number: 104208

Page.

Appendix E'- Precast Yard and Material Reports

Material Safety Data Sheets are available at www.nucorbar.com or by contacting your inside sales representative. NBMG-08 January 1, 2012

LOT # HEAT #	DESCRIPTION	PHYSICAL TESTS			CHEMICAL TESTS															
		YIELD P.S.I.	TENSILE P.S.I.	ELONG % IN 8"	BEND	WT%	DEF	C	Ni	Mn	Cr	P	Mo	S	V	Si	Cb	Cu	Sn	C.E.
ALL BUNDLES MUST HAVE TAGS ALL MATERIAL MUST BE CLEAN/NO PITTING/NO RUST DOT INSPECTION AS TRUCK ARRIVES ALL DELIVERIES B/4 3:00 FRIDAYS B/4 NOON																				
PO# => BR1110477301 BR11104773	104534 Nucor Steel - Birmingham Inc 22/#7 Rebar 40' A615M Gr 420 (Gr60) ASTM A615/A615M-09b GR 60[420] AASHTO M31-07	69,600 480MPa	111,500 769MPa	13.0%	OK	-2.3% .053	.41 .10	.128 .14	.021 .022	.038 .008	.28 .003	.38	.65							
PO# => BR1110478201 BR11104782	104534 Nucor Steel - Birmingham Inc 22/#7 Rebar 40' A615M Gr 420 (Gr60) ASTM A615/A615M-09b GR 60[420] AASHTO M31-07	73,000 503MPa	110,100 759MPa	13.0%	OK	-3.1% .053	.43 .14	1.22 .15	.014 .028	.036 .015	.22 .003	.38	.66							
PO# => BR1110509801 BR11105098	104534 Nucor Steel - Birmingham Inc 10/#3 Rebar 40' A615M GR 420 (Gr60) ASTM A615/A615M-09b GR 60[420] AASHTO M31-07	72,100 497MPa	109,500 755MPa	13.0%	OK	-1.9% .019	.38 .14	1.18 .15	.020 .040	.038 .006	.21 .003	.44	.61							

I hereby certify that the material described herein has been manufactured in accordance with the specifications and standards listed above and that it satisfies those requirements.  
 1) Weld repair was not performed on this material.  
 2) Material was not heat treated.  
 3) Mercury, Radium, or Alpha source materials in any form have not been used in the production of this material.

*George F. Milgrom*

QUALITY ASSURANCE:

**Dura - Stress, Inc.**



*Load cell  
ASTM F44  
calibrated*

**CERTIFICATE OF CALIBRATION**

Serial Number: <b>T12</b> <b>DRO ONLY</b> Manufacturer: <b>Hercules with Strainsense DRO</b> Description: <b>Stressing Jack # T12</b> Capacity: <b>47,000 lbf</b> Divisions: <b>50 lbf</b> Tolerance: <b>+/- 1.5% of applied load</b> Initial Findings: <b>Out of calibration</b> Action Taken: <b>Recalibrated</b>	<u>Report Number</u> <b>T12-007</b> <u>Date</u> <b>10/3/2011</b> <u>Date Due</u> <b>10/3/2012</b> <u>Calibration interval</u> <b>12 months</b>  <u>AMB. Temp.</u> <b>78Deg F</b>
* When available: (1) As stated by manufacturer; (2) Accepted by tolerances; or (3) Observed accuracy of unit.	

DRO Calibration Before Recalibration								
Range: 48,000 lbf			Range: 48,000 lbf			Range: 48,000 lbf		
Standard	Reading	% Error of applied load	Standard	Reading	% Error of applied load	Standard	Reading	% Error of applied load
2053	2000	-2.58	10145	10000	-1.43	30298	30000	-0.98
3054	3000	-1.77	15144	15000	-0.95	35301	35000	-0.85
4056	4000	-1.38	20164	20000	-0.81	40351	40000	-0.87
5052	5000	-1.03	25351	25000	-1.38	45566	45000	-1.24
						48621	48200	-0.87

After Calibration								
Range: 5,500 lbf Initial Gauge			Range: 50,000 lbf Final Gauge			Range: 50,000 lbf Final Gauge		
Standard	Reading	% Error of applied load	Standard	Reading	% Error of applied load	Standard	Reading	% Error of applied load
2010	2000	-0.50	10027	10000	-0.27	30042	30000	-0.14
2998	3000	0.07	15038	15000	-0.25	35106	35100	-0.02
4012	4000	-0.30	20650	20550	-0.48	40264	40250	-0.03
4991	5000	0.18	25078	25000	-0.31	45040	45100	0.13
						48140	48150	0.02

\* Unit capable of 60,000 but only calibrated to 48,000+. Low range calibrated to 5,500 lbf

Remarks: Calibrated within 1.5% of applied load in accordance with ASTM E-4 with NIST traceable standards used in accordance with ASTM E-74.

Equipment used:  
 Strainsense/IDS loadcell/digital indicator Capacity 50,000 lbf - Serial # 0404D/411351

*Craig A. Hill* Quality Control Technician      *Wenon D. ...* Engineer  
 1-10-11

Appendix E - Precast Yard and Material Reports



MATERIAL CERTIFICATION OF COMPLIANCE

Sanderson, FL

DURA STRESS INC  
11325 COUNTRY ROAD 44  
LISBON FL 34788

Bill of Lading: 00103248  
Order Number: 378873  
PO Number: 104832

Insteel Wire Products Company hereby certifies that the specimens taken from production lot(s) consisting of one or more of the following Lot/serial numbers were tested in accordance with and met the specification requirements of A 416 - 10. The attached test report(s) represent the result of such test(s).

1/2 (12.7mm) 7W 270 LR ASTM A416

Test Report Number: 10071136

Lot/Serial Numbers

- 1302461112054 ✓
- 1302461112055 ✓
- 1302461112056 ✓
- 1302461112057 ✓
- 1302461112058 ✓
- 1302462112839 ✓
- 1302462112842 ✓

Heat Number/Lot Number

15048

3-8  
P-1

The products listed in this certification were manufactured and fabricated in the United States of America.

Insteel Wire Products Company hereby certifies that the prestressing strand described above meets or exceeds the minimum bonding requirements as currently accepted in the NASP (North American Strand Producers) pull-out test and the Moustaffa block pull-out test.

All Domestic Prestressing Strand was made from steel rod that was manufactured and processed completely in America. The rod was then manufactured into PC Strand in the United States at Insteel Wire Products Company plant in either Jacksonville, FL or Gallatin, TN. The material meets the "Buy America" requirements of 23 CFR 635.410.

The products listed in this certification were manufactured in the U.S.A. from wire rod which was manufactured in the U.S.A.

Quality Assurance Manager: Channing L. R. ...

Date: 07-MAR-2012

Appendix E - Precast Yard and Material Reports



**INSTEEL WIRE PRODUCTS**®

Sanderson Plant - Sanderson, FL 32087

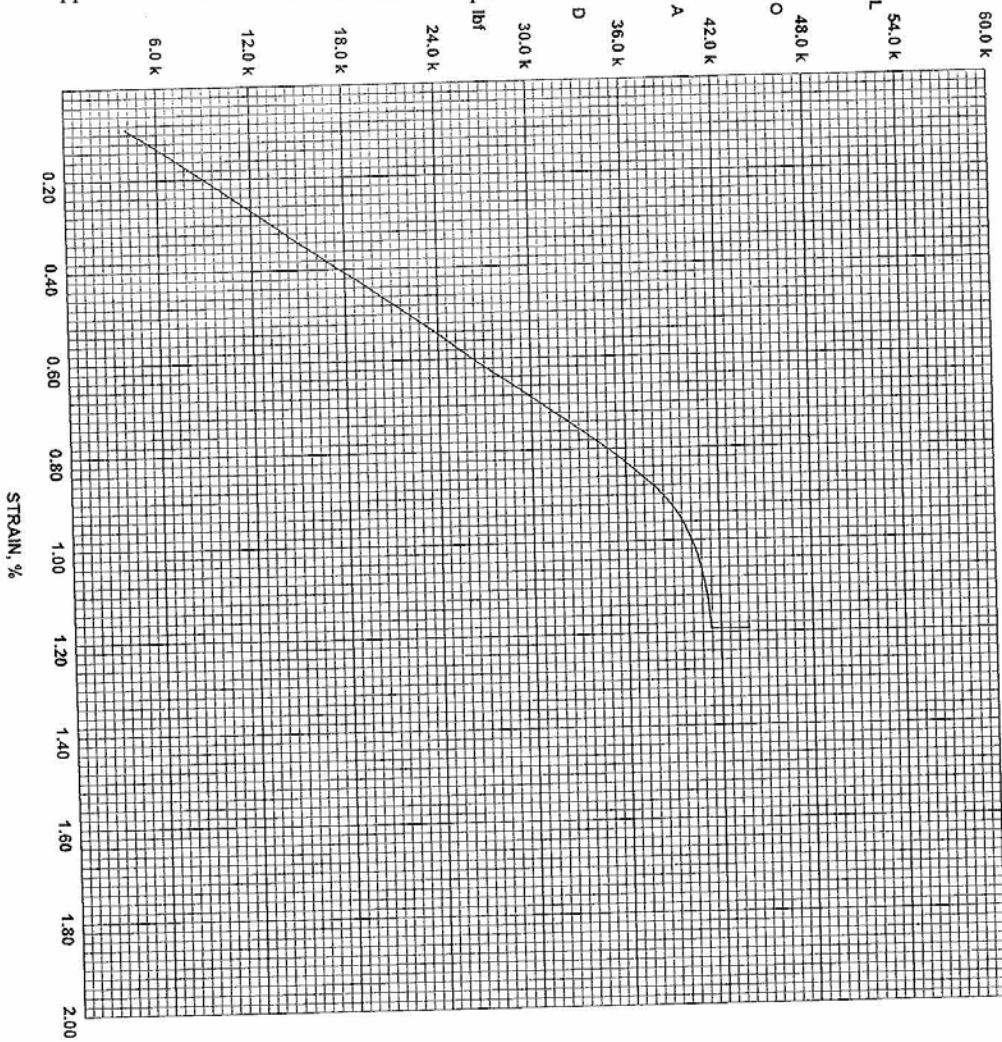
## Packing List

DURA STRESS INC  
11325 COUNTRY ROAD 44  
LISBON FL 34788

Bill of Lading Number: 00103248  
Page: 1 of 1  
Date: 07-MAR-12  
Sales Order Number: 378873  
Customer PO Number: 104832

Lot Number	Description	Length	Weight
1302461112054	1/2 (12.7mm) 7W 270 LR ASTM A416	13700	7132
1302461112055	1/2 (12.7mm) 7W 270 LR ASTM A416	13700	7132
1302461112056	1/2 (12.7mm) 7W 270 LR ASTM A416	13700	7132
1302461112057	1/2 (12.7mm) 7W 270 LR ASTM A416	13700	7132
1302461112058	1/2 (12.7mm) 7W 270 LR ASTM A416	13700	7132
1302462112839	1/2 (12.7mm) 7W 270 LR ASTM A416	13700	7132
1302462112842	1/2 (12.7mm) 7W 270 LR ASTM A416	13580	7070
<b>Total Number of Packs 7</b>		<b>Totals</b>	<b>95780 49862</b>

Appendix E - Precast Yard and Material Reports



Steel Wire Products  
Prestressed Concrete Strand

1/2" 270 7W LOW RELAXATION

Test Number: 10071136  
 Tested By: CER  
 Ultimate Breaking Strength, lbF: 43862  
 Ultimate Breaking Strength, kN: 195  
 Load @ 1% Extension, lbF: 40218  
 Load @ 1% Extension, kN: 179  
 Ultimate Elongation, %: 5.73  
 Representative Area, in<sup>2</sup>: 0.153  
 Representative Area, mm<sup>2</sup>: 98.7  
 Actual Area, in<sup>2</sup>: 0.1527  
 Actual Area, mm<sup>2</sup>: 98.5470  
 Avg Modulus of Elasticity, Mpsi: 29.0  
 Avg Modulus of Elasticity, MPa: 199947.6  
 Reference:

Mar 7, 2012 11:58:49 AM  
 SN: 206250-R2 V7.02.07

**STRAIGHT BILL OF LADING - NOT NEGOTIABLE**  
Appendix E - Precast Yard and Material Reports

**NUCOR**  
NUCOR STEEL BIRMINGHAM, INC.

Nucor Steel Birmingham, Inc.  
2060 Avenue A  
KISSIMMEE, FL 34788  
321-219-0191

Page: 1 of 1

Bill of Lading No.:  
406520 Rev 0

PICKED: 01-30-2012 7:12 AM  
PRINT: 01-30-2012 7:35 AM

SOLD TO: 000

DURA-STRESS INC  
PO BOX 490779  
LEESBURG, FL 34749  
(352) 787-1422

SHIP TO: 010

DURA-STRESS INC  
11325 COUNTY RD 44  
LEESBURG, FL 34788  
(352) 787-1422

Subject to section 7 of conditions, of applicable bill of lading. If this shipment is to be delivered to the consignee without recourse on the consignor, the consignor shall sign the following statement.

(Signature of Consignor)  
EXW (Incoterms 2000) loaded.  
If charges are to be prepaid, write "to be prepaid" here.  
**To Be Prepaid**

Rec \$ \_\_\_\_\_ to apply in prepayment of the charges on the property described herein.

Agent or Carrier

Per \_\_\_\_\_  
(The signature here acknowledges only the amount prepaid)

Freight Mode: Over Length Truck

CUSTOMER NO.	CUSTOMER ORDER NUMBER	OUR ORDER NUMBER	SHIPPER NUMBER	TERMS
10099	See Below	See Below	O1-104175	Prepaid
SHIP VIA		VEHICLE NUMBER	ROUTING	
Paul Horne Trucking Inc		92		
NO. OF BUNDS.	NO. OF PIECES	DESCRIPTION	PRODUCT CODE	WEIGHT
		<b>SPECIAL INSTRUCTIONS</b> ALL BUNDLES MUST HAVE TAGS ALL MATERIAL MUST BE CLEAN/NO PITTING/NO RUST DOT INSPECTION AS TRUCK ARRIVES ALL DELIVERIES B/4 3:00 FRIDAYS B/4 NOON DELIVER TO SOUTHSIDE		
2	70	32/#10 Rebar 60' A615M Gr 420 (Gr60) OUR ORDER NUMBER - 314552/1 CUSTOMER PO# - 104461 Tag# 1 : BR0711231310 Heat #: BR07107800 Lot #: BR0710780001 Tag# 2 : DL1011040295 Heat #: DL10103396 Lot #: DL1010339601	900000327204200  Pieces: 35 Pieces: 35	18,072  9,036 9,036
5	945	13/#4 Rebar 40' A615M GR 420 (Gr60) OUR ORDER NUMBER - 314552/2 CUSTOMER PO# - 104461 Tag# 3 : BR1111082793 Heat #: BR11104059 Lot #: BR1110405901 Tag# 4 : BR1111082964 Heat #: BR11104065 Lot #: BR1110406501 Tag# 5 : BR1111082968 Heat #: BR11104065 Lot #: BR1110406501 Tag# 6 : BR1111082971 Heat #: BR11104065 Lot #: BR1110406501 Tag# 7 : BR1111082972 Heat #: BR11104065 Lot #: BR1110406501	900000134804200  Pieces: 189 Pieces: 189 Pieces: 189 Pieces: 189 Pieces: 189	25,250  5,050 5,050 5,050 5,050 5,050
		<b>Total Tags: 7</b>	<b>Total Pieces: 1015</b>	<b>43,322</b>

*DAVID*

Name of Carrier: Paul Horne Trucking Inc  
RECEIVED subject to the classifications and tariffs in effect on the date of the issue of this bill of lading.

Carrier's No. 92

**Charges Advanced**

\$ \_\_\_\_\_  
\*Shippers imprint in lieu of stamp; not a part of bill of lading approved by the Interstate Commerce Commission.\*

If the shipment moves between two ports by a carrier by water the law requires that the bill of lading shall state whether it is "carrier's or shipper's weight."

NOTE - Where the rate is dependent on value, shippers are required to state specifically in writing the agreed or declared value of the property.

The agreed or declared value of the property is hereby specifically stated by the shipper to be not exceeding

per \_\_\_\_\_ This shipment is correctly described  
CORRECT WEIGHT IS \_\_\_\_\_

bs. T&M9

The property described above in apparent good order, except as noted (contents and condition of contents of packages unknown), marked, consigned, and destined as indicated above, which said carrier (the word carrier being understood throughout this contract as meaning any person or organization in possession of the property under the contract) agrees to carry to its usual place of delivery at said destination, if on its route, otherwise to deliver to another carrier on the route to said destination. It is mutually agreed, that every service to be performed hereunder shall be subject to all the terms and conditions of the Uniform Domestic Straight Bill of Lading set forth (1) in Official, Southern, Western, and Illinois Freight Classifications in effect on the date hereof, if this is a rail or a rail-water shipment, or (2) in the applicable motor carrier classification or tariff if this is a motor carrier shipment.

Shipper hereby certifies that he is familiar with all the terms and conditions of the said bill of lading, including those on the back thereof, set forth in the classification or tariff which governs the transportation of this shipment, and the said terms and conditions are hereby agreed to by the shipper and accepted for himself and his assigns.

NBMG-07 April 29, 2008

**STRAIGHT BILL OF LADING - NOT NEGOTIABLE**

Appendix E - Precast Yard and Material Reports

**NUCOR**  
NUCOR STEEL BIRMINGHAM, INC.

Nucor Steel Birmingham, Inc.  
2060 Avenue A  
KISSIMMEE, FL 34788  
321-219-0191

Page: 1 of 1

Bill of Lading No.:  
406520 Rev 0

PICKED: 01-30-2012 7:12 AM  
PRINT: 01-30-2012 7:35 AM

SOLD TO: 000

SHIP TO: 010

DURA-STRESS INC  
PO BOX 490779  
LEESBURG, FL 34749  
(352) 787-1422

DURA-STRESS INC  
11325 COUNTY RD 44  
LEESBURG, FL 34788  
(352) 787-1422

Subject to section 7 of conditions, of applicable bill of lading. If this shipment is to be delivered to the consignee without recourse on the consignor, the consignor shall sign the following statement.

(Signature of Consignor)  
EXW (Incoterms 2000) loaded.  
If charges are to be prepaid, write "to be prepaid" here.  
**To Be Prepaid**

Rec. \$ \_\_\_\_\_ to  
Apply in prepayment of the charges on the property described herein.

Agent or Carrier

Per \_\_\_\_\_  
(The signature here acknowledges only the amount prepaid)

Freight Mode: Over Length Truck

CUSTOMER NO.	CUSTOMER ORDER NUMBER	OUR ORDER NUMBER	SHIPPER NUMBER	TERMS
10099	See Below	See Below	O1-104175	Prepaid
SHIP VIA		VEHICLE NUMBER	ROUTING	
Paul Horne Trucking Inc		92		
NO. OF BUNDS.	NO. OF PIECES	DESCRIPTION	PRODUCT CODE	WEIGHT
		<b>SPECIAL INSTRUCTIONS</b> ALL BUNDLES MUST HAVE TAGS ALL MATERIAL MUST BE CLEAN/NO PITTING/NO RUST DOT INSPECTION AS TRUCK ARRIVES ALL DELIVERIES B/4 3:00 FRIDAYS B/4 NOON DELIVER TO SOUTHSIDE		
2	70	32/#10 Rebar 60' A615M Gr 420 (Gr60) OUR ORDER NUMBER - 314552/1 CUSTOMER PO# - 104461 Tag# 1 : BR0711231310 Heat #: BR07107800 Lot #: BR0710780001 Tag# 2 : DL1011040295 Heat #: DL10103396 Lot #: DL1010339601	900000327204200 Pieces: 35 Pieces: 35	18,072 9,036 9,036
5	945	13/#4 Rebar 40' A615M GR 420 (Gr60) OUR ORDER NUMBER - 314552/2 CUSTOMER PO# - 104461 Tag# 3 : BR1111082793 Heat #: BR11104059 Lot #: BR1110405901 Tag# 4 : BR1111082964 Heat #: BR11104065 Lot #: BR1110406501 Tag# 5 : BR1111082968 Heat #: BR11104065 Lot #: BR1110406501 Tag# 6 : BR1111082971 Heat #: BR11104065 Lot #: BR1110406501 Tag# 7 : BR1111082972 Heat #: BR11104065 Lot #: BR1110406501	900000134804200 Pieces: 189 Pieces: 189 Pieces: 189 Pieces: 189 Pieces: 189	25,250 5,050 5,050 5,050 5,050 5,050
		Total Tags: 7	Total Pieces: 1015	43,322

*James Green*  
1-30-12  
Green

*DAVID*

Name of Carrier: Paul Horne Trucking Inc  
RECEIVED subject to the classifications and tariffs in effect on the date of the issue of this Bill of Lading.

Carrier's No. 92

The property described above in apparent good order, except as noted (contents and condition of contents of packages unknown), marked, consigned, and destined as indicated above, which said carrier (the word carrier being understood throughout this contract as meaning any person or corporation in possession of the property under the contract) agrees to carry to its usual place of delivery at said destination, if on its route, otherwise to deliver to another owner on the route to said destination. It is mutually agreed, that every service to be performed hereunder shall be subject to all the terms and conditions of the Uniform Domestic Straight Bill of Lading set forth in Official Southern, Western, and Illinois Freight Classifications in effect on the date hereof, if this is a rail or a sea-water shipment, or (2) in the applicable motor carrier classification or tariff if this is a motor carrier shipment.

Shipper hereby certifies that he is familiar with all the terms and conditions of the said bill of lading, including those on the back thereof, set forth in the classification or tariff which governs the transportation of this shipment, and the said terms and conditions are hereby agreed to by the shipper and accepted for himself and his assigns.

NBMG-07 April 29, 2008

Charges Advanced

\$ \_\_\_\_\_  
"Shippers import in lieu of stamp; not a part of bill of lading approved by the Interstate Commerce Commission."

If the shipment moves between two ports by a carrier by water the law requires that the bill of lading shall state whether it is "carrier's or shipper's weight."

NOTE - Where the rate is dependent on value, shippers are required to state specifically in writing the agreed or declared value of the property.

The agent or declared value of the property is hereby specifically stated by the shipper in the not exceeding per \_\_\_\_\_

This shipment is correctly described  
CORRECT WEIGHT IS \_\_\_\_\_

kg. TGM9

SOLD DURA-ST, JS INC  
 PO BOX 490779  
 TO: LEESBURG, FL 34749-

**NUCCOR**  
 NUCOR STEEL BIRMINGHAM, INC.

**CERTIFIED MILL TEST REPORT**

Page: 1

SHIP DURA-STRESS INC  
 11323 COUNTY RD 44  
 TO: LEESBURG, FL 34788-

Ship from:  
 Nucor Steel Birmingham, Inc.  
 2060 Avenue A  
 KISSIMMEE, FL 34758  
 321-219-0191

Date: 30-Jan-2012  
 B.L. Number: 406520  
 Load Number: 104175

Material Safety Data Sheets are available at [www.nucorcar.com](http://www.nucorcar.com) or by contacting your inside sales representative.

LOT # HEAT #	DESCRIPTION	PHYSICAL TESTS				CHEMICAL TESTS										
		YIELD P.S.I.	TENSILE P.S.I.	ELONG % IN 8"	BEND	WT% DEF	C	Mn	Cr	P	Mo	S	V	SI	Co	Cu

ALL BUNDLES MUST HAVE TAGS  
 ALL MATERIAL MUST BE CLEAN/NO PITTING/NO RUST  
 DOT INSPECTION AS TRUCK ARRIVES  
 ALL DELIVERIES B/4 3:00 FRIDAYS B/4 NOON

PO# => 104461  
 BR0710780001 Nucor Steel Birmingham, Inc. 71,800 111,600 10.0% OK -4.5% .40 1.28 .018 .044 .26 .45 .64  
 BR07107800 32#10 Rebar 495MPa 769MPa .067 .14 .14 .036 .010 .010 .005 .005

PO# => 104461  
 BR1110405901 Nucor Steel - Birmingham Inc 71,000 108,300 13.0% OK -2.8% .42 1.17 .010 .029 .22 .36 .64  
 BR11104059 13#4 Rebar 490MPa 747MPa .033 .13 .14 .032 .017 .017 .002 .002

PO# => 104461  
 BR1110406501 Nucor Steel - Birmingham Inc 67,400 105,600 13.0% OK -2.2% .42 1.19 .009 .038 .22 .34 .64  
 BR11104065 13#4 Rebar 465MPa 728MPa .034 .11 .12 .024 .008 .008 .004 .004

Material Re  
 40' A615M GR 420 (Gr60)  
 ASTM A615/A615M-09b GR 60[420]  
 AASHTO M31-07

I hereby certify that the material described herein has been manufactured in accordance with the specifications and standards listed above and that it satisfies these requirements.  
 1) Weld repair was not performed on this material.  
 2) Material was manufactured in the United States.  
 3) Material has been used in the production of this material.

QUALITY ASSURANCE: 

SOLD DURA-STEEL, INC.  
 PO BOX 490779  
 TO: LEESBURG, FL 34749-

**NUCOR**  
 NUCOR STEEL BIRMINGHAM, INC.

**CERTIFIED MILL TEST REPORT**

Page: 2

SHIP DURA-STRESS INC  
 11325 COUNTY RD 44  
 TO: LEESBURG, FL 34788-

Ship from:  
 Nucor Steel Birmingham, Inc.  
 2060 Avenue A  
 KISSIMMEE, FL 34758  
 321-219-0191

Date: 30-Jan-2012  
 B.L. Number: 406520  
 Load Number: 104175

Material Safety Data Sheets are available at [www.nucorbar.com](http://www.nucorbar.com) or by contacting your inside sales representative.

MEMO-08 January 1, 2012

Appendix E - Precast Yard and Material Reports

LOT # HEAT #	DESCRIPTION	PHYSICAL TESTS				CHEMICAL TESTS														
		YIELD P.S.I.	TENSILE P.S.I.	ELONG % IN 8"	BEND	WT% DEF	C	NI	Mn	CR	P	Mo	S	V	SI	CB	Cu	Sn	C.E.	
PO# => 104461																				
DL1010339601	Nucor Steel - South Carolina	69,000	110,000	9.0%	OK	-2.6%	.44	1.24	.007	.019	.16	.26	.66							
DL10103396	32#10 Rebar 60' A615M Gr 420 (Gr60) ASTM A615/A615M-09b GR 60(420) AASHTO M31-07	476MPa	758MPa			.070	.07	.07	.010	.013	.003									

I hereby certify that the material described herein has been manufactured in accordance with the specifications and standards listed above and that it satisfies these requirements.

Weld repair was not performed on this material.

1) Weld repair was not performed on this material.  
 2) Heat of material is as shown on the source materials in any form have not been used in the production of this material.

QUALITY ASSURANCE: *[Signature]*

REBAR REPORT  
[Type the document title]

---

DATE: 3/8/12

JOB#

BED#

MARK#

TYPE OF BEAM:

BAR SIZE: 4 HEAT: BR110405901

BAR SIZE: HEAT:

BAR SIZE: HEAT:

BAR SIZE: HEAT:

Appendix E - Precast Yard and Material Reports

**CONCRETE MIX DESIGN**

Class: II DECK

Mix Design Number: 03-1668

Minimum Strength: 4500 psi

Effective Date: 12/21/2009

Hot Weather? Yes

Issuer's Name: R.D. Hager

Status: APPROVED

Project #:

Producer: A Materials Group

Plant #:

**Source of Materials**

Product Product Name	Quantity	Producer Plant #	QPL # Spec:	SSD FM	Geological Type
Cement: Type II Cement	510 LB	SUWANNEE AMERICAN CEMENT - BRANFORD CMT29	AASHTO M 85 - Type II	3.15	
Fly Ash: Class F Fly Ash	127 LB	HEADWATERS-GASTON FA31	ASTM C 618 - Class F	2.27	
Coarse Aggregate: # 67 Stone	1705 LB	A GROUP CABBAGE GROVE MINE 38627		2.50	Limestone
Fine Aggregate: Silica Sand	1246 LB	CROWDER EXCAVATING & LAND CL, INC 50471		2.64	2.40 Silica Sand
Air Ent Admixture: AEA92 S	3.0 OZ	EUCLID CHEMICAL CO.	S924-0023 AASHTO M 154 - AEA		
Type D Admixture: Eucon WR	70.0 OZ	EUCLID CHEMICAL CO.	S924-0307 AASHTO M 194 - Type D		
Water:	33.50 GA				
Water for Concrete					
Water:	279.0 LB				
Water for Concrete					

**Specification Limits**

Temperature	Less than or equal to 100
Slump	1.50 to 4.50
Compressive Strength	Greater than or equal to 4500
Air Content	1.00 to 6.00
W/C Ratio	Less than or equal to 0.44
Aggregate Correction Factor:	1.0

**Producer Data**

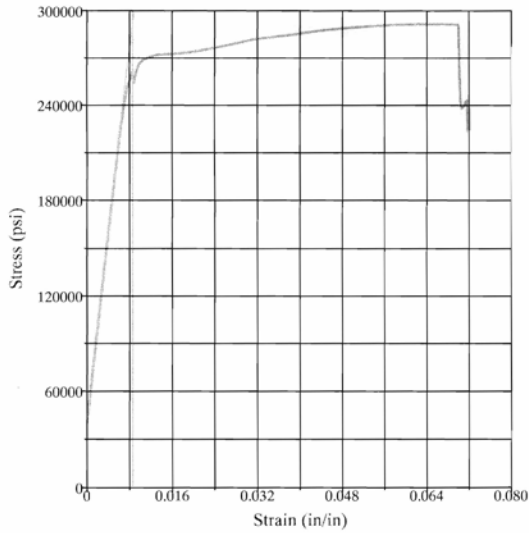
W/C Ratio	0.44	LB per LB
Theoretical Yield	27.00	CF
Temperature	97	degree F
Slump	3.50	inches
Density	143.2	LB per CF
Chloride Content	0.357	LB per CY
Air Content	3.00	percent
28 DAY	5980	avgpsi

Comments:

Mix Designer: First Name Last Name

Conc\_Mix-4.rpt 12/22/09 slb

Appendix E - Precast Yard and Material Reports

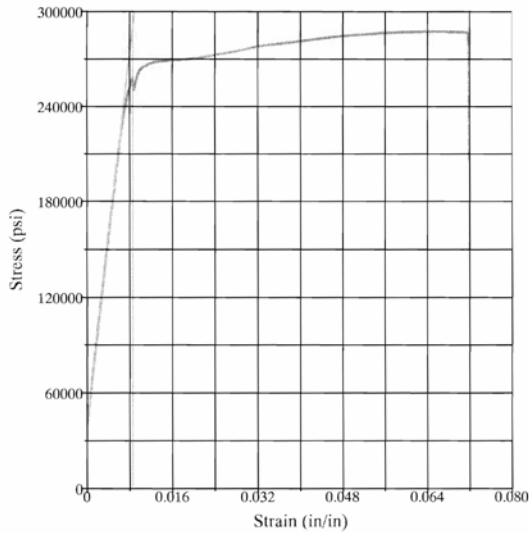


**Test Results**  
 Specimen Gage Length: **31.0000** in  
 Area: **0.1500** in<sup>2</sup>  
 Total Load: **43750** lbf  
 Tensile Strength: **291650** psi  
 Correlation Coefficient: **0.9999**  
 Modulus of Elasticity: **29362200** psi  
 Stress at 1% EUL: **261160** psi  
 Load at 1% EUL: **39170** lbf  
 Est. Elongation: **0.1**  
 Position at Break: **2.405** in  
 Total Elongation: **7.17** %

**Test Summary**

Counter: **6950**  
 Elapsed Time: **00:01:50**  
 LIMS Number: **UF Research**  
 Project Number: **UF Research**  
 Sample Number: **57**  
 Size: **0.5**  
 Grade: **270 K**  
 Coil:  
 Operator: **Mark**  
 Condition of Sample: **Satisfactory**  
 Comments:  
 Procedure Name: **ASTM A416 - 7 wire strand - Epsilon**  
 Start Date: **5/24/2012**  
 Start Time: **2:53:45 PM**  
 End Date: **5/24/2012**  
 End Time: **2:55:35 PM**  
 Workstation: **FLORIDA-DOT**  
 Tested By: **tech**

Appendix E - Precast Yard and Material Reports

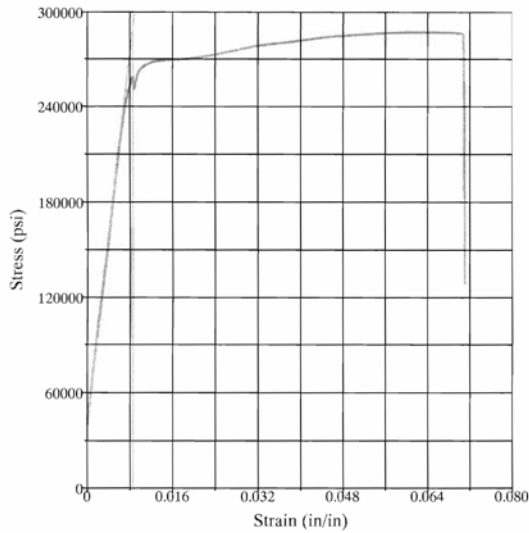


**Test Results**  
 Specimen Gage Length: **31.0000** in  
 Area: **0.1520** in<sup>2</sup>  
 Total Load: **43700** lbf  
 Tensile Strength: **287490** psi  
 Correlation Coefficient: **0.9999**  
 Modulus of Elasticity: **28987600** psi  
 Stress at 1% EUL: **257620** psi  
 Load at 1% EUL: **39160** lbf  
 Est. Elongation: **0.1**  
 Position at Break: **2.429** in  
 Total Elongation: **7.19** %

**Test Summary**

Counter: **6951**  
 Elapsed Time: **00:01:56**  
 LIMS Number: **UF Research**  
 Project Number: **UF Research**  
 Sample Number: **57**  
 Size: **0.5**  
 Grade: **270 K**  
 Coil:  
 Operator: **Mark**  
 Condition of Sample: **Satisfactory**  
 Comments:  
 Procedure Name: **ASTM A416 - 7 wire strand - Epsilon**  
 Start Date: **5/24/2012**  
 Start Time: **3:28:12 PM**  
 End Date: **5/24/2012**  
 End Time: **3:30:08 PM**  
 Workstation: **FLORIDA-DOT**  
 Tested By: **tech**

Appendix E - Precast Yard and Material Reports

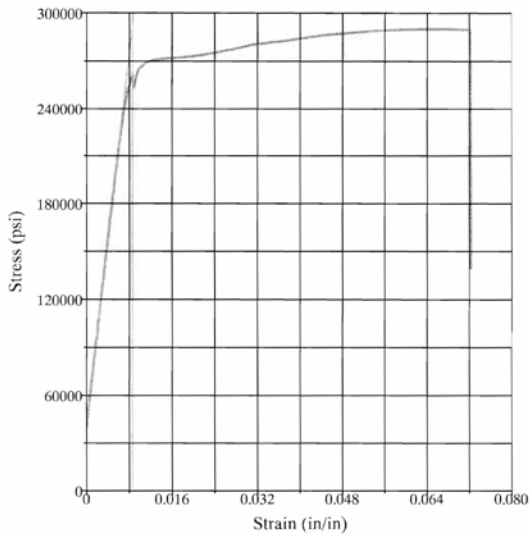


**Test Results**  
 Specimen Gage Length: **31.0000** in  
 Area: **0.1520** in<sup>2</sup>  
 Total Load: **43660** lbf  
 Tensile Strength: **287210** psi  
 Correlation Coefficient: **0.9999**  
 Modulus of Elasticity: **28928900** psi  
 Load at 1% EUL: **39260** lbf  
 Stress at 1% EUL: **258300** psi  
 Est. Elongation: **0.1**  
 Total Elongation: **7.10** %  
 Position at Break: **2.360** in

**Test Summary**

Counter: **6948**  
 Elapsed Time: **00:01:56**  
 LIMS Number: **UF Research**  
 Project Number: **UF Research**  
 Sample Number: **55**  
 Size: **0.5**  
 Grade: **270 K**  
 Coil:  
 Operator: **Mark**  
 Condition of Sample: **Satisfactory**  
 Comments:  
 Procedure Name: **ASTM A416 - 7 wire strand - Epsilon**  
 Start Date: **5/24/2012**  
 Start Time: **2:36:33 PM**  
 End Date: **5/24/2012**  
 End Time: **2:38:29 PM**  
 Workstation: **FLORIDA-DOT**  
 Tested By: **tech**

Appendix E - Precast Yard and Material Reports



**Test Results**  
 Specimen Gage Length: 31.0000 in  
 Area: 0.1510 in<sup>2</sup>  
 Total Load: 43800 lbf  
 Tensile Strength: 290090 psi  
 Correlation Coefficient: 0.9999  
 Modulus of Elasticity: 29244600 psi  
 Load at 1% EUL: 39320 lbf  
 Stress at 1% EUL: 260430 psi  
 Est. Elongation: 0.1  
 Total Elongation: 7.23 %  
 Position at Break: 2.417 in

**Test Summary**

Counter: 6949  
 Elapsed Time: 00:01:54  
 LIMS Number: UF Research  
 Project Number: UF Research  
 Sample Number: 55  
 Size: 0.5  
 Grade: 270 K  
 Coil:  
 Operator: Mark  
 Condition of Sample: Satisfactory  
 Comments:  
 Procedure Name: ASTM A416 - 7 wire strand - Epsilon  
 Start Date: 5/24/2012  
 Start Time: 2:47:21 PM  
 End Date: 5/24/2012  
 End Time: 2:49:15 PM  
 Workstation: FLORIDA-DOT  
 Tested By: tech

Appendix E - Precast Yard and Material Reports



FDOT

September 6, 2012

Re: FDOT Structure Lab, Tallahassee, FL

Attn:

Enclosed please find the following for your approval:

<u>Product</u>	<u>Strength</u>	<u>Description</u>
FC80JE	8500 psi	8500 PSI SCC
JB85EC	8500 psi	8500 PSI

Please direct inquires or replies to:

Spooner, Justin  
Technical Services, North FI

The recipient acknowledges and confirms that this information is confidential and is being disclosed to the recipient for purposes of review only. By accepting this information, the recipient agrees:

- to maintain this information in confidence at all times;
- to not disclose this information, in whole or in part, by way of summary or analysis, to anyone except as explicitly agreed to by Florida Rock Industries, Inc.

Florida Rock Industries, Inc. has no knowledge or authority regarding placement location of the above mix designs. It is the responsibility of the engineer/architect and/or contractor to determine that the above mix designs are in compliance with all applicable building codes and standards for all properties, environments and uses.

ACI 302.1 recommends that an air-entrainment not be used when a smooth, dense, hard-troweled finish is desired.

Contractor assumes responsibility for ordering and placing by Mix Number, as approved by the engineer/architect. Changes in mix properties may require a change in the Mix Number.

By accepting this information, the recipient agrees to insure copies of the test results are supplied to Florida Rock Industries, Inc. as soon as they become available.

FDOT

September 6, 2012

Re: FDOT Structure Lab, Tallahassee, FL

**Concrete Mixtures**

			Mixture Proportions †	
Mix Number			FC80JE	JB85EC
Strength (psi)			8500	8500
W/C Ratio			.29	.29
Slump (in)			27 +/- 3"	8 +/- 1"
Air Content (%)			3	3.0 +/- 1.5
Plastic Unit Weight (lbs/cf)			145.0 +/- 1.5	153.3 +/- 1.5
Material	ASTM	Type		
Cement	C 150	I/II	900	900
Flyash	C 618	Class F	150	140
Water	--	Potable	300	292
Aggregate	C 33	Sand	1408	1100
Aggregate	C 33	#67 Stone	--	1700
Aggregate	C 33	#89 Stone	1150	--
Admixture	C 260	AEA	‡	‡
Admixture	C 494	HRWR	‡	‡
Admixture	C 494	W/Reducer	‡	‡

† quantities may vary in accordance with ACI 301 4.2.3.6.a & 4.2.3.6.b, ACI 318 5.6.3.4 and ASTM C 94.

‡ admixture dosage rates in accordance with manufactures recommendations.

The recipient acknowledges and confirms that this information is confidential and is being disclosed to the recipient for purposes of review only. By accepting this information, the recipient agrees:

- to maintain this information in confidence at all times;
- to not disclose this information, in whole or in part, by way of summary or analysis, to anyone except as explicitly agreed to by Florida Rock Industries, Inc.

Concrete mixtures were developed based on the specifications, written and/or verbal, as supplied to Florida Rock Industries, Inc. for the referenced project.

Florida Rock Industries, Inc. can be responsible for concrete strength only:

- if sampling, specimen molding, curing and testing of specimens are done by certified personnel and an accredited laboratory;
- if testing conforms with applicable ASTM standards (ASTM C 31, C 39, C 94 and C 1077) for Standard Cured specimens under ASTM C 31;
- if the maximum slump and air content are not exceeded;
- if we are supplied a copy of all test results as they become available.

Florida Rock Industries, Inc. is not responsible for concrete strength as tested by Field Cured specimens under ASTM C 31 or results of testing in accordance with ASTM C 42. If core results are equal to or greater than 75% of f'c, Florida Rock Industries, Inc. will not be responsible for charges incurred, including, but not limited to the cost of coring, delays, structural analysis, etc.

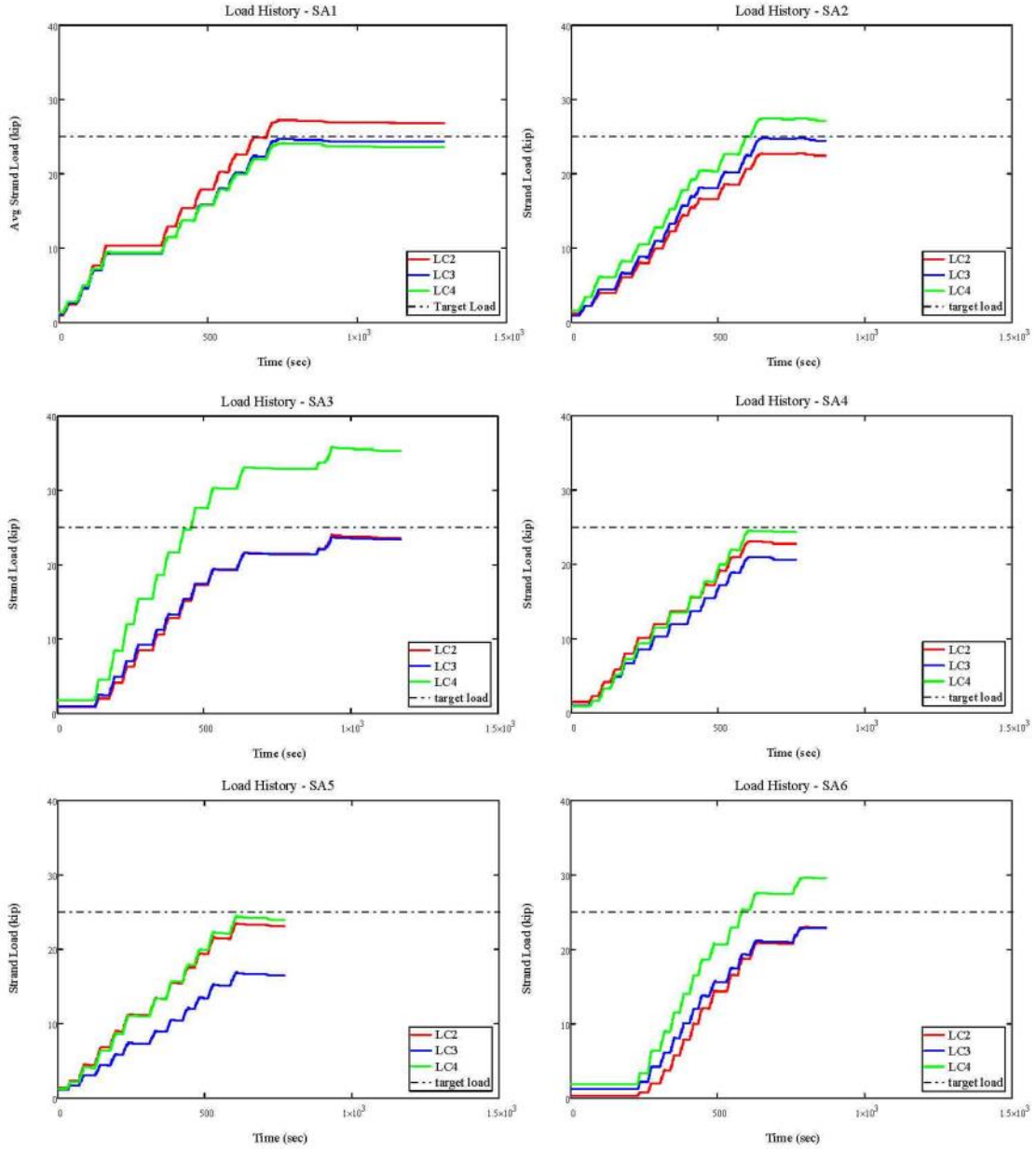
## Appendix F–Splice Assembly Plots

This appendix includes the data taken during the splice assembly procedure. Data is included for all six of the spliced specimens. Table 36 relates each spliced specimen to the load test performed on the completed beam. The “splice assembly” nomenclature is used in the plots contained in this appendix.

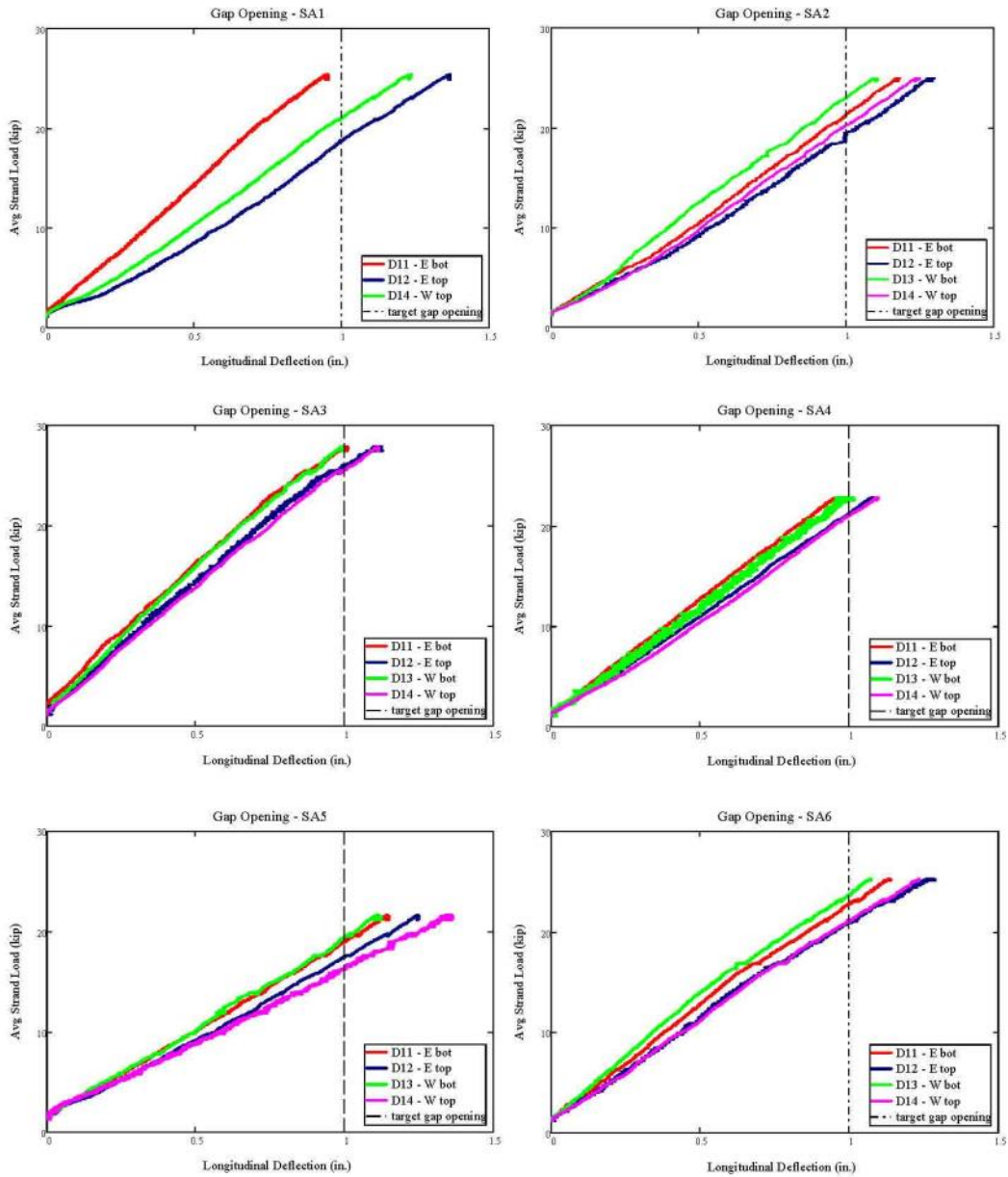
**Table 36–Splice Assembly IDs**

Spliced Specimen Assembly ID	Load Test ID
SA1	X1
SA2	SB
SA3	SU
SA4	SU2
SA5	F1
SA6	F2

### Load History

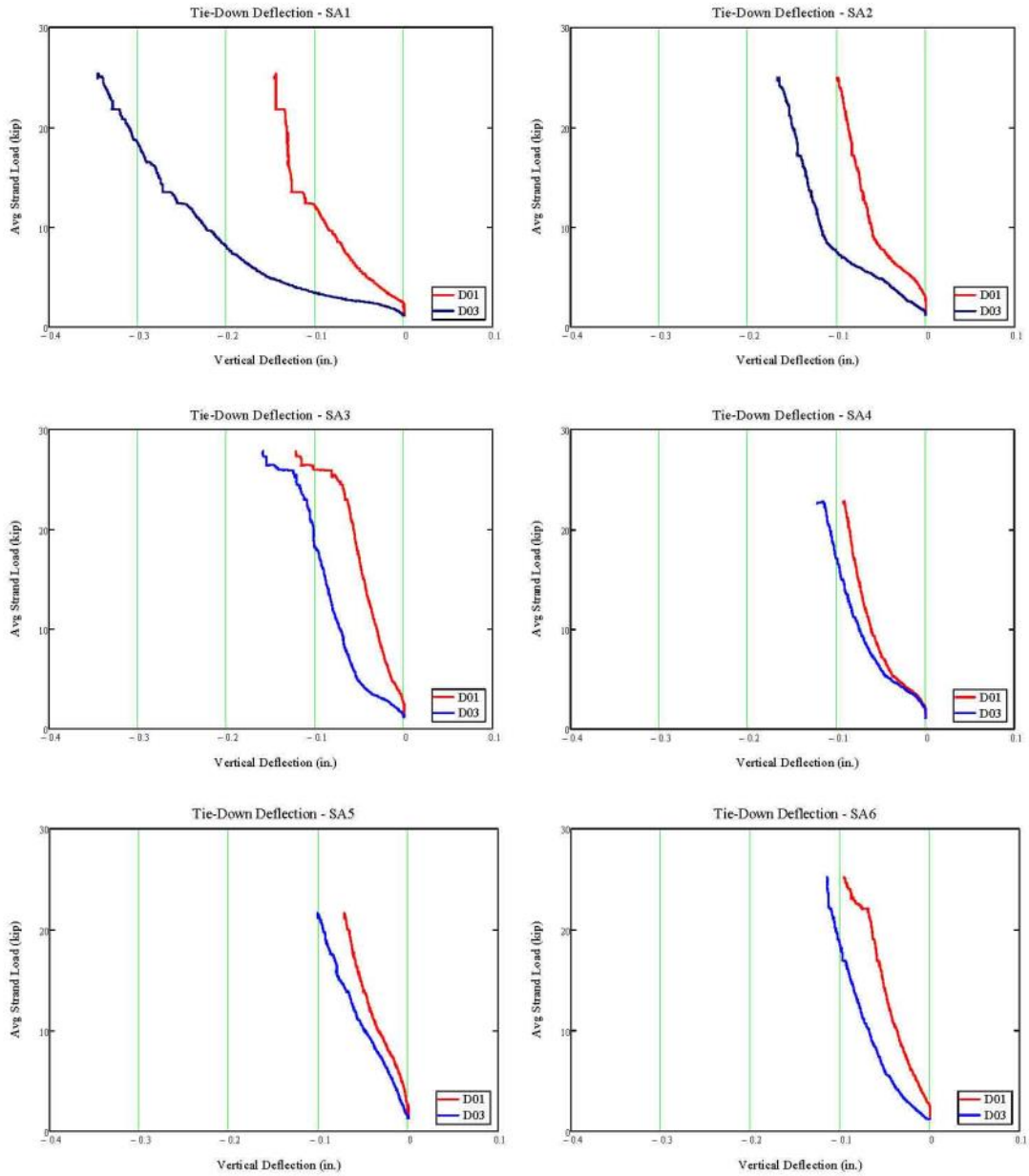


Gap Opening



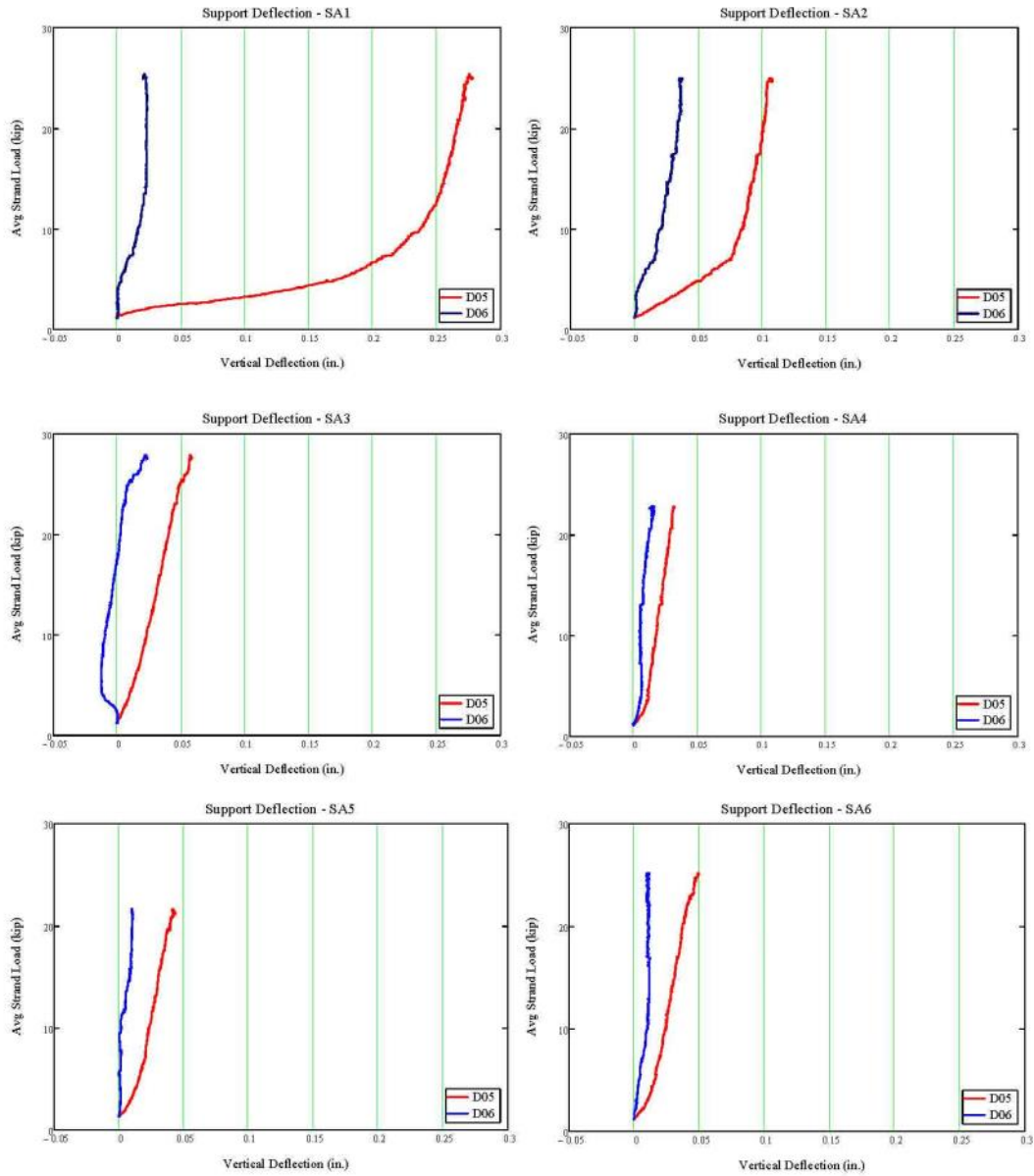
Appendix F - Splice Assembly Plots

**Tie-Down Deflection**



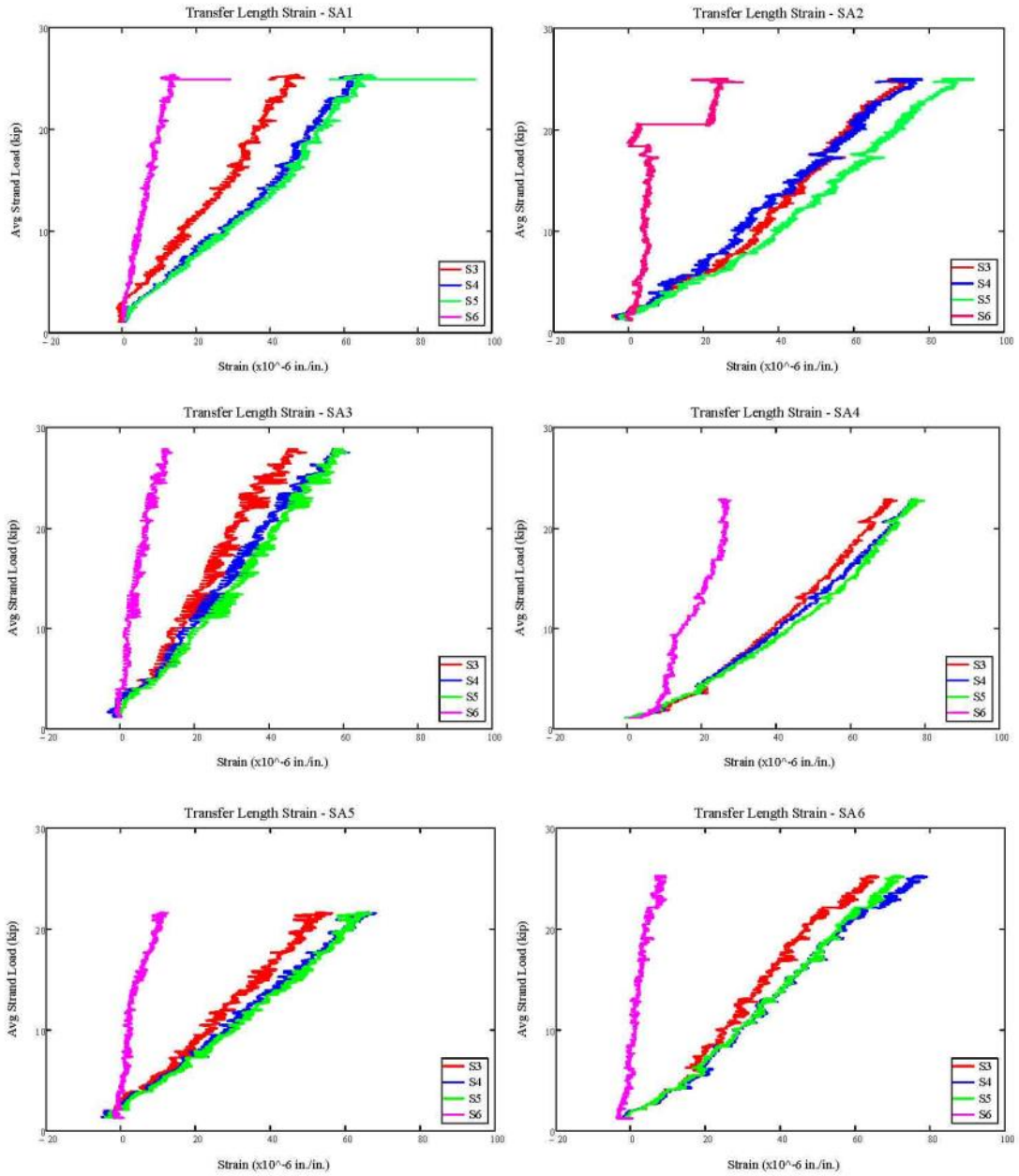
Appendix F - Splice Assembly Plots

Support Deflection

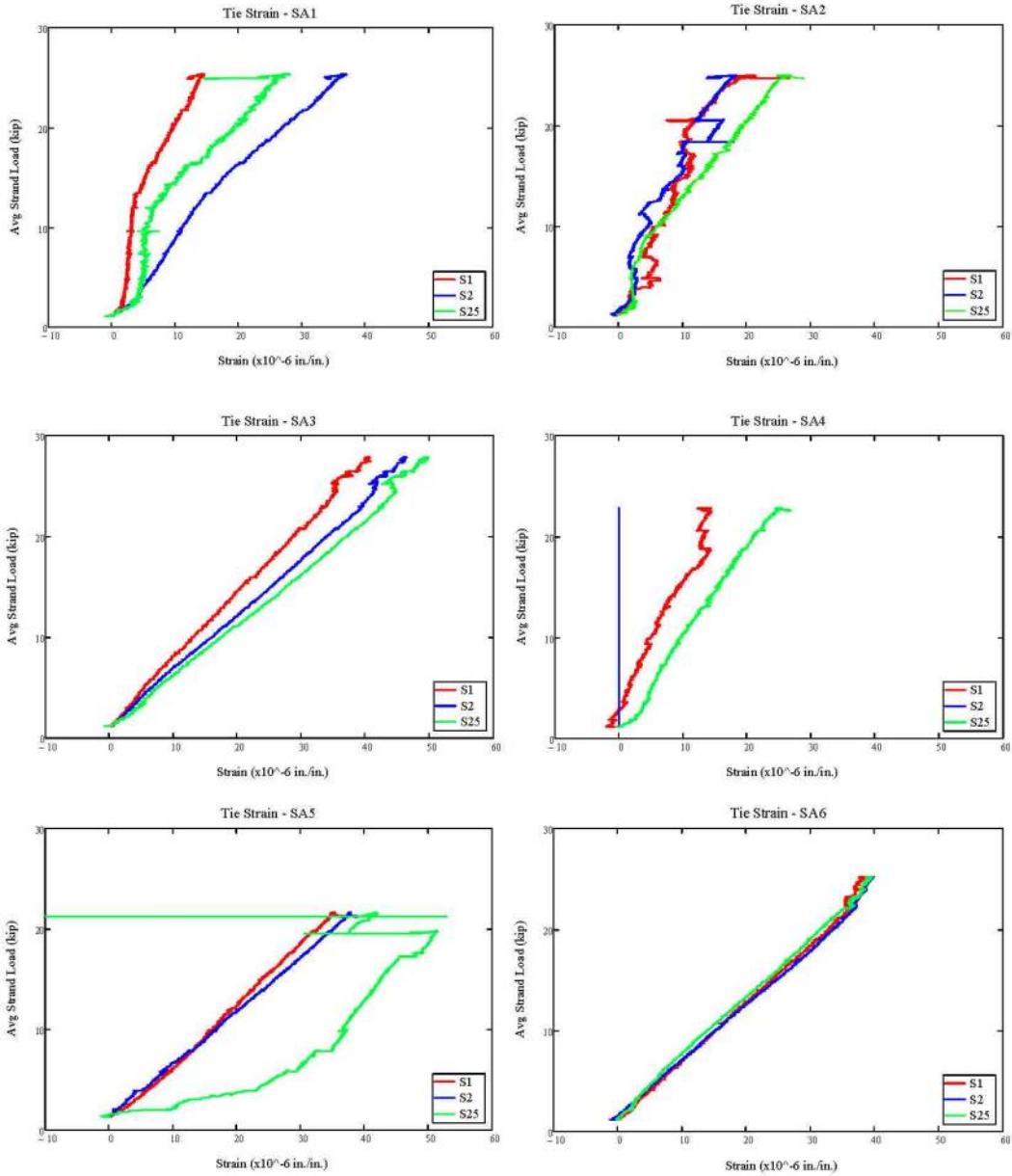


Appendix F - Splice Assembly Plots

Transfer Length Strain

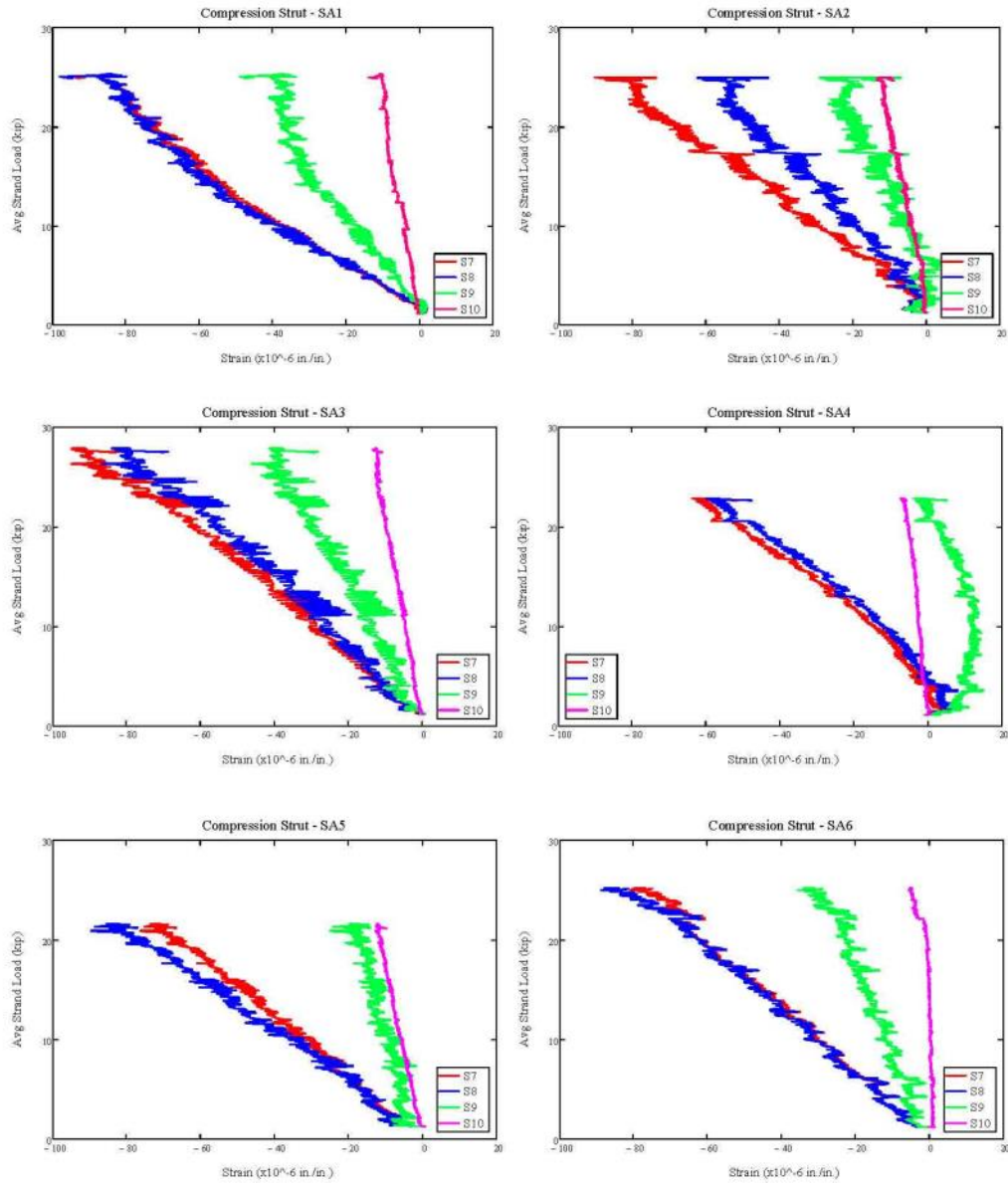


**Tie Strain**



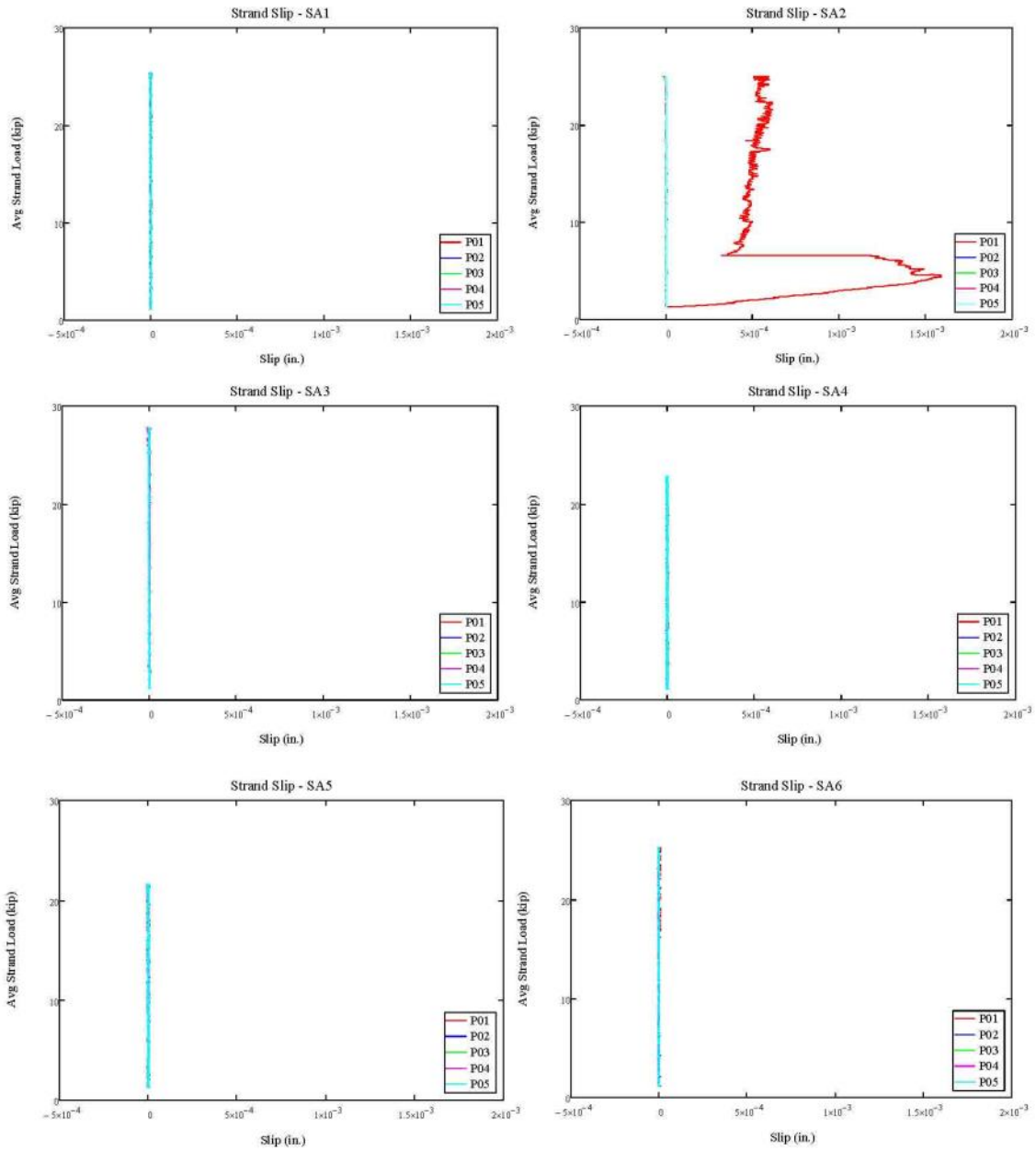
Appendix F - Splice Assembly Plots

Compression Strut



Appendix F - Splice Assembly Plots

Strand Slip



Appendix F - Splice Assembly Plots

Grabb-It Strain

